Interaction of positron beams with surfaces, thin films, and interfaces

Peter J. Schultz

Department of Physics, The University of Western Ontario, London, Ontario, Canada N6A 3K7

K. G. Lynn

Department of Physics and Department of Applied Science, Brookhaven National Laboratory, Upton, New York 11973

Recent advances in the study of solid surfaces and thin films using variable-energy positron beams are reviewed. In the first part the authors discuss the process of positron moderation and technical aspects of positron beam production and application. The second part is (roughly) organized in sections that apply to increasing time scales appropriate to the positron-solid interaction. These are (a) first encounter and scattering effects, (b) energy loss and stopping profiles, (c) diffusion of thermalized positrons, (d) positron-surface interactions, and (e) studies of defects near surfaces and interfaces. The review is written with more emphasis on the most recent measurements and interpretations than on the chronology of various developments.

CONTENTS

LIST OF SYMBOLS

a_0	Bohr radius (0.529 Å)
$C(z)$	depth distribution of defects [Eq. (52)]
D	surface dipole potential [Eq. (1)]
D_{Ps}	positronium diffusion coefficient [Eq. (37)]
D_+	positron diffusion coefficient [Eq. (13)]
E_B	Ps binding energy in the solid [Eqs. (3) and (4)]
E_a	activation energy for positrons trapped at the surface to form Ps in vacuum [Eq. (45)]
E_b	binding energy for positrons at the surface [Eq. (47)]
E_f	Fermi energy [Eq. (29)]
E_0	incident energy at which 50% of the positrons return to the surface [Eqs. (22) and (28)]
E_{1v}^f	monovacancy formation energy [Eq. (51)]
e^+	moderated positrons
$\mathcal{F}_0$	direct (i.e., $\varepsilon_{\mathrm{Ps}}$) fast Ps formed [Eq. (45)]
$\mathcal{F}_s$	surface-state trapped e^+ which are desorbed as Ps
$f(E)$	Ps fraction formed at the surface [Eqs. (9) and (25)]
f_0	Ps extrapolated to zero energy (branching ratio)
L_+	positron diffusion length [Eq. (28)]
$\mathcal{L}$	Laplace transform of e^+ stopping profile [Eq. (21)]
m	shape parameter for Mavkhovian profile [Eq. (10)]
$\mathcal{N}(a)$	number of positrons that diffuse back to the surface from depth a [Eqs. (19) and

	(20)]
n	power dependence of stopping on energy [Eq. (12)]
o-Ps	$^3S_1$ triplet state, ortho-positronium
$P(z)$	positron stopping profile [Eq. (10)]
Ps	positronium atom
p-Ps	$^1S_0$ singlet state, para-positronium
R_∞	Rydberg constant (13.6 eV)
S	Doppler-broadening line-shape parameter (Fig. 27)
S_{1v}^f	monovacancy formation entropy [Eq. (51)]
U_K	K-shell binding energy (Fig. 46)
V_{corr}	positron/conduction-electron correlation [Eq. (32)]
V_0	positron/lattice (zero-point) potential [Eq. (32)]
v_d	drift velocity [Eq. (53)]
$Y(E)$	fractional yield of reemitted positrons
Y_0	yield extrapolated to zero energy (branching ratio)
z	one-dimensional depth parameter [Eq. (10)]
$\bar{z}$	average positron stopping depth [Eq. (12)]
z_0	depth-related constant [Eq. (11)]
$\langle z \rangle$	mean depth of defect distribution [Eq. (58)]
α	thermal expansion coefficient [Eq. (43)]
β	proportional to positron reflection [Eq. (15)]
$\langle \beta_{\text{Ps}} \rangle$	positronium reflection coefficient [Eq. (46)]
ε	positron moderation efficiency
ε_d	deformation potential [Eqs. (32) and (44)]
ε_{Ps}	positronium formation potential [Eq. (2)]
κ_{bv}	transition rate from free to vacancy-trapped [Eq. (50)]
κ_{vb}	transition rate from vacancy to bulk state [Eq. (50)]
κ_0	trapping rate for vacancies [Eq. (51)]
κ_t	general trapping rate in arbitrary defects [Eq. (52)]
λ_b/τ_b	bulk solid (freely diffusing) positron annihilation rate/lifetime
λ_d/τ_d	positron annihilation rate/lifetime trapped at subsurface defects
$\lambda_{\text{eff}}/\tau_{\text{eff}}$	"effective" rate/lifetime as a freely diffusing particle, including a combination of the above [Eq. (14)]
λ_e/τ_e	positron-conduction-electron scattering rate/time
λ_i/τ_i	positron-impurity scattering rate/lifetime
$\lambda_{\text{ph}}/\tau_{\text{ph}}$	positron-acoustic-phonon scattering rate/time
λ_s/τ_s	positron surface annihilation rate/time
λ_t/τ_t	thermalization rate/time
μ	mobility [Eq. (33)]
μ_+	positron band energy [Eq. (1)]
μ_-	electron chemical potential [Eq. (1)]
μ_{Ps}	positronium chemical potential [Eq. (5)]
φ_+	positron work function [Eq. (1)]
φ_-	electron work function [Eq. (1)]
φ_0	$=(\varphi_+ + \varphi_-) = -(\mu_+ - \mu_-)$ [Eqs. (39) and (43)]
φ_{Ps}	positronium work function [Eqs. (3) and (4)]

I. THE TECHNIQUE

A. Introduction

Almost 40 years ago DeBenedetti *et al.* (1949) discovered that the two γ rays arising from the annihilation of a thermalized positron with an electron in a solid were not exactly collinear. This observation, which was correctly attributed to the effects of electron momentum, marked the birth of solid-state investigations with positrons, a field that grew rapidly and continues to grow (see West, 1973, or Hautojärvi, 1979, for general reviews).

Almost from the outset, Madanski and Rasetti (1950) realized that the continuous energy distribution of positrons emitted from standard positron sources was a limitation on the capabilities of the probe. They tried to moderate the positrons from a radioactive source to lower energies in order to obtain a source of positrons that were more or less monoenergetic, but they were unsuccessful. At that time they concluded that positrons were trapping in the solid or at the surface, or that positronium was being formed which their measurement would not be sensitive to. It was about 20 years before the processes of positron thermalization and diffusion were understood to a level that one could begin to speculate about the interaction of a positron inside a metal with the metal/vacuum interface. It was several more years before relatively efficient positron reemission was observed, and the late 1970s saw the first careful preparations of surfaces that were useful as positron "moderators" (Mills, 1978; Lynn, 1979a). The present high efficiency of conversion (a fraction of a percent) from the continuous β energy spectrum to monoenergetic beams of positrons has resulted in a new approach to the study of solids with positrons, emphasizing the surface and near-surface regions which were only indirectly accessible before.

The development of *slow*-positron beams (i.e., as distinct from the positron beams used in high-energy physics) has been motivated not only by materials science but also by atomic physics. For example, positron and positronium gas scattering and fundamental studies of positronium are both research areas that have required the intensity and energy resolution of modern beams. In this review we shall restrict our discussion primarily to the solid-state applications of the probe, and refer the interested reader to any of a variety of reviews of the atomic physics (Stein and Kauppila, 1982; POS84; Charlton, 1985; Dupasquier and Zecca, 1985) or astrophysical (Leventhal and MacCallum, 1985) applications.

An introduction to the field of experimentation with low-energy positron beams was given by Mills (1982). Dale, Hulett, and Pendyala (1983), Nieminen (1983), and

Corbel (1987) have reviewed some of the solid-state applications of the field, and Dupasquier and Zecca (1985) have briefly discussed various aspects of beam formation and research on both atomic and solid-state problems. As yet the most complete reviews of low-energy-positron studies related to solid-state applications are the lecture notes of Mills (1981a) and Lynn (1981) for the International School of Physics Enrico Fermi Course LXXXIII (POS81), which are now somewhat dated for a field that has seen the majority of its activity since 1980 (see Fig. 14). It is our intention to provide an up-to-date review and a critical survey of solid-state research with slow-positron beams, leaving out as much of the technical discussion of the apparatus and technique as we feel is reasonable. In addition to the open literature, there are several collections of individual papers to which we shall occasionally refer that are both general in nature (ICPA references: International Conferences on Positron Annihilation) or specific workshops on slow-positron beam studies (SLO84, SLO85).

The organization of this review is as follows. The first part starts with a general but brief summary of positron interactions with solids, progressing from the more traditional bulk studies to the processes at surfaces which are common both to the production of positron beams and to much of the resulting solid-state research. We complete the first part with sections concerning beam production and the more generally applied experimental techniques. In the second part we discuss some of the experimental results relevant to the study of solids with positron beams, supporting these where possible with some of the underlying assumptions behind theoretical models of the positron/near-surface interaction. The organization of this part will generally follow the time sequence of the positron's encounter with the solid. Scattering and channeling effects are presented first, followed by inelastic collisions (which cause the positron to thermalize), then epithermal processes and thermal diffusion. Finally, surface and defect studies, which are the two major areas of research, are reviewed. In this way we hope to build on the concept of "time scales" for positron interactions introduced in the first section. The third part of the review is a brief summary.

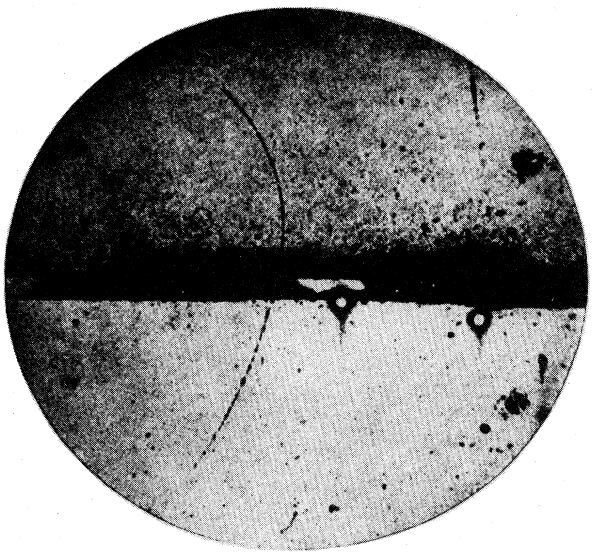

FIG. 1. One of Anderson's (1933) original photographs illustrating the historic discovery of the positron. In the cloud chamber, there is a lead plate 6 mm thick and a magnetic field oriented in the page. The change of energy (63 MeV below the plate to 23 MeV above) with the known thickness of lead and magnitude of the field proves that the particle is positive and of the same mass as the electron.

In general it is our aim to emphasize the present understanding of the research, so that in cases where early interpretations have been reevaluated we shall usually defer to current rather than historical perspectives. It is not our intention to provide an in-depth review of the experimental or theoretical details for the specialist, but rather to give the reader an overview of the interesting developments in this rapidly evolving area of condensed matter studies. It is hoped that this review will provide nonpractitioners with an understandable and up-to-date perspective on the solid-state applications of variable-energy positron beams.

B. Positrons

The positron was postulated by Dirac (1930) as the "negative" energy extension of his theory of electron energy levels. Anderson's discovery (1932a, 1932b, 1933) followed soon afterwards, and the historic cloud-chamber photograph of his 1933 paper is reproduced in Fig. 1. The positron, which is the antiparticle of the electron, has the same mass within current experimental limits (511.0034 ± 0.0014 keV$/c^2$; Cohen and Taylor, 1973) and the same spin ($\frac{1}{2}$), but the opposite charge and magnetic moment. It is stable in vacuum ($\tau > 2 \times 10^{21}$ yr; Bellotti *et al.*, 1983), although in metals it rapidly thermalizes, and annihilates with an electron predominantly via 2-γ-ray decay (~ 511 keV) with a mean lifetime that is typically only a few hundred picoseconds (psec).

In some circumstances the positron can bind with an electron to form a positronium atom (Ps) with a vacuum binding energy of ~ 6.8 eV. The singlet $^1S_0$ state (parapositronium, or p-Ps) has a vacuum lifetime of approximately 125 psec, and it decays predominantly into two γ rays of ~ 511-keV energy. Its total spin is $S=0$ ($m_s=0$), as opposed to that of the triplet $^3S_1$ state (orthopositronium, or o-Ps), which has a total spin $S=1$ ($m_s=0, \pm 1$). The lifetime of o-Ps, is about 142 nsec, and in vacuum it decays into three or more γ rays. The continuous energy distribution arising from o-Ps decay was predicted by Ore and Powell (1949) and was measured by Chang and co-workers (1985; Fig. 2). The relative amount of p-Ps:o-Ps formed in the absence of external disturbances is 1:3; this ratio can be derived on kinematical grounds. Reviews of fundamental properties of posi-

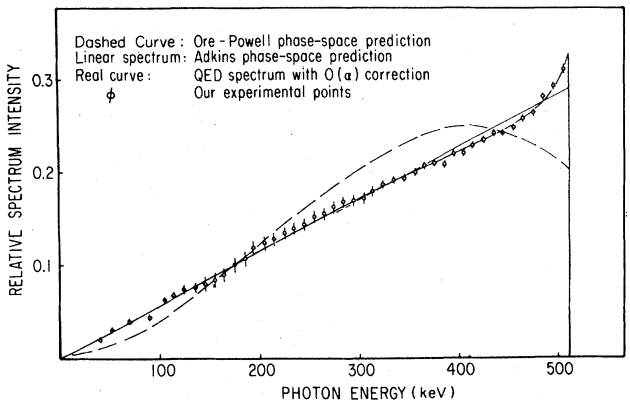

FIG. 2. The energy distribution of the 3γ decay of o-Ps. The points are the experimental results of Chang *et al.* (1985) and the QED models of Ore and Powell (1949) and of Adkins (1983). The 2γ decay of either p-Ps or positrons in delocalized or trapped states would produce a narrow peak (a few keV FWHM) at 511 keV. The experimental points in the figure were obtained by a coincidence measurement with a high-resolution intrinsic Ge spectrometer.

trons and/or Ps are given by Berko and Pendleton (1980) and Rich (1981).

1. Studies of solids

When a positron from some radioactive source enters a solid, it rapidly loses its kinetic energy (~ 10 psec) until it is near thermal energy, scattering between Bloch states to diffuse through the solid. We shall discuss this process in more detail in Secs. II.A–II.C, but it suffices for the present discussion to state that the "thermalization" time is short relative to the average lifetime of the positron in the solid. Kubica and Stewart (1975) demonstrated this experimentally by showing that the positron contribution to the center-of-mass momentum of the annihilating pair was negligibly small down to ~ 10 K in the alkali metals. After thermalization, the positron remains essentially as a "free" or delocalized particle, although strongly correlated with conduction electrons in its environment, until it annihilates in the bulk solid with $\tau_b \sim 10^{-10}$ sec.

The formation of Ps has not been observed either directly or indirectly inside defect-free metals or semiconductors. This absence is explained by the fact that a bound positron-electron pair in an electron gas would polarize the medium, which would, in turn, screen the positron-electron interaction. The Ps binding energy approaches zero at an electron density slightly below that found in Cs, which is the most dilute alkali metal (Kahana, 1960; Lowy and Jackson, 1975). Unlike metals and semiconductors, Ps does form in some molecular and ionic solids (see, for example, Dupasquier, 1981).

The foundation upon which almost all of the traditional defect-free bulk studies of solids with positrons rests is the fact that the positron annihilates with an electron in the solid, contributing very little extra momentum to the center of mass of the annihilating pair. This is because there is, on average, only one positron in the solid at any one time, so that after thermalization ($\sim 3/2k_BT$) it resides near the bottom of its own band as a delocalized Bloch wave. The electron, by contrast, has significant momentum because of the effect that the Pauli exclusion principle has on the sea of $\sim 10^{22}$ electrons/cm^3. The two γ rays normally arising from the annihilation are nearly collinear because of conservation of momentum, and the effect of electron momentum is to cause them to be emitted at a slight angle relative to each other. The measurement of the angular correlation of the annihilation radiation (ACAR) is one of the common experimental techniques used for studying positron annihilation in solids, and the effect of electron momentum discussed above is demonstrated dramatically in Fig. 3, where the upper curve shows the two-dimensional (2D) ACAR spectrum for a virtually momentum-free system (p-Ps in quartz), and the lower curve shows a similar measurement for delocalized positrons in a single crystal of Cu. Given this sensitivity, it is not surprising that the technique is widely used for measuring Fermi surfaces of metals and alloys (see, for example, Berko, 1981, or West, 1985).

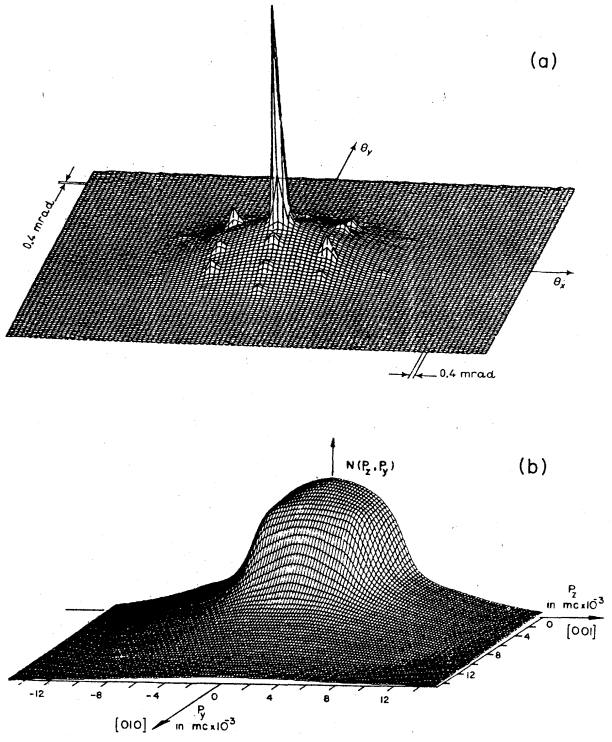

FIG. 3. Two-dimensional electron momentum distributions obtained using angular correlation of annihilation radiation (ACAR) measurements. The upper curve is for p-Ps annihilations in single-crystal quartz (after Manuel, 1981), which is a system with close to zero center-of-mass momentum. The lower curve is for delocalized positron annihilations in single-crystal Cu (from Haghgooie *et al.*, 1978), showing the much broader distribution due to the energetic electrons in the solid.

The positron's sensitivity to details of the *local* electronic environment is reflected not only in angular correlation but also in the Doppler broadening of the energy of the annihilation γ rays, as well as the mean positron lifetime before annihilation. These techniques are also often used for studies of lattice defects, since a freely diffusing positron can localize in regions of minimum potential in a periodic lattice created by the missing ion cores, as illustrated schematically in Fig. 4 (we can consider the positron as a Bloch-type wave packet extending over dimensions characterized by the de Broglie wavelength). The ability of positrons to localize or trap in thermally generated vacancies was first demonstrated clearly by MacKenzie and co-workers (1967), and the volume of activity that followed has since exceeded all other areas of bulk solid research with positrons, including Fermi-surface studies. It should be mentioned that localization of a particle as light as the positron, which is fundamentally quantum mechanical, is not as straightforward a conclusion as the highly schematic image of Fig. 4 would suggest. The de Broglie wavelength of a thermalized positron is

$$\lambda_{\rm th}=\frac{2\pi\hbar}{(3mk_BT)^{1/2}}=(62\ \text{Å})\left[\frac{300}{T}\right]^{1/2}$$

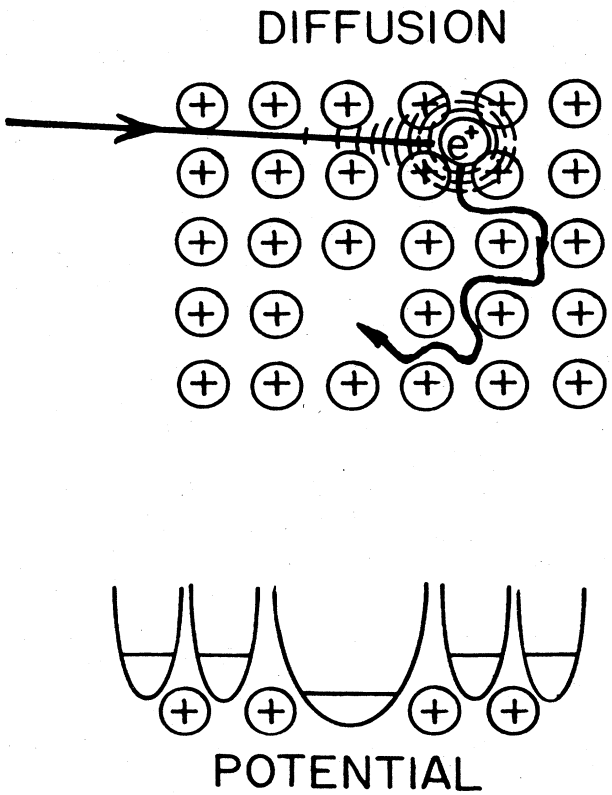

FIG. 4. The potential minimum for a point defect in a lattice. The positron rapidly thermalizes in the lattice and diffuses by scattering between delocalized Bloch states. The de Broglie wavelength of a positron at room temperature is ~20 times the lattice spacing. The transition from this extended state to the "trapped" state in the vacancy is very efficient ($\sim 10^{-15}$ sec^{-1}).

(where T is in degrees K and m is the positron mass), which, at room temperature, is roughly 20 times larger than typical interionic separations in metals. Nevertheless, it does localize at open-volume defects, and Hodges (1970) first explained the process theoretically by using the Golden Rule to evaluate the transition probability from the delocalized to trapped states, considering plane waves only. The trapping rates calculated in this way turn out to be on the order of $\sim 10^{15}$ sec^{-1} per unit concentration of vacancies, and the binding energies are as large as a few eV, consistent with the efficient process that is observed experimentally.

The way in which positron trapping is identified depends on which of the above methods is used. When the positron wave function collapses into a vacancy, its overlap with the more energetic core electrons in the solid is decreased relative to the less tightly bound conduction electrons. This leads to a significant reduction in the Doppler broadening of the annihilation radiation, or (equivalently) a reduced deviation from collinearity of the two annihilation γ rays. Both of these effects result in narrower distributions. There is also a decrease in the electron density in a vacancy relative to the undefected lattice, so that the mean positron lifetime is increased. The technique is in general extremely sensitive, indicating observable changes at defect concentrations as low as 10^{-7}. The measurement and interpretation of all of these effects has been discussed at length in several articles (e.g., West, 1973, or Hautojärvi, 1979), and we summarize the observable results of positron localization for the three basic techniques in Fig. 5.

2. A positronic calendar

Since the prediction and discovery of the positron more than 50 years ago, there has been a tremendous increase in the volume and variety of applications for the study of condensed matter physics, especially in the last 30 years. In the early 1930s there was a flurry of activity as researchers attempted to learn more about this newly discovered antiparticle, which continues to be simple to study in a relatively modest laboratory. As the general understanding of the particle increased, fundamental particle research began to decline, and DeBenedetti's discovery in 1949 inspired new solid-state applications. The spirit of the development of the field is captured in Fig. 6, where we reproduce Lambrecht's plot (1975) of the number of annually published papers relating to both positrons and positronium from 1930 to the mid 1970s. Some of the key events in the history of bulk studies of solids with positrons are summarized in Table I. The table is by no means complete and is intended to highlight only a few of the events that helped shape the present field.

C. Surfaces and beams

Most of the positrons implanted in a solid from a typical radioactive source reach equilibrium between 0.1 and

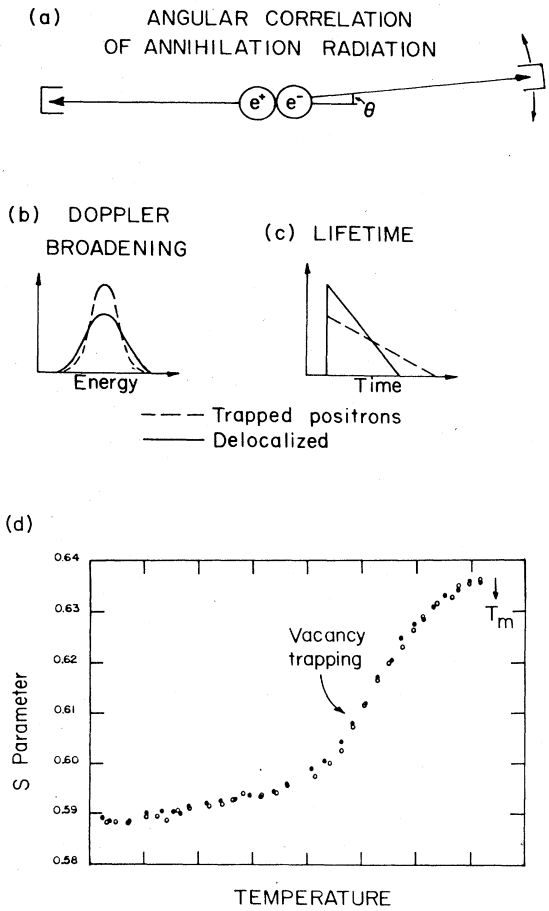

FIG. 5. Electron momentum reflected in (a) the deviation of γ-ray collinearity in ACAR measurements, or in (b) the width of the γ-ray annihilation line shape. When positrons trap in defects there is a reduced overlap with energetic core electrons, leading to narrow momentum (or γ-ray energy) spectra, and there is a general decrease in the electron concentration, leading to longer positron lifetimes (c). The narrowness of the line shape, characterized by an "S" parameter (Fig. 27), is sensitive to vacancy concentrations of $\sim 10^{-7}$ as illustrated by the increase in curve (d), and it usually saturates at some level ($\sim 10^{-3}$) below the melting point of the material T_m, which in this case is a CuZn alloy.

1 mm deep in the crystal. This is illustrated in Fig. 7, where the experimentally determined (Hansen *et al.*, 1982) implantation or stopping profile for positrons from ^{22}Na in Ni foils is shown. It is also clear that a significant number of positrons will thermalize near the surface of the solid. In fact, something on the order of 1% will stop within 1500 Å of the surface (1000 Å$\approx$0.09 mg/cm^2 for Ni), which is about the distance a thermalized positron will diffuse in a defect-free metallic solid in one mean lifetime. These are the positrons that can, if the sample and surface conditions are suitable, contribute to the "monoenergetic" reemitted flux from which the beam can be extracted.

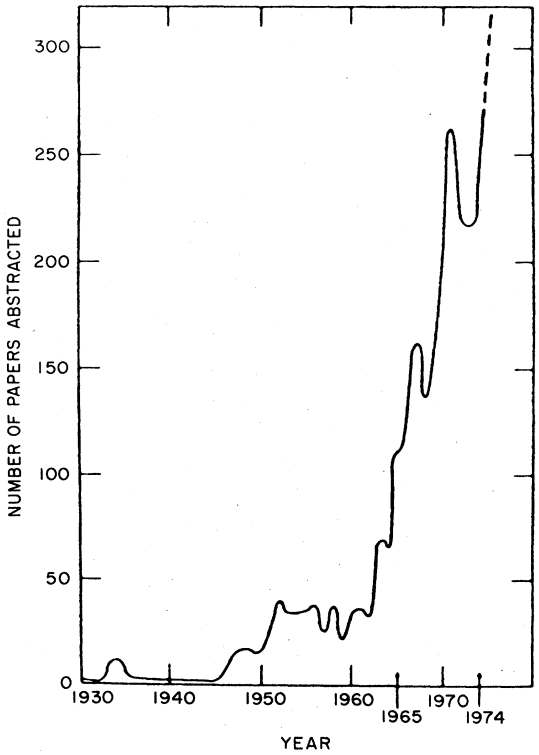

FIG. 6. The number of papers published annually relating to positrons and positronium from 1930 through to the height of activity in the field, around the mid-1970s (from Lambrecht, 1975).

1. The positron work function

The electron work function φ_- for a solid is defined as the minimum energy required to remove a bulk electron from a point inside to one just outside the surface (see, for example, Ashcroft and Mermin, 1976). This includes

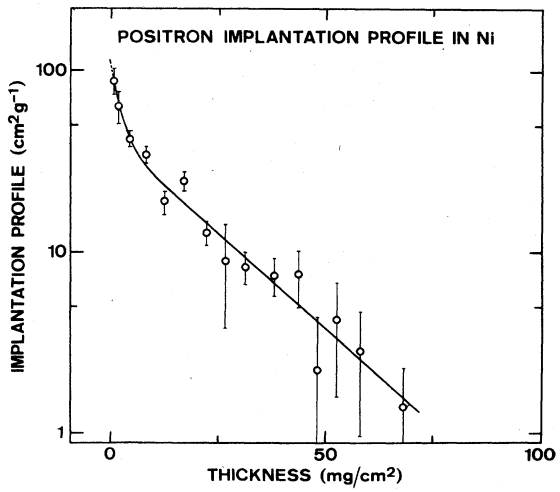

FIG. 7. The profile of energetic positrons from a ^{22}Na source stopping in Ni. This was measured by transmission through multiple layers of thin foils (from Hansen *et al.*, 1982).

TABLE I. A positronic calendar for solid state.

Year	Researcher	Event
1930	Dirac	Prediction of positron
1932	Anderson	Discovery
1933	Blackett and Occhialini	Pair production
1934	Klemperer	2γ annihilation
1934	Mohorovicic	Prediction of Ps existence
1949	DeBenedetti *et al.*	θ not 180°
1951	Deutsch	Discovery of Ps
1953	Bell and Graham	Two lifetimes in quartz
1955–1965	Berko, Stewart, and others	Advances in Fermi studies
1960	Kahana	Theory: enhanced annihilation
1960	Bell and Jorgensen	Material dependence of τ
1965	Brandt	Trapping model: alkali halides
1967	MacKenzie *et al.*	Thermal vacancy effects
1969	Bergersen and Stott	Trapping model: metals
1969	Connors and West	Trapping model: metals
1970	Hodges	Trapping theory
	... the field takes off	Fermi studies
		Defect studies
		Ps chemistry
		Astrophysics
		Gas scattering
		etc.

a "bulk" contribution, which is just the electron's chemical potential μ_- (or the absolute value of the Fermi energy for metals), and a surface contribution, which is called the surface dipole barrier D. The dipole is primarily caused by the tailing of the electron distribution into the vacuum, although it can also be affected by the relaxation and reconstruction of the surface layers (Lang and Kohn, 1973).

The positron work function φ_+ is defined in exactly the same way as φ_-, where μ_+ is defined as the difference between the bottom of the lowest positron band and the crystal zero level (at $T=0$). The reference level for the potentials involved in calculating φ_- and φ_+ must be chosen consistently. The "crystal zero" as we use it is the potential averaged over only the interstitial regions between the atoms. Other reference levels have been used in the literature (for a full discussion, see Hölzl and Schulte, 1979). The contributions to μ_+ include repulsion from the ion cores (zero-point potential, V_0) and attraction to the electrons (correlation potential V_{corr}) (Heine and Hodges, 1972; Hodges and Stott, 1973b; Nieminen and Hodges, 1976a, 1976b). The effect of the dipole D is positive for electrons and negative for positrons (i.e., directed out of the solid), where D is also measured relative to the crystal zero of the electrostatic potential. It is this reversal that causes φ_+ to be very nearly zero and, in some cases, even negative, allowing the reemission of slow, monoenergetic positrons into the vacuum (Tong, 1972). These contributions to the work function are given by

$$\varphi_+ = -D - \mu_+ ,$$
$$\varphi_- = +D - \mu_- , \tag{1}$$

and they are shown schematically in Fig. 8.

Following the unsuccessful attempt of Madanski and Rasetti (1950), Cherry (1958) was the first to observe moderated slow-positron emission, with an efficiency of $\sim 10^{-8}$. Experimental evidence of *efficient* ($\sim 10^{-7}$ -10^{-6}) generation of slow (eV) positrons was reported at a 1968 meeting of the American Physical Society (Groce

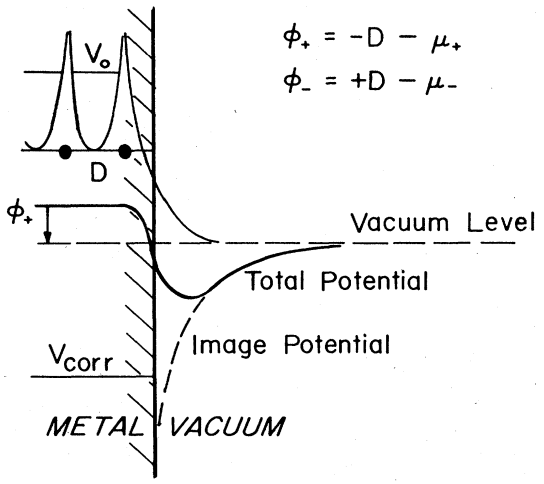

FIG. 8. The single-particle potential for a thermalized positron in a metallic lattice. The work function φ_+ is a combination of the bulk chemical potential μ_+ and the surface dipole layer D. The positron chemical potential includes terms due to correlation with the conduction electrons (V_{corr}) and the repulsive interaction with the ion cores (V_0). The opposite sign of D for positrons relative to that for electrons is the important difference that can, in many cases, result in a negative φ_+ like that shown in the figure.

et al., 1968), and again by the same group in 1972 (Costello *et al.*). In Fig. 9 examples are shown of the reemitted positron energy distributions measured for various metallic moderators that this group studied (McGowan, 1972). These are the first high-resolution differential measurements of positron energy distributions to be made, and they demonstrate the narrow energy width that is a characteristic result of the positron emission process. The negative work function was predicted by Tong (1972), who first reported the significance of the dipole contribution, and this model was subsequently corrected for positron-electron screening by Hodges and Stott (1973b).

It is important to emphasize that there are several unique advantages to producing a beam of positrons using a moderator, as opposed to the simpler energy selection of a traditional β-ray spectrometer. The first is that positrons are emitted from a moderator preferentially normal to the surface, and the energy width of the beam is extremely narrow, being (typically) limited only by the thermal energy of the positron in the lattice (<0.1 eV) (Murray and Mills, 1980; Gullikson *et al.*, 1985; Fischer, Lynn, and Gidley, 1986). This property is essential for many experiments, such as energy-loss or cross-section measurements, where energy resolution is critical. The second, and perhaps more important, feature of moderator-produced beams is that the efficiency ($\sim 10^{-3}$) of typical systems is much higher than that of β-ray spectrometers, even with wide energy windows. For example, the spectrometer employed by Ito *et al.* (1980) produced a beam with $\sim 2-3\times 10^{-5}$ efficiency at 300 keV, with >50 keV full width at half maximum (FWHM). The combination of narrow energy resolution with relatively high efficiency is illustrated in Fig. 10, where we show the differential yield of positrons from a $W(110)$ moderator, together with the ^{58}Co β^+ spectrum.

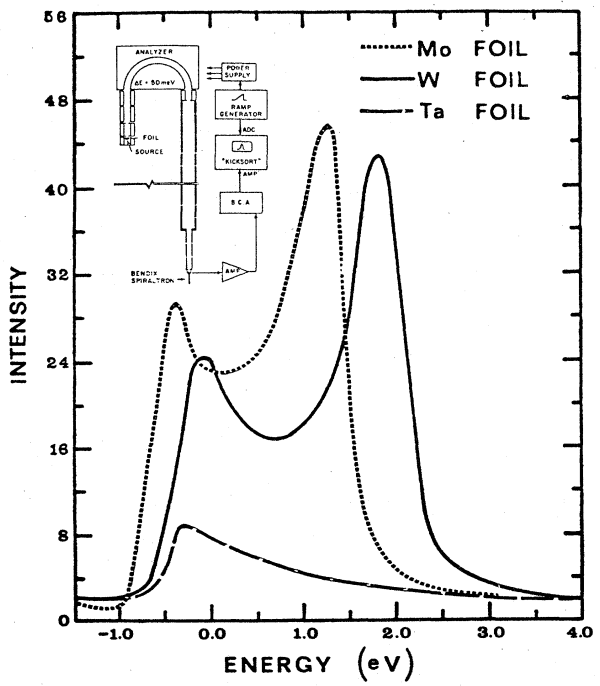

FIG. 9. The first measurement of a relatively "narrow" energy distribution of positrons reemitted from a solid moderator. The abscissa is the positron energy from the tantalum-mica-gold sandwich moderator, which was biased to 15 V (after Groce *et al.*, 1968).

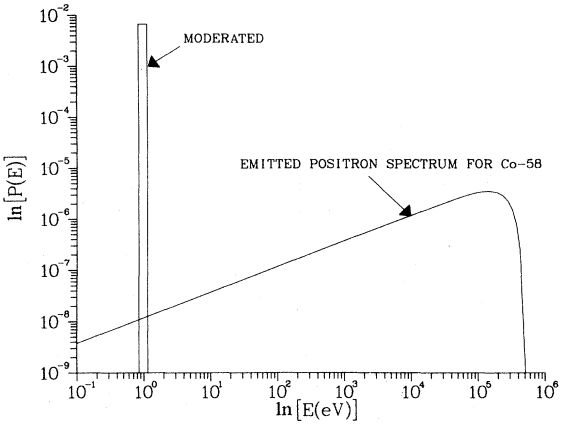

FIG. 10. Comparison of positron yield from a moderator with the original β^+-particle energy spectrum for ^{58}Co (normalized). The benefit of the nonconservative process of positron moderation relative to simple velocity selection is obvious.

2. Time scales for positrons

Even though a typical positron lifetime in a solid is only 10^{-10} sec, it is important to realize that this is in fact long compared with most other times that are significant (see Table II). In this review we shall consider what is known about positron interactions with solids and surfaces with emphasis on the time sequence in which these processes take place, rather than the chronology of discovery and/or understanding.

A summary of some of the important processes that can occur at and near surfaces when studied with a beam of slow positrons is presented in Fig. 11. The figure is divided into four sections, each representing a progressively "expanded" time frame, and illustrating those features that are appropriate to the frame. There is a great deal of information in the figure, and it is highly schematic. Nevertheless, it demonstrates that the reemission of thermalized positrons is just one branch of a fairly involved set of interactions, which include the scattering and energy-loss processes that dominate the first few picoseconds, and the diffusion and surface interactions of the thermalized particle occurring at longer times.

3. The positronium work function

Many of the processes illustrated in Fig. 11 involve the formation of Ps at the surface of the solid. As yet there is no evidence that Ps will form in the undefected bulk of

TABLE II. Time scales for positrons.

	Time	Footnotes
Lifetime in vacuum	$\sim 2\times 10^{22}$ yr	a
Scattering or diffraction	$\sim 10^{-15}$ sec	b
Thermalization (to $\sim$ Fermi energy)	$\sim 10^{-13}$ sec	c
Thermalization (to $\sim \frac{3}{2}kT$)	$\sim 10^{-12}$ sec	b
Trapping (after thermalization)	$\sim 10^{-15}$ sec	d
e^+ lifetime		
Freely diffusing	$\sim 1\times 10^{-10}$ sec	e
Monovacancy trapped	$\sim 2\times 10^{-10}$ sec	e
Multivacancy/void trapped	$\sim 4\times 10^{-10}$ sec	f
Surface state	~ 4–6×10^{-10} sec	g,h
Annihilation time	$\sim 10^{-21}$ sec	i
Ps lifetime		
Singlet, vacuum	$\sim 1.25\times 10^{-10}$ sec	j
Triplet, vacuum	$\sim 1.42\times 10^{-7}$ sec	j
Triplet, in solids (molecular crystals and insulators)	$\leq 10^{-9}$ sec	k

[a]Bellotti *et al.*, 1983.
[b]Perkins and Carbotte, 1970.
[c]Nieminen and Oliva, 1980.
[d]Hodges, 1970.
[e]West, 1973.
[f]Hautojärvi, 1979.
[g]Lynn, Frieze, and Schultz, 1984.
[h]Kögel *et al.*, 1988.
[i]Schrader, 1985.
[j]Gidley, Rich, Sweetman, and West, 1982.
[k]Dupasquier, 1981.

crystalline metals or semiconductors (Sec. I.B.1). In all such materials there is, on the other hand, a finite probability that Ps will form as a delocalized positron leaves the solid surface and travels through the decreasing electron density just outside. Conservation of energy gives a potential, ε_{Ps}, for Ps "just outside" the surface,

$$\varepsilon_{Ps}=\varphi_- +\varphi_+ -\tfrac{1}{2}R_\infty \ . \tag{2}$$

The binding energy of Ps in vacuum, $\frac{1}{2}R_\infty \simeq 6.8$ eV, is large enough to ensure that ε_{Ps} is often negative, so that Ps formation becomes one of the main branches for positrons that diffuse back to the surface of many systems. The first evidence of efficient Ps formation was that presented by Canter *et al.* (1974). Mills (1978) later observed Ps formation on well-characterized surfaces, shown in Fig. 12. These data indicate not only the magnitude of the effect (from 30% to 100%), but also the dependence on incident positron energy, which can be related to the positron diffusion in the solid (Sec. II.C).

Over the last several years researchers in the field have referred to ε_{Ps} as the "Ps work function," which is not appropriate, since in the variety of situations described above (and pictured in Fig. 11) there can be no Ps inside the solid. We shall, instead, refer to ε_{Ps} as a Ps *formation potential,* and reserve the term "work function" for the more appropriate situation described below. Ps formed (with a thermalized positron) at the surface has a maximum kinetic energy, given by $-\varepsilon_{Ps}$, which is discussed in more detail in Sec. II.D.2.

In many solids (such as molecular and ionic crystals) Ps can form when an energetic positron loses some of its energy by liberating an otherwise bound electron. When in a solid, the binding energy of the Ps is less than the vacuum value of $\frac{1}{2}R_\infty$ because of (among other things) a repulsive exchange interaction between the Ps electron and the surrounding electrons. This is what creates the negative Ps work function φ_{Ps}, which is given by

$$\varphi_{Ps}=-\mu_{Ps}+E_B-\tfrac{1}{2}R_\infty \ , \tag{3}$$

where E_B is the binding energy of Ps while in the solid and μ_{Ps} is the chemical potential of the Ps, which can be described as the center-of-mass energy of the lowest-energy "dressed" Ps Bloch wave while in an excitonlike state. Ps diffuses in the solid, and if it reaches the surface it may escape into the vacuum. In this case, we describe the potential difference between the point "just outside" the solid surface and the point "in the bulk" as the Ps work function φ_{Ps}.

Energy can be balanced in a way that is equivalent to Eq. (3) above by describing the Ps work function as the energy required to completely separate the positron from the electron in the solid (E_B), plus the energy required to remove both from the solid ($\varphi_+ +\varphi_-$), less the energy

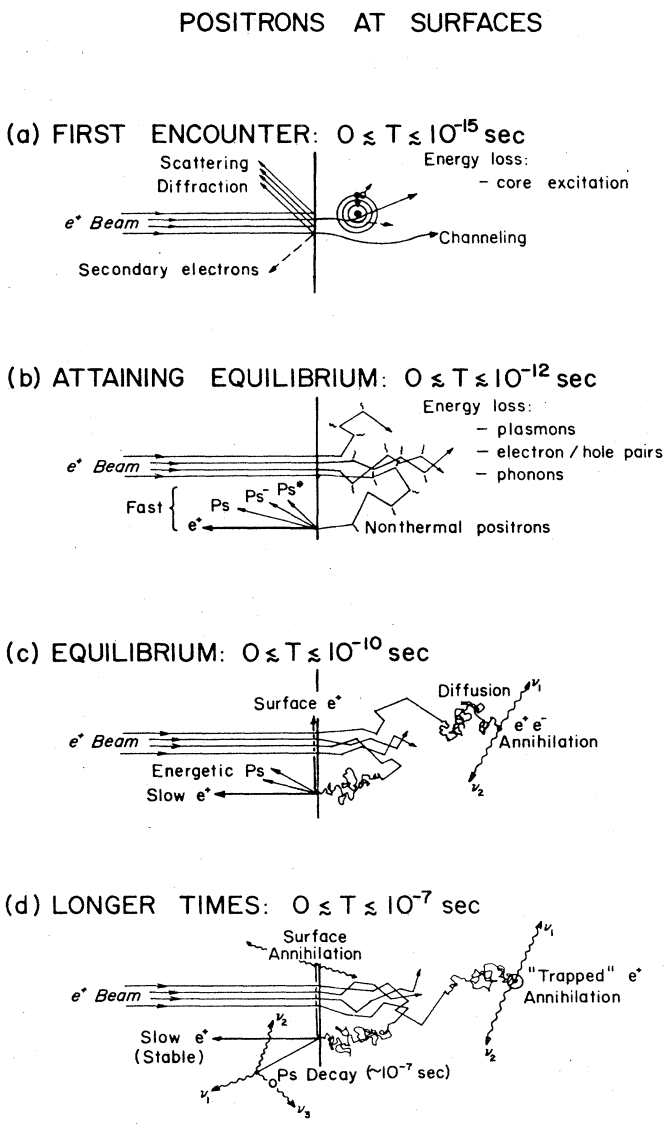

FIG. 11. The interaction of a positron beam ($E \lesssim 100$ keV) with the near-surface region of a solid. The figure is organized in four parts according to the appropriate time scales, as discussed in the text.

gained by reassembling the Ps in vacuum ($\frac{1}{2}R_\infty$):

$$\varphi_{Ps} = E_B + \varphi_+ + \varphi_- - \tfrac{1}{2}R_\infty \ . \tag{4}$$

It is interesting to note that this description (which is essentially a definition for E_B) implies that the Ps chemical potential is in equilibrium with those of the positron and electron:

$$\mu_{Ps} = \mu_+ + \mu_- \ . \tag{5}$$

There is, in general, less certainty at this time about the details of formation in bulk, diffusion, and subsequent escape of Ps from a solid than there is for the bare positron.

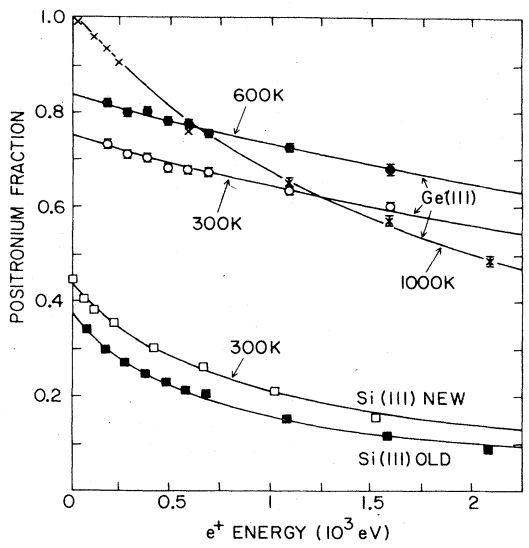

FIG. 12. The efficient formation of Ps at a surface for variously prepared and treated semiconductor samples. The "new" and "old" Si(111) refer to samples immediately after cleaning and after two weeks in the vacuum system, respectively. The decrease of the Ps fraction f with energy is due to the finite diffusion length of positrons in the solid (from Mills, 1978).

4. Time scales for positronium

The Ps atom is the lightest hydrogenic system that can be used to probe a solid, and recent developments have resulted in the availability of Ps beams. Mills (1983) demonstrated that a small fraction of Ps^- can be formed by passing an energetic positron beam through a thin foil. The charged Ps state has the attractive feature of allowing electrostatic acceleration, but the decay rate [$\lambda_{Ps^-} = 2.09(9)$ nsec^{-1}], low yield ($\sim 10^{-5}$), and wide energy distribution were not promising for beam development. More recently, Ps atoms with energies of up to a few tens of eV have been produced with efficiencies of up to a few percent by the same beam-foil technique (Mills and Crane, 1985a). Energetic Ps has also been produced by passing a positron beam through a dilute gas cell (Brown, 1986; Laricchia *et al.*, 1987) and by "skipping" a low-energy positron beam off a surface (Gidley *et al.*, 1987). The first measurements of specularly reflected Ps from solid surfaces have been made at Brookhaven National Laboratory (Berko *et al.*, 1985). Recently both angle and energy dependences of Ps scattering from a LiF(100) surface have been measured at Brookhaven National Laboratory (≈ 1 part in 10^3) that are consistent with zero-order diffraction (Weber, 1988). In addition, new theories for Ps interactions are being developed, such as the work of Melezhik and Vukajlovic (1987) on cross sections for spin flip during Ps-electron scattering. The promise of usable beams of Ps in the near future inspires the summary of their possible interactions with solid surfaces presented in Fig. 13, in analogy with earlier such summaries for positron beams.

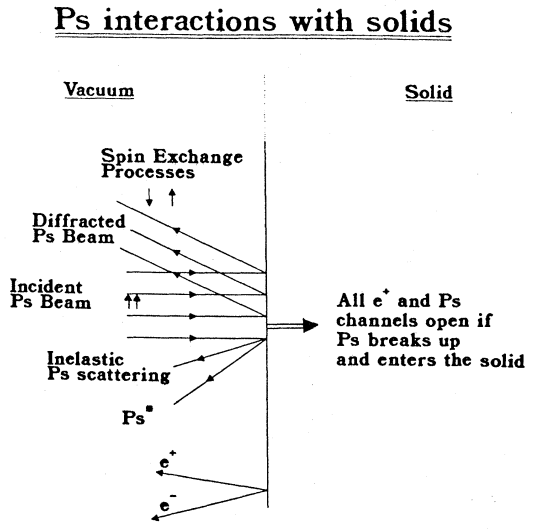

FIG. 13. Possible interactions of Ps beams with surfaces are suggested. The incident beam is shown in the long-lived triplet state, *o*-Ps: $\tau \approx 142$ nsec, since the singlet *p*-Ps which decays with $\tau \approx 125$ psec in vacuum would not survive in a beam long enough to be of any practical use. These processes have not yet been studied in detail, since variable-energy beams of Ps are only now available.

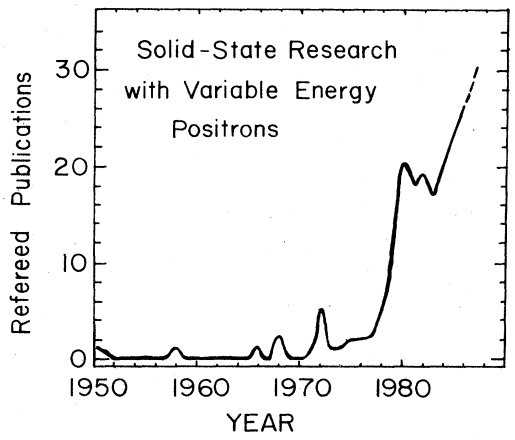

FIG. 14. The number of papers published annually tha to the solid-state applications of positron beams. By c ison with the general field of study with positrons and 6), this figure clearly shows the relative youth of the fi well as the rapid growth that is presently occurring.

5. A slow-positronic calendar

As indicated in Sec. I.B.2, studies of solids with positrons have been pursued since the mid 1950s. The development of efficient positron beams is more recent, and the field of surface and near-surface studies with positrons has evolved only since about 1980. Since that time, however, the interest and activity associated with positron beam studies has steadily increased, as is demonstrated in Fig. 14. This curve represents the positron beam publications that are relevant to the development of solid-state applications only, and it was abstracted from the references contained in this article. It is clear that the activity of the field is rising. Some of the important contributions leading to the current beam efficiencies are summarized in Table III.

D. Beam production

The experimental problems associated with the efficient production of slow-positron beams have required significant effort to solve. This is demonstrated by the fact that the first published suggestion of the process (Madanski and Rasetti, 1950) predates the "near-theoretical" efficiencies approaching 1% we now attain by about 30 years. We are continually striving to improve moderator efficiencies and beam intensities, largely because of the cost of primary positron sources and an ever-expanding interest in more demanding experiments requiring more beam current. Examples of current attempts to find even better moderators are discussed in the following subsection. It is true, nonetheless, that for several years now the basic details of positron beam production have been well understood, resulting in a rapid increase in both numbers of facilities and publications. For this reason we shall cover as little of the technical information as continuity allows, referring where possible to original publications for details. Two examples of the

TABLE III. A slow positronic calendar.

Year	Researcher	Event
1950	Madanski and Rasetti	Right idea, no results
1958	Cherry	First observation ($\epsilon \sim 10^{-8}$)
1968	Groce *et al.*	LINAC: usable rates ($\epsilon \sim 10^{-6}$)
1972	Canter *et al.*	MgO moderator ($\epsilon \sim 3 \times 10^{-5}$)
1972	Tong	Negative e^+ work-function theory
1979	Mills	Cu(111)+S ($\epsilon \sim 1 \times 10^{-3}$)
1982	Howell *et al.*	Intense LINAC beam (pulsed)
1983	Vehanen *et al.*	W(110) ($\epsilon \sim 3 \times 10^{-3}$)
1985	Lynn *et al.*	Intense dc reactor beam
1987	Mills and Gullikson	Solid Ne ($\epsilon \sim 7 \times 10^{-3}$)

variety of descriptions of sources, moderators, and beam design considerations that can be found are Canter and Mills (1982) and Dupasquier and Zecca (1985).

1. Sources and moderators

Monoenergetic ("slow") positron beams all start with primary sources that have continuous energy distributions, arranged in some geometrically convenient fashion near a positron "moderator" or "converter." The primary source is most often a radioactive isotope, although in some cases a LINAC is used to generate positrons by pair production (Groce *et al.*, 1968; Howell, Alvarez, and Stanek, 1982; Graff *et al.*, 1984; Ito *et al.*, 1985). In this case, the pulsed electron beam is stopped in a dense high-Z absorber, creating bremsstrahlung γ rays. Dorikens *et al.* (1987) suggested that LINAC-based beams could be improved by designing the electron absorber, or "converter," to take advantage of β^+-emitting isotopes produced by nuclear reactions.

Other methods for source production have been used. For example, protons from a 4.75-MV Van de Graaff accelerator incident on a boron target were employed by Stein *et al.* (1974) to generate positrons through nuclear reactions. Another idea recently suggested by Skalsey and Van House (1988) involves production of an intense ^{126}I source by neutron irradiation of ^{124}Xe in a fairly typical reactor ($\sim 10^{14}$ n/sec cm^2). This source would act as its own moderator (see Gullikson and Mills, 1986). However, the most common methods are all variations of those involving radioactive sources or LINAC. Some of the source/moderator configurations are presented in Fig. 15.

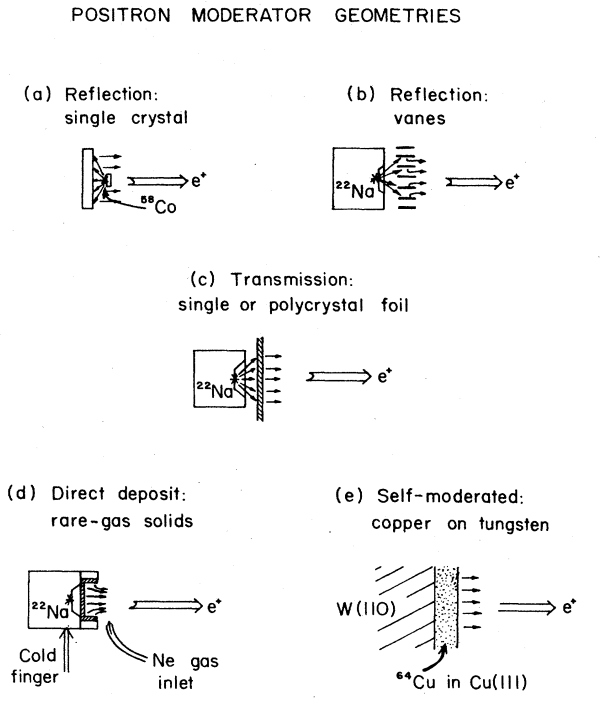

FIG. 15. Some of the various source/moderator geometries employed. A common mode used with ^{58}Co sources ($\tau_{1/2} \approx 71$ d) is the "back-reflection" geometry shown in (a), with the source plated on a thin rhodium foil or needle in front of a thick single-crystal moderator (usually W, Ni, or Cu). Various other geometries have been adopted for ^{22}Na sources ($\tau_{1/2} \approx 2.6$ yr), which are commercially available in sealed vacuum capsules.

As yet, most of the high-efficiency moderators are all negative-work-function materials, which emphasize features such as narrow energy width [e.g., Ni(100), Gullikson *et al.*, 1985)], or maximum yield [e.g., W(110), Vehanen *et al.*, 1983)]. The back-reflection geometry depicted in Fig. 15(a) is one of the most common arrangements, using a ^{58}Co source in front of a single-crystal moderator to produce the beam (Mills, 1979a). Recent demonstrations of transmission moderation [Fig. 15(c)] through thin single crystals of W (Chen *et al.*, 1985; Lynn, Nielsen, and Quateman, 1985) and Ni (Schultz, Gullikson, and Mills, 1986) do not have the problem of source shadowing that limits the back-reflection geometry, but so far problems with defects in the foils and self-absorption of positrons in the source material and window have resulted in consistently poorer efficiencies (Massoumi *et al.*, 1988; Schultz, 1988; Gramsch *et al.*, 1987). Annealed polycrystalline materials are occasionally used, such as the W vanes which are arranged in "Venetian blinds" shown in Fig. 15(b) (Dale *et al.*, 1980), and the 5-μm Ni foils first used by Gidley and Frieze (1986) in transmission geometry. Various single and polycrystalline moderator foils have been compared by Gramsch *et al.* (1987).

Recently Gullikson and Mills (1986) have shown that rare-gas solids (e.g., Ne) reveal unusually high yields of "hot" positrons, because of the inability of the positrons to thermalize completely in the rare-gas solids [see Fig. 15(d) and Sec. II.B.4]. The efficiency of 7×10^{-3} (Mills and Gullikson, 1986) for a solid Ne moderator with a ^{22}Na source is the highest quoted (see Table IV). An increase of moderator efficiencies over those possible with simple diffusion of thermalized positrons might also be possible by using electric fields in semiconductors or insulators to increase the mobility of positrons to the emitting surface. This so-called "field-enhanced" moderator was originally suggested by Lynn and McKee (1979), but their attempts to produce such a moderator were not successful, probably because of impurities or defects in the contacts. Beling *et al.* (1987a, 1987b) have recently discussed the field-enhanced moderator in the context of modern epitaxial metal/semiconductor systems, although so far no experimental results have been reported.

The energy width of positrons elastically reemitted from clean single-crystal moderators is almost always $\sim$75 meV at room temperature (Gullikson *et al.*, 1985; Fischer *et al.*, 1986), as illustrated for clean Ni(100) in Fig. 16. This is consistent with thermal broadening only of a beam with a Maxwell-Boltzmann velocity distribution [Sec. II.D.1 and Eq. (38)]. Further evidence of the

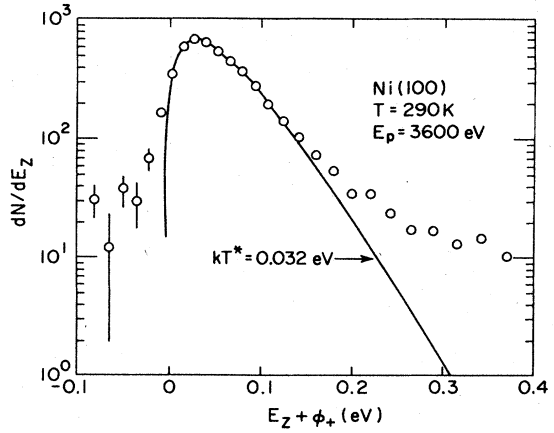

FIG. 16. The differential total energy distribution of positrons reemitted from a Ni(100) surface. The energy is shown relative to the positron work function $\varphi_+ = -1.3 \pm 0.1$ eV, where E_z is the longitudinal energy. The positrons were implanted with 3600-eV incident energy, and the solid line is a fitted beam Maxwell-Boltzmann distribution [Eq. (38)] with an effective temperature of $k_B T^* = 32$ meV (after Gullikson *et al.*, 1985).

"elasticity" of the emission process is supplied by the narrow angular spread ($\sim 10°$ FWHM) shown in Fig. 17 for positrons reemitted from a W(110) crystal (Fischer *et al.*, 1986). The width represented by this curve is quite close to what would be expected for elastic emission from a simple step of height φ_+, which predicts for the most probable half angle of emission $\theta_{1/2}$,

$$\theta_{1/2} = \left[\frac{k_B T}{\varphi_+} \right] . \tag{6}$$

A widely quoted figure of merit for positron beams is the efficiency ε, which is the ratio of positrons extracted in a beam to the number being produced by the radioisotope (or, for LINAC's, to the number of incident electrons). This is impossible to calculate reliably, since it involves all the details of the source/moderator arrangement, such as self-absorption of primary β^+'s in the source, moderator material, defect properties, surface roughness and impurities, geometry, extraction fields, and so on. In spite of this, it is instructive to list (Table IV) "typical best" efficiencies and overall beam strengths for systems ranging from relatively modest non-UHV laboratory beams to large "intense" facilities, since the kind of research that can be done is to some degree controlled by the tradeoff between available resources and desired intensity.

2. Beam transport

Once the positron beam is extracted from the moderator, it is guided through a vacuum system to the target. Various methods of beam transport have been used, including fully electrostatic systems (Cherry, 1958; Rosenberg *et al.*, 1980a; Van House and Zitzewitz, 1984; Frieze, Gidley, and Lynn, 1985), axial magnetic fields (Costello *et al.*, 1972; Lynn and Lutz, 1980b; Mills, 1981a; Hutchins *et al.*, 1985, 1986; Weiss, 1985; Lahtinen *et al.*, 1986; Schultz, 1988), and hybridized electrostatic/magnetic systems (e.g., Rich, 1986). The fundamental difference between the electrostatic and magnetic system of beam transport is simply that some experiments require the measurement of scattering angles (and therefore are hindered by magnetic fields), whereas other experiments are simplified by the ability to confine all scattered charged particles. Other advantages or disadvantages of specific systems are discussed in the references listed above.

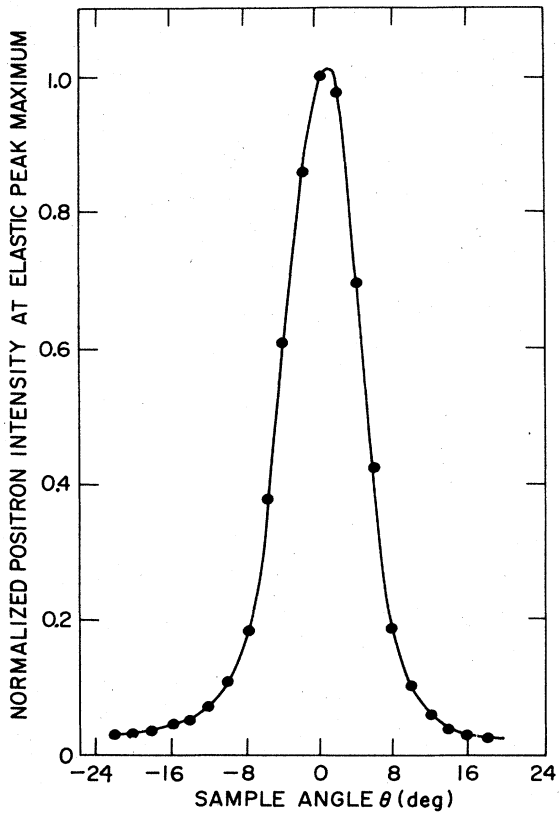

FIG. 17. The angular distribution of elastically emitted positrons for W(110). The FWHM is about 10°, which is close to the predicted value of $\sim 5.6°$ based on Eq. (6) assuming $\varphi_+ = 2.9$ eV (from Fischer *et al.*, 1986).

In Fig. 18 we show a fairly typical laboratory-based beam. This particular apparatus is magnetically guided and uses crossed electric and magnetic fields (Mills, 1980c) to separate the desired slow-positron beam from the fast-positron and γ-ray background of the source. The target region of any vacuum system is specific to the experiments of interest. The beam in Fig. 18 is set up with emphasis on inner-shell ionization, positron channeling, and defect profiling studies, all of which are discussed in later sections. Other facilities are optimized for

different purposes, such as the system being assembled by Rice-Evans *et al.* (1987), which will be able to study samples at temperatures as low as ~2 K.

Until relatively recently, particle acceleration in magnetically guided systems was accomplished by adjusting the potential on the target to be studied (e.g., Lynn and Lutz, 1980b). While this is simple enough, it tends to limit the versatility of the sample holder, as well as to restrict the maximum attainable energy. Most facilities that continue to operate this way are limited to a maximum of ~5 keV, although there are facilities of this type that can handle a few tens of keV (Triftshäuser and Kögel, 1982a). The more common approach for newer beams is to float some portion of the source end of the vacuum system electrically, thereby removing the problem of beam energy from the target end (see Fig. 18). Beams of this type (occasionally referred to as "high-energy" positron beams) are usually designed for maximum accelerations of about 100 keV, since most of the *near-surface* solid-state research they are used for does not require higher energies. However, there are some facilities (applied to solid-state research) that are designed

TABLE IV. Positron source/moderator efficiencies. The efficiency ϵ of conversion for source/moderator geometries, listed for the various configurations in common use. The number listed is the total efficiency, including losses due to source construction, geometrical arrangement, and moderator quality. It is important to note that the numbers listed are *normalized* to standard primary-source sizes, although the efficiencies listed in the original references were taken with various-size sources. There is a dependence of efficiency on source strength, which for simplicity we neglect here (Massoumi *et al.*, 1988).

Primary sources

(A1) 500 mCi ^{58}Co on W needle or ribbon
(A2) 500 mCi ^{58}Co on inside of W ring
(A3) 100 mCi ^{22}Na in sealed capsule
(A4) 60 Ci ^{64}Cu in ^{63}Cu, on W(110) substrate
(A5) LINAC: Livermore Laboratory, 100 MeV at 400 μA.
(A6) LINAC: Germany, 160 MeV at 1 μA.
(A7) LINAC: Japan, 25 MeV at 100 mA.

Moderator	Source	Fig. 15	ϵ	e^+/sec	Footnotes/notes
Laboratory beams					
Cu(111)+*S*	(A1)	(a)	$\sim 1\times10^{-3}$	2.8×10^{6}	a
W(110)	(A1)	(a)	$\sim 2\times10^{-3}$	5.6×10^{6}	b,c
W(110)	(A2)	(a)	$\sim 3\times10^{-3}$	8.4×10^{6}	d/untested
W vanes	(A3)	(b)	$\sim 7\times10^{-4}$	2.2×10^{6}	e
Ne (~1 μm)	(A3)	(d)	$\sim 7\times10^{-3}$	2.2×10^{7}	f
Foils	(A3)	(c)			
W(100)			$\sim 6\times10^{-4}$	1.9×10^{6}	g,h/~1 μm
Ni(100)			$\sim 7\times10^{-4}$	2.2×10^{6}	h/~0.3 μm
W polycrystalline			$\sim 2.6\times10^{-4}$	8.3×10^{5}	h/~6 μm
W polycrystalline			$\sim 1\times10^{-4}$	3.2×10^{5}	i/~15 μm
Ni polycrystalline			$\sim 1\times10^{-4}$	3.2×10^{5}	h–j/~5 μm
Ni polycrystalline			$\sim 2.5\times10^{-4}$	8.0×10^{5}	h/~2 μm
Intense beams					
Cu(111)+*S*	(A4)	(e)	2.4×10^{-4}	8×10^{7}	k/dc beam
W vanes	(A5)	(b)	1.5×10^{-6}	8.6×10^{8}	l/1440 pps
W vanes	(A6)	(b)	$\sim 9\times10^{-6}$	5×10^{7}	m/100 pps
W vanes	(A7)	(b)	2.4×10^{-8}	2×10^{6}	n/estimated only

[a]Mills, 1979a.
[b]Vehanen, Lynn, Schultz, and Eldrup, 1983.
[c]Vehanen, 1987.
[d]Brusa, Grisenti, Oss, Zecca, and Dupasquier, 1985.
[e]Dale, Hulett, and Pendyala, 1980.
[f]Mills and Gullikson, 1986.
[g]Lynn, Nielsen, and Quateman, 1985.
[h]Gramsch, Throwe, and Lynn, 1987.
[i]Schultz, 1988.
[j]Gidley and Frieze, 1986.
[k]Lynn, Mills, West, Berko, Canter, and Roellig, 1985.
[l]Howell, Alvarez, and Stanek, 1982.
[m]Ley, Niebling, Osipowicz, Picard, and Werth, 1985.
[n]Ito, Azuma, Sueoka, Mori, Katsumura, Kobayashi, and Tabata, 1985.

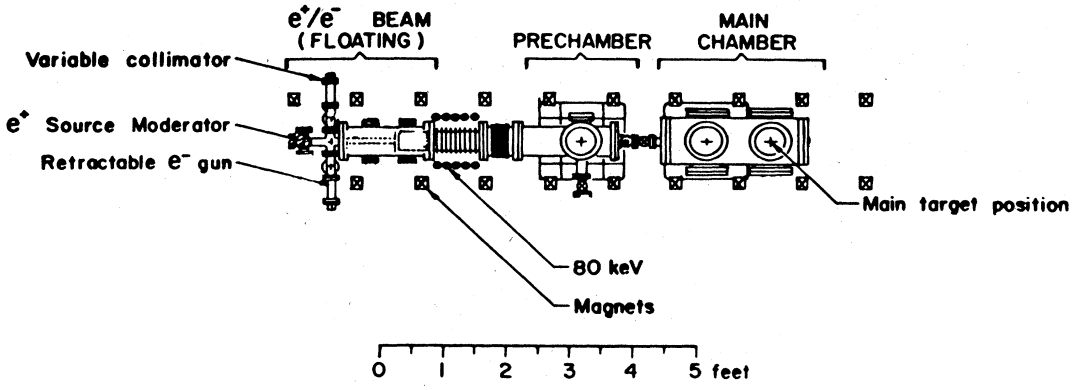

FIG. 18. A typical magnetically guided positron beam. This beam uses transmission moderation [Fig. 15(c)] and accelerates the beam from 0 to 80 keV by floating the source end of the apparatus (after Schultz, 1988).

for operation in the MeV range (see, for example, Andersen *et al.*, 1971; Bauer *et al.*, 1987). Electrostatic beams require appropriate tuning of the lens elements to attain the desired beam energy (see, for example, Canter, 1986). Although these beams are most often used only in the low-energy (<10 keV) regime, new designs will extend the energy range to several tens of keV.

3. Time-resolved beams

The average positron lifetime is a sensitive function of the electronic environment of the positron, as can be seen by reviewing Table II. This fact has long been recognized (Bell and Graham, 1953; Bell and Jorgensen, 1960) and has been exploited in bulk lifetime studies for about two decades (Hautojärvi, 1979; Vehanen and Rytsölä, 1981). Positron lifetime spectrometry in beam research has a similarly promising future, although attaining respectable resolution (i.e., FWHM $\ll 1$ nsec) by "tagging" positrons in a beam is technically more demanding than the bulk technique, which makes use of a γ ray emitted simultaneously with the positron as a start signal.

One method of timing with beams involves collecting the positrons in equally separated (in time) bunches. This has been done by Mills (1980a) using magnetic mirrors to bunch a nominally dc magnetically guided beam, attaining so far a best reported time resolution of ~ 8 nsec (Mills, Pfeiffer, and Platzman, 1983). A new system being developed by the Munich group (Schödlbauer *et al.*, 1985, 1987) combines similar magnetic bunching techniques with a high-speed chopper, which they expect will yield an ultimate time resolution of around 100 psec. This system, which is shown in Fig. 19, has so far been tested to a resolution of ~ 200 psec. Bunched positron beams can also be produced at LINAC's, where the pulsed electron beam automatically results in bunches ranging from a few nsec to a few μsec in width (Howell, Fluss, Rosenberg, and Meyer, 1985).

Subnanosecond timing of positron beams has recently

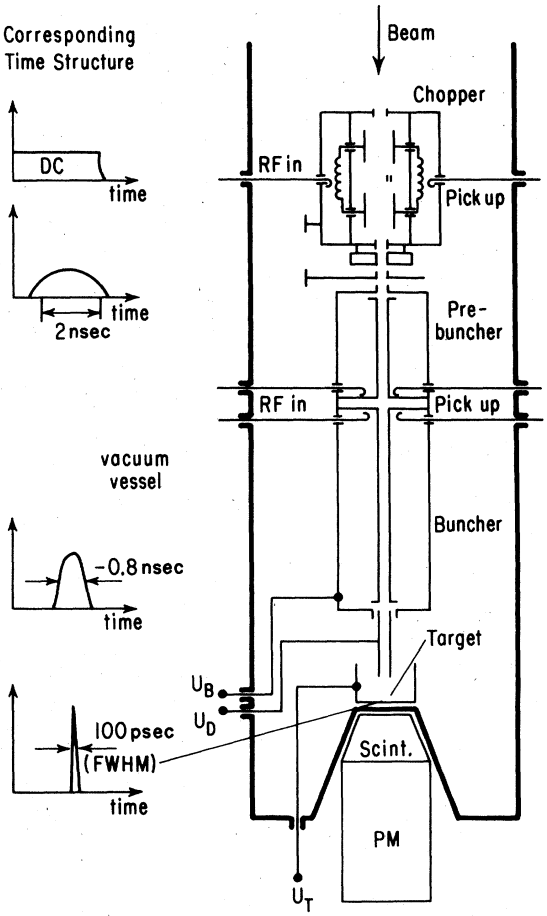

FIG. 19. A recent design for a beam buncher. This design uses an RF modulated chopper to produce 2-nsec-wide bunches, followed by a pair of matched bunches (which decelerate those at the front of the bunch and accelerate those at the back). The current time resolution of this system is ~ 200-psec FWHM, although the design goal shown on the figure is 100 psec (from Schödlbauer *et al.*, 1985, 1987).

been described by Crane and Mills (1985), who employ a rapidly pulsed electric field to bunch the beam. The nonuniform electric field accelerates those positrons at the entrance of a sample "cup" more than those near the sample surface. The authors report that as long as the surface to be studied is positioned correctly, this yields a time resolution of ~0.47-nsec FWHM. As yet there is too much uncertainty in the shape of the resolution function for this technique to be applied to new measurements, but the initial demonstration certainly shows promise for the future.

In yet another approach, the Stuttgart group (Bauer *et al.*, 1987) has developed a positron beam in a commercial pelletron accelerator that can be accelerated to MeV energies. They intend to time-tag the positrons using a thin transmission scintillator in front of the sample to be studied, and expect to achieve a time resolution of a few hundred picoseconds or less.

Other methods for time-tagging the positrons in beams have been used which are closely related to the experimental details and so are discussed in the next section with reference to the experimental observables.

4. Brightness enhancement

The physical diameter of most positron beams is generally limited by the geometry of available primary sources and moderators. Typical beams range from ~1 to 6 mm in diameter, and the relatively low primary beam currents (Table IV) make collimation an unattractive alternative. Many experiments (e.g., diffraction) require a beam that not only is physically small, but also has the minimum possible spread in both angle and energy. This may be quantified by the brightness "B" of the beam, by

$$B = \frac{I}{\theta^2 d^2 E} , \tag{7}$$

where d is the diameter, E is the positron energy, I is the intensity (particles/sec), and θ is its angular divergence. The limitation on particle beam brightness is usually imposed by the initial conditions of the source and Liouville's theorem, which states that the volume occupied in phase space of the beam will be a constant under the influence of conservative forces. Thus, if the diameter of the beam is decreased, it is at the expense of angular divergence, and so on. Canter and Mills (1982) discuss both brightness and, more specifically, the "brightness per volt" of positron moderators.

The process of positron energy moderation is nonconservative and is, therefore, not restricted by the same phase-space limitations. A beam can be focused to a small spot and remoderated to achieve the original angular and energy characteristics, at a cost of about 50% or less of the beam intensity. This concept was originally suggested for positrons by Mills (1980b), and the implications in terms of theoretically attainable "brightness" are demonstrated in Fig. 20. Frieze and co-workers (Frieze, Gidley, and Lynn, 1985) successfully remoderated an electrostatically focused beam twice to attain an increase in brightness of more than a factor of 100. Their system was used for the low-energy positron diffraction (LEPD) studies discussed in Sec. II.A.1. In a more recent construction of a similar style of remoderated beam, Canter and co-workers (see Canter, 1986) have achieved an increase in brightness of a factor of ~500. Their beam can be focused to a few microns in diameter and can be rastered over an area of 0.2 mm^2, as demonstrated in Fig. 21 (Brandes *et al.*, 1987). In a related development, Van House and Rich (1988) have recently reported a transmission positron microscope (TPM), which has a magnification of 55.

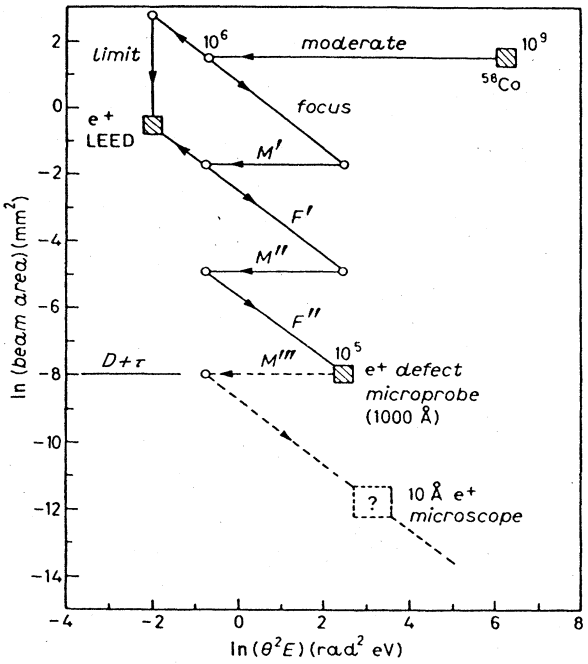

FIG. 20. The concept of brightness enhancement for a positron beam is illustrated in this log plot of beam area vs divergence. The lines at 45° represent decreasing the beam area at the cost of angular divergence, which does not change the "brightness" [Eq. (7)]. The horizontal lines represent moderation, which increases the brightness by regaining the small angular spread at a cost of about half the beam intensity per stage of remoderation (from Mills, 1981a).

5. Beam polarization

It is an interesting property of positrons emitted from the decay of radioactive nuclei that they possess a longitudinal polarization, or helicity, in the direction that they are emitted. Zitzewitz *et al.* (1979) found that the positrons moderated in MgO maintained their polarization down to thermal energies, thus allowing the formation of a preferentially spin-polarized beam. By sacrificing beam intensity, Van House and Zitzewitz (1984) have achieved

up to 70% polarization of a positron beam, and it has been used (at 50% polarization) by the Michigan group (Gidley, Köymen, and Capehart, 1982) in conjunction with an axial magnetic-field spin rotator to measure the spin states of electrons at metallic surfaces (Sec. II.D).

Van House and Zitzewitz (1984) made a careful study of the beam polarization and its measurement under various experimental conditions. To summarize, the technique utilizes the fact that in a magnetic field the $m=0$ singlet and $m=0$ triplet Ps are mixed to form two field-perturbed states. This is quantified by measuring the changes in the intensity of the perturbed to unperturbed triplet component when the positron spin or B field is flipped by 180°. Van House and Zitzewitz show how the intensity change can be directly related to the spin polarization. An apparatus similar to theirs is shown in Fig. 22. Many of the solid-state, atomic, and general-physics experiments done or proposed by the Michigan group are discussed by Rich (1986; also Rich, Van House *et al.*, 1987).

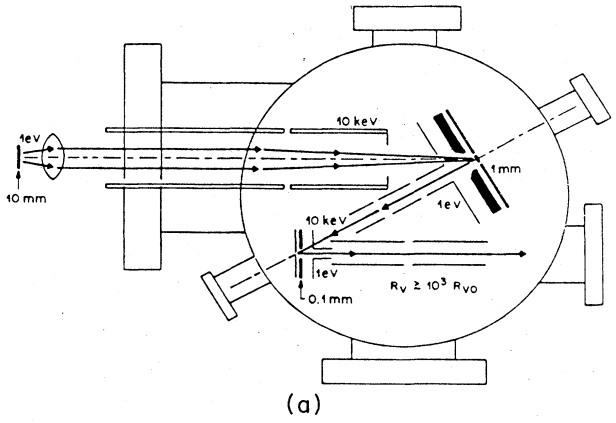

(a)

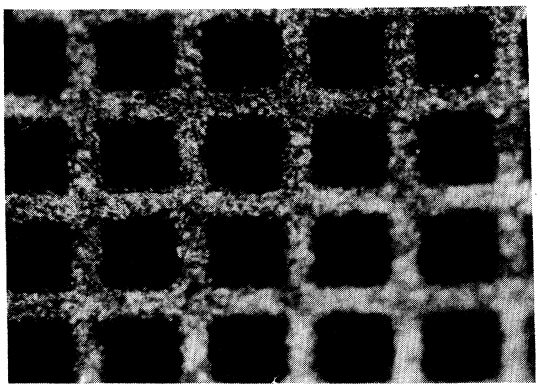

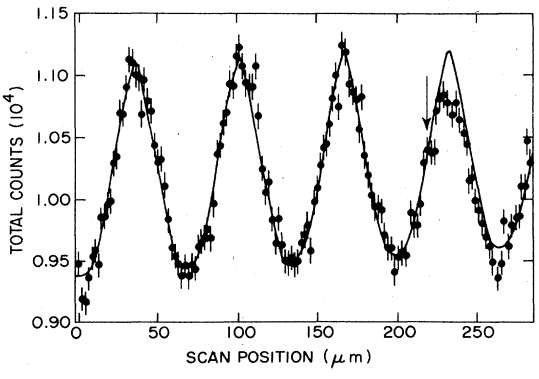

(b)

FIG. 21. A doubly remoderated electrostatic positron beam. The increase of the brightness of the beam is a factor of 10^3. This apparatus produces a focused spot size of ~ 15-μm diam. The resolution of the beam is indicated in (b), where the one-dimensional image of a fine-mesh grid is obtained by rastering the beam across it (after Brandes *et al.*, 1988).

E. Observables

Much of the research undertaken with variable-energy positron beams can be reduced, at least in the first instance, to measurements of the γ rays resulting from annihilation of positrons in delocalized, trapped, or Ps states. In some cases positrons are detected directly, and occasionally other signals are employed such as direct Ps detection, characteristic x rays, secondary or Auger electrons, and even uv photons. In this section we shall briefly survey the properties and detection of the primary experimental "observables."

1. Positrons

Because positron beams are of such low current ($\sim 10^{-13}$ A), simple methods for characterizing incident or scattered particles (such as charge collection or monitoring a phosphor) are not useful. Channel electron multipliers are typically used either singly (CEM, or "channeltrons") or in the channel electron multiple arrays (CEMA). For higher-energy positrons (≥ 15 keV), stan-

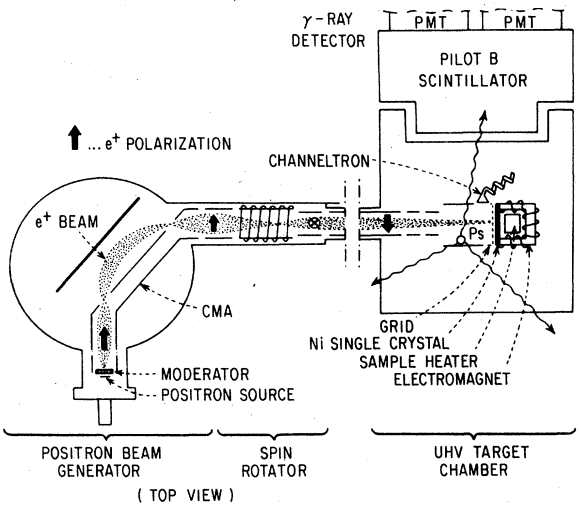

FIG. 22. A spin-polarized (~ 50–70%) positron beam. Positrons in this facility are electrostatically focused and transported, and a magnetic "spin-flipper" selects polarization (after Gidley, Köymen, and Capehart, 1982).

dard Si surface-barrier detectors can also be used. The angle and/or energy of scattered (or reemitted) positrons can be characterized using modifications of techniques that are standard for electron spectroscopy, such as the hemispherical analyzer employed by Fischer *et al.* (1986) in an electrostatic beam, shown in Fig. 23. This particular instrument has been used for measuring the energy distribution of positrons reemitted from clean metal surfaces, as illustrated schematically in Fig. 23(a).

In magnetically guided positron beams, the confining field does not allow the use of conventional hemispherical or cylindrical analyzers, so detailed energy measurements are made with a retarding-field analyzer, such as the one shown in Fig. 24. A typical spectrum of the "integral" yield versus energy of the reemitted positrons is shown in Fig. 25, which is obtained by relative biasing of the sample and retarding grids of the analyzer. In general, this type of analyzer measures only one component (i.e., the field axis) of energy. Gullikson *et al.* (1985) have demonstrated that the use of strong-focusing magnetic fields can reduce the total energy of the emitted positrons (at any angle) to the one direction measured. Because of the strong magnetic focusing, this technique requires incident positron energies of 1 keV or more, but these authors show that this type of data can be combined with various reconstruction techniques to extract similar angle and energy information to the hemispherical analyzer in an electrostatic system. One limitation of electrostatic analyzers is that they cannot easily measure absolute intensities, or reemission yields. This is relatively simple with the retarding-field analyzer, since the yield is just the relative difference in the measured rate at sample biases well below and above the value characteristic of the work function (Fig. 25).

A variation of the retarding-field analyzer which has been used at Brookhaven National Laboratory to measure differential (rather than integral) positron energy distributions is shown in Fig. 26(a). In this system, the crossed electric and magnetic fields ($\mathbf{E}\times\mathbf{B}$ analyzer) are used to sweep across the energy distribution of the emit-

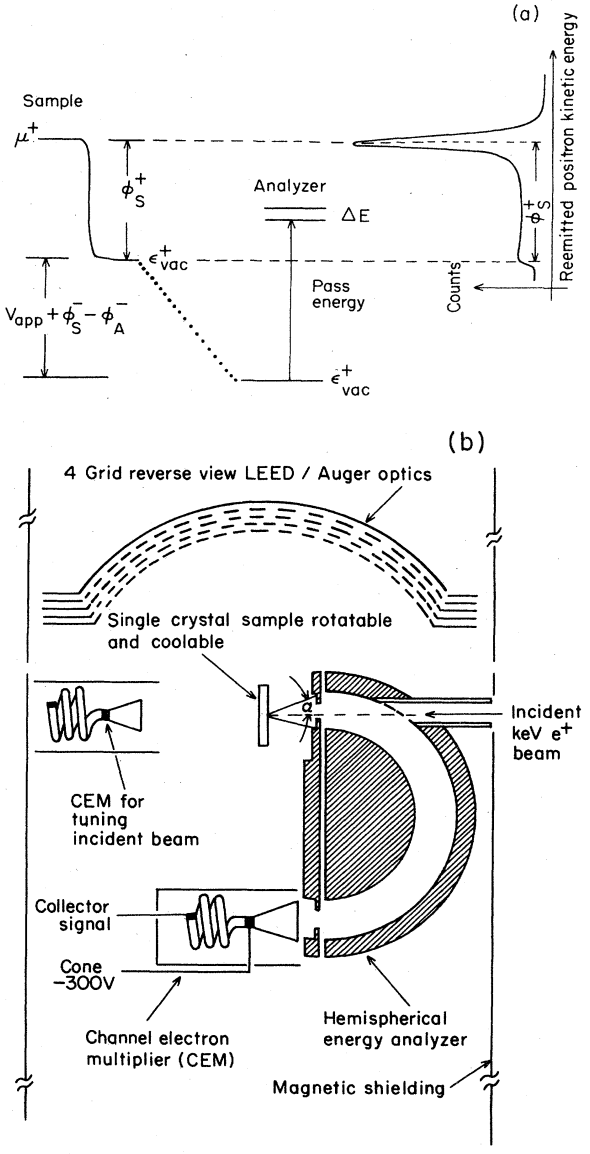

FIG. 23. A hemispherical analyzer for measuring reemitted positron angle and energy distributions. The analyzer is shown in (b), and the relationship between the applied potential V_{app} and the various sample and contact potentials for the system is illustrated in (a). In this figure μ_+ is the positron chemical potential, φ_s^+ and φ_s^- are the positron and electron work functions for the sample, φ_A^- is the contact potential of the analyzer, and ΔE is the analyzer resolution (from Fischer *et al.*, 1986).

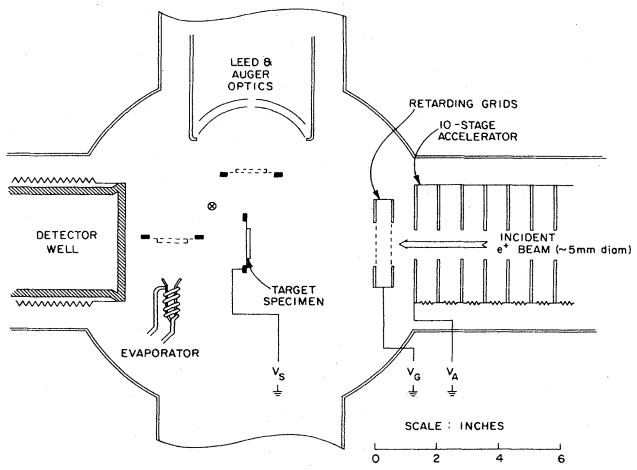

FIG. 24. A simple retarding-field analyzer for measurement of reemitted positron energy distributions. In this apparatus an axial magnetic field keeps both incident and reemitted positrons confined to the original beam axis. The incident beam is normally implanted into the sample at 1–5 keV, and those positrons which thermalize and are reemitted are retarded or transmitted by the pair of retarding grids, depending on the relative bias between the grids and sample. The positrons are detected either by the annihilation γ rays (resulting in a spectrum similar to that in Fig. 25 after background subtraction) or by direct counting in a particle detector, e.g., Fig. 26 (from Schultz, Lynn, Frieze, and Vehanen, 1983).

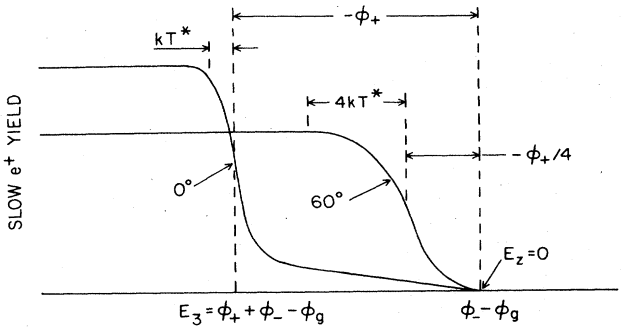

FIG. 25. Integral positron reemission spectra taken with a retarding-field analyzer. The positrons are retarded when the applied bias ($V_{app}=V_s-V_g$) is less than the effective "zero," which is the difference between the electron contact potentials of the sample and grids. The steepest portion of the curve corresponds to the elastically emitted "peak" of Fig. 23, which is broadened by the thermal spread k_BT^*. The two spectra are taken at different angles between the sample normal and incident beam (i.e., B field) directions, showing how the $E_z=0$ position is defined (after Murray, Mills, and Rowe, 1980).

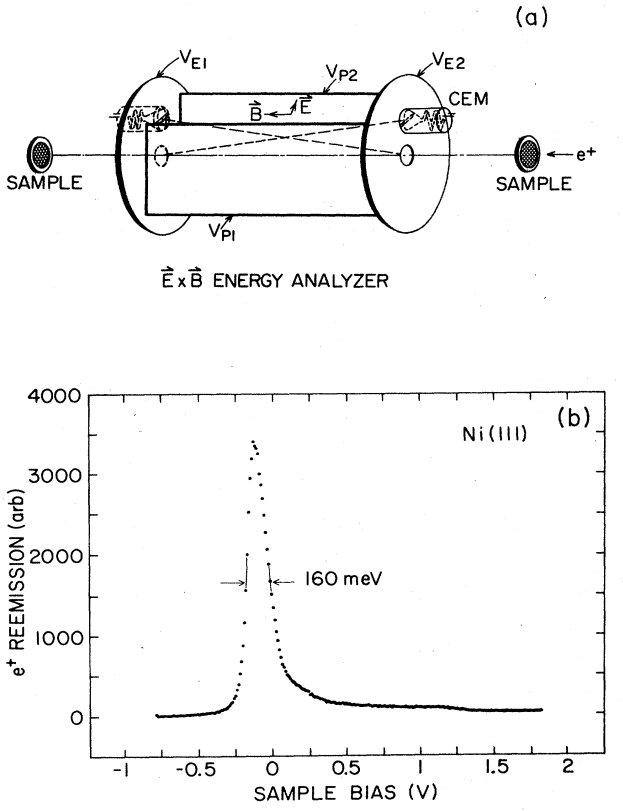

FIG. 26. Energy analyzer for differential measurements. Reemitted positrons are swept across a slit in front of a CEM counter. The best sensitivity is achieved by using the plates at the end of the $E\times B$ drift region as electrostatic "mirrors" and passing the beam back and forth several times in the same space. The resolution achieved for the measurement shown in (b) was ~160 meV (Chen, Schultz, and Lynn, 1984).

ted positrons in much the same way as a conventional electrostatic analyzer would. The width of the distribution shown in Fig. 26(b) for Ni(111) is ~160-meV FWHM, which is due to the thermal smearing of the positron energy distribution (~75 meV) and the instrumental resolution (~140 meV).

In conventional retarding-field measurements, such as the ones described above, what is actually measured is not the positrons themselves, but rather the annihilation γ rays from those positrons forced by the retarding potential to return to the sample surface. The type of energy-dispersive spectrometer that is used is determined by experimental requirements. For example, if maximum count rate without concern for resolution is required, then a NaI(Tl) detector is often used. However, if details of the annihilation line shape are of interest, then the superior resolution of a semiconductor detector [intrinsic Ge, or Ge(Li)] is required. The annihilation line shape can be deconvoluted to extract the electron momentum distribution, but more often it is simply quantified by a line-shape parameter such as "S," which is the ratio of counts in a central portion of the annihilation photopeak to the total counts in the peak (Fig. 27). Parameters like this have been used extensively in traditional bulk studies with positrons (Sec. I.B), and their high sensitivity to the

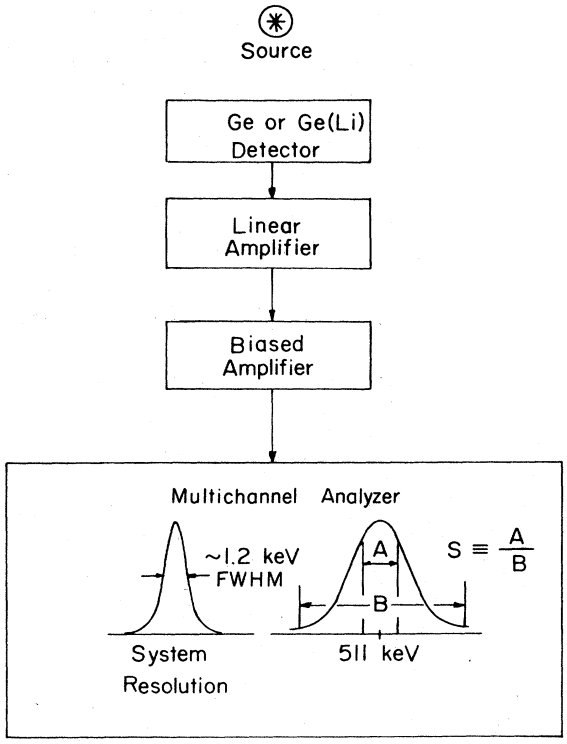

FIG. 27. System for measuring annihilation γ rays. The 511-keV line shape is broadened by the electron momentum. The environment in which the positron annihilates (i.e., in which it becomes delocalized, trapped at defects, or trapped at the surface) can be parametrized by the line shape; an example of such parametrization is the parameter "S" shown in the figure.

environment of the annihilating positron (see Fig. 5) find similar application in the "near-surface" studies of solids now done with e^+ beams.

As mentioned previously, the sensitivity of a positron to its environment is reflected not only in the annihilation momentum distribution, but also in its lifetime spectrum. Since characteristic lifetimes in metals and semiconductors are on the order of 10^{-10} sec (Table II), most of the techniques currently used for time-bunching the beam are not adequate for experiments of this type. The new techniques for beam bunching discussed previously (Fig. 19) will provide suitable time resolution for studies of this type. Positrons can be tagged by using secondary electrons released from the target surface as the start signal. This method was first employed by Gidley *et al*, (1976) for a measurement of the *o*-Ps vacuum annihilation rate (FWHM $\sim$7 nsec), and more recently by Gidley, Köymen, and Capehart (1982) for measurements of Ps formation at a Ni(110) surface. Lynn, Frieze, and Schultz (1984) used a similar technique for measurements of the positron surface-state lifetime at an Al(110) surface. The apparatus used for this particular experiment (Fig. 28) had a time resolution of $\sim$0.6-nsec FWHM.

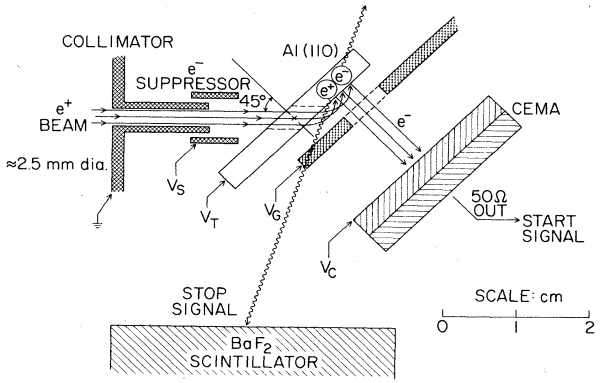

FIG. 28. Positron lifetime apparatus. The arrival of the positron at a surface is "tagged" by the ejection of secondary electrons, and the annihilation quanta are measured with a fast scintillator for the stop signal. The system shown achieved a resolution of $\sim$600-psec FWHM (from Lynn, Frieze, and Schultz, 1984).

2. Positronium

The presence of Ps can be identified by an analysis of the γ-ray energy spectrum. The continuous energy distribution (Fig. 2) arising from the 3γ decay of *o*-Ps results in a much different spectrum from that produced by the 2γ decay of either positrons or *p*-Ps, as is evident in the spectrum shown for a high-resolution Ge spectrometer in Fig. 29. It is important to note that this technique for Ps detection is sensitive only to Ps in vacuum, because any *o*-Ps that does form in a solid is much more likely to encounter an electron with the appropriate "opposite" spin to the positron, and annihilate (i.e., via pick-off) into 2γ rays than by the normal 3γ rays (e.g., Dupasquier, 1981; Eldrup, 1981).

In order to quantify the differences in the γ-ray spectra, such as those shown in Fig. 29, one defines the ratio

$$R = \frac{T-P}{P} , \tag{8}$$

where T and P refer, respectively, to the integrated counts in the total and peak regions of the spectrum. This quantity, which compensates for any fluctuation in incident beam current, varies continuously from a minimum value R_0 when no Ps is formed through to a maximum R_1 when 100% of the incident positrons end up as Ps. By considering the various processes available for the positron, it can be shown that the Ps fraction f is related to these ratios by (Marder *et al.*, 1956; Mills, 1978; Lynn and Welch, 1980)

$$f = \left[1 + \frac{P_1}{P_0}\frac{R_1 - R_f}{R_f - R_0}\right]^{-1} . \tag{9}$$

There are of course systematic and calibration problems associated with these measurements that we shall not discuss here, some of which are covered in various references (Lynn, 1981; Schultz *et al.*, 1984; Nielsen, Lynn, Vehanen, and Schultz, 1985).

A particularly informative way of studying Ps is with the aid of Anger cameras to produce two-dimensional ACAR spectra discussed in Sec. I.B.1. Although significantly more involved, this technique has recently been employed by the groups at Lawrence Livermore National Laboratory (Howell, Meyer, Rosenberg, and Fluss, 1985) and Brookhaven National Laboratory (Lynn, Mills, West, Berko, Canter, and Roellig, 1985). The 2D ACAR images are preferentially sensitive to the 2γ rays from *p*-Ps as opposed to the 3γ *o*-Ps annihilations, and recently they have been used for studies of the

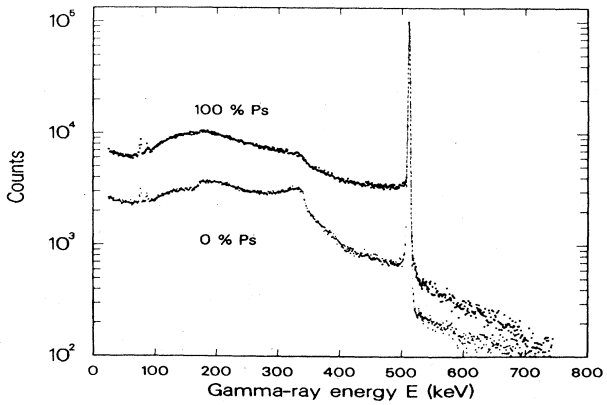

FIG. 29. The annihilation spectra measured with a high-resolution Ge detector for situations representing $\sim$100% and 0% Ps. The continuous energy spectrum for γ rays resulting from the decay of *o*-Ps was shown in Fig. 2. The fraction of Ps being formed at a surface is determined by scaling the measured spectrum between these two extremes, using Eq. (9) (from Lahtinen *et al.*, 1986).

positron surface state as well as Ps velocity spectroscopy (see Sec. II.D.3). The contributions of p-Ps, bulk, and surface annihilations to surface 2D ACAR spectra are shown in the example in Fig. 30 (Chen *et al.*, 1987). The high-energy distribution (top) is dominated by annihilations in the bulk Si, and the lower left distribution at room temperature represents surface and p-Ps events. The spectrum in the lower right-hand side of the figure, at 600 °C, is almost entirely p-Ps, since the surface bound positrons are all thermally desorbed as Ps (Sec. II.D.3). The asymmetry visible in the contribution of p-Ps to these distributions is due to the fact that the p-Ps is traveling away from the surface, and it is therefore a measure of the velocity distribution. One advantage of this kind of measurement is that it is possible to determine the absolute Ps fraction (i.e., 0% or 100%), without the calibration problems referred to above.

In order to obtain the p-Ps spectrum shown in Fig. 30(c), one must first remove the underlying contribution due to the surface-localized annihilations from data like those shown in 30(b). This component is symmetric in $p_\perp$, since there is no average center-of-mass current of the annihilating pair normal to the surface. It is therefore approximated by a twofold symmetrizing of the data at $p_\perp > 0$ [i.e., right-hand side of Fig. 30(b)] and subtracted from the total spectrum. This process is discussed in detail by Chen (1987).

Because of the relatively long lifetime of o-Ps (142 nsec), it travels considerable distances in the vacuum system if it leaves a sample surface with any kinetic energy. For example, 1-eV Ps would travel ~ 6 cm in one lifetime. This fact has been exploited (Sec. II.D.2) for studies of o-Ps velocity by using collimating slits outside the vacuum system of time-tagged positron beams to determine the time-of-flight distribution. These experiments can yield similar results to the 2D experiments mentioned above (assuming that p-Ps and o-Ps have the same energy when formed), with the exception that angular information requires a series of runs. The first experiment of this kind was that of Mills, Pfeiffer, and Platzman (1983), whose apparatus is shown in Fig. 31.

The decay rate of o-Ps was studied in detail by Gidley *et al.* (1976) using secondary electrons as their start signal, and they have subsequently used the long lifetime as a convenient means of determining total Ps fractions (Gidley, Köymen and Capehart, 1982). Other ways in which Ps has been studied or observed include direct detection of energetic o-Ps in a CEMA (Gidley *et al.*, 1976) and laser ionization followed by detection of the released positron (Chu and Mills, 1982a, 1982b; Chu, Mills, and Hall, 1984; Mills and Chu, 1983). An interesting extension of the laser ionization technique which has so far not been attempted would be to determine the Ps time of flight by ionizing it at various positions in front of a target of interest, collecting the positrons. This would offer much better precision and flexibility than physical collimation in determining angle and energy distributions of Ps emitted from surfaces.

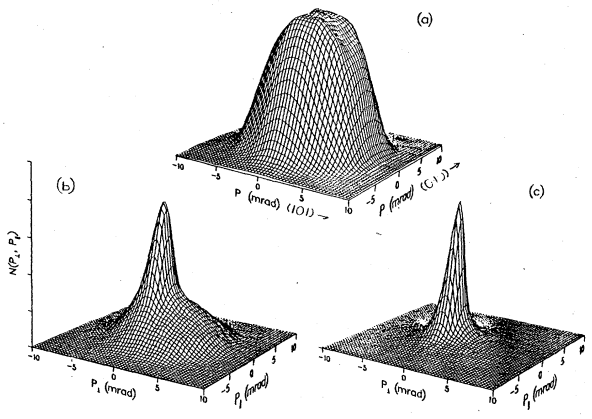

FIG. 30. Representative spectra measured with a 2D ACAR system. The result in (a) (15-keV incident positrons) is representative of "bulk" annihilations in the Si(111) sample, showing the characteristically broad momentum distribution. The result in (b) is for energetic p-Ps (the narrow component) and annihilations in the surface state (symmetric broad component). The p-Ps component has a slight asymmetry which is hard to see in this type of plot (see Sec. II.D) and which is due to the Ps momentum normal to the surface. In (c) the sample is heated to 600 °C, so that most of the positrons previously trapped at the surface are desorbed as Ps as well (from Chen *et al.*, 1987).

II. RESEARCH—FUNDAMENTAL TO APPLIED

A. First encounter

The interaction of an incident beam of energetic positrons with a solid surface is different from that for electrons. This is primarily associated with the difference in charge, but there is also a difference due to the fact that there is no Fermi sea of positrons in the sample, and therefore the exchange part of the potential is not present. For these reasons, much of what has been studied with positrons complements other work and provides

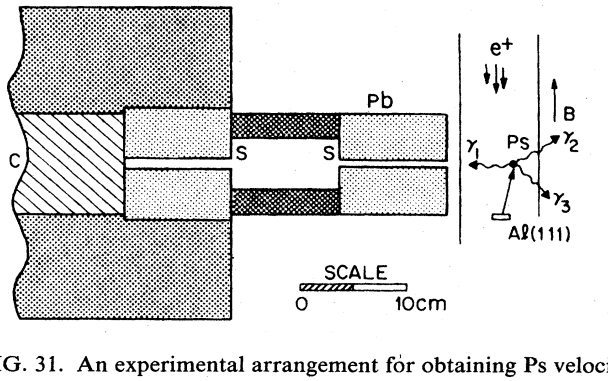

FIG. 31. An experimental arrangement for obtaining Ps velocity distributions by time-of-flight measurements. The parts labeled are S, Pb collimator slits; C, $4'' \times 8'' \times 8''$ plastic scintillator detector; e^+, 5-nsec burst of about 80 positrons; B, 150-G magnetic guiding field; γ_1–γ_3, three-photon annihilation of $^3S_1$ o-Ps; Al(111), aluminum sample on heater stage (from Mills and Pfeiffer, 1985).

unique insight into the fundamental interactions of charged particles with matter.

One difference is brought out by Valkealahti and Nieminen's (1984) calculation of the scattering of 100-eV and 1-keV electrons and positrons. Their results show that the differential elastic scattering probability is larger for 1-keV electrons than it is for positrons (Fig. 32). This relative difference in scattering cross sections is generally expected for energetic electrons and positrons. The angle-dependent calculations plotted in the figure show very little scattering in the backward direction, but these are for single-ion-core events, and plural scattering of this type results in larger ($\sim 10\%$) total backscattering fractions. Backscattering probabilities for β particles emitted from radioactive sources are expected to be different for electrons and positrons, primarily because of two effects ($\approx 30\%$ larger for electrons, for most values of Z and energies from a few tens of keV up to several MeV; Bisc and Braicovich, 1964; Kuzminikh *et al.*, 1974). The most important is the fact that the ion-core potential for electrons is attractive, which makes large-angle (i.e., nearly unscreened *relativistic* Rutherford) scattering more favorable. The second, which is of much less importance, is the fact suggested above that the exchange-correlation potential makes the tails of the atomic potential larger in amplitude for electrons, thereby increasing the small-angle scattering.

In addition to these factors it must also be remembered that positrons are unique, which means that only one exists on average in the solid at any one time. Energetic electrons, on the other hand, can transfer their energy to others in the solid, which may subsequently be scattered and counted in the total intensity. Backscattering intensities are strongly dependent on the material thickness

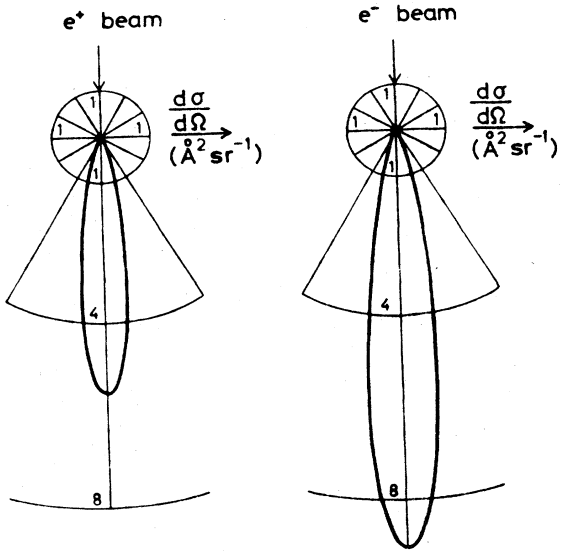

FIG. 32. Polar plots of the differential (elastic) scattering cross sections for 1-keV positrons and electrons on a Cu crystal atom (from Valkealahti and Nieminen, 1984).

for *both* positrons and electrons (Cosslett and Thomas, 1965), which must be considered for studies of thin films or multilayer structures. In general, there is still a large degree of uncertainty in the absolute backscattering probabilities for monoenergetic positrons, particularly in the low-energy (≤ 10 keV) regime.

1. The surface potential

At various incident positron energies, the single-particle potential depicted in Fig. 8 can be studied, with the results generally revealing a sensitivity to various aspects of the surface. Several examples of surface potential studies are discussed in the following sections, including incident (Sec. II.B.2) and reemitted (Sec. II.D.1) positron energy loss, surface-state localization and lifetime (Sec. II.D.3), and the possible implications of surface defects (Secs. II.D.3 and II.E.2). In this section we briefly discuss two novel ideas for probing the surface potential, which have not as yet been tested experimentally, but which may reveal interesting results in the future.

A theoretical proposal for the direct experimental determination of the electrostatic dipole barrier D of a metal was discussed in detail by Oliva (1979). The basic concept involves the determination of the specular reflection coefficient as a function of the normal component of energy for a positron scattering off the metal surface. Simplistically, a drop in the reflection coefficient would occur where the value of the normal component of energy was equal to D. Corrections due to electron correlations, core scattering, and inelastic effects (plasmons) are required; Oliva shows that these corrections can be minimized by using a high-energy (~ 30 keV) incident beam at grazing angle ($\leq 1°$). He estimates that a determination of D could be made to within 10% of the actual value. It is worth noting that this measurement, if possible, would be the first direct measurement of D.

Another potentially interesting source of information about solid surfaces is the study of fine structure for low-incident-energy positrons. Using an asymmetric square well to approximate the surface potential, Read (1983) has suggested that low-incident-energy positrons would scatter with strong energy-dependent features. Her calculations for the 00 beam scattering from Ag(001) show significant differences over a small range in energy (16–25 eV) due to changes in the potential well width of only fractions of an angstrom. As she concludes, this technique may allow determination of the detailed shape and position of the potential well for a variety of surfaces, independent of the sign of the positron work function. Jennings and Neilson (1988) have recently carried out similar calculations for a Cu(111) surface. They also find that the scattering probability of low-energy positrons contains fine structure that is dependent on the details of the surface potential, as shown in Fig. 33.

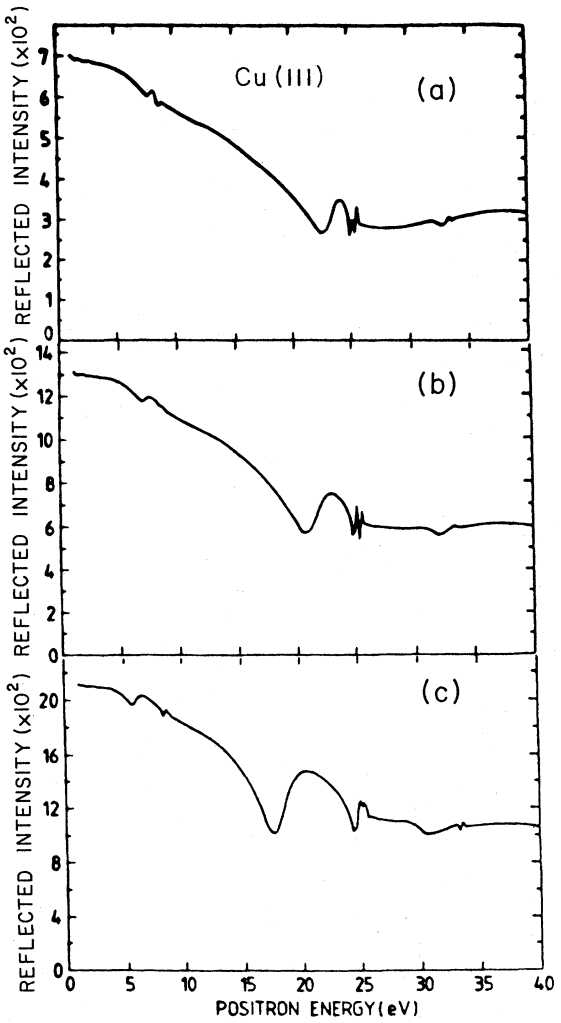

FIG. 33. Simulations of LEPD fine structure for Cu(111) with angle of incidence $\theta = 60°$ along the (11) azimuth. Curves (a)–(c) are for progressively wider surface potential wells, as modeled by the authors (from Jennings and Neilson, 1988).

2. Low-energy positron diffraction (LEPD)

One of the first solid-state projects undertaken with monoenergetic positron beams was the study of low-energy positron diffraction, or LEPD, and the comparison of the results with those for electrons (LEED). Lynn and Dickman (1978) reported scattered positron intensity variations for single-crystal samples, which they attributed to Bragg reflection, and Mills and Platzman (1980) measured the specular intensity versus voltage (I-V) curves for Cu(111) and Al(111). Around the same time Rosenberg *et al.* (1980a) published both specular and nonspecular I-V curves for Cu(111), using the system shown in Fig. 34. Their data for the 00 (specular) beam, together with the theoretical fit done by Read and Lowy (1981), are shown in Fig. 35. This group continued their

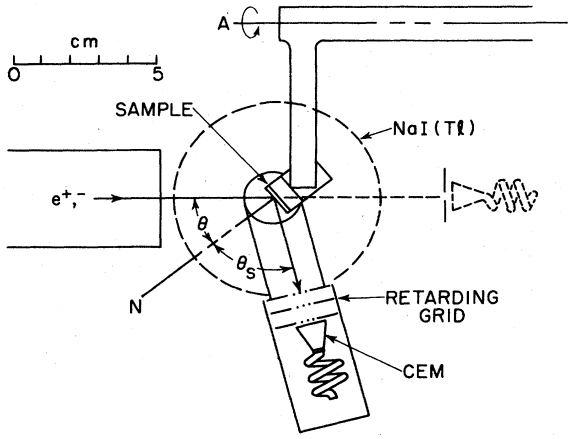

FIG. 34. Apparatus used for early LEPD studies. I-V curves were measured for the specularly reflected positron beam from a Cu(111) surface (from Rosenberg *et al.*, 1980).

study of positron diffraction and subsequently reported more detailed measurements, which they compared with various theories (Weiss *et al.*, 1983).

Specularly reflected positrons in nonmetallic systems were also observed by Cook *et al.* for LiF (1984) and by Mills and Crane in alkali halides (1985b). From the earliest work it was clear that the fundamental limitation was the relatively poor quality of the positron beam, as measured by angular and momentum spread (i.e., phase space). Typical singly moderated positron beams have angular spreads of ~20 mm deg, whereas typical LEED guns provide ~1 mm deg beams with about the same energy resolution (20 mm deg means that a beam of 20 mm

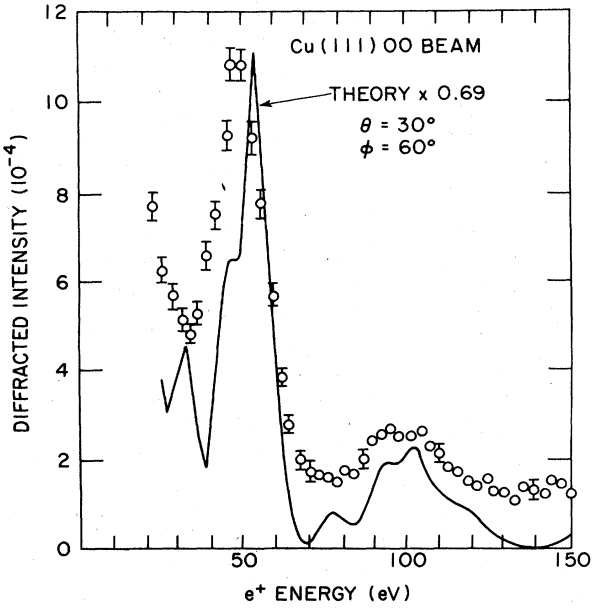

FIG. 35. The positron diffraction (LEPD) results obtained with the system shown in Fig. 34 (from Rosenberg *et al.*, 1980).

diam. has an angular divergence of 1°). A doubly remoderated positron beam was used to measure the improved results shown in Fig. 36 (Frieze, Gidley, and Lynn, 1985). This beam has an angular resolution of ~ 1 mm deg for both positrons and electrons, which is comparable to that for commercial LEED guns. Different intensities for scattering of positrons relative to electrons arise from the change in the sign of the potential. This is clearly demonstrated by the reversed intensity of the $(0\bar{1})$ and (10) beams in the figure.

Using the same remoderated beam, Mayer, Zhang, Lynn, Frieze *et al.* (1987) have recently made a detailed comparison of LEED and LEPD for Cu(100). Their data and theoretical fits are reproduced in Fig. 37, showing broader peaks in the *I-V* distributions for positrons than for electrons. The theoretical fits shown in Fig. 37 required larger inelastic scattering cross sections for positrons than for electrons in order to explain the broader peaks, which could not be interpreted as due to normal energy-loss processes (electron-hole and plasmon formation). As a result, the authors have suggested that the imaginary part of the potential is larger for positrons than for electrons, which may be caused by rapid Ps formation and breakup. This would provide an efficient means of losing energy for positrons in the topmost layers of a surface. Zhang, Tzoar, and Platzman (1988) have pointed out that higher-order corrections to the positron energy loss at a surface are important in this energy range (50–400 eV). Horsky *et al.* (1988) have recently done a similar comparative LEED/LEPD study for CdSe surfaces, in which they were able to determine the surface structure.

In addition to the above work, LEPD measurements

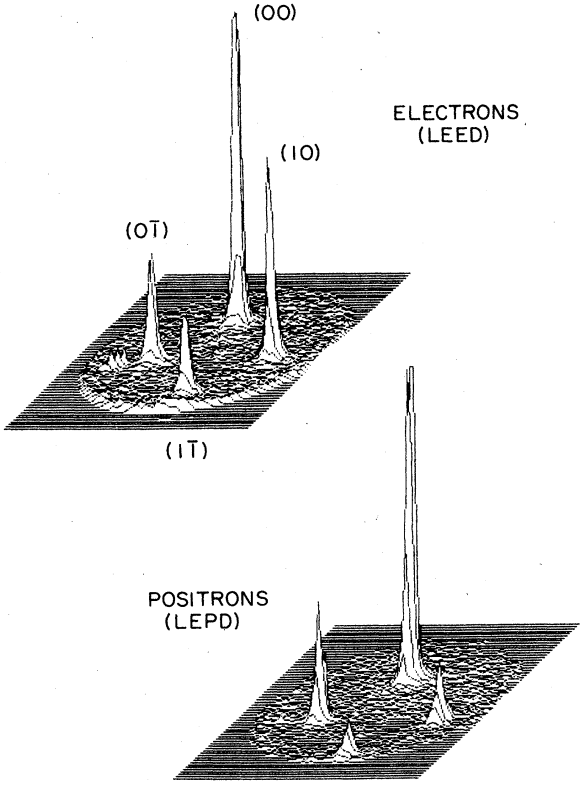

FIG. 36. Isometric plots comparing low-energy diffraction results for electrons (LEED) and positrons (LEPD) from W(110). The specular and three diffracted spots for each were obtained with the first brightness-enhanced positron beam [similar design to that shown in Fig. 21(a)]. The absolute scattering probabilities were twice as high for positrons into the specular beam (2%) as for electrons (1%). The incident beam energy was 250 eV (from Frieze, Gidley, and Lynn, 1985).

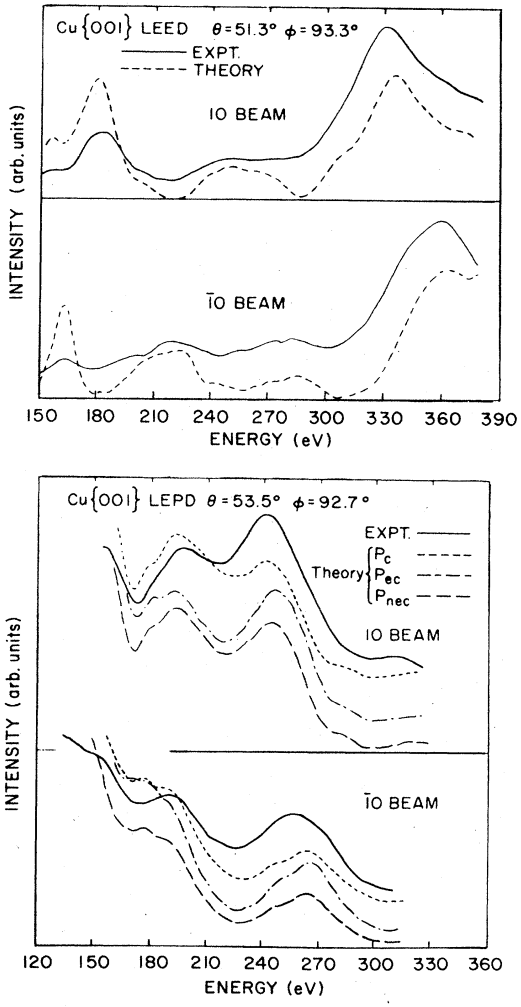

FIG. 37. LEED and LEPD *I-V* characteristics are compared for two nonspecular beams scattering from Cu(100). The theoretical calculation for the LEED results is fairly standard and is described by the authors in the original text. For the LEPD theory, the structural parameters determined from the LEED results were used, and the potentials were varied for visual fit. The curve labeled P_c is constructed from the same potential as used for LEED, with the sign of the Coulomb interaction reversed, the exchange interaction eliminated, and the correlation (with conduction electrons) retained. P_{ec} is as above, but with both exchange and correlation terms retained. P_{nec} was constructed with both exchange and correlation terms eliminated (from Mayer, Zhang, Lynn, Frieze *et al.*, 1987).

were also made at glancing angle. Some examples of the results are shown in Fig. 38, together with theoretical calculations supporting the observations. Although experimental LEPD studies are not yet revealing significant new fine structure, the level of understanding implicit in the agreement between experiment and theory is encouraging.

Gullikson, Mills, and McRae (1988) have recently measured the specular elastic reflection of e^+ from rare-gas solids. In this case the first Bragg peak occurs within the band gap, so that electronic excitation and multiple scattering effects are negligible and almost perfect reflection of positrons is observed. The positron inner potential in rare-gas solids is small, unlike that for electrons, thus allowing the low internal particle energies required for a direct observation of this effect. Their results are reproduced in Fig. 39, where the Bragg-peak profiles all approach the flat-topped shape characteristic of perfect crystals. The authors state that the rounding of the edges is associated with amorphous domains in the crystals, and they use the energy and width of the Bragg peaks to determine the positron energy gap and inner potential for the rare-gas solids.

Until very recently it had never been certain that any unique information LEPD could offer (that LEED could not) would justify the experimental difficulty of the technique. It had always been argued that the lack of exchange processes would not only allow a test of electron exchange in LEED theories, but would also make LEPD distributions intrinsically easier to calculate. In addition to this advantage, Read and Lowy (1981) have suggested that certain structural problems, such as surface relaxation for W(100) and Mo(100), cannot be unambiguously determined with LEED, but can in fact be resolved with LEED and LEPD together. LEPD has the interesting

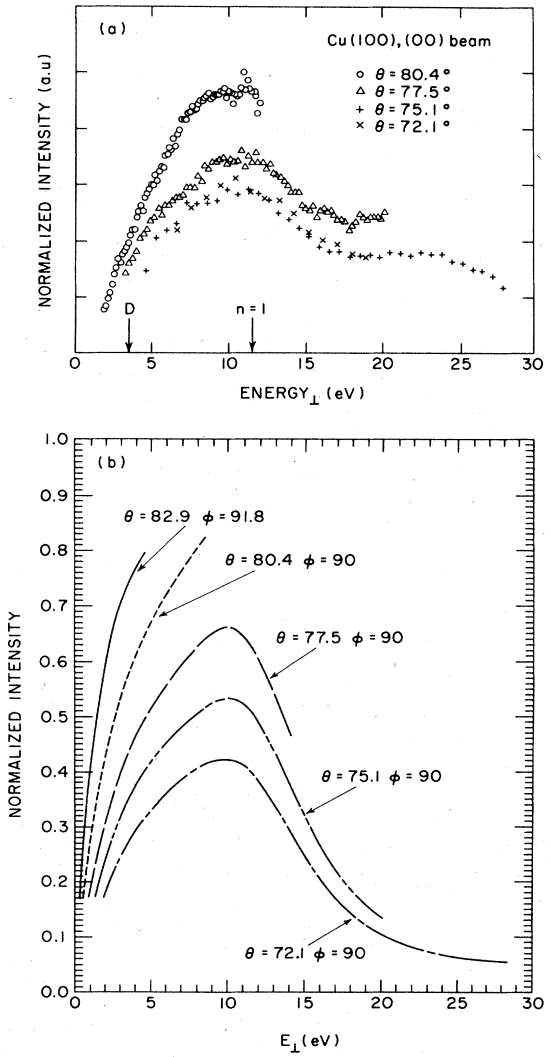

FIG. 38. LEPD data (a) taken at glancing angle compared with the theory (b) (Mayer, Zhang, Lynn, Throwe *et al.*, 1987).

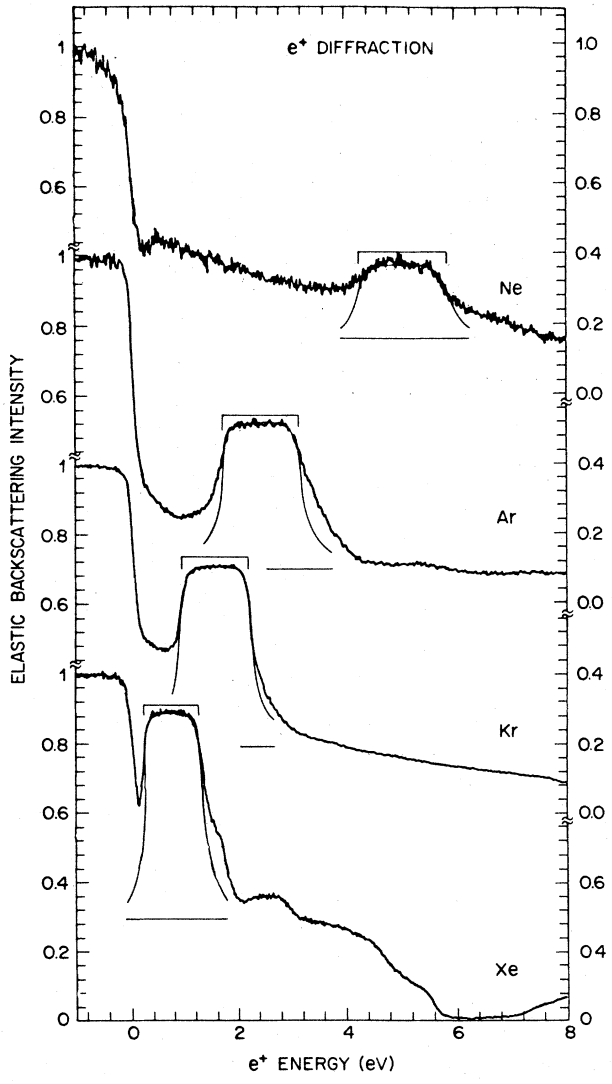

FIG. 39. Positron specular reflection probability vs positron energy E, for the (111) surfaces of Ne, Ar, Kr, and Xe (from Gullikson, Mills, and McRae, 1988).

property that changing the positron-electron correlation by unrealistically large amounts produces only small changes in the corresponding *I-V* profile (Jona *et al.*, 1980). This is in marked contrast to the situation for LEED, and it could assist in producing more accurate structure determinations, since the correlation term is not well known for either particle. Although the full potential of LEPD is yet to be demonstrated, it is the development of the field itself that is providing its own justification, as is so often the case. The new physics is coming out of the unforeseen, such as the apparent difference in the inelastic cross section mentioned above.

3. Positron channeling

When an energetic beam of particles is incident on a crystalline solid, there is a strong variation of the scattering and penetration of the beam with crystal orientation. The particles can be steered by the atomic potentials of the host crystal and channeled along axes or planes of the lattice as illustrated schematically in Fig. 40.

The potential used to estimate channeling properties is Lindhard's (1965) "standard" potential, which is an approximation to the screened Thomas-Fermi (Molière) potential. This allows an analytic calculation of the average potential along atom strings or planes, which is the basis of the so-called continuum approximation. Experimental evidence of channeling is a decrease in any measurable close-encounter process, such as Rutherford backscattering or inner-shell ionization. In the "classical" regime applicable to high-energy ions (hundreds of keV to MeV) the effect can be quite dramatic, with "dips" observable for most major axes and planes that have minimum values (χ_{min}) of only a few percent of the values for randomly oriented crystals. The phenomenon of channeling, first observed in the early 1960s, has been studied extensively and is reviewed in several general reports (e.g., Gemmell, 1974; Feldman, Mayer, and Picraux, 1982).

Most of the work that has been done to date has been concerned with the interactions of H^+ and heavier ions, although there have been a number of experimental studies of β-particle channeling. Electron channeling in particular has been investigated at all energies from a few tens of keV up to several MeV, the lower energies having particular importance in transmission electron microscopy. Positron channeling, on the other hand, has not been studied extensively primarily because of the difficulty in obtaining a sufficiently intense monochromatic beam of incident positrons.

Uggerhoj (1966; Uggerhoj and Andersen, 1968) reported measurements of blocking patterns for electrons and positrons emitted from ^{64}Cu embedded in a Cu single crystal. In this type of experiment, the source of particles is not a beam but a substitutional impurity in the solid, so what is observed is the "blocking" of the emitted particles by the other atoms in the crystal. Uggerhoj and Andersen were able to show that the channeling in the 150–500-keV energy range studied was consistent with the classical approximation, and they applied the technique to lattice location measurements of β-emitting impurities in Si. The first successful observation of channeling with an incident beam of β particles (Andersen *et al.*, 1971) was axial channeling for 1-MeV positrons incident on Au(110); it is shown in Fig. 41 together with the comparable energy-scaled result for protons. Pedersen *et al.* (1972) studied planar channeling for 1.2-MeV positrons on Si soon afterwards, for several different high- and

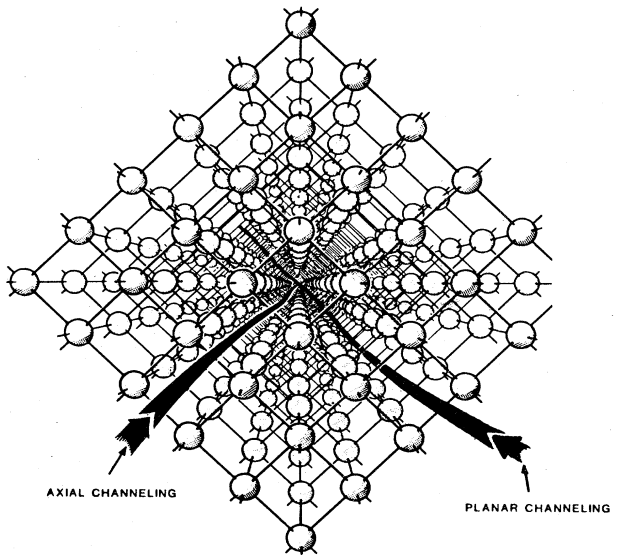

FIG. 40. Schematic illustration of axial and planar channeling of energetic particles. The potentials that steer the incident beam are usually modeled by a continuum approximation, using cylindrically symmetric string potentials for axial channeling and two-dimensional planar potentials for planar channeling.

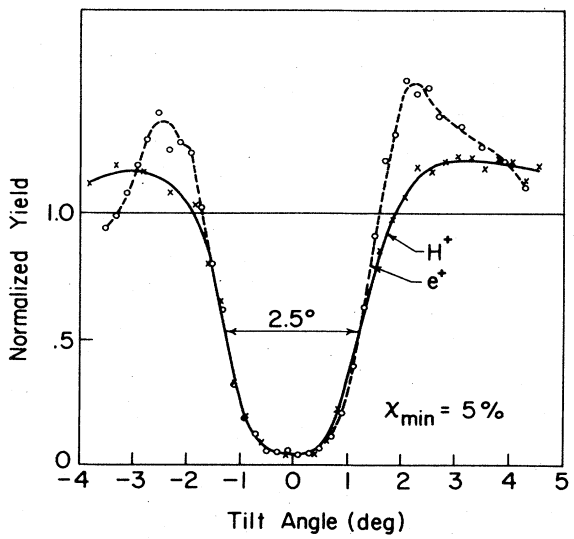

FIG. 41. Classically channeled particles show a pronounced dip in any measurable close-encounter process, such as Rutherford backscattering. Results shown here are for 1-MeV positrons and 0.670-MeV protons incident in the ⟨110⟩ axis of a gold single crystal (from Andersen *et al.*, 1971).

low-symmetry planes. Both results were more or less consistent with classical channeling, although there is structure in the data for planar channeling that is related to interference effects.

Schultz, Logan, *et al.* (1988; Logan *et al.*, 1988) have recently used a variable-energy beam to study e^+ channeling at 50 keV and below. Their studies included measurements of the positrons transmitted through a 0.26-μm-thick Si(100) crystal, which are reproduced in Fig. 42. The upper curve, which shows strong peaks in the aligned directions, was taken with a surface-barrier detector on the original beam axis, and the lower curve was taken with a detector off-axis measuring the randomly scattered particles. The crystal was tilted along a line that passed through the ⟨100⟩ axis (at $\varphi \approx 3.2°$). The data show strong channeling effects at 50 keV which are similar to the "classical" results typical for higher energies.

In addition to the above-noted results, several axes and planes were studied, with the result that in almost all cases the channeling effects were consistent with the classical description. This observation was not predictable by the usual semiclassical estimates discussed by Gemmell (1974) and others. The extent to which the classical behavior dominates the ⟨100⟩ axial channeling is shown in Fig. 43. The basic shape is observed to be the same from 50 to ~ 10 keV, with the exception of a broadening proportional to $E^{-1/2}$ and a decreased magnitude attributable to an increase in *dechanneling*. The multiple scattering of the positrons as they penetrate the crystal causes the dechanneling, and it is in fact responsible for masking any quantum structure that might otherwise be visible in the data. The changes in width and dechanneled fractions can both be predicted by simple extrapolation of the scaling laws determined for high-energy classical channeling of protons in Si.

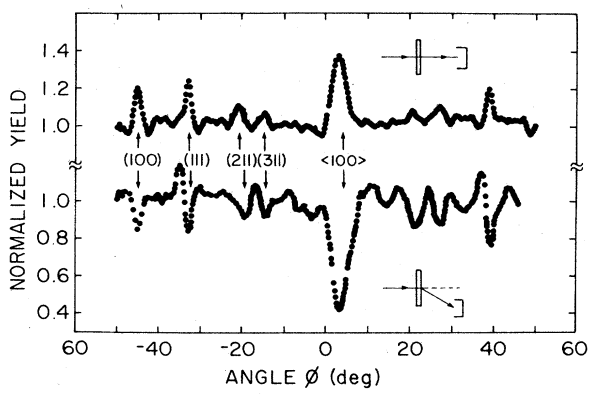

FIG. 42. Channeling of 50-keV positrons in a 0.26-μm-thick Si(100) crystal. The two curves show the transmitted positron intensity; the upper curve was obtained with a surface barrier detector on the original beam axis, and the lower curve was obtained by measuring positrons scattering off-axis. The data, together with other spectra taken for different orientations of the same crystal, show that the effect is classical at 50 keV (from Logan, Schultz, *et al.*, 1988).

The study of positron channeling may lead to potential uses quite apart from the academic interest in the problem. One application would be studies of interstitial impurities in metals or semiconductors, since energetic ions are often too destructive. It is also evident that the classical nature of positron channeling at energies as low as a few tens of keV must have implications for the shape and depth of positron implantation profiles (Sec. II.B), which have so far not been considered in theoretical or Monte Carlo calculations.

B. Slowing down

The processes involved in positron energy loss in solids are similar to those for electrons, but with certain impor-

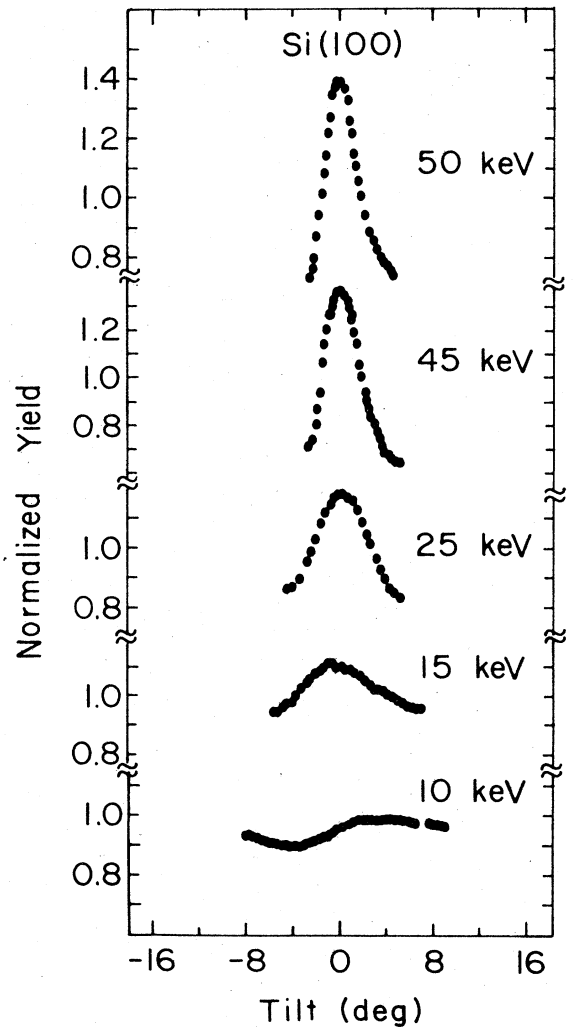

FIG. 43. ⟨100⟩ axial channeling for the thin Si crystal angle for several different incident positron energies. The width of the peak is proportional to $E^{-1/2}$, consistent with classical channeling of light particles, and the magnitude of the peak decreases with decreasing energy due to the increase of dechanneling effects in the 0.26-μm crystal (from Schultz, Logan, *et al.*, 1988).

tant differences. For energies in the range of a few MeV, the stopping process is dominated by mass radiative stopping (bremsstrahlung), in which the electron or positron interacts with the screened Coulomb field of the nucleus or one of the atomic orbital electrons, emitting a photon. This energy-loss mechanism is significantly *less* efficient for positrons than it is for electrons, since electrons are attracted by the nuclear charge and repelled by the atomic electrons. Recently Kim *et al.* (1986) have generated an approximate scaling law for the ratio of e^+ to e^- bremsstrahlung energy loss, which quantifies the difference as a function of target atomic number Z. Another fundamental difference arises because positrons annihilate in flight, thus decreasing the expected range. Heitler (1947) showed that the range of positrons in Pb would decrease due to this effect by $\sim 1.7\%$ at 0.511 MeV and $\sim 4.2\%$ at 5.11 MeV (i.e., as the energy increases, the cross section for annihilation in flight decreases, but the total probability increases).

In the next stage of slowing down, β-particle directions are randomized primarily by Mott (relativistic nuclear) scattering and energy is lost by electron scattering. Rohrlich and Carlson (1954) have shown theoretically that (almost independent of Z) positron-electron scattering is more efficient than electron-electron scattering below about 345 keV, but the reverse is true above that energy (see also Seltzer and Berger, 1974, and Hansen and Ingerslev-Jensen, 1988). This is due to differences in the electron scattering cross sections for positrons and electrons, which have two basic sources.

(i) The upper limit of the energy transfer for positrons is 100%, whereas for electrons it is 50%. This is because electrons are not distinguishable.

(ii) Collisions with large energy transfer are different. The relativistic electron-electron collision cross section (Moller) has to be replaced with the corresponding positron-electron cross section (Bhabha).

These differences are evident in Fig. 44, which shows the percentage positron-electron difference in average energy loss for Pb, Sn, and Al in units of m_0c^2. Some of the differences for energy loss of positrons and electrons are relatively well understood and quantified, while others are only beginning to be measured now that controllable positron beams are available over wide ranges of incident energy. One example that follows from the preceding section is the possibility that channeling effects may play a role in the mean depth at which positrons stop in single crystals. This could be significantly different for positrons and electrons of comparable energy.

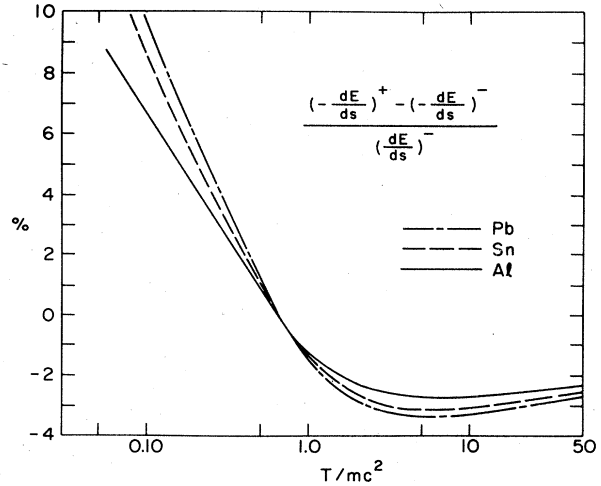

FIG. 44. Electron and positron energy-loss differences highlighted for Pb, Sn, and Al. The kinetic energy is $T=(\gamma-1)mc^2$, and dE/ds is the average collision loss per unit path length s (after Rohrlich and Carlson, 1954).

In general, most of the important scattering processes through which electrons lose their energy to a lattice are similarly important for positrons. Other than specific cases, such as the channeling mentioned above, or the inner-shell ionization discussed below, differences predicted theoretically are usually small, although there are so far few experimental tests. Lennard, Schultz, and Massoumi (1988) have initiated detailed studies of these differences in the *intermediate* energy range of 5–50 keV, comparing the energy distributions of monoenergetic positrons and electrons transmitted through thin metal foils. Examples of the energy distributions they observe for positrons transmitted through an 8-μm Be foil (≈ 1.4 mg/cm^2) are shown in Fig. 45. Spectra measured in the same geometry using similar-velocity electrons are almost identical.

In the remainder of this section we shall discuss some of the factors important to positron energy loss in solids, starting with inner-shell ionization and following with three sections more specific to metals, semiconductors and ionic solids, and insulators, respectively.

1. Core excitations

Most of the energy of an energetic positron (≤ 100 keV) that enters a solid is lost through core and valence-electron excitations, as is also the case for energetic elec-

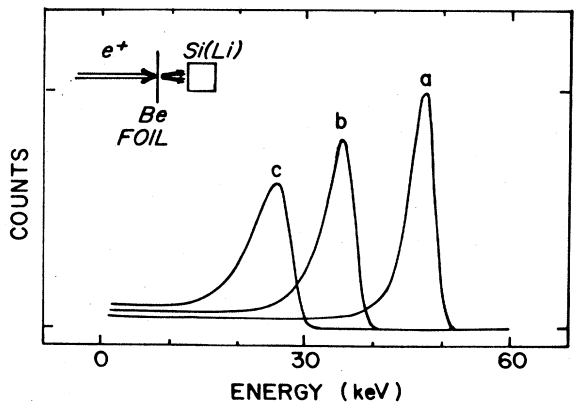

FIG. 45. Positron energy-loss spectra for transmission through ≈ 1.4 mg/cm^2 Be foil. Spectra are shown after area normalization for incident energies: (a) 56.2 keV, (b) 45.3 keV, and (c) 37.9 keV (from Lennard, Schultz, and Massoumi, 1988).

trons (Adesida *et al.*, 1980). Through such interactions the positron's energy is reduced to a few tens of electron volts in about 10^{-13} sec (Perkins and Carbotte, 1970). At relatively high incident energies (i.e., several tens to hundreds of keV), Schultz and Campbell (1985) and Ito *et al.* (1980) have compared K-shell ionization cross sections for positrons and electrons in thin foils of copper and silver, respectively. As can be seen from their data, which are shown in Fig. 46, the cross sections are comparable at incident energies higher than a few times the threshold energy U_K ($U_K \approx 8.98$ keV for Cu and 25.51 keV for Ag). The important result first demonstrated by the data for Cu is the fact that at energies below $\sim 3U_K$ the cross section for positrons becomes significantly less than that for electrons. Similar measurements comparing cross-section ratios σ^-/σ^+ for the L-shell in Au have been made from 25 to 55 keV (Lennard, Massoumi, and Schultz, 1988).

At much lower energies, Lynn and Fischer (1986) have observed positron-induced Auger electron emission, caused by L-shell ionization of a Ni target with 3.0-keV incident positrons. Their results, which are qualitatively similar to the more familiar electron-induced Auger process, are shown in Fig. 47.

Valkealahti and Nieminen (1983, 1984) have done Monte Carlo simulations of the implantation profiles of lower-energy (i.e., keV) electrons and positrons incident on solids, including both elastic and inelastic scattering. They describe core and valence-electron excitations in terms of Gryzinski's excitation function (1965), and through various assumptions show that the total inelastic cross section should be slightly less for electrons than for positrons (Valkealahti and Nieminen, 1984). It is noteworthy that these assumptions do not include channeling effects or realistic angular effects in inelastic collisions. Corrections due to these effects could lower the

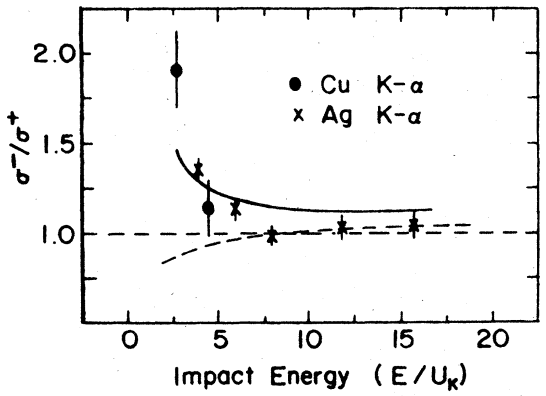

FIG. 46. Cross sections for K-shell ionization of Cu and Ag compared for electrons and positrons. The abscissa is scaled in terms of the ionization potentials, which are 8.98 and 25.51 keV for Cu and Ag, respectively. The dashed curve is the theoretical prediction including differences due to exchange only, and the divergence observed at low impact energy is due to the Coulomb repulsion of positrons from the ion cores (from Schultz and Campbell, 1985).

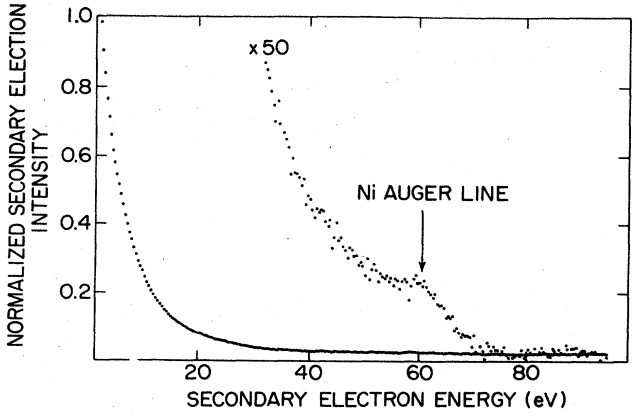

FIG. 47. Positron-induced Auger electron emission for Ni(100). The incident positrons were 3.0 keV, ionizing the L shell (from Lynn and Fischer, 1986).

probability of a close encounter of the positron with the nucleus. However, these effects are probably of less importance than the general scattering considerations included for determining the overall shape of the stopping, or implantation, profile. Moreover, Gryzinski's excitation function for the valence electrons does not include the proper particle-hole or plasmon terms which has a significant effect on the inelastic mean free path as well as the stopping profiles. Examples of profiles calculated are shown in Fig. 48 for 5-keV positrons incident on aluminum and in Fig. 49 for both 3- and 5-keV positrons incident on copper. The solid curves in Fig. 49 are their fits of a Makhovian distribution,

$$P(z) = \frac{m z^{m-1}}{z_0^m} \exp[-(z/z_0)^m] , \tag{10}$$

to the Monte Carlo data (Makhov, 1960a, 1960b, 1960c). The *shape* parameter they find is $m \approx 1.9$, and the parameter z_0 is a function of incident positron energy, given by

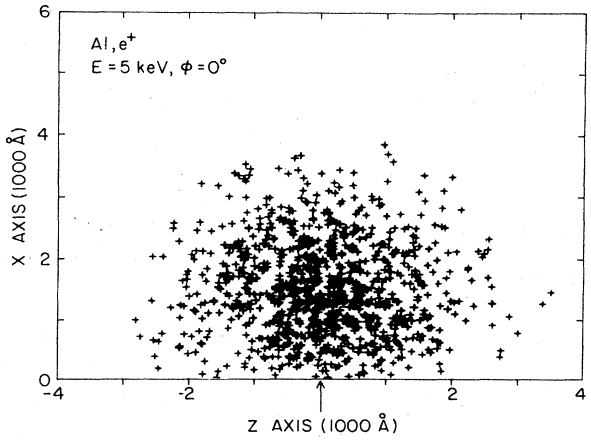

FIG. 48. Monte Carlo distribution of trajectory end points for 5-keV positrons at normal incidence on Al. The arrow shows the entrance position of the positrons (from Valkealahti and Nieminen, 1984).

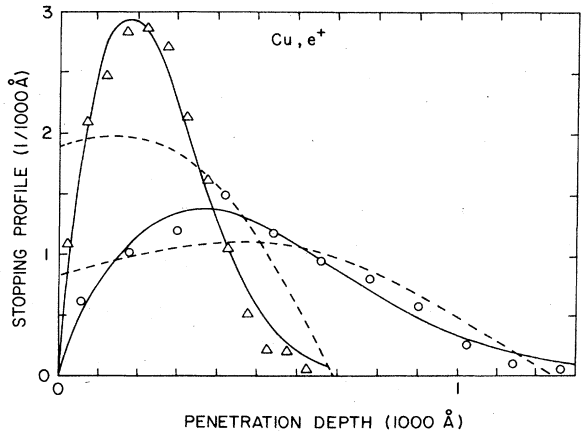

FIG. 49. Stopping profiles obtained by reducing the two-dimensional data of Fig. 48 to one dimension. The two sets of data shown are for 3- and 5-keV positrons incident on Cu. The solid lines are the Makhovian profile [Eq. (10)], and the dashed lines are the experimentally measured profiles for thin films of Cu of varying thickness (from Valkealahti and Nieminen, 1984).

$$z_0 = \frac{\bar{z}}{\Gamma[(1/m)+1]} , \tag{11}$$

where $\bar{z}$ is the mean stopping depth. The dependence of z_0 on the Γ function simplifies for certain profiles (discussed in detail in Sec. II.C.1), such as the exponential profile for which $m=1$ and $\Gamma(2)=1$, or the Gaussian-derivative profile for which $m=2$ and $\Gamma(\frac{3}{2})=\pi^{1/2}/2$.

The dependence of mean depth on energy is assumed to be a power law,

$$\bar{z} = AE^n , \tag{12}$$

which was originally developed for electron stopping. The constant A in Eq. (12) was found empirically to be $A \sim 400/\rho$ Å/keV^n, where ρ is the target density in g/cm^3, $\bar{z}$ is in Å, and E is in keV (Mills and Wilson, 1982; Vehanen, Saarinen, *et al.*, 1987), and the power $n \approx 1.6$ for positrons incident on most materials (Lynn and Lutz, 1980a).

Different experimental determinations of the constant A vary by up to 20%, which leads to some uncertainty in attempts to do quantitative depth studies. This is especially important in multilayer systems, where both density and backscattering variations are contributing to uncertainties in positron stopping depths. It is also not clear that the constant A is necessarily independent of both atomic number Z and incident energy E. For example, there is a well-established energy dependence of the ratio of (calculated) positron to electron ranges in any given material (ICRU, 1984), which may indicate an energy dependence to the constant, A, or may be explained by a difference in the power n (n for positrons would have to be bigger than for electrons by ~ 0.03 to explain the energy dependence in Si).

The power n is also cause for some concern, as the results that do exist for both positrons *and* electrons are not all in agreement, particularly in the low (few keV) energy ranges of most interest in e^+ beam research. For high-energy electrons, n has been measured to be a decreasing function of energy, going from ~ 1.68 at 10 keV down to ~ 1.16 at 3 MeV (Katz and Penfold, 1952). At lower energies, one experimental study of electron stopping in evaporated metal films of Al, Cu, Ag, and Au (Cosslett and Thomas, 1964) found that n was a strong function of energy, ranging from ~ 1.2 ($1 \leq E \leq 5$ keV) to ~ 1.4 ($5 \leq E \leq 10$ keV) to 1.7 ($10 \leq E \leq 15$ keV).

The only direct measurements that exist for monoenergetic positrons are those of Mills and Wilson (1982). Their experiment measured the transmitted positron flux through thin wedge-shaped foils of Al and Cu supported on a thin carbon foil, and they extracted not only the profile shapes but also the mean depth versus energy (Fig. 50). Their results are that $n = 1.60^{+0.15}_{-0.08}$ for $1 \leq E \leq 6$ keV e^+ in Al, and $n = 1.43^{+0.07}_{-0.11}$ for $1 \leq E \leq 6$ keV e^+ in Cu. One problem that was not considered in the analysis of these data is the fact (Cosslett and Thomas, 1965) that the backscattered fraction of positrons varies as the film thickness, ranging (in the case of Cu) from 0 to 30% from the thin-to-thick edge of the target film.

The Monte Carlo results of Fig. 49 also show the direct profile measurements (dashed curve) of Mills and Wilson. The discrepancy of the measured profile shapes with the Monte Carlo results at low energy in Fig. 49 was attributed to a reduction in the amount of backscattering in the experimental measurement, since positrons that are transmitted through the thin crystals can no longer

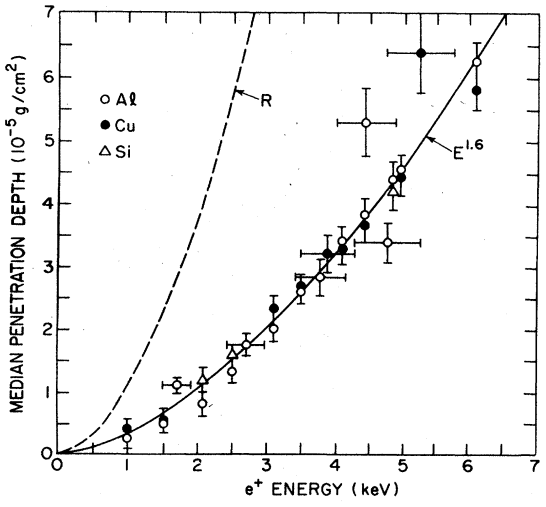

FIG. 50. Experimentally determined median stopping depth χ_+ for monoenergetic positrons in Si, Al, and Cu. χ_+ is related to the more familiar mean depth by $\chi_+ = z_0(\ln 2)^{1/m}$, which (for $m=2$) is $2\bar{z}(\ln 2/\pi)^{1/2} \sim 0.94\bar{z}$ [see Eqs. (10)–(12)]. The solid curve is a best fit to the data, yielding $\chi_+ = (332/\rho)E^n$ (Å), where ρ is the material density, E is given in keV, and n is approximately 1.6. Curve R is the mean penetration depth for positrons in Al as calculated by Nieminen and Oliva, 1980 (from Mills and Wilson, 1982).

scatter. Lynn, McKay, and McKeown (1987) have shown that the stopping profile can be affected by reimplanting positrons that were originally backscattered from the sample.

The details of where the positrons stop or reach near-thermal energies in a solid are determined almost entirely by these very fast inelastic collisions described above. The actual loss of energy in the final stages of thermalization (i.e., below a few tens of eV) is, however, different for the different classes of solids, and will be discussed in the following sections.

2. Metals

Perkins and Carbotte (1970) have shown that inelastic conduction-electron scattering, and specifically plasmon excitation (Oliva, 1980a), dominates the slowing down of positrons around energies near the Fermi energy E_f. Plasmon losses are evident in the results obtained by Dale *et al.* (1981), Fig. 51, where they show the energy distribution of 785-eV incident positrons and electrons scattered from a tungsten sample. They speculate that the differences they observe in the inelastically scattered fractions might be the results of *d*- and *f*-shell excitations.

Zhang *et al.* (1988) have recently considered the positron-electron interaction in metals in detail for $0 < E < 200$ eV. They include virtual Ps formation by

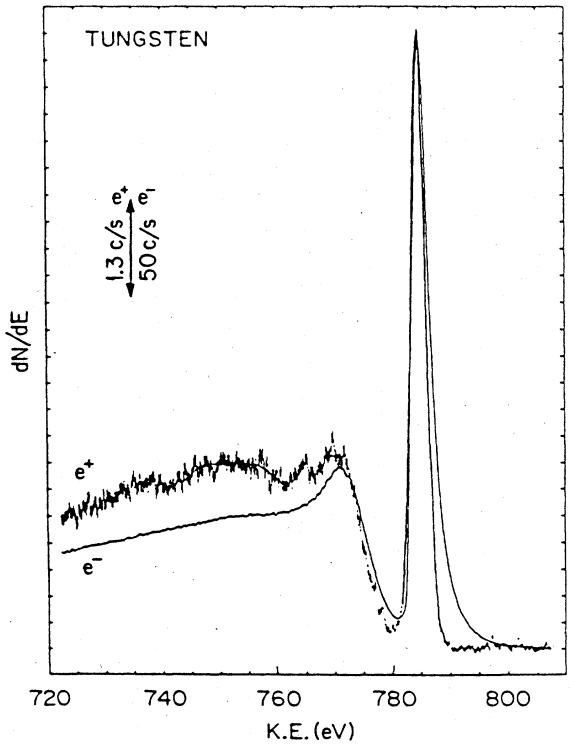

FIG. 51. Positrons and electrons at 785 eV are scattered off tungsten, showing the elastic peak and the inelastic distribution. Plasmon excitations are primarily responsible for the energy losses in this region (from Dale *et al.*, 1981).

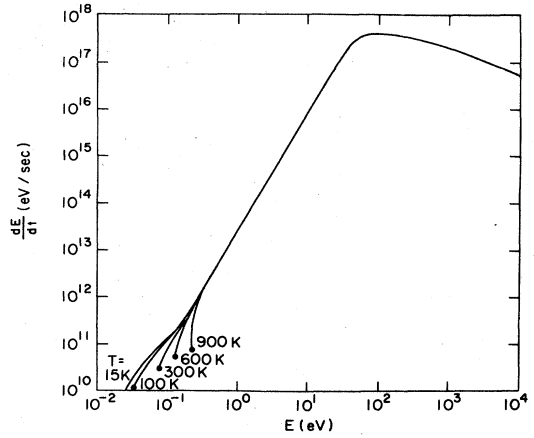

FIG. 52. Positron energy loss dE/dt vs energy E in Al due to combined effect of positron-conduction electron and positron-phonon scattering for several temperatures (from Nieminen and Oliva, 1980).

treating it as a multiple-scattering interaction, and their results show that the electron wave function is enhanced at the positron by comparison with previous RPA (random-phase approximation) calculations. The rate of inelastic positron-electron scattering is significantly increased by this enhancement, relative to previously determined RPA estimates.

The last stage of thermalization of a positron in a metal, at energies well below E_f, is dominated by phonon scattering (Perkins and Carbotte, 1970). In Fig. 52 the rate of energy loss dE/dt is plotted as a function of positron energy E for positrons in Al at various temperatures. This figure shows that, as the energy falls below a few tenths of an eV, the effects of phonon scattering begin to dominate relative to the electron gas. Nieminen and Oliva (1980) have pointed out that the very long mean free paths (shown in Fig. 53) and the high probability of large-angle scattering at low positron energies (Oliva, 1979) contribute significantly to the overall

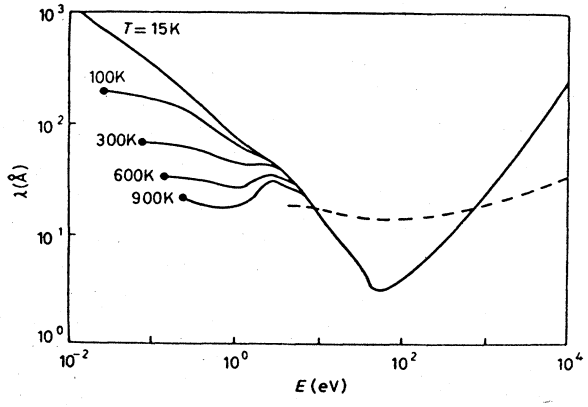

FIG. 53. Mean free path vs energy of a positron in Al due to the combined effect of positron-conduction electron and positron-phonon scattering. The dashed line is associated with elastic core scattering (from Nieminen and Oliva, 1980).

broadening of the final thermalized profile of positrons. The thermalization times they obtain are on the order of 1–10 psec, in reasonable agreement with previous estimates (Carbotte and Arora, 1967).

A subtle yet important point made by Carbotte and Arora (1967) is that increasing electron density (decreasing r_s) leads to more screening of the positron-electron interaction in the metal, and therefore a longer thermalization time. This is illustrated in Fig. 54. Theoretical estimates all predict that thermalization times increase significantly as temperature decreases, in some cases even exceeding the mean positron lifetime in the solid (Carbotte and Arora, 1967). Kubica and Stewart (1975) measured high-resolution 1D ACAR spectra for several materials down to low temperature, and by careful examination of the *sharpness* of the Fermi edge in the momentum distributions they concluded that the positron thermalizes down to $T=25\pm25$ K in potassium, $T=10\pm10$ K in Mg, and $T=30\pm25$ K in Al. Their results for Na indicated that the positron was not completely thermalized ($T=50\pm30$ K), but the interpretation was uncertain due to the possibility of defects induced by a martensitic transformation. This evidence of low-temperature thermalization in a material with a very low conduction-electron density is in apparent conflict with Carbotte and Arora's *early* theory, which did not include positron-phonon interactions. A later work (Perkins and Carbotte, 1970), which included this effect, demonstrated that low-temperature thermalization would be expected. The thermalization time predicted as a function of temperature by the Perkins-Carbotte theory is shown in Fig. 55.

For positrons incident on a metal surface at energies up to a few keV, thermalization times are sufficiently long and the large-angle scattering processes sufficiently important that a small fraction will be reemitted into the vacuum before they are completely thermalized. This is demonstrated by the differential energy distribution (Sec. I.E.1) of low-energy positrons emitted from a

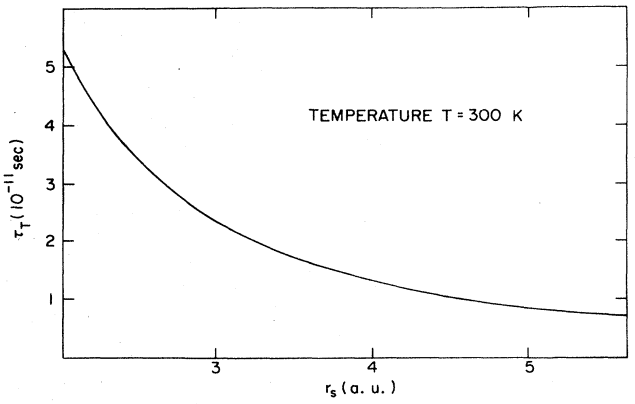

FIG. 54. Positron thermalization time vs electron density. The decrease is due to an increased positron-electron interaction (from Carbotte and Arora, 1967).

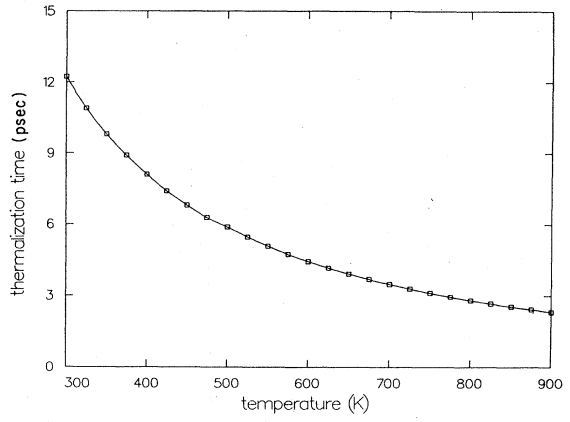

FIG. 55. Positron thermalization time vs temperature. The inclusion of the positron/phonon interaction leads to both shorter thermalization times than those predicted previously (e.g., Fig. 53), and a dependence on temperature (after Perkins and Carbotte, 1970).

Ni(100) + CO surface, shown in Fig. 56. The importance of the nonthermal component at low energies can be gauged relative to the tail at 3.0 keV incident energy, where the nonthermal fraction is small. It has also recently been demonstrated (Nielsen *et al.*, 1986) that the nonthermal positrons have a finite probability for trapping in open volume lattice defects, contrary to some previous theoretical calculations. These results are shown in Fig. 57, where a reduction of the nonthermal component is caused by the introduction of thermally activated vacancies [small points, Fig. 57(a)] or by damaging the near-surface region of the solid with Ar^+ ion sputtering [Fig. 57(b)]. Recent theoretical models are now consistent with the existence of resonances in the cross sections for trapping of epithermal positrons in vacancies and vacancy clusters (McMullen and Stott, 1986; Puska and Manninen, 1987; Shirai and Takamura, 1987).

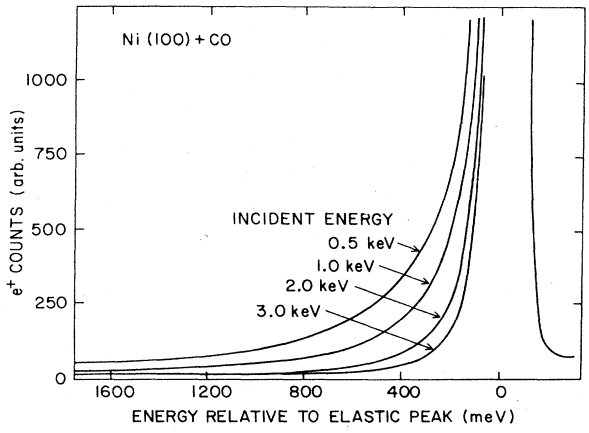

FIG. 56. Reemitted positron-energy distributions for Ni(100) + CO. The various spectra indicate emission of nonthermal positrons after being implanted in the sample at energies below 3 keV (from Fischer, 1984).

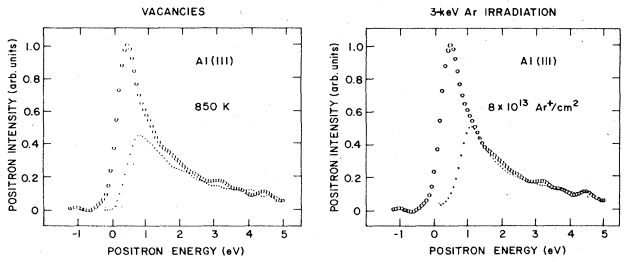

FIG. 57. Emission of 50-eV incident positrons before complete thermalization in Al(111) (open circles). The small points were obtained (a) at 850 K (where thermal vacancies are present) and (b) after sputtering the surface with 3-keV Ar^+ ions. The fact that these curves are both below the open circles is evidence for prethermalized trapping of positrons in defects (see Sec. II.E). From Neilsen *et al.*, 1986.

The observation that positrons can trap prior to complete thermalization indicates not only that the thermalization time of a positron is *relatively* long, but also the the trapping process above thermal energies is very efficient. This result would also be expected to apply to the interaction of a low-energy positron with the potential well at the surface of a metal. The interaction is fundamentally important to many of the processes studied with positron beams, such as the low-energy diffraction discussed above (Sec. II.A.1) and the positron reemission and Ps formation discussed in Sec. II.D.

A single-particle potential such as that pictured in Fig. 8 can be simplified for low-energy positrons as a series of step potentials, and the interaction of the positron with this potential (which is kept static and does not adjust to the presence of the positron) can be calculated simply. Using this model, energy loss of positrons as they pass over the potential well at the surface would lead to an inelastic component of the reemitted positron energy distribution. The fraction that is inelastic is a complicated function of the magnitude of φ_+. As $|\varphi_+|$ increases, the time spent over the well (and therefore the probability of losing energy) decreases, although this is compensated to some extent by the fact that there are more lower-energy states available into which the positron can scatter. This number of states depends on both the positron and the electron band structure at the surface. Another result of this simple model is the prediction of internal reflection of the positron off the potential step at the surface (Nieminen and Oliva, 1980). Since the reflection probability β varies as the ratio of energy width (of the positron distribution) to step height, one would expect that (i) β should decrease as temperature decreases, and (ii) β should become large as the kinetic energy of the positron becomes much smaller than $|\varphi_+|$ (see Wilson, 1983, and references therein).

Lynn, Schultz, and MacKenzie (1981) showed that the formation of Ps at a Cu(111) + S surface as a function of temperature did not show the decrease at low temperatures that would be expected from internal reflection of thermally diffusing positrons approaching the simple step potential described above. Their results are shown in Fig. 58, together with two theoretical predictions based on kinetic desorption (upper curve; Kreuzer *et al.*, 1980) and the step potential with reflection discussed above (lower curve; Nieminen and Oliva, 1980). The increase at higher temperatures which is evident in Fig. 58 is due to thermally activated Ps (discussed in more detail in Sec. II.D.3). The relatively weak dependence on temperature below this activated desorption was also observed for the yield of reemitted positrons (Schultz and Lynn, 1982), and it was suggested at that time that the inelastic losses during the reemission process were in fact much stronger than anticipated. In both of these studies, the incident positron energies were relatively low ($\sim$500–2000 eV), and so it is possible that part of the temperature dependence observed can be attributed to reemission of nonthermal positrons or nonthermal Ps emission.

Wilson (1982, 1983) investigated positron energy loss at the image-induced potential well by guiding very-low-energy ($\leq$25 eV) positrons at Cr(100) and Al(100) surfaces. His data, shown in Fig. 59, show the total annihilation rate for positrons as a function of target bias V_T. For this study the beam voltage V_B was maintained at a small value ($\sim$22 V), and a grid near the sample was at ground potential ($V_G = 0$ V) to ensure that all reemitted or reflected positrons would escape from the detection region. At $V_T \leq V_G$ the reemitted positrons were returned to the sample showing the same sort of integral energy distribution that was described in Sec. I.E.1.

The sharp increase labeled V_{thresh} in Fig. 59 corresponds to the target bias at which the beam reaches and interacts with the surface, and the kinetic energy the pos-

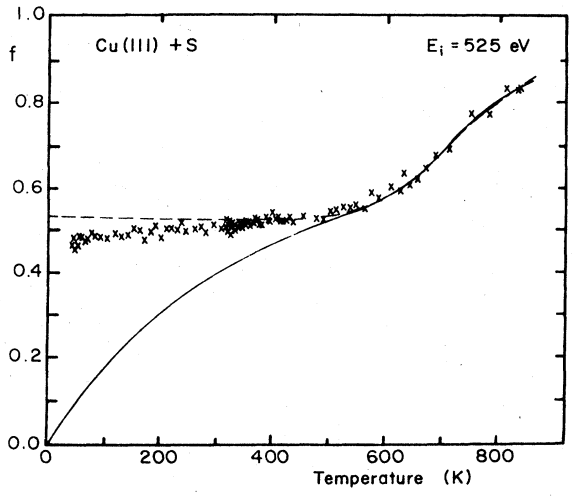

FIG. 58. The fraction of Ps formed at a Cu(111) + S surface for 525-eV incident positrons. The solid curve is a theoretical prediction based on quantum-mechanical reflection of a plane wave from an attractive potential step (the surface). The fact that the data do not follow the simple model is attributed to inelastic processes near the surface, or positrons that are not fully thermalized which return to the sample surface (from Lynn, Schultz, and MacKenzie, 1981).

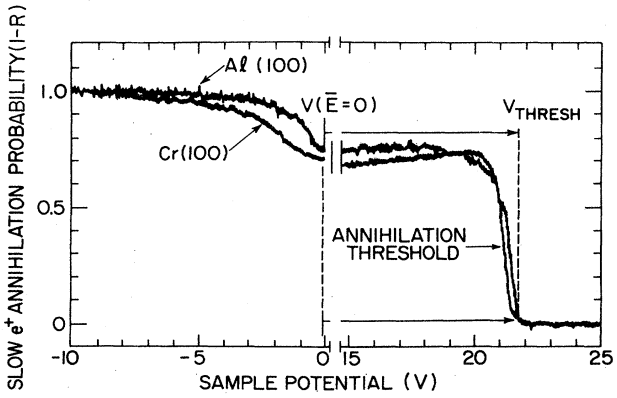

FIG. 59. Positron reflection from Cr(100) and Al(100). Annihilation of positrons in the target region, after correction for background, is proportional to $(1-R)$, where R is the reflection probability (from Wilson, 1982).

itrons have when they reach the surface is $E_i = V_{\text{thresh}} - V_T$. Wilson points out that the rough equality of the trapped (annihilating) fraction at $E_i \approx 2$ and 20 eV indicates that the inelastic processes are very strong, and that reflection of the incident beam off the sample is not observed even at the lowest incident energies. These results are the first direct evidence that the interaction of the positron with the surface potential must be considered dynamically, and that a nonadiabatic distortion of the charge at the surface which produces the image potential may be important. Another possibility is that the above-mentioned resonant trapping of positrons into the surface state is dominating at these energies. So far, theoretical calculations of resonant trapping cross sections have not been performed for the surface state. These calculations are now being performed.

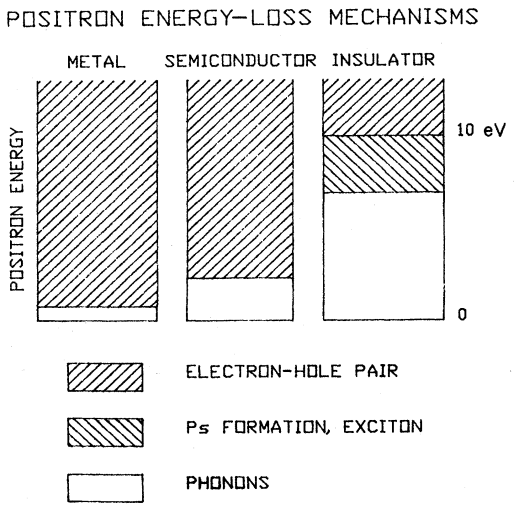

FIG. 60. Schematic representation of the relative importance of various energy-loss mechanisms for positrons in metals, semiconductors, and insulators.

3. Semiconductors and ionic solids

Positron energy loss in semiconductors is similar to that in metals, except that electron-hole creation ceases to be possible when the positron energy becomes less than the band gap. This is indicated schematically in Fig. 60, which shows a wider region of energy that must be lost to phonon modes in the absence of more efficient mechanisms. The effect of the band gap is seen in the results of Mills and Crane (1985a), who measured the energy distribution of 500-eV incident positrons reemitted from a series of ionic crystals. The particularly wide distributions observed (reproduced in Fig. 61) are suggested to be evidence of Ps formation and subsequent dissocia-

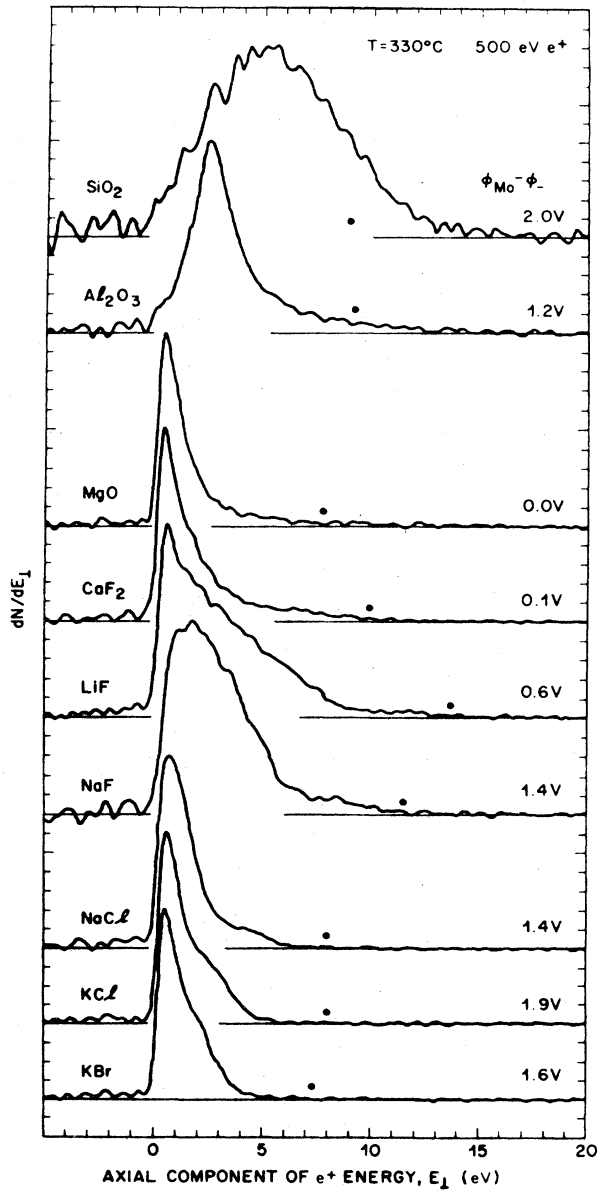

FIG. 61. Positron emission spectra for nine ionic crystals (from Mills and Crane, 1985a).

tion (Mills and Crane, 1985a), although it has also been suggested (Lynn and Nielsen, 1987) that the energetic positrons are the result of a slower rate of energy loss to phonons relative to electron-hole excitations. Gullikson and Mills (1986) supported this model in their results for rare-gas solids, discussed in the next section. The inhibition of energy loss caused by a band gap, which has recently been confirmed in Si (Nielsen, Lynn, and Chen, 1986), is in fact evident in some of the earliest data on work-function emission of positrons (Mills, Platzman, and Brown, 1978).

The implication of the band gap for slowing down of positrons in a semiconductor was discussed well before positron beams were operating efficiently by Pendyala (1973), who was studying the positron emission process in an attempt to develop a slow-positron beam. He suggested that the inability to thermalize positrons efficiently at energies below the gap width may reduce the annihilation rate and lead to relatively intense emission of "hot" positrons from semiconductor surfaces.

The formation of positronium in many solids is not favored because of the screening of the attraction by the high density of electrons, as was mentioned in an earlier section (Kahana, 1960). It has been a fairly widespread belief that all metals and semiconductors belonged to this class of materials. However, Dupasquier and Zecca (1985) have pointed out that Ps formation may be energetically possible in Si. There is so far no experimental evidence of Ps formation in semiconductors, although further studies on clean semiconductors at low temperatures may substantiate their claim.

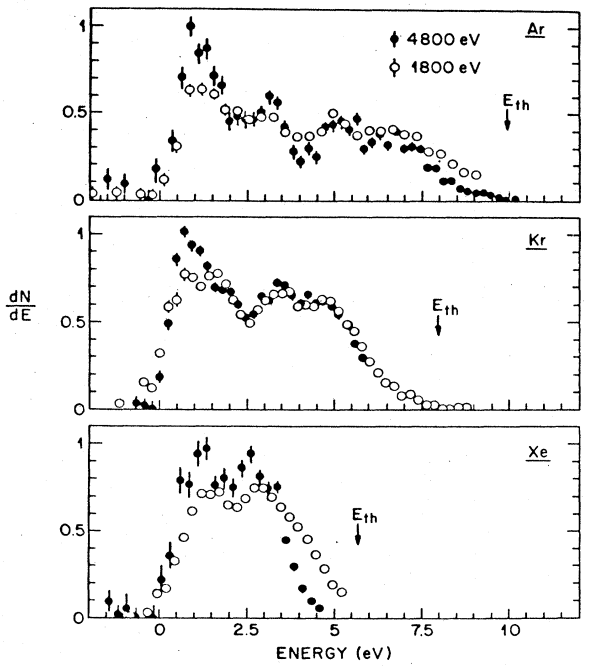

FIG. 62. Positron emission spectra for solid noble gases Ar, Kr, and Xe. The spectra are effectively the same for the two different incident positron energies studied (4800 and 1800 eV). E_{th} is the minimum energy to which positrons thermalize in these solids, as determined by the band gap (from Gullikson and Mills, 1986).

4. Insulators

The prolonged thermalization time caused by band gaps in semiconductors and ionic solids is even more pronounced in insulators, which are also represented on the schematic in Fig. 60. This was first identified by Gullikson and Mills (1986), whose data for rare-gas solids are shown in Fig. 62. The absence of an optical-phonon branch in these simple solids (which is available for the ionic solids) reduces the efficiency of the energy loss even more. Gullikson and Mills point out that the average energy lost per collision in solid Ne is only about 6 meV, in agreement with the average phonon energy in this system.

Positron energy loss in many insulators involves Ps formation in one way or another. This has long been studied by bulk lifetime studies of insulators, liquids, and molecular solids (ICPA65; ICPA82, ICPA85) and has stimulated at times lively debate between competing models (see Eldrup *et al.*, 1985, and references therein). One of the crucial points in the dynamics of Ps in insulators is whether or not it thermalizes completely prior to annihilation. In a high-resolution ACAR study, Kubica and Stewart (1975) showed that the width of the narrow *p*-Ps peak (e.g., Fig. 3) depends on sample temperature, consistent with the change in center-of-mass momentum that would be expected at thermal equilibrium. Their results showed that free Ps thermalized down as low as $T=10^{+2}_{-5}$ K, indicating complete thermalization within experimental limits, although the details (of energy loss for low-energy Ps) are still not well understood.

Eldrup and co-workers (1983) demonstrated that Ps formation in ice was enhanced when energetic positrons (i.e., ~ 1 keV) lost a large fraction of their energy to ionization and breakup of the ice molecules (Fig. 63) in the so-called *spur* mechanism of Ps formation (Mogensen, 1974, and 1975). The data shown in Fig. 63 also confirmed the model of excitonic Ps formation within the so-called Ore gap (Dupasquier, 1981, p. 546), which is the energy range between the ionization threshold and the limit of stability for energetic Ps in the solid. This is seen in the figure as a peak from ~ 6 to 10 eV, while the second (less distinct) peak at ~ 25 eV is evidence for the second level of ionization. These results were subsequently supported by Monte Carlo calculations done by Van House *et al.* (1984b) and Eldrup *et al.* (1985), which are shown in Fig. 64.

The dynamics of Ps formation in LiF have been studied by Howell, Rosenberg, and McMullen (1988) by measuring the emitted Ps energy distribution as a function of incident e^+ energy. They estimate that the deformation potential for Ps coupled to the phonons in the lattice is ~ 3 eV. Structure is observed in the Ps energy spectrum, which they discuss in terms of the detailed Ps

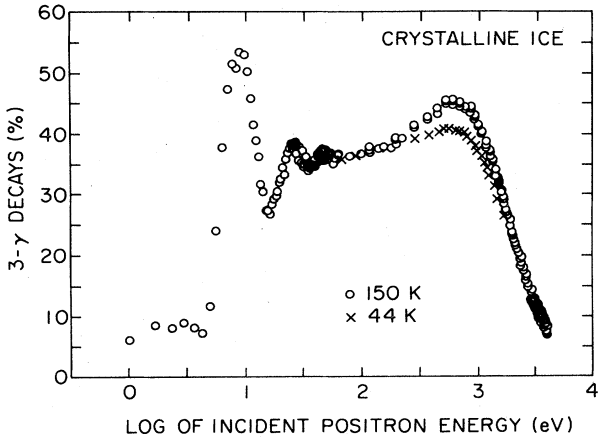

FIG. 63. The 3γ annihilation fraction of o-Ps vs incident positron energy. Some of the positrons in ice form Ps, which then diffuses to the surface and escapes into the vacuum. There is no significant contribution in the above due to Ps annihilation in the solid, since it almost all decays by 2γ emission (from Eldrup *et al.*, 1983).

formation mechanism, and the Ps work function φ_{Ps} is estimated to be 3.0±0.4 eV.

C. Diffusion

In Sec. I.E.2, we described how a measurement of the fraction f of Ps emitted from a surface is made. By measuring f as a function of incident positron energy, it is possible to learn something about the diffusion of the *thermalized* positrons. In fact, in this context the measurement of f is just a convenient measure of the flux of positrons back to the surface, and the discussion that follows is applicable to any measurement of back diffusion whether it is the Ps fraction, reemitted positrons, or the measurement of annihilation line-shape parameters (Sec. I.E). Almost all of the earliest work in this area was done using f as the experimentally determined parameter, but more recently the line-shape parameter S has been used more extensively. In this section we shall review some of the underlying assumptions and properties of positron diffusion, in terms both of our current theoretical understanding and of the experimental research done to the present time. These concepts will be referred to in Sec. II.E in the discussion of defect studies of the near-surface region of solids.

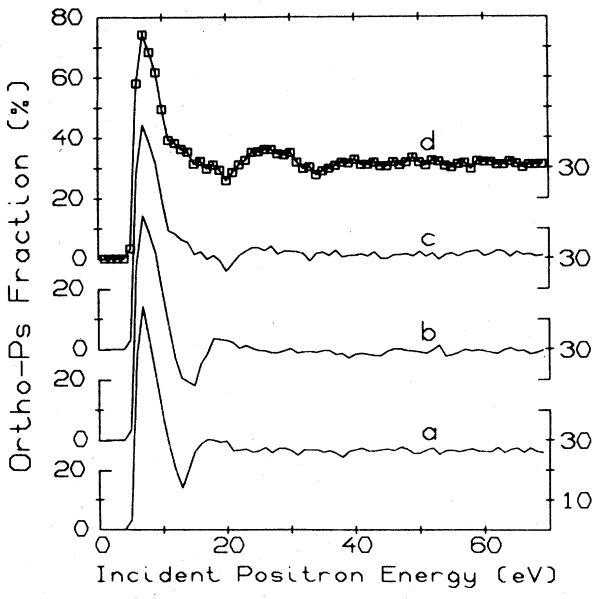

FIG. 64. Calculated fractions (Monte Carlo) of positrons forming o-Ps as a function of incident positron energy. The curves (a)–(d) represent cumulative contributions of various electronic bands to the total Ps formation probability. The ionization energies for these bands are (a)–(d) 9.8 eV, (b)–(d) 11.5 eV, (c)–(d) 16.3 eV, and (d) ~30 eV. From Eldrup *et al.*, 1985.

1. Data analysis

Positrons from a monoenergetic beam reach near-thermal energies in a time that is fairly short compared to their lifetime in most solids, as discussed in the preceding section. The so-called stopping or implanation profile looks something like that shown in Figs. 48 and 49, and the subsequent motion of the positrons in the lattice could be described using the Boltzmann equation, which accounts for normal drift and collisional effects on the positron's motion. Since the mean free path for positron scattering is much less than typical penetration depths (cf. Fig. 53), it is assumed that the diffusion equation adequately describes the positron motion (Mills, 1978; Lynn, 1981, and references therein; Case and Zweifel, 1967).

In a discussion of the limitations of the diffusion equation, Brandt and Arista (1979) have pointed out that, at least in cases where defects are present in the lattice, the energy distribution of the ensemble of diffusing positrons may not be Maxwellian, due to positron trapping into defects. This would necessitate the application of the Boltzmann equation. An energy-dependent trapping rate (below 1 eV) has been observed both in bulk studies of solids (Warburton and Shulman, 1977; Fluss *et al.*, 1978; Luhr-Tanck *et al.*, 1985) and in near-surface studies with positron beams (Nielsen, Lynn, and Chen, 1986) in cases where equilibrium concentrations of defects are present. Theoretical descriptions of *resonance* trapping in vacancies (McMullen and Stott, 1986; Puska and Manninen, 1987) support these observations, and Lynn, McKay, and Nielsen (1987) have shown that prethermalized trapping may significantly affect measurements of bulk positron lifetimes. The significance of observed energy-dependent trapping rates for positron diffusion is not yet determined. Brandt and Arista also state that the Boltzmann equation must be used in constrained or confined media, which may pose special problems for the near-surface regions of a solid studied with positron beams, but again the distance scales are determined by the scattering length, which is typically only several tens of angstroms.

In summary, it appears that the assumptions underlying the use of the diffusion equation are acceptable (McMullen, 1985).

The three-dimensional diffusion equation is given by

$$\frac{\partial n(r,t)}{\partial t}=D_+\nabla^2 n(r,t)-\lambda_{\text{eff}}n(r,t)-\frac{\partial}{\partial r}[v_d n(r,t)] \quad (13)$$

where D_+ is the positron diffusion coefficient, $n(r,t)$ is the positron density as a function of both time and position, ($\lambda_{\text{eff}}^{-1}=\tau_{\text{eff}}$) is the effective lifetime of the positron in a freely diffusing state, and v_d is the field-dependent drift velocity. Several authors have solved the diffusion equation with the drift-velocity term included (Mills and Murray, 1980; Jorch *et al.*, 1984; Beling *et al.*, 1987a). Although not important for diffusion in metals, it is required for the semiconductor studies now being done (cf. Fig. 72 and Sec. II.E). Dupasquier and Quartapelle (1987) have specifically addressed the near-surface polarization effects in semiconductors.

The diffusion equation above includes normal annihilation in the bulk solid (lifetime, λ_b^{-1}) as well as trapping (rate, κ_t) in a depth-dependent concentration of defects $C(z)$,

$$\lambda_{\text{eff}}=\frac{1}{\tau_{\text{eff}}}=\lambda_b+\kappa_t C(z) . \quad (14)$$

Applying a radiative boundary condition (Waite, 1957), one finds that the transmission coefficient through the surface is variable:

$$n(0,t)=\beta\left[\frac{\partial n}{\partial z}\right]_{z=0} , \quad (15)$$

where β is a coefficient that takes account of internal reflection at the surface. As β approaches zero, the surface is totally absorbing (i.e., no reflection), and as β approaches infinity the surface becomes totally reflecting. The eigensolution of Eq. (13) for $v_d=0$ can be written in one dimension as (Lynn, 1981)

$$n_K(z,t)=\theta(z)\frac{\sin(Kz)+K\beta\cos(Kz)}{(1+\beta^2K^2)^{1/2}}\exp(-\delta t) , \quad (16)$$

where the step function $\theta(z)$ sets the density to zero in the region outside the surface ($z<0$). The time/space separation constant δ is related to K in the above by $\delta=D_+K^2+\lambda_{\text{eff}}$.

The general solution for the positron wave-function density, $\Psi(z,t)$, is just the integration over the solutions in Eq. (16), and is given by

$$\Psi(z,t)=\int_0^\infty C_K n_K(z,t)dK , \quad (17)$$

where the coefficients C_K can be solved in the trivial case of an initial profile that is a δ function, $\Psi(z,0)=\delta(z-a)$,

$$C_K=\frac{2}{\pi}\frac{\sin(Ka)+K\beta\cos(Ka)}{(1+K^2\beta^2)^{1/2}} . \quad (18)$$

This approach can be applied to more realistic profiles by simply using a weighted integral of the δ-function solution. The experimentally measured quantity is the number of positrons that diffuse back to the surface, which is the total flux through the plane of the surface due to the initial δ-function profile at a, or

$$\mathcal{N}(a)=\int_0^\infty |J(0,t)|\,dt=\int_0^\infty \left|-D_+\left[\frac{\partial\Psi}{\partial z}\right]_{z=0}\right| dt , \quad (19)$$

where $J(0,t)$ is the positron current through the surface ($z=0$). Equations (16)–(19) above are solved to yield

$$\mathcal{N}(a)=\frac{\exp[-a/(D_+\tau_{\text{eff}})^{1/2}]}{1+\beta/(D_+\tau_{\text{eff}})^{1/2}} . \quad (20)$$

For a general and more realistic profile $P(z)$ of positrons, the number that escape through the surface is given by

$$\mathcal{L}=\int_0^\infty P(z)\mathcal{N}(z)dz , \quad (21)$$

which is the Laplace transform of the stopping profile (Lynn, 1981). The implantation profile $P(z)$ is characterized by a mean depth $\bar{z}$, as shown previously in Eqs. (10)–(12). The increase of $\bar{z}$ with energy is dramatically illustrated in the log-log plot of $P(z)$ in Fig. 65, together with the decrease in the fraction that diffuse back to the surface F_s, and the resulting increase in the fraction that annihilate in the bulk, F_b. These profiles were generated assuming a shape parameter of $m=1.9$, which appears to be close to optimum. Deriving the diffusion coefficient

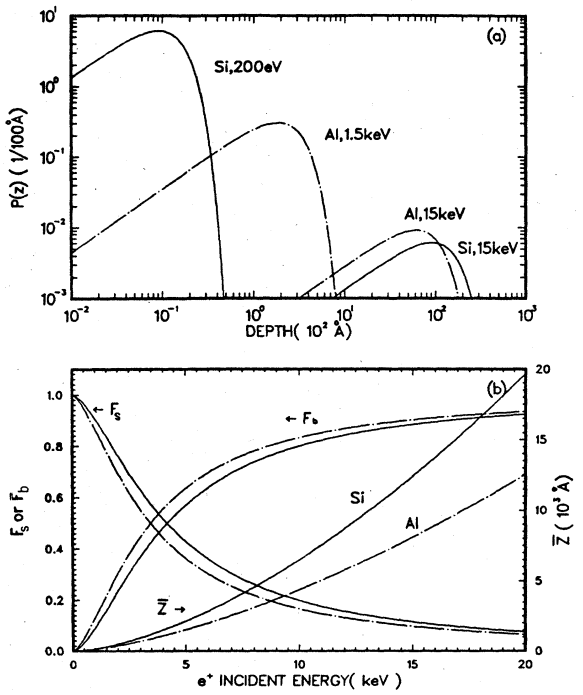

FIG. 65. A schematic representation of the positron implantation properties for Al and Si. (a) Positron stopping profiles in Si and Al; (b) the fractions that diffuse back to the surface F_s, and annihilate from bulk states F_b. The mean depth at which the positrons stop, $\bar{z}$, is also shown.

D_+ from Ps fraction data (or any other measure of back-diffused positrons) according to Eq. (21) involves a nonlinear fit of a numerically integrated function, which is prohibitively time consuming for many applications (Nielsen, Lynn, Vehanen, and Schultz, 1985). If the shape parameter m in Eq. (10) is set equal to unity, $P(z)$ reduces to an exponential and Eq. (21) can be solved analytically. Assuming the power-law relationship between mean depth and energy [Eq. (12)], and neglecting the reflection coefficient ($\beta \rightarrow 0$) (Mills, 1978; Lynn, 1981), we find that the exponential profile yields for the fraction returning to the surface

$$F_s = \frac{1}{1+(E/E_0)^n} . \tag{22}$$

This is shown in Fig. 65(b), together with the bulk fraction, which is

$$F_b = 1 - F_s . \tag{23}$$

For a measurement of Ps this is written

$$f = f_0 F_s , \tag{24}$$

where f_0 is the branching ratio for Ps, which is the relative fraction of those positrons at the surface that form Ps.

At present, most of the experimental data to be found in the literature have been fit using the exponential profile and Eq. (24). As Valkealahti and Nieminen (1983) have pointed out, this simplification would probably result in an extracted D_+ that was too small by $\sim 25\%$. Their estimate was confirmed by the results of Nielsen, Lynn, Vehanen, and Schultz (1985) for silicon, which show that the exponential profile cannot be made to fit the data over a wide range of positron energies [Figs. 66(a) and 66(b)] and that the value for $D_+ \sim 1.9 \pm 0.3$ cm^2/sec was about 40% less than that obtained using nonlinear fitting to the general Makhovian profile [Fig. 66(c); $D_+ \sim 2.7 \pm 0.3$ cm^2/sec].

It is interesting to note that the fit to the data shown in Fig. 66(c) requires a profile shape parameter of $m = 1.4$, rather than the $m = 1.9$ predicted theoretically (Valkealahti and Nieminen, 1984). This is closer to the experimental profiles of Mills and Wilson (1982), as demonstrated by the Monte Carlo results in Fig. 49. It may be significant that the data for Si were fit over all energies from 500 eV up, which may introduce systematic effects due either to variations of the stopping power (Sec. II.B.1) or to emission of epithermal positrons (Huomo *et al.*, 1987). The profile may also have been affected by the experimental geometry (as discussed at the beginning of this section) which, in this case, caused all backscattered positrons to be returned to the sample.

In addition to the simple exponential profile considered above, it is also possible to obtain an analytical solution to Eq. (21) with a shape parameter of $m = 2$, to yield the profile

$$P(z) = \frac{\pi z}{2(\bar{z})^2} \exp[-(\pi/4)(z/\bar{z})^2] \tag{25}$$

which is the (negative) derivative of a Gaussian. The evaluation of the Laplace transform of Eq. (25) yields for the fraction returning to the surface the expression

$$F_s = [1 - \pi^{1/2} \sigma_g \exp(\sigma_g^2) \mathrm{erfc}(\sigma_g)] , \tag{26}$$

where erfc is the complimentary error function, and

$$\sigma_g = \frac{z_0}{2L_+} = \frac{\bar{z}}{L_+ \pi^{1/2}} . \tag{27}$$

As above, the Ps fraction would be given by $f = f_0 F_s$. In spite of the fact that $m = 2$ is a long way from the apparent parameter $m \approx 1.4$ observed experimentally, McMullen (1984) has demonstrated that Eq. (26) is much better than the exponential profile at reproducing the Laplace transform [Eq. (21)] of the experimental profiles of Mills and Wilson (1982), as shown in Fig. 67. The use of the Gaussian-derivative profile above was also found to be superior to the exponential profile by Lynn, Chen, *et al.* (1986) in defect-profiling studies of He in Ni (see

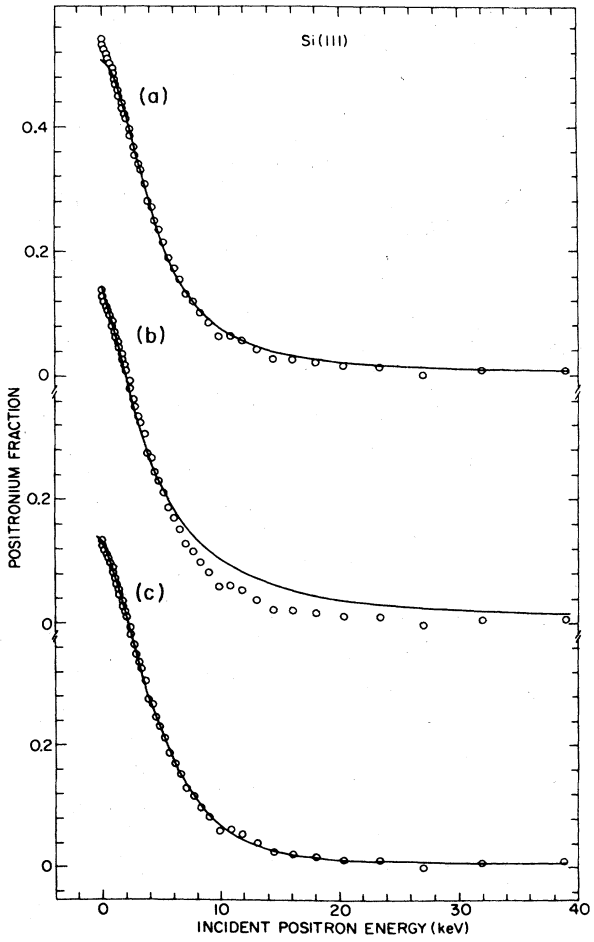

FIG. 66. Ps fraction vs energy for Si(111). The three curves are all the same data compared with fits to (a) exponential profile [Eq. (22)], $n = 2.0$; (b) exponential profile, $n = 1.6$ and energy confined to $0.5 \text{ keV} \leq E \leq 6.0$ keV; (c) Makhovian profile [Eq. (10)] with $n = 1.6$ and $m = 1.4$ (from Nielsen, Lynn, Vehanen, and Schultz, 1985).

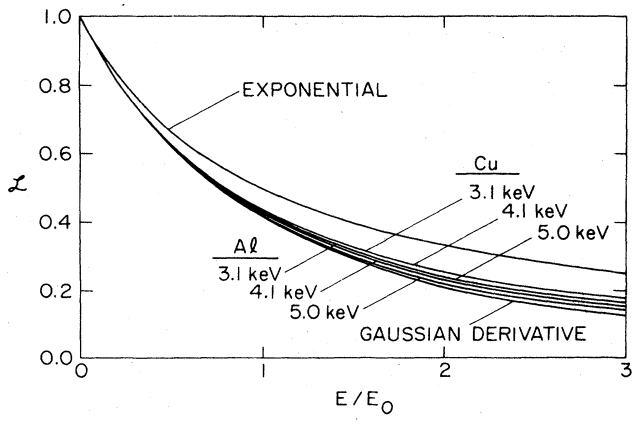

FIG. 67. The Laplace transform of positron stopping profiles [Eq. (21)]. Shown are fits to the experimental results (Mills and Wilson, 1982) for 3.1-, 4.1-, and 5.0-keV positrons incident on Al and Cu. Also shown are the predictions based on the exponential profile [Eq. (22), $m=1$] and the Gaussian-derivative profile [Eq. (26), $m=2$] (after McMullen, 1984).

Sec. II.E) and by Vehanen, Saarinen, *et al.* (1987) in multilayer profiling. The Gaussian-derivative profile is now used almost exclusively, but still needs further scrutiny.

As is clear from the preceding discussion, the ability to extract precise values of D_+ (or L_+, the mean diffusion length) is complicated by uncertainties in the details of the positron stopping profile. The Laplace transforms of different profiles [Eq. (21)] lead to different relationships between D_+ and energy. This is usually expressed for convenience in terms of a characteristic energy E_0 at which half the positrons return to the surface ($F_s=\frac{1}{2}$) by

$$L_+=(D_+\tau_{\rm eff})^{1/2}=(A/A')E_0^n \ , \tag{28}$$

where A ($\sim 400/\rho$ Å/keV^n) is the same constant introduced in Eq. (12), and A' depends on the profile [$A'=1.0$ for the exponential profile, Eq. (22); $A'\sim 1.26$ for the Gaussian-derivative profile, Eq. (26)].

In addition to uncertainties in the profile, there are a variety of experimental parameters that are important, such as knowledge of the reference states of 0% and 100% Ps formation and the response function of the detection system. Dependence of the magnitude of L_+ on such parameters has been discussed by Lynn (1981), Jorch *et al.* (1984), and Schultz, Lynn, and Jorch (1984). There is some evidence that measurements of Ps fractions at energies below a few keV may be influenced by formation with nonthermal positrons (Huomo *et al.*, 1987), but most evidence supports the claim that systematics of L_+ (such as temperature dependence) are not overly sensitive to experimental or profile parameters (Schultz, Lynn, and Nielsen, 1985; Nielsen *et al.*, 1986).

2. Positrons in metals: theory

Positron diffusion in metals is calculated in the relaxation time approximation, which relates the positron diffusion coefficient $D_+(T)$ to the mean (relaxation) time between collisions through the Einstein equation. The model accounts for scattering from phonons, conduction electrons, and impurities (Bergersen *et al.*, 1974). In general it is found that impurity scattering is negligible at temperatures above ~ 25 K or so, and that acoustical-phonon scattering is about 2 orders of magnitude more important than electron scattering, resulting in a dependence on temperature that is universally like $T^{-1/2}$. Because of recent conflicting experimental results for $D_+(T)$, it is useful to review some of the assumptions underlying the theory.

Woll and Carbotte (1967) have calculated the transition rate, $M_e(\underline{k},\underline{k}')$, for conduction-electron scattering of the positron from state $\underline{k}$ into $\underline{k}'=\underline{k}+\mathbf{q}$ in the small-$|q|$ limit required for thermalized positrons. For this they assumed a static screened interaction and the low-temperature limit of the electron Fermi function. Using their result with the additional assumption of diffuse scattering, Bergersen *et al.* (1974) found a relaxation time τ_e, for conduction-electron scattering at temperature T is given by

$$\tau_e=\frac{4}{\pi}(m/m^*)\frac{\hbar E_f}{(k_BT)^2} \ , \tag{29}$$

where E_f is the Fermi energy, k_B the Boltzmann constant, and m the electron rest mass. The phenomenological "effective" mass in the above, m^* (sometimes called the quasiparticle mass), is usually larger than the more familiar band mass used in electron transport theory and arises from three principle contributions (Hyodo *et al.*, 1986). The most important (Mikeska, 1967) is phonon scattering. Since it is more likely for a low-energy positron to absorb a phonon than to create one (because of the number of available phonon states above and below the positron wave vector), there is an asymmetric broadening of the positron's momentum distribution. The other contributions to m^* are the effect of electron density enhancement in the vicinity of the positive particle (Hamann, 1966) and band effects.

Conwell (1967) has calculated the relaxation time for electron-phonon scattering employing the deformation-potential approximation (Bardeen and Shockley, 1950). This approximation represents the coupling of the electron energy with dilations of the lattice. Because carriers and holes in semiconductors have long wavelengths at normal temperatures (~ 100 Å), and so interact primarily with acoustic lattice vibrations of similar wavelength, they can be treated by a continuum theory. Thus the deformation potential ε_d can be seen to represent the weak, long-range potential that results from the shifting of the band edges in nonpolar semiconductors when acoustic phonons set up localized regions of dilated and contracted lattice. Adapting this for positron scattering with phonons in metals, Bergersen *et al.* (1974) obtained

$$\tau_{\rm ph}=\frac{\pi\hbar^4B}{\sqrt{3}\varepsilon_d^2(m^*k_BT)^{3/2}} \ , \tag{30}$$

TABLE V. Positron diffusion coefficients: metals. Positron diffusion coefficient D_+ and its temperature T dependence. All data that were quoted as E_0 rather than D_+ or L_+ were converted using Eq. (28), in which the constant $(A/A')\sim(4/1.26)\sim 3.2$ μgm/cm^2 (determined empirically by Mills and Wilson, 1982, and Vehanen, Saarinen, *et al.*, 1987). η is the power relating D_+ to T: $D_+ \approx D_+(300)(T/300)^{\eta}$. Values for D_+ obtained by other techniques are given by Dupasquier and Zecca (1985) and Paulin (1979). Key to techniques for Tables V and VI are as follows: e^+, positron beam measurement; yield, positron yield vs energy; Ps, Ps vs energy; S, line-shape parameter vs energy; [a] exponential profile, $m=1$, $n=1$; [b] exponential profile, $m=1$, $n=1.6$; [c] Gaussian profile, $m=2$, $n=1.6$, E-min$=0$; [d] Gaussian profile, $m=2$, $n=1.6$, E-min$=4$ keV; [e] Makhovian profile, $m=1.4$, $n=1.6$; bulk, bulk positron technique (Sec. I.B); *e*SR, depolarization measurements.

Material	$D_+(300)$	η	T (K)	Technique	Footnotes
Ag(111)	0.3(1)[a]			e^+-Ps [a]	b
Al	0.4	−0.5		Theory	c
Al		−0.4(2)	80–300	e^+-Ps [a]	d
Al	0.39			e^+-Ps [a]	e
Al poly	2				f
Al foil	0.76(14)			e^+ (transmission)	g
Al(100)		−1.0(4)	370–500	e^+-Ps [b]	h
Al(100)	0.31(1)	−0.8(1)	160–500	e^+-Ps [a]	i
Al(100)	0.33			e^+-Ps [b]	j
Al(110)		−0.7(5)	160–300	e^+-Ps [b]	h
Al(110)		−0.5	20–500	e^+-Ps and S [e]	k
Al(111)		−1.0(3)	160–300	e^+-Ps [b]	h
Al(111)	0.19(1)			e^+-Ps [a]	i
Surface					
Al(100)	1.2	0		Theory	l
Al(110)	1.4	0		Theory	l
Al(111)	1.4	0		Theory	l
C(0001)	0.16			e^+-Ps [c]	m
Cd(1120)		−2.6(4)	170–375	e^+-Ps [b]	h
Cd(0001)		−1.0(2)	40–375	e^+-Ps [b]	h
$CoSi_2$	0.002[n]			e^+-yield	o
Cu	1.56	−0.5		Theory	p
Cu	0.9			e^+-Ps [a]	e
Cu foil	1.06(20)		300	e^+ (transmission)	g
Cu poly	0.415(2)		300	e^+-Doppler	q
Cu(111)	0.9(1)[a]			e^+-Ps [a]	b
Fe	>1.0			*e*SR-diffusion	r
Fe	$<4\times10^{-5}$			*e*SR-hopping	r
Ga	0.4	−0.5		Theory	c
In	0.4	−0.5		Theory	c
InP	0.10(3)[s]			Bulk	t
K	0.4	−0.5		Theory	c

where B is the bulk modulus. In Eq. (30) a factor $(1-\cos\theta)$ was neglected, which would lead to a small numerical correction but essentially the same result (McMullen, private communication). The relaxation time is related to the mobility μ given by Bardeen and Shockley (1950) through the positron effective mass, or

$$\tau=\tfrac{3}{2}(m^*\mu)\ . \tag{31}$$

The applicability of the deformation potential to calculations of positron-phonon interactions in metals is somewhat complicated since, as Bardeen (1956) originally pointed out, conduction electrons would effectively screen any local potential induced by deformation. Nevertheless, in evaluating Eq. (30), Bergersen *et al.* (1974) calculated ε_d [following Hodges and Stott (1973b)] including the volume dependence of the potential due to the positron's zero-point motion, V_0, electron-positron correlation $V_{\rm corr}$, and electron chemical potential μ_-, as

$$\varepsilon_d=\frac{r_s}{3}\frac{dV_0}{dr_s}+\frac{r_s}{3}\frac{dV_{\rm corr}}{dr_s}+\Omega\frac{d\mu_-}{d\Omega}\ , \tag{32}$$

where r_s is the usual free-electron radius and Ω is the unit-cell volume. The above is the volume dependence of the positron's energy in the lattice, which is discussed further in Sec. II.D.2.

The connection between relaxation time and D_+ is made through the mobility μ, using the Einstein relation

$$\mu=\frac{D_+}{k_BT}\ , \tag{33}$$

TABLE V. (*Continued*).

Material	$D_+(300)$	η	T (K)	Technique	Footnotes
Li	0.7	−0.5		Theory	c
Mg	0.5	−0.5		Theory	c
Mo(110)		−0.9(3)	475–1000	e^+-Ps [b]	h
Mo(111)		−0.86(3)	300–1400	e^+-Ps [c]	u
Mo(111)	1.2(1)	−0.50(4)	300–1400	e^+-Ps [d]	u
Na	0.7	−0.5		Theory	c
Nb(110)		−0.8(1)	300–1750	e^+-Ps [b]	h
Ni	0.7			e^+-Ps [a]	e
Ni poly	0.73(1)		300	e^+-Doppler	q
Sn(100)	0.04			e^+-Ps [a]	v
Tl	0.4	−0.5		Theory	c
W	1.26	−0.5		Theory	p
W	1.4			e^+-Ps [a]	e
W(111)	8.5(4.0)			e^+-yield [a]	w
Zn	0.5	−0.5		Theory	c
Zn-22% Al	0.6			Bulk	x

[a]Data for 400 K.
[b]Lynn and Welch, 1980.
[c]Bergersen, Pajanne, Kubica, Stott, and Hodges, 1974.
[d]Lynn, Schultz, and MacKenzie, 1981.
[e]Vehanen, Lynn, Schultz, Cartier, Güntherodt, and Parkin, 1984.
[f]McKee, Stewart, Manis, and Sang, 1979.
[g]Mills and Wilson, 1982.
[h]Schultz, Lynn, and Nielsen, 1985.
[i]Lynn and Lutz, 1980a.
[j]Lynn and Schultz, 1985b.
[k]Vehanen, 1988.
[l]Nieminen and Puska, 1983.
[m]Sferlazzo, Berko, Lynn, Mills, Roellig, Viescas, and West, 1988.
[n]Assuming $\tau=220$ psec.
[o]Gullikson, Mills, and Phillips, 1988.
[p]Schultz, 1983, unpublished [based on theory of (c) above].
[q]Triftshauser and Kögel, 1982a.
[r]Seeger, Major, and Jaggy, 1985.
[s]Data for 77 K.
[t]Beling, Simpson, Stewart, Wang, Fung, Wai, and Sun, 1987.
[u]Huomo, Vehanen, Bentzon, and Hautojärvi, 1987.
[v]Mills, 1981a.
[w]Wilson and Mills, 1983a.
[x]McKee, Carpenter, Watters, and Schultz, 1980.

which is generally applicable for any charged particle that obeys Maxwell-Boltzmann statistics. Recently Hyodo, McMullen, and Stewart (1986) have shown that the positron momentum is not a Maxwell-Boltzmann distribution in potassium single crystals, but the difference is probably not significant in the present context. The positron-phonon interaction, and in particular the strength of the coupling, has been reviewed recently by McMullen (1985). He concludes that strong positron–acoustic-phonon coupling effects are not seen in the metals for which data are available, so that the $T^{-1/2}$ dependence of D_+ resulting from Eqs. (30) and (33) should be correct as far as the assumptions outlined at the beginning of this section are valid. Theoretical estimates of D_+ for metals are listed in Table V, together with experimental results.

3. Surface diffusion theory

Applying the same type of diffusion model to the surface, Nieminen and Puska (1983) have shown that surface (i.e., two-dimensional) diffusion can be calculated for positrons localized in the two-dimensional surface state (see Sec. II.D.3). In their model, the relaxation time for scattering from acoustic phonons, $\tau_{\rm ph}^{\rm 2D}$, is

$$\tau_{\rm ph}^{\rm 2D}=\frac{\hbar\rho_a\langle c^2\rangle}{m''(\varepsilon_d'')^2 k_B T}\ , \tag{34}$$

and for impurities

$$\tau_i^{\rm 2D}=\frac{2\pi\hbar^3}{n_i A_{\rm cell} V_i^2 m''}\ , \tag{35}$$

where ρ_a is the areal mass density of the surface, $\langle c \rangle$ the average surface sound velocity, m'' and ε_d'' the *surface* effective positron mass and deformation potentials, respectively, n_i the impurity concentration, A_{cell} the surface unit-cell area, and V_i the average potential difference between a host and impurity cell. Nieminen and Puska (1983) used a corrugated-mirror model for the surface potential to evaluate ε_d'', which simply replaces the planar approximation with a more realistically modulated potential. They calculated D_+^{2D} for Al surfaces and found (a) D_+^{2D} is in general larger than D_+ for three-dimensional bulk diffusion in the same material. This is primarily due to the fact that ε_d'' for the surface is smaller than ε_d for the bulk. (b) The smaller ε_d'' coupled with the fact that the host-impurity potential difference V_i is in general larger on a surface than in the bulk means that impurity scattering may be much more important for surface diffusion. (c) The T^{-1} dependence in Eq. (34) results in a temperature-independent surface-diffusion coefficient [cf. with Eq. (33)].

Their calculations for surface-diffusion coefficients D_+^{2D} are included in Table V, although there have so far been no experimental measurements of surface diffusion. It may turn out that a delocalized positron does not exist in the surface state for most materials, but rather all positrons are coupled with surface defects or impurities (see Sec. II.D).

4. Positrons in metals: observations

Until ~1980 experimental studies of positron diffusion in solids were limited to bulk techniques (cf. Sec. I.B), which were briefly reviewed by Paulin (1979). Two examples more recent than this are the study by McKee *et al.* (1980) of positron trapping at grain boundaries in Zn/Al alloys and the study of positron depolarization in Fe presented by Seeger *et al.* (1985). While the results of some of these bulk studies are included in Table V, the current emphasis is on studies done with variable-energy positron beams.

Values for D_+ and L_+, as discussed in Sec. II.C.1, can be taken from measurements of the positron back-diffusion probability to the sample surface as a function of incident positron energy. In the earliest reports of temperature-dependent studies it was generally assumed that the simple $T^{-1/2}$ dependence predicted theoretically was correct (e.g., Lynn and Lutz, 1980a; Mills, 1980c; Schultz *et al.*, 1982). A systematic compilation of data for L_+ [Eq. (28)] versus temperature in a variety of materials was presented by Schultz, Lynn, and Nielsen (1985), showing the first evidence that the temperature dependence of D_+ was possibly more negative than $T^{-1/2}$. These results, which are shown in Fig. 68, also indicate that the diffusion in Cd is anisotropic. Because defects are very difficult to anneal out of Cd in vacuum, it may be that some of the results were affected by defect interactions (e.g., nonthermal trapping). However, as mentioned in the original report (Schultz, Lynn, and Nielsen, 1985), this would only lead to a stronger dependence of D_+ on temperature than is indicated in Fig. 68. Neither the anisotropy nor the large values of the temperature dependence are as yet understood, although various suggestions offered have included dynamic screening of the positron when scattering from phonons, or contributions from (previously neglected) transverse phonon scattering (Singh *et al.*, 1988).

The change of the temperature dependence for aluminum data in Fig. 68 (below ~100 K) has recently been shown to be associated with nonthermal positrons. When the data are analyzed using only those positrons with 2000-eV incident energy or higher, the Finnish group finds that the temperature dependence of D_+ is consistent with $T^{-1/2}$ from ~20–500 K (Vehanen, 1988). This observation coupled with the recently observed resonant trapping at vacancies (see Secs. II.B.2 and II.E.1) suggests that nonthermal positron trapping in the surface state may be responsible for the low-temperature discrepancy.

Huomo, Vehanen, Bentzon, and Hautojärvi (1987) have in fact suggested that the anomalously large values of the temperature dependence indicated in Fig. 68 may all be the result of systematic problems with the fitting procedure of the Ps fraction data [see Eqs. (22) to (24)]. Their conclusion is that data acquired below 4 keV (for

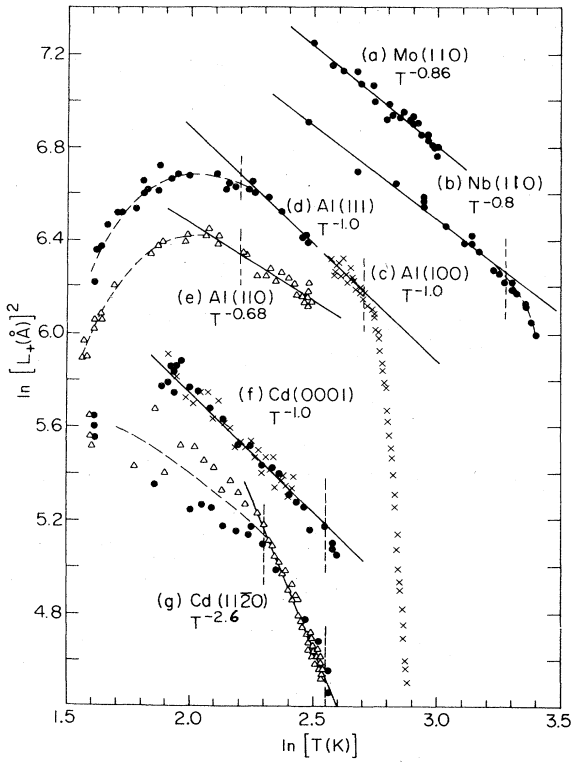

FIG. 68. Positron diffusion length squared, L_+^2 vs temperature for several metals. The slopes of the lines are larger than the theoretically predicted $-\frac{1}{2}$, which is based on positron/acoustic phonon scattering (from Schultz, Lynn, and Nielsen, 1985).

Mo and Ag) should not be used because reemission of nonthermal positrons leads to erroneous values of L_+ (and therefore D_+). Their results when fit in this way (Fig. 69) exhibit a weaker dependence on temperature than those of Schultz *et al.* (1985), yielding $T^{-0.5}$ for Mo and $T^{-0.6}$ for Ag. Huomo and co-workers have also recently obtained a similarly weak temperature dependence for D_+ in Al (Huomo, Vehanen, and Hautojärvi, 1987). The most important point that these authors make is that results obtained for positron back-diffusion to a solid surface still contain uncertainties in *both* the data acquisition and the analysis procedure. One aspect of data analysis presently being investigated by this group is whether or not nonlinearities in the analysis for f [Eqs. (8) and (9)] may be introducing errors that are not present when data are analyzed using the line-shape parameter S.

Howell, Rosenberg, Meyer, and Fluss (1987a) have observed emission of nonthermal Ps from Pb up to incident positron energies of 3 keV. By measuring the energy distribution of the nonthermal Ps (i.e., $K \gtrsim 1$ eV), they were able to show that the *intensity* of the nonthermal component varies as K^{-2}, where K is the Ps energy. This dependence can be seen from the data to vary slightly with incident energy. They attribute this power-law dependence, also observed by Mills and Crane (1985a), to details of the positron energy loss in the solid. The study of nonthermal contributions to both e^+ and Ps emission from surfaces is certainly one that will be studied in much greater detail in the future, since the motion of thermalized positrons in metals is not only of fundamental interest but also important for the application of the technique to other areas (e.g., defect and interface studies; see Sec. II.E).

5. Positrons in semiconductors

The experimental results for positron diffusion in semiconductors are even more poorly understood than those

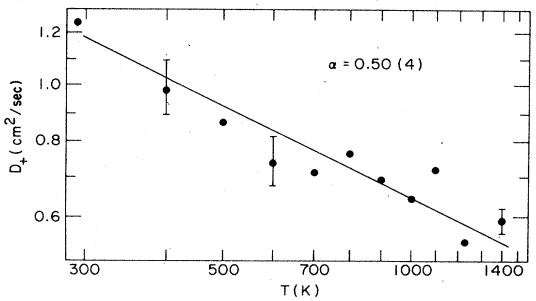

FIG. 69. Positron diffusion coefficient ($D_+ \alpha L_+^2$) vs temperature for Mo(111). The temperature dependence is in this case consistent with the predicted $-\frac{1}{2}$ slope, when the minimum incident positron energy included in the fit of Eq. (26) to the data is 4 keV (from Huomo, Vehanen, Bentzon, and Hautojärvi, 1987).

for metals. The comparison is in fact quite general for experimental positron studies of semiconductors and metals. The first studies were *bulk* Doppler-broadening measurements of the positron mobility in solid-state Ge and Si detectors (Mills and Pfeiffer, 1976, 1977), yielding values for D_+ that were comparable with other solids (i.e., ~ 1 cm^2/sec) but a particularly weak dependence of D_+ on temperature for Ge (see Table VI). These measurements were followed by positron beam studies of D_+ vs temperature in Ge (Jorch, Lynn, and MacKenzie, 1981). In this work it was observed that E_0 [see Eq. (28)] and therefore D_+ did not follow any simple model. These data, which are shown in Fig. 70, were fit instead by a model that included the formation of a small positron-polaron state (solid lines in the figure). The positron coupling with the Ge lattice was examined in more detail by Jorch, Lynn, and McMullen (1984). It should be noted that it was assumed in all of the above work that the measurements were of diffusion of thermal positrons in the crystalline solid. The recent observations of in-

TABLE VI. Positron diffusion coefficients: semiconductors. Experimental values of D_+ and its temperature dependence η. See Table V for key to techniques.

Material	$D_+(300)$	η	T (K)	Technique	Footnotes
Ge	0.9[a]	−0.1	36–93	Doppler shift	b
Ge(100)	0.5	See text	300–1000	e^+-Ps [b]	c
Ge(110)	0.2	See text	300–1000	e^+-Ps [b]	c
Ge(111)	0.5	See text	300–1000	e^+-Ps [b]	c
Si	3.2[a]	−0.4	80–184	Doppler shift	d
Si(111)	2.7(3)			e^+-Ps [e]	e
Cz-Si(100)	2.1(2)			e^+-S [e]	f
FZ-Si(100)	2.7(2)			e^+-S [e]	f

[a]Data for 80 K rather than 300 K.
[b]Mills and Pfeiffer, 1976.
[c]Jorch, Lynn, and MacKenzie, 1981; Jorch, Lynn, and McMullen, 1984.
[d]Mills and Pfeiffer, 1977.
[e]Nielsen, Lynn, Vehanen, and Schultz, 1985.
[f]Schultz, Tandberg, Lynn, Nielsen, Jackman, and Denhoff, 1988.

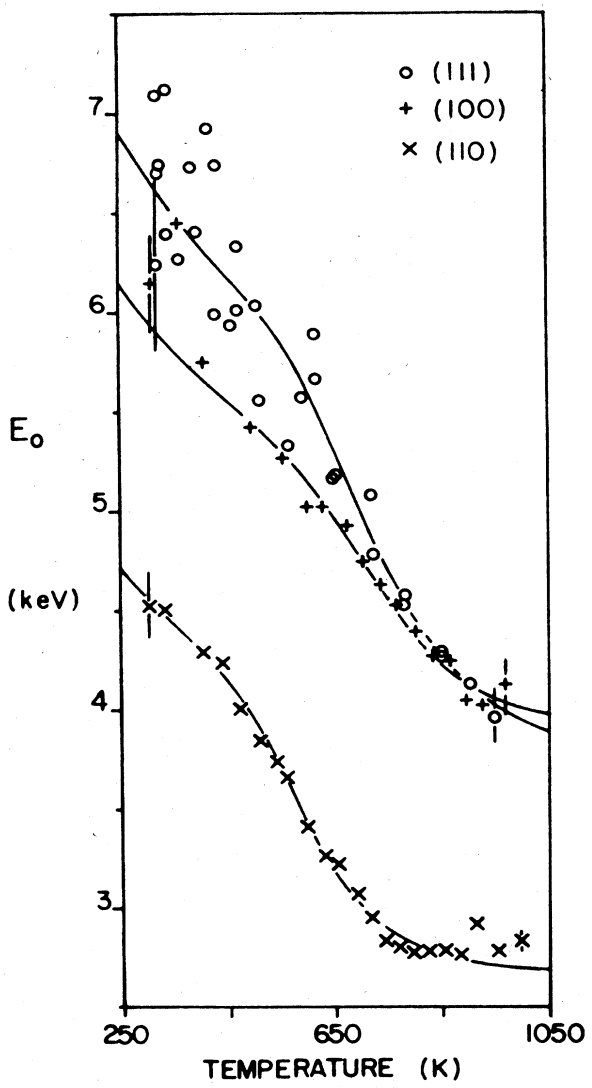

FIG. 70. Positron diffusion parameter E_0 for Ge [see Eq. (28)]. These data were fit (solid lines) by a polaron model for the positron motion as opposed to the conventional diffusion model (from Jorch *et al.*, 1981).

complete thermalization of positrons in insulators, discussed in Sec. II.B, suggest that the interpretation of the results shown in Fig. 70 may be influenced by the temperature dependence of positron thermalization.

Another detailed study of positron diffusion was carried out for several Si crystals by Nielsen, Lynn, Vehanen, and Schultz (1985). This work, which was discussed in Sec. II.C.1 in relation to the data analysis (see Fig. 66), also revealed unusual features of the temperature dependence of E_0. As the results in Fig. 71 show, there is a sharp decrease in the diffusion length near room temperature relative to the tendency expected from results at higher temperatures. This decrease is attributed to an electric field caused by an inversion layer at the surface of the Si. It is well known that thermal treatment of Si can deplete the oxygen near the surface [normally

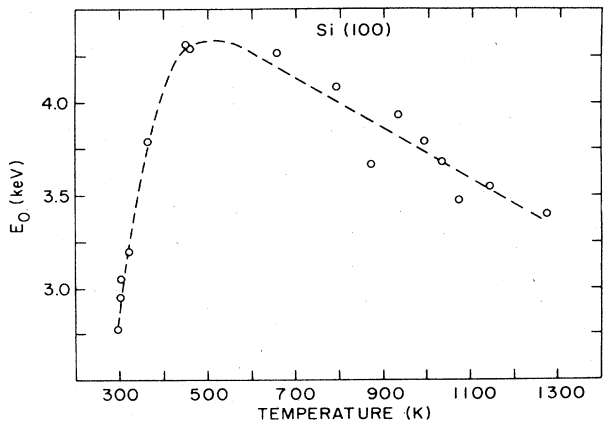

FIG. 71. Positron diffusion parameter E_0 as a function of temperature for Si(100). The low-temperature effect (300–500 K) is reproducible, following annealing of the sample to ~1300 K (from Nielsen, Lynn, Vehanen, and Schultz, 1985).

$\sim 10^{18}$ cm^{-3} for Czochralski-grown (Cz-), silicon], which would lead to trapping of charge in the surface region. The effect observed did not show any hysteresis with temperature, and it was removed by low-energy sputtering of the sample, confirming that the cause was related to the electric field at the surface.

Now that semiconductors are being studied more routinely using bulk-positron and positron beam techniques, the influence of electric field on positron motion must be considered. For example, some of the silicon-silicon epilayers studied by Schultz, Tandberg, Lynn, *et al.* (1988) show clear evidence of polarization effects due to known impurities trapped at the epilayer interface (see Fig. 118 and the discussion in Sec. II.E.4). In Fig. 72 we show fairly typical line-shape parameter (S) data for a Cz-Si(100) crystal. The solid curve that goes through the data is generated by an iterative solution to the diffusion

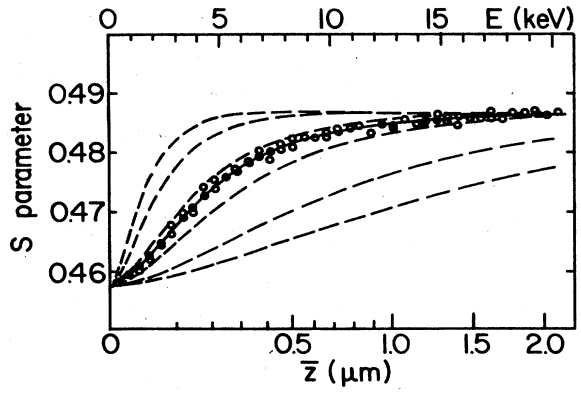

FIG. 72. Positron annihilation line-shape parameter S vs incident energy E for Czochralski-grown (Cz) Si(100). The data are fit (solid line) assuming $D_+ = 2.1$ cm^2/sec and no effect due to electric field. The other six curves show the effect of electric fields of strengths 10^3, 5×10^3, and 10^4 V/cm on positron motion, with the fields directed into the bulk (upper three curves) and out towards the surface (lower three curves).

equation (13), assuming $D_+ = 2.1$ cm^2/sec, and no effect due to either field-induced mobility or defect trapping. Also shown on the figure are curves generated including the effects of uniform electric fields of 10^3 V/cm, 5×10^3 V/cm, and 1×10^4 V/cm originating from negative (curves above the data) and positive (below the data) charges at the surface. Fields of 10^3–10^5 V/cm are fairly typical for abrupt *p-n* junctions (e.g., Sze, 1981, p. 248).

Results for D_+ and its temperature dependence η are summarized for semiconductors in Table VI. Although there are relatively few studies of positron motion in semiconductors, the analogy with hole mobility and the possible extension of such studies to new kinds of materials (e.g., superlattices; see Sec. II.E) will ensure that this area will be emphasized much more in the future.

6. Positronium diffusion

If the deformation-potential approximation described above can be used for describing Ps diffusion properties in solids, then the formalism is also much the same as that derived above for positrons (Hyodo, 1985). The most important scattering mechanism for neutral Ps is the interaction with longitudinal-acoustic phonons. Here we get

$$\Gamma(\rho,\omega)=\frac{\varepsilon_d^2 (M_{\rm Ps}^*)^{3/2}\omega^{1/2}k_B T}{2^{1/2}\pi\hbar^3\rho s^2}\ , \tag{36}$$

where $\Gamma(\rho,\omega)$ is the imaginary part of the Ps self-energy, ω is the phonon frequency, $M_{\rm Ps}^*$ is the Ps effective mass, ρ is the density, and s is the sound velocity in the solid. The simplest description of the self-energy of a particle is the difference between its *bare* energy and its energy in an interacting system. In this case, the imaginary part of the self-energy depends on the relaxation time for Ps scattering (McMullen, 1985) as $\tau_{\rm ph}^{\rm Ps}=\hbar/\Gamma$, and the Ps diffusion coefficient is therefore estimated as

$$D_{\rm Ps}\approx\frac{\hbar}{\Gamma(\rho,k_B T)}\frac{k_B T}{M_{\rm Ps}^*}\ . \tag{37}$$

As an example, Kakimoto *et al.* (1985) found $\varepsilon_d = 7.6$ eV and $M_{\rm Ps}^* = 2.10 m_e$ for MgF_2 and estimated a Ps diffusion coefficient at 300 K to be about 1.7 cm^2/sec. Bulk measurements of this type, done using ACAR (see Sec. I.E), complement the $D_{\rm Ps}$ estimates that can be deduced using positron beam techniques and are discussed in reviews by Paulin (1979), Dupasquier (1981), and Dupasquier and Zecca (1985).

Incident beams of positrons have been used to study Ps diffusion in crystalline and amorphous ice (Eldrup *et al.*, 1983, 1984, 1985), in a variety of ionic solids (Mills and Crane, 1984), and on oriented crystals of quartz (Sferlazzo *et al.*, 1987), all of which are summarized in Table VII. The diffusion coefficients are all small (on the order of 0.1 cm^2/sec or less). The thermally assisted diffusion usually predicted for Ps would lead to a very small diffusion coefficient, $D_{\rm Ps}\le 10^{-3}$ cm^2/sec, which is consistent with many of the observations or calculations listed in Table VII. In addition, the temperature dependence where measured is usually found to be small, if not zero. An example of this is shown in Fig. 73 where E_0 is plotted for two separate crystals of ice (Eldrup *et al.*, 1985). These data correspond to values of $D_{\rm Ps}$ ranging from $\sim$0.10 cm^2/sec ($E_0 = 1700$ eV) to $\sim$0.33 cm^2/sec ($E_0 = 2100$ eV) using Eq. (28), where the E_0 values are

TABLE VII. Positronium diffusion: The Ps diffusion coefficient $D_{\rm Ps}$ and its temperature dependence η for a variety of materials. The techniques referred to are positron beam studies (e^+), such as those discussed in the text, and angular correlation of annihilation radiation (ACAR), which was described in the first part of the review.

Material	$D_{\rm Ps}(300)$	η	T (K)	Technique	Footnotes
Crystalline ice	0.17(9)	$\approx$0	44–150	e^+	a
SiO_2(0001)	0.07(3)		300	e^+	b
SiO_2	$>$0.26	$\approx$0	100–700	ACAR	c
SiO_2	0.047(13)			e^+	d
SiO_2 powder	1.5×10^{-5}			ACAR	e
MgF_2	1.7		300	ACAR	f
NaF	$>$0.31(2)	$\approx$0	4.5–155	ACAR	c
NaF	0.008(4)		600	e^+	g
NaF	0.09			Theory	h
KCl	0.0010(5)		600	e^+	f
KCl	0.005			Theory	h

[a]Eldrup, Vehanen, Schultz, and Lynn, 1985.
[b]Sferlazzo, Berko, and Canter, 1987.
[c]Dupasquier, 1984.
[d]Sferlazzo, Berko, and Canter, 1985.
[e]Brandt and Paulin, 1968, 1972.
[f]Kakimoto, Hyodo, and Fujiwara, 1985.
[g]Mills and Crane, 1984.
[h]Boev and Arefiev, 1985.

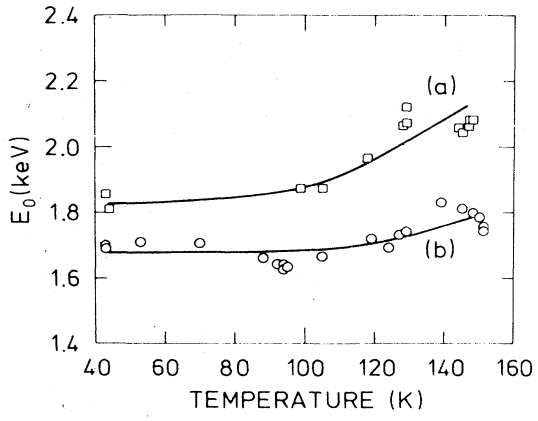

FIG. 73. Diffusion parameter E_0 for Ps in crystalline ice as a function of temperature. The lines are only guides for the eye, and the two curves are for two different ice crystals grown *in situ* in the vacuum system (from Eldrup *et al.*, 1985).

deduced from the slope of data such as the extreme right-hand side of Fig. 63 ($E > 10^3$ eV). The discrepancies being found between D_{Ps} as measured by positron beams and bulk ACAR techniques remain as unsolved problems to be studied in the future.

D. Surface processes

Much of the research done with variable-energy positron beams involves the surface in one way or another. For example, most of the diffusion studies described in Sec. II.C are possible because of the unique signature of positrons that return to the surface after thermalizing at some distribution of depths in the solid. This sensitivity can be understood, at least qualitatively, by referring to the single-particle potential for a positron near a surface (shown previously in Fig. 8). For a thermalized positron approaching the surface from inside the metal, the most common interaction processes are the following.

(i) Reemission into the vacuum as a free positron either without energy loss (elastically) or having lost energy (inelastically). This will occur for thermalized positrons only if the positron work function, φ_+, is negative.

(ii) Localization of the positron in a surface state. This occurs because of the image-induced potential well at the surface (Fig. 8). It is possible that surface defects or impurities may bind positrons in even deeper traps, or that a Ps-like state may form (Sec. II.D.3), but these details are not yet known.

(iii) Energetic Ps emission by the pickup of a *near-surface* electron, which is possible if the binding energy (6.8 eV) is greater than the sum of electron (φ_-) and positron (φ_+) work functions. Excited (Ps*) and negatively charged (Ps^-) states of energetic Ps have been observed, but they are generally of lower intensity (Mills, 1981b; Schoepf *et al.*, 1982).

(iv) Thermal Ps emission by excitation of a surface-bound positron out of the "surface state." For most metal and semiconductor surfaces, this occurs at elevated (approximately a few hundred °C) temperatures.

(v) Reflection of the positron wave function by the attractive (if φ_+ is negative) or repulsive (if φ_+ is positive) potential step at the surface.

It is important to recognize that these fates are fundamentally different from those available to a positron approaching the surface from outside the metal, with the exception of trapping and energy loss at the surface potential well (including reflection), which were discussed in Sec. II.B.2. In this section we shall restrict our discussion to the case of those positrons which interact with the surface by approaching from inside the solid.

The positron reflection coefficient, which is proportional to β in Eq. (15), Sec. II.C.1, was predicted by Nieminen and Oliva (1980) to be dependent on temperature. However, various experimental results (Lynn, Schultz, and MacKenzie, 1981; Schultz and Lynn, 1982) indicate that the fraction of positrons transmitted through the potential step at the surface is weakly dependent on temperature. This discrepancy was explained by Wilson (1983) as being the result of inelastic processes (see Sec. II.B.2), but it has also been suggested to be the result of multiple approaches (from inside the solid) of positrons to the surface (Neilson *et al.*, 1986a). There is also some disagreement on a theoretical description for the branching ratios (i.e., relative probabilities) of the above processes, although most models are correlated with the magnitude of the positron work function φ_+ (e.g., Kreuzer, Lowy, and Gortel, 1980; Nieminen and Oliva, 1980; Neilson, Nieminen, and Szymanski, 1986a). Discrepancies between predicted and measured branching ratios may be related to many-body effects (Wilson, 1982) or (as above) to the "multiple approach" model of Neilson, Nieminen, and Szymanski, (1986a). Specific differences will be discussed in the following sections. It is, nevertheless, a relatively general result for metals where φ_+ is negative that at room temperature the division is roughly equal between (i) reemitted positrons, (ii) surface trapped positrons, and (iii) energetic Ps.

A technical, but nevertheless important, feature of the branching ratios for the various positron fates at the surface has been discussed by Schut *et al.* (1988) and Baker *et al.* (1988). The study of positron back-diffusion to the surface, which is of particular importance for the defect studies described in Sec. II.E, is usually done by monitoring either the Ps fraction f or a line-shape parameter S (see Sec. I.E). Any change in the surface that affects the branching ratio for Ps (such as adsorbtion of an impurity, or temperature changes) must be considered in the analysis of the data. The fraction of the incident positron beam which would normally be backscattered or reemitted as thermal or epithermal positrons can be (experimentally) returned to the target or allowed to escape. By measuring both f and S for both of these situations, Schut and co-workers show how careful accounting of all the particles allows a determination of the exact branch-

ing ratios. A point they emphasize is that whenever the branching ratio for Ps is nonzero, both parameters f and S must be simultaneously measured for accurate results, since the very narrow line shape resulting from p-Ps will affect the determination of back-diffusion.

1. Reemitted positrons

The following discussion of the positron reemission process will in general be restricted to metal surfaces for which φ_+ is (necessarily) negative. There is much less known about the mechanism of positron reemission from nonmetallic surfaces primarily because there are fewer experimental results than for metals. A notable exception is the recent observation of nonthermal positron emission from rare-gas solids discussed in Sec. II.B.4. This is the result of the inability of positrons to thermalize completely before reaching the surface of any material with filled electronic shells and no optical phonons (which would allow greater energy loss than the acoustic branch). Positron work functions that have been measured or calculated so far are listed in Table VIII.

The earliest indirect measurements of the angular distribution of positrons reemitted from negative φ_+ surfaces (Murray and Mills, 1980) supported the view that the emission process was relatively elastic and that the angular distribution of positrons was sharply peaked about the surface normal. These data also indicated that the positron yield, or emission rate Y_0, increases as φ_+ becomes more negative for many metals. Recently Gullikson, Mills, and Murray (1988) measured Y_0 for Ni(100) and Cu(111) surfaces by systematically varying φ_+. They found that the data (as earlier) are consistent with two models. The first is a resonant-electron-transfer model derived from the theory for ion neutralization (Yu and Lang, 1983; Lang, 1983), which predicts that lower-energy positrons form Ps more efficiently than those at higher energies (solid curve, Fig. 74). The second model relates the positron emission rate to the density of final states of the emitted positron (dashed curve; Mills, Pfeiffer, and Platzman, 1983). At the present time, neither model includes effects due to recoil or many-body processes, although these are likely to be small.

As more data were acquired for various surfaces, it became evident that inelastic processes were also important, and (depending on the surface) that virtually any fraction of the reemitted positrons could have kinetic energies between 0 and φ_+ (see, for example, Schultz and Lynn, 1982; Wilson, 1982, 1983; Wilson and Mills, 1983a, 1983b). When measuring the integral energy distribution with a magnetically guided beam, one finds that the angular distribution is convoluted with the total energy, so the interpretation of a broad energy distribution can be ambiguous (see Sec. I.E.1). The broad energy contribution for a variety of surfaces is clearly shown in Fig. 75, which is a plot of the integral energy distributions of reemitted positrons (Wilson, 1983). Data of this type were described in Sec. I.E, but the important feature is that the elastic contribution leads to a steep slope in the integral distribution, broadened only by the instrumental resolution (which is of the order of $\sim$0.1 eV) and the thermal spread of the positron ensemble. Reemission from the oxygenated W(111) surface appears to be almost entirely inelastic or spread over large angles, whereas that for either Al(100) or Cu(111) + S is primarily elastic. There are still insufficient data for well-characterized surfaces for us to fully understand the extent to which the positron reemission process is inelastic.

This work was supported by other studies which revealed that contaminated surfaces were often responsible for wide energy distributions of reemitted positrons. The differential total energy measurements reported by Fischer (1984; Fischer, Lynn, and Gidley, 1986) demonstrated

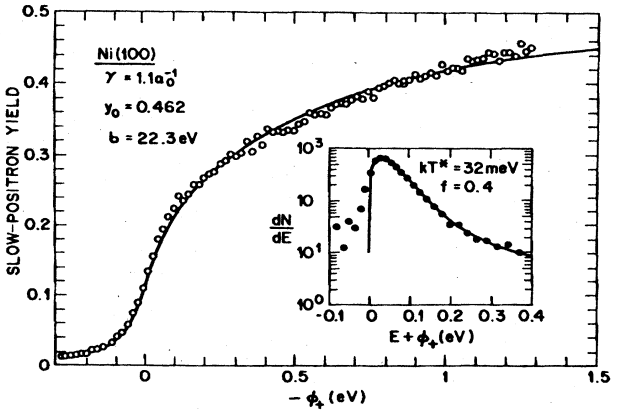

FIG. 74. The slow-positron yield for Ni(100) and Cu(111) vs the positron work function. The curves through the data points are fits: the solid curve is derived from a resonance tunneling model (Yu and Lang, 1983), and the dashed curve is derived from a theory for Ps production (from Gullikson, Mills, and Murray, 1988).

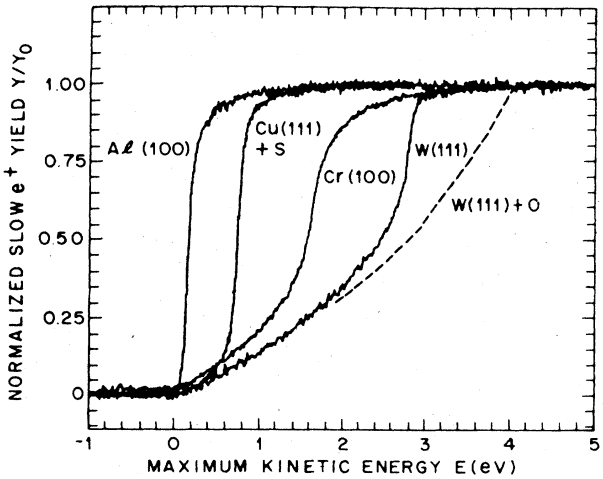

FIG. 75. Integral energy distributions for positrons reemitted from various surfaces. The spectra give the ratio of the number of positrons emitted with energy less than E to the total number emitted (from Wilson, 1983).

TABLE VIII. Work functions and potentials. Values of positron and electron chemical potentials (μ_+ and μ_-), work functions (ϕ_+ and ϕ_-), and energetic Ps formation potentials (ϵ_{Ps}). Positron yield Y and Ps emission fractions f are listed where known, as are the thermal desorption properties, including the binding E_b and activation energies E_a. All quantities are experimentally determined, unless indicated with (th) for theoretical.

	(a) Face-independent properties					(b) Face-dependent properties: e^+ and e^-				(c) Face-dependent properties: Ps		
Material	ϵ_{Ps} (eV)	μ_-(th) (eV)[c]	μ_+(th) (eV)[c]	ϵ_{Ps}(th) (eV)[c]	Face	ϕ_-[a,b] (eV)	ϕ_+(th) (eV)	ϕ_+ (eV)	Y_0 (%)	E_b (eV)	E_a (eV)	f_0 (%)
Ag					Ag(100)	4.64(2)	+0.72[c]	>0[d]	0	2.4(1)	0.4(1)[e]	40[e]
							+2.4[f]					
					(110)	4.52(2)	+0.84[c]					
					(111)	4.74(2)	+0.62[c]			2.5(1)	0.5(1)[e]	35[e]
							+2.4[f]					
Al	−2.8(3)[g]	−0.74	−3.35	−2.71	Al(100)	4.41(3)	−0.32[c]	−0.16(3)[h]	20[i]	2.80	0.41(2)[i]	62[i]
	−2.58(3)[j]						−0.5[i]	−0.19(5)[k]	21[a]			
					(110)	4.28(3)	−0.19[c]		9[a]			
					(111)	4.24(3)	−0.15[c]	+0.065(3)[h]	6[i]	2.89	0.33(2)[l]	60[i]
									14[a]			
Au	−2.0(2)[g]				Au(111)	5.2	+1.1[f]	>0[m]	0			
Be					Be(0001)	5.10(2)	−0.5[n]	>0[o]				
Cr	−4.10(4)[o]	−0.42	−4.57	−4.10	Cr(100)	4.46(6)	−1.76[c]	−1.76(5)[o]				21[o]
Cu	−2.5(3)[d,e,g,a]	−1.59	−3.22	−1.99	Cu(100)	4.59(3)	+0.22[c]			2.77(5)	0.56(2)[p]	
					+S	4.87		−1.2[q]		2.91(8)	0.98(3)[p]	50(5)[r]
					(110)	4.48(3)	+0.33[c]	−0.13(8)[s]		2.97(5)	0.64(2)[p]	
					+S	4.88		−0.4[s]		2.54(7)	0.61(2)[p]	50(3)[p]
					(111)	4.85(3)	−0.13[c]	−0.4(1)[s]	39(5)[t]	2.45	0.5(1)[e]	
								−0.33[q]	28(3)[r]			
					+S	5.14		−0.87[q]	55(5)[r]	2.56	0.9(1)[d]	50(5)[u,e,a]
								−0.78(5)[k]				
Mo		−0.04	−1.88	−4.88	Mo(100)	4.53	−2.65[c]	−1.7[v]	23[v]			
					+O			−2.7[v]	37[v]			
					(110)	4.95	−3.03[c]					
					(111)	4.55	−2.67[c]					
Ni	−2.6(3)[g]	−1.55	−2.91	−2.35	Ni(100)	5.22(4)	−0.77[c]	−1.0(1)[w]	39(2)[a]	2.33(7)	0.75(5)[x]	52
							−0.4[f]	−1.3(1)[y]	45(5)[t]			
					+O			−0.95[x]				
					C2×2-CO			−1.6[x]				
					C2×2-S			−1.6[x]				
					(110)	5.04	−0.59[c]	−1.4(1)[q]				
					(111)	5.35	−0.90[c]					
							−0.4[d]					
Pb	−0.73(7)[g]	−1.58	−3.98	−1.25	Pb(100)	4.01	+1.55[c]	+2.06[z]	0			
Pt					Pt(100)			−1.9(1)[aa]	14[aa]			
					+CO			−2.2(1)[aa]	24[aa]			
Sn					Sn(100)	4.4	+2.7[bb]	>0[cc]	0	2.8	0.38(2)[cc]	47[cc]
W	−4.9(1)[dd]				W(100)			−3.0[ee]				
					(110)			−3.0(2)[ff]	33[ff]			

TABLE VIII. (*Continued*).

	(a) Face-independent properties				(b) Face-dependent properties: e^+ and e^-				(c) Face-dependent properties: Ps		
Material	ϵ_{Ps} (eV)	μ_-(th) (eV)[c]	μ_+(th) (eV)[c]	ϵ_{Ps}(th) (eV)[c]	Face	ϕ_-[a,b] (eV)	ϕ_+(th) (eV)	ϕ_+ (eV)	Y_0 (%)	E_b (eV)	E_a (eV)	f_0 (%)
					+ C			−2.9(1)[q]				
					+ O			−4.1(2)[q]				
					+ Cu/θ=1.5			−3.0/−1.2(1) (W/Cu)[q]				
					+ Cu/θ=3			−3.1/−0.6(1) (W/Cu)[q]				
					(111)	4.47(2)	−2.1[f]	−2.6(1)[dd]	40(5)[dd]			
					+ O			−4.0(1)[dd]	53(5)[dd]	2.8(1)	0.5(1)[dd]	
Metal polycrystals												
Mo					Mo			<0[gg]				
Nb					Nb			<0[gg]				
Ni					Ni			<0[w,gg,hh]				
Ta					Ta			−1.2				
W	−4.3[ii]				W			−3(1)[hh]				
Other solids												
C(0001)					C(0001)			+ 1.4(5)[jj]				
Si					Si(100)	4.91(5)	+ 2.04[c]			2.06(7)	0.17(3)[p]	50(5)[v]
					(111)	4.74(5)	+ 2.21[c]	~0[kk]	10[a]	2.69(7)	0.49(5)[p]	50(5)[v,ll]
Ge					Ge(111)	4.8	+ 1.98[c]			2.8	0.83(7)[a]	75(5)[ll]
$CoSi_2$					$CoSi_2$	4.62(7)[mm]		−0.46(5)[mm]	23(1)[mm]			
Ne	2.2(2)[nn]				Ne			+ 0.6(1)[nn]	70(3)[oo]			
Ar	4.0(2)[nn]				Ar			+ 1.55(5)[nn]	67(3)[mm]			
Kr	5.1(2)[nn]				Kr			+ 2.00(5)[nn]	63(3)[mm]			
Xe	5.4(2)[nn]				Xe			+ 2.30(5)[nn]	50(3)[mm]			
SiO_2					SiO_2				15[pp]		0.15[qq,pp]	40[pp]
LiF					LiF			−0.7[rr]				
NaF					NaF			+ 0.5[rr]	40[rr]			

[a]Mills, 1981a.
[b]Hölzl and Schulte, 1979.
[c]Boev, Puska, and Nieminen, 1987.
[d]Lynn, K. G., 1980, unpublished.
[e]Lynn and Lutz, 1980b.
[f]Nieminen and Hodges, 1976b.
[g]Howell, Rosenberg, Fluss, Goldberg, and Laughlin, 1987; and Howell, Rosenberg, and Fluss, 1986.
[h]Gullikson and Mills, 1987b.
[i]Lynn and Lutz, 1980a.
[j]Mills, Pfeiffer, and Platzman, 1983.
[k]Murray and Mills, 1980.
[l]Lynn, 1980.
[m]Lynn, K. G., 1980, unpublished.
[n]Brandt, 1976.
[o]Wilson and Mills, 1983b.
[p]Mills, 1979b.
[q]Fischer, Lynn, and Gidley, 1986.
[r]Mills, 1979a.
[s]Murray, Mills, and Rowe, 1980.
[t]Gullikson, Mills, and Murray, 1988.
[u]Lynn, Schultz, and MacKenzie, 1981.
[v]Nielsen, Lynn, Vehanen, and Schultz, 1985.
[w]Gidley, 1986, private communication.
[x]Fischer, 1984.
[y]Gullikson, Mills, Crane, and Brown, 1985.
[z]Howell, Meyer, Rosenberg, and Fluss, 1985.
[aa]Schultz, Jackman, Jorch, and Lynn, 1983.
[bb]Hodges and Stott, 1973b.
[cc]Jean, Lynn, and Carroll, 1980.
[dd]Wilson, 1983.
[ee]Chen, Lynn, Pareja, and Nielsen, 1985.
[ff]Schultz, Lynn, Frieze, and Vehanen, 1983.
[gg]Gramsch, Throwe, and Lynn, 1987.
[hh]Schultz, 1987.
[ii]Howell, private communication.
[jj]Gullikson and Mills, 1987b; Sferlazzo *et al.*, 1988.
[kk]Chen, 1987.
[ll]Mills, 1978.
[mm]Gullikson, Mills, and Phillips, 1988.
[nn]Gullikson, Mills, and McRae, 1988.
[oo]Mills and Gullikson, 1986.
[pp]Sferlazzo, Berko, and Canter, 1985.
[qq]0.15-eV activation energy for Ps, not positrons.
[rr]Mills and Crane, 1984.

that positrons reemitted from a variety of clean surfaces [Ni(100); W(110); Cu(111)] were almost all elastic, with an energy distribution consistent with Maxwell-Boltzmann statistics. This gives the distribution of speeds $N(v)$, for a beam of positrons emitted into a solid angle $d\Omega$, as

$$N(v)dv \propto v^3 \exp(-mv^2/2k_bT)dv\,d\Omega\ . \tag{38}$$

Spectra for a Ni(100) surface measured using the spherical analyzer (Fig. 23) are shown in Fig. 76. The data are fitted well by the distribution in Eq. (38) over the temperature range 23–300 K studied. This conclusion was also reached by Gullikson *et al.* (1985), who used total energy measurements (see Sec. I.E.1) to show that emission is elastic for Ni(100) and W(110) + C and that angular spread of the emitted positrons is responsible for much of the inelastic emission falsely suggested by the tails in the distributions of Fig. 75.

In an attempt to explain the inelastic emission process, Pendry (1980) suggested that the positron surface state (see Sec. II.D.3) can be regarded as a mixed positron/Ps-like entity, which is stable because of reflection from both the solid and the vacuum. The dissociation of the Ps-like state from this mixed state leads to the large spread in angle and/or energy that was observed. The important point is that either description may correctly describe the energy distribution of the inelastic component, but neither can predict the integral of the distribution or its importance relative to the elastic component.

Other theories for positron emission that do not involve Ps formation are based on transition rates for available scattering mechanisms at the surface, with the height of the step (φ_+) and the depth and width of the image-induced potential well (Fig. 8) being important. It is generally accepted that inelastically emitted positrons lose most of their energy to creation of electron-hole pairs (Nieminen and Oliva, 1980), with other processes such as bulk or surface plasmons (energetically impossible), or phonons (small energy loss), being less important (Neilson, Nieminen, and Szymanski, 1986a). The most recent theoretical models of the reemission process (Neilson, Nieminen, and Szymanski, 1986a, 1986b; Kato and Ishii, 1987) achieve reasonable agreement with experimental results for describing both energy and angular distributions when an adjustable screening parameter is used. Examples of calculated angular distributions of positrons reemitted from smooth surfaces of Al, Cr, and W are shown in Fig. 77.

One interesting application of measurements of reemitted positron total energy distributions has been given the

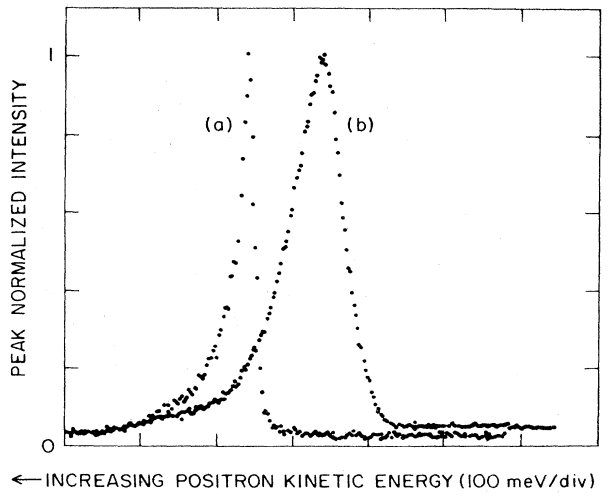

FIG. 76. Differential reemitted positron total energy distributions for Ni(100). Curve (a) was taken at 23 K (FWHM ~24 meV), and curve (b) was taken at 300 K (FWHM ~80 meV). From Fischer, Lynn, and Gidley, 1986.

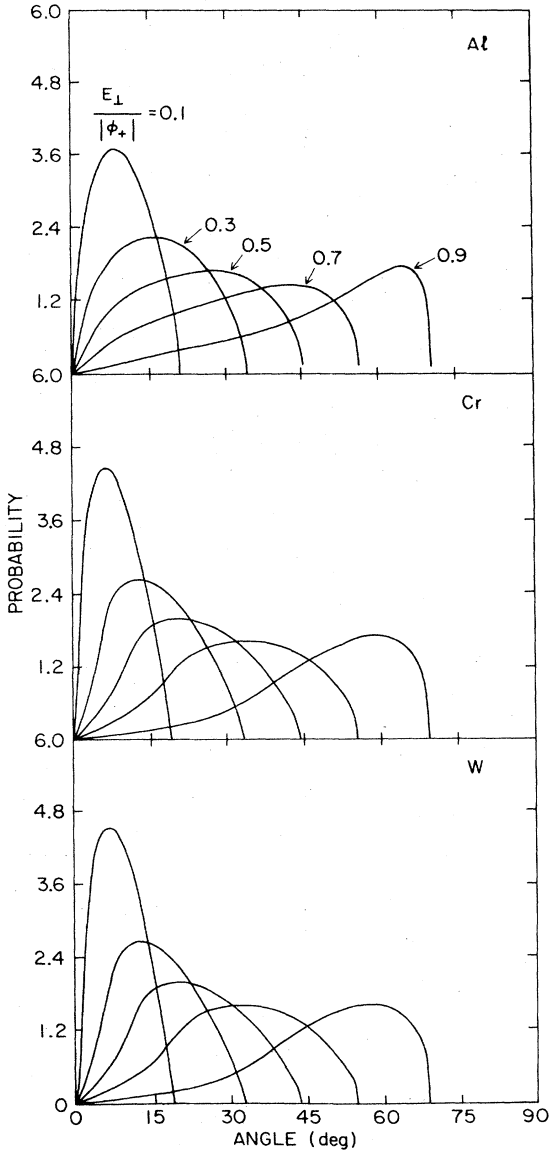

FIG. 77. Angular distributions of positrons leaving Al(100), Cr(100), and W(111) metal surfaces at 300 K. The various curves represent fixed final energy in the z (surface normal) direction, $E_\perp/|\varphi_+| = 0.1$, 0.3, 0.5, 0.7, and 0.9 (from Neilson, Nieminen, and Szymanski, 1986b).

acronym "REPELS," which stands for reemitted positron energy-loss spectroscopy, and which is similar to the more familiar electron energy-loss spectroscopy (EELS). The first REPELS results were those of Fischer *et al.* (1983), who demonstrated the technique by observing the carbon/oxygen and carbon/nickel vibrational modes (248 and 57 meV, respectively) for CO on a Ni(100) surface. The width of the discrete energy-loss peaks that they measured (Fig. 78) was dominated by the thermal spread of the positrons. In a subsequent study (Fischer, 1984; Fischer *et al.*, 1986) the thermal spreading was reduced by lowering the sample temperatures, which improved the resolution of the technique considerably. Although somewhat more difficult to do than EELS (primarily because of positron beam availability and intensities) and limited in available energy to the magnitude of the negative positron work function (if it exists), the technique, as they point out, has some advantages. These include the relative ease of probing very small energy losses ($\ll 1$ eV), which is very hard to do with conventional particle optics in an EELS spectrometer, as well as the absence of exchange effects, which may prove important for studies of adsorbed paramagnetic molecules.

The techniques for measuring reemitted distributions of positrons were briefly described in Sec. I.E.1 and, as Murray, Mills, and Rowe (1980) first pointed out, a series of spectra taken with a simple retarding-field analyzer (Figs. 24 and 25) reveals not only the absolute magnitude of φ_+ but also any changes that may have occurred in φ_- for the surface. Much of the earlier work on temperature effects and correlations between positron and electron work functions suffers either from poor statistics or uncertain experimental conditions. For Cu(111) + *S* (Schultz and Lynn, 1982) it was shown that φ_+ and φ_- do not change by the same amount with changing temperature. This was revealed by a temperature dependence of the point E_3 (as defined in Fig. 25):

$$E_3=\varphi_+ +\varphi_- -\varphi_g \ . \tag{39}$$

Since the work function of retarding grids (φ_g) remains constant, it is easily seen from Eq. (39) above and the definitions for φ_+ and φ_- [Eq. (1)] that the cancellation of the dipole contribution D in E_3 means that it is sensitive to changes in the bulk chemical potentials μ_+ and μ_-. This fact was subsequently exploited by Schultz, Lynn, *et al.* (1983) to test competing calculations of μ_+ and μ_-, finding in general good agreement with the sum of the chemical potentials (E_3) and the theoretical estimates. A difference in the temperature dependence of φ_- and φ_+ was also observed for Ni(100) by Fischer, Lynn, and Gidley (1986). By comparing Eq. (39) with Eq. (2) it can be seen that systematic changes in E_3 (assuming constant φ_g) can also be compared with those observed for the Ps formation potential ε_{Ps}. Bulk solid information derived from temperature-dependent studies of both ε_{Ps} and E_3 is discussed in more detail in Sec. II.D.2.

The equivalence of the dipole contribution to both φ_+ and φ_- means that detailed comparisons of φ_+ with φ_- as a function of well-characterized systematic changes to the experimental system allows the separation of bulk effects from surface effects, as discussed above. This is not directly possible from measurements of φ_- alone. For example, any change to the surface which causes only the surface dipole to change would be expected to affect φ_- and φ_+ by equal and opposite amounts, so that the point E_3 should not move. Such a change is demonstrated in Fig. 79, where the energy distribution of reemitted positrons is shown for (a) clean and (b) CO-covered Pt(100). The CO coverage, which is signaled by a C(2×2) LEED pattern, has been shown to be accompanied by an increase in φ_- of ~200 meV (Thiel *et al.*, 1983). The results in Fig. 79(b) show that φ_- and φ_+ changed by 250±140 meV and −290±140 meV, respectively, consistent with a changing surface dipole.

Gullikson and Mills (1987a) have measured φ_+ changes as a function of temperature in Al (discussed in the next section) and were able to show that the "$E_z=0$" point (Fig. 25), and thus φ_-, moved by less than 20 meV over the temperature range 20 to 300 K. This precision (with a simple retarding-field analyzer) was made possible by turning the sample off the beam axis, as described in Sec. I.E.1, and it provided a check on the surface impurity concentrations over the time required to do their experiment. In the future, accurate measurements of the absolute changes in work-function curves of this type may help to resolve questions about subsurface adsorption and interfacial potentials for thin epitaxial overlayers.

Gidley and Frieze (1988) have recently initiated a systematic study of the bulk chemical-potential sum, $\mu_+ +\mu_- =-(\varphi_+ +\varphi_-)=-\varphi_0$ [as deduced from Eqs. (1)

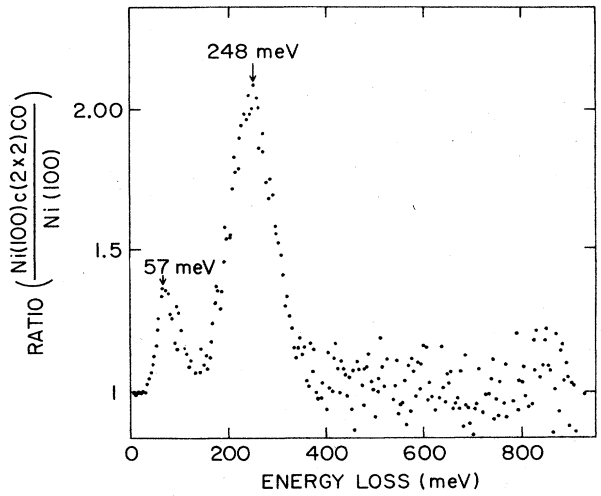

FIG. 78. REPELS (Reemitted positron energy-loss spectroscopy) spectrum for CO on Ni(100). The data shown are the ratio of normalized peak counts in the case of Ni(100)$c(2\times2)$CO to clean Ni(100), showing the loss peaks for the Ni-C stretch (57 meV) and the C-O stretch (248 meV). From Fischer, Lynn, and Frieze, 1983.

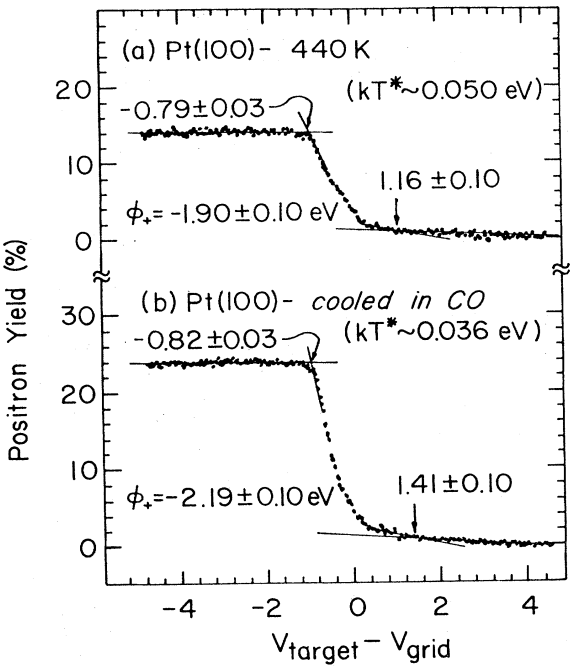

FIG. 79. Integral positron reemission energy distributions for (a) clean Pt(100) and (b) Pt(100)$c(2\times2)$CO. The previously measured change in φ_- for the adsorption of CO on Pt(100) is $\sim$200 meV, which is consistent with the results above [$\Delta\varphi_- = +250\pm140$ meV; see Fig. 25 and Eq. (39)]. The measured change $\Delta\varphi_+ = -290\pm140$ meV in the spectra above is consistent with the view that the adsorption affects only the surface dipole contribution to the work function (from Schultz, Jackman, Jorch, and Lynn, 1983).

and (39)], for a variety of thin-film bimetallic systems. They point out that the matching of electron Fermi levels that occurs at an interface due to charge transfer has no equivalent for the positron ground-state energy. The reemitted positron elastic peak position (E_3) of any layer depends only on the bulk chemical potentials of that layer, independent of any overlayers. The motion of positrons between dissimilar layers is prevented, according to their model, if the direction is to a layer where $\mu_+ + \mu_-$ is more positive (i.e., φ_0 more negative). This is illustrated schematically in Fig. 80, where a thermalized positron is energetically allowed to cross an interface if the peak position of the new layer is to the *left* of that for the host layer.

Measurements of positron work functions have been made not only for bulk single-crystal surfaces, but also in a few thin (unsupported) single-crystal foils. Both transmission and back reemission studies were done for W(100) films of 1000-, 2500-, and 5000-Å thickness by Chen, Lynn, Pareja, and Nielsen (1985). The work function was $\varphi_+ = 3.0\pm0.3$ eV, and the reemitted positrons were found to be in a narrow angular cone with a FWHM $\sim$30°. The maximum transmission reemission yields were 18% and 12% for 1000 and 2500 Å foils, respectively. In Fig. 81 both the forward and back reemis-

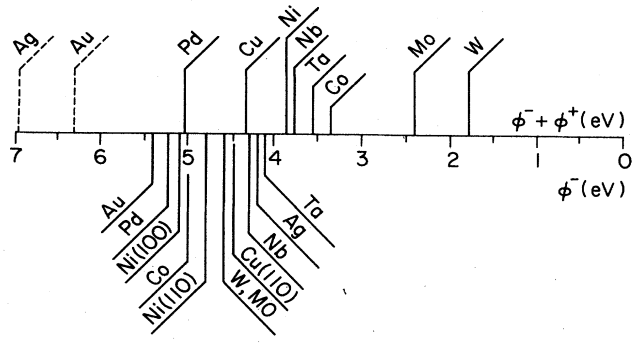

FIG. 80. Measured, reemitted positron elastic peak energies (top), and top-layer electron work functions (bottom; from Hölzl and Schulte, 1979), for multilayer systems. From Gidley and Frieze, 1988.

sion data are shown for two foils, as well as the theoretical fits of the diffusion equation. In solving the diffusion equation, the authors assumed *perfectly absorbing* boundaries and a Makhovian implantation profile [Eq. (10)] with $n=1.8$ and $m=1.14$. The diffusion-related parameter E_0 (Sec. II.C.1) was found to be $\sim$10 keV, corresponding to a mean diffusion length $L_+ \sim 1380$ Å. These values were obtained after heating the foils to tem-

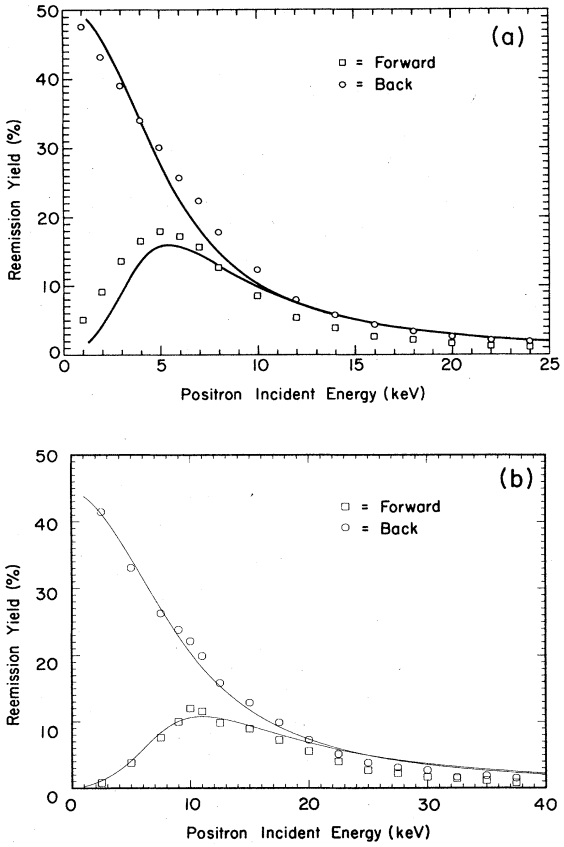

FIG. 81. Yield of reemitted positrons vs incident positron energy for (a) $\sim$1000-Å-thick W(100) and (b) $\sim$2500-Å-thick W(100) films. The solid curves are theoretical fits to the data (from Chen *et al.*, 1985).

peratures >2000 °C to remove defects. Schultz, Gullikson, and Mills (1986) also studied transmission reemission for a Ni(100) single crystal approximately 1200 Å thick, and they found ~20% reemission for 8-keV incident positrons, with a narrow angular spread consistent with elastic emission.

2. Energetic positronium formation

As discussed in the Introduction (Sec. I.C.3), the term work function, as applied to Ps emission from solid surfaces, will be reserved for the case in which Ps is removed from a point just inside the bulk to one just outside the surface (Sec. II.D.4). For metal surfaces, the energetics of Ps formation at the surface is determined by the so-called formation potential ε_{Ps} [Eq. (2)] which is often negative due to the relatively large binding energy of the positron-electron pair (~6.8 eV for Ps in vacuum). The first observation that Ps formation at surfaces is relatively efficient (Canter, Mills, and Berko, 1974) was followed by observations of $n=2$ excited Ps (Canter, Mills, and Berko, 1975), time-of-flight measurements to deduce the triplet *o*-Ps decay rate (Gidley *et al.* 1976; Gidley and Zitzewitz, 1978), and then quantitative measurements of the fraction of Ps formed as a function of incident positron energy (Mills, 1978; Lynn, 1979a, 1979b). Based on limited experimental data, a correlation was established by Murray, Mills, and Rowe (1980), relating the fraction of free positrons emitted to the absolute magnitude of φ_+. Nieminen and Oliva (1980) also predicted theoretically that the amount of Ps formed at a surface should be inversely correlated with $|\varphi_+|$. Their model used dynamical arguments to compare the time it takes Ps to form with the time a positron would spend in the surface region. The electronic density of states at the surface must also play an important role which would be difficult to assess, but which they included approximately in coupling constants.

The differential energy distribution of Ps emitted from an Al(111) surface was measured by Mills, Pfeiffer, and Platzman (1983) using the time-of-flight (TOF) apparatus previously described (Fig. 31). Their model for the formation process, which is represented by the lines through their data in Fig. 82, is that the capture of the electron is a nonadiabatic one-step process, which leaves the metal in an excited state. This means that the kinetic energy of the Ps, which has a maximum given by ε_{Ps}, is representative of the density of states of the electrons from which the Ps is formed. Furthermore, since Ps is formed outside the surface, where the electron density falls to $\sim\frac{1}{10}$ the bulk value (Held and Kahana, 1964; Lowy and Jackson, 1975), this interpretation would imply that the kinetic energy distribution of Ps is an exceedingly local probe, specific to the surface electronic structure. Technically this model is analogous to the dynamic Berglund-Spicer (1964) three-step model of photoemission, which separates the process of photoinduced release of an electron from a solid surface into the stages of (i) ionization,

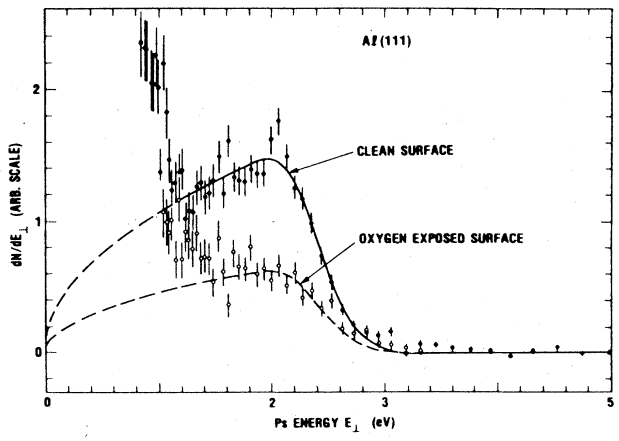

FIG. 82. Normal component of kinetic energy for Ps emitted from Al(111). The solid curve is modeled assuming the Ps is formed nonadiabatically, leaving the solid in a one-hole excited state, the velocity therefore representative of the local electronic density of states at the surface (from Mills, Pfeiffer, and Platzman, 1983).

(ii) electron transport, and (iii) ejection from the solid. The analogy is based heavily on the premise that the initial process of ionization (and thus emission of Ps) can be considered independently of the deexcitation of the host lattice (Walker and Nieminen, 1986).

The *sudden* emission process for Ps was also supported by the TOF measurements of Howell, Rosenberg, Meyer, and Fluss for Pb(100) (1987) and for a variety of dissimilar metals (Howell, Rosenberg, Fluss *et al.*, 1987). Their results, shown in Fig. 83, also show the increase at *low* energies (<1 eV) found in the data of Mills *et al.* This increase is not explained either by thermal emission of Ps (next section) or by the simple nonadiabatic models represented by the solid lines in Figs. 82 and 83. There are so far two theoretical treatments that may explain this low-energy contribution (which is nevertheless *greater* than thermal energy). Levine and Sander (1982) attempted to describe thermal Ps emission by a tunneling process of positrons localized in the surface state and occupying discrete excited levels. There is not much support for this as a mechanism for thermal Ps emission, primarily because the levels in the surface state are expected to be much wider apart and more diffuse than predicted by Levine and Sander. However, it is possible that tunneling from the surface state is contributing to the low-energy Ps. It is perhaps more likely that the low-energy component is the result of dynamic effects of the ejection process. Adapting techniques developed for ion neutralization, Ishii (1987; Ishii and Shindo, 1987; Isii, 1984) has shown that the inelastic component of the energy distribution for *energetic* Ps can be described in this way. The second Ni(100) curve in Fig. 83 was obtained by reducing the angle of acceptance of the TOF apparatus from ~30° half angle to 15°. The authors conclude from these higher-resolution data that the discrepancy near 1 eV that still remains in the experimental data must be real,

while the lower-energy contribution that was removed by this process is actually due to scattering of more energetic Ps within the chamber. This conclusion is in apparent contradiction with the inelastic models described above.

The most convincing evidence that the *sudden* approximation is reasonable and that Ps velocity is influenced by the surface electron density of states is provided by the surface 2D ACAR data from Brookhaven National Laboratory, reported by Chen *et al.* (1987). As discussed in Sec. I.E.2, the Ps momentum perpendicular ($k_\perp$) and parallel ($k_\parallel$. . .one component) to the target surface can be separated from the total annihilation spectrum (Fig. 30). Conservation of energy demands

$$k^2=k_\perp^2+k_\parallel^2=\frac{2mE}{\hbar^2}\ , \tag{40}$$

where E is the Ps kinetic energy, limited to a maximum given previously [Eq. (2)] by the formation potential

$$\varepsilon_{Ps}=\varphi_+ +\varphi_- -\tfrac{1}{2}R_\infty\ .$$

Figure 84(a) shows the surface band structure projected along high-symmetry lines for Al(100), which is expanded and shown again in Fig. 84(b) together with the curve of the lowest measurable energy states, as determined by the momentum balance given above. It is energetically favorable for Ps to form with electrons taken from anywhere in the D-shaped region of E vs k space above this line and below the Fermi level. The band gap (hatched area) suggests a reduced density of electrons available at low $k_\parallel$ relative to what would be predicted by a simple free-electron density of states. This is clearly evident in Fig. 85, where the two-dimensional Ps momentum distributions that would be predicted from this band

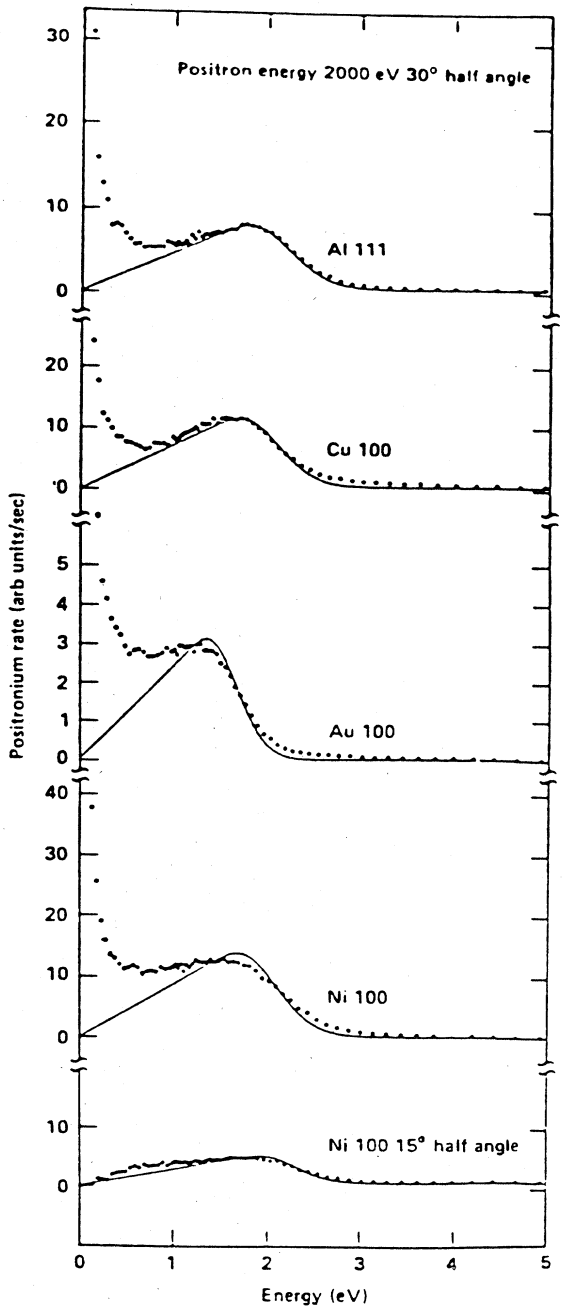

FIG. 83. Ps (normal) energy distributions for various metal surfaces. The nonadiabatic model of Fig. 82 is applied to these spectra, and the explained intensity at low energies is again evident (from Howell *et al.*, 1987).

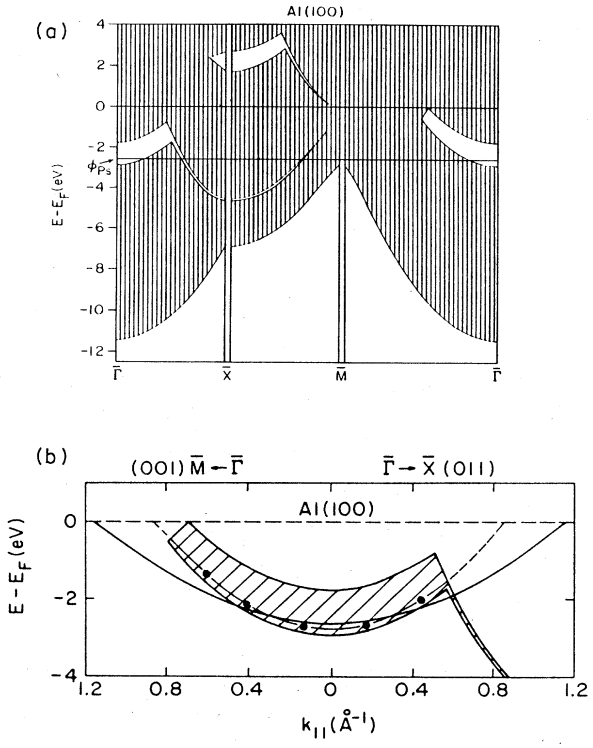

FIG. 84. Projected band structure for the (100) surface of Al. The shaded portion of the lower figure is a band gap, and the solid curve is the dispersion of the lowest occupied states that can form Ps in terms of the final Ps momentum *parallel* to the surface [see Eq. (40)]. The dashed curve is the dispersion of the true surface state and surface resonance state (Hansson and Flodström, 1978). From Chen, 1987.

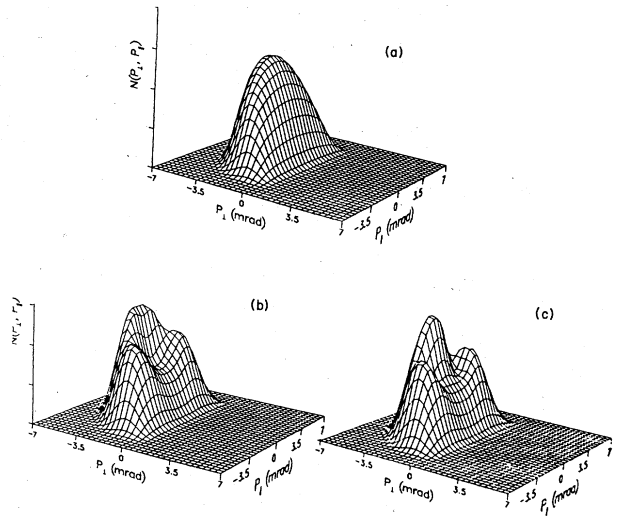

FIG. 85. Theoretical intensity distributions of Ps formed at an Al(100) surface. Curve (a) is based on a free-electron model, while curves (b) and (c) are based on the band structure of Fig. 84 (cuts parallel to [011] and [001] directions, respectively). From Chen *et al.*, 1987.

structure are shown. These predictions are also shown as contour plots in Figs. 86(a) to 86(c), together with the experimental results 86(d) and 86(e) for two different surface directions. The three-lobed distributions expected can be seen in both sets of data. Schultz, Lynn, and Frieze (1984) have suggested that the particular sensitivity of the process to surface densities of states would lead to an enhancement of the large-$k_{\parallel}$ regions of the distributions due to electrons which originate in surface states. Chen *et al.* (1987) demonstrated that this would be a small effect relative to the projected band gaps (i.e., lack of bulk electron states) presented in Figs. 84–86. It is interesting to note that a higher intensity of low-energy Ps is seen in the experimental results in Fig. 86 than there is in the theoretical predictions. This contribution is similar to that discussed above with reference to Figs. 82 and 83. Similar theoretical *p*-Ps momentum distributions to those of Chen *et al.* (Fig. 86) have been presented by Walker and Nieminen (1986) and by Shindo and Ishii (1987).

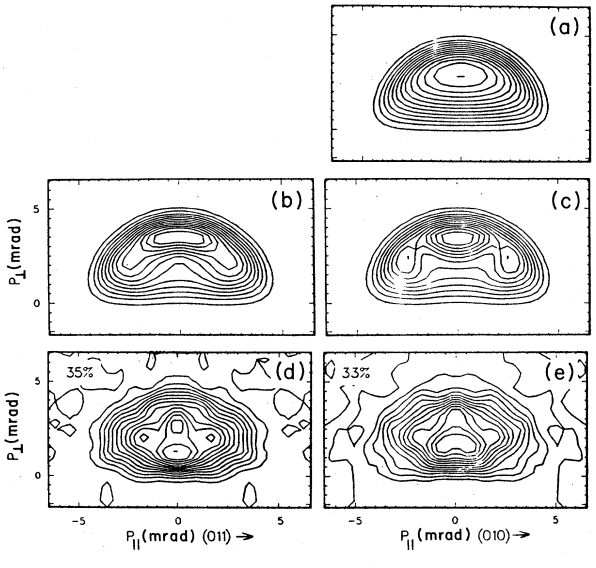

FIG. 86. Symmetrized contour plots of the spectra shown in Figs. 85(a)–85(c), compared with experimental results in Figs. 85(d) and 85(e). The "three-lobed" structure is supported in the experimental data, and the low-energy component seen in Figs. 82 and 83 is also present in these data (from Chen *et al.*, 1987).

Another mechanism for Ps emission has recently been suggested to explain unusual results for graphite (Sferlazzo *et al.*, 1988). In graphite the band structure does not support the usual one-electron-hole process for Ps emission because the electron momentum *parallel* to the surface is too large [cf. Eq. (40)]. The observation of Ps emission in spite of this fact led to the proposal that momentum conservation is satisfied by the emission and absorption of phonons, which fits the observed dependence of the Ps emission on temperature.

In addition to the energy-balanced processes discussed above, Howell and co-workers (1986, 1987) noted evidence of *fast* Ps formation (10 to 20 eV) in their TOF results. This process is quite different, involving pickup of electrons by *epithermal* backscattered positrons. Fast Ps has also been reported by Mills and Crane (1985a), who saw ~0.5% formation of 10–500-eV Ps from keV positrons directed through a 50-Å carbon foil. Gidley *et al.* (1987) measured approximately 3% to 5% formation of energetic Ps for glancing-angle positrons (~100 eV) skipping off various solid surfaces at glancing angles of about 6°. Their results showing the angular distribution for Ps formed at a Cu(100) surface are reproduced in Fig. 87. In their paper they proposed a simple kinematic model whereby a glancing-angle positron could produce a quasi-elastic Ps atom, which they predicted to be ejected at 45° relative to the surface plane. The maximum in the Ps emission angle in Fig. 87 is ~27° (relative to the surface plane) for Cu(100). Ishii (1987b) has recently extended

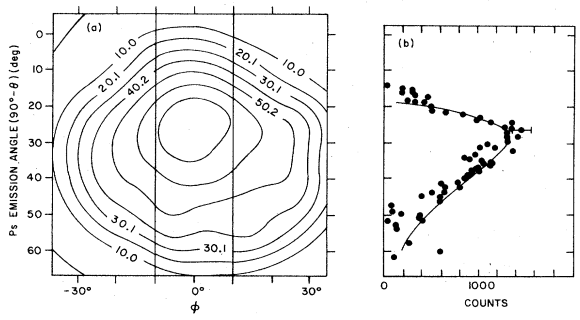

FIG. 87. Formation of Ps by low-energy (100-eV) positrons incident on a Cu(100) surface at glancing angle (6°). The emission angle is measured relative to the plane of the surface (from Gidley *et al.*, 1987).

his dynamical model of the positron-surface interaction to describe the glancing-angle pickup. He finds that direct Ps formation combined with formation directly from a dynamical positron-surface *skipping* state qualitatively reproduces the experimentally observed distributions. Future applications of energetic neutral beams of Ps include surface diffraction and reflection studies (Weber, 1988), as well as Ps/atom collision cross-section measurements.

Gidley, Köymen, and Capehart (1982) have used the preferential surface sensitivity of Ps formation together with a highly polarized (50%) incident positron beam to study surface magnetism. Positrons will only form triplet *o*-Ps ($m_s=\pm 1$) with electrons if the spins are aligned, and will form both *p*-Ps and *o*-Ps ($m_s=0$) with equal probability if they are antialigned. The resulting ratio, which is normally 3:1 for a random arrangement of electrons, can be significantly affected by a preferential alignment of the spins of the electrons at the surface. The results of this study for Ni(110) as a function of temperature are shown in Fig. 88. The solid curve in the figure is the bulk magnetization, and the dashed curves are fits of a two-dimensional model to their data. In an experiment of this type, reproducibility is crucial to the results, since the Ps fraction is extremely sensitive to small changes of the surface (see, for example, Sec. II.D.3).

This measurement clearly reveals the temperature dependence of the spin polarization of the electron captured to form Ps, but the interpretation has possible complications. As in the above technique of Ps velocity studies, this only samples the electrons at the surface which lie within the Ps formation potential [$\varepsilon_{Ps}\approx 3.1$ eV for Ni(110)], and it must be assumed that the pickup process reflects only the near-surface electron density of states. The relatively large fraction of the Ps which is emitted at very low energies (discussed above) is still not understood. This component may be partly responsible for the discrepancy between the results shown in Fig. 88 and other electron polarization studies, which usually report larger values for surface polarization. For example, if the low-energy Ps is due to the inelastic processes suggested by Ishii (1987), then spin-flip of an electron in the measured Ps might occur, which would lead to an error in the analysis. Further work on the influence of positron polarization on both fast Ps formation and, as yet unstudied, thermally desorbed Ps is needed to resolve these uncertainties.

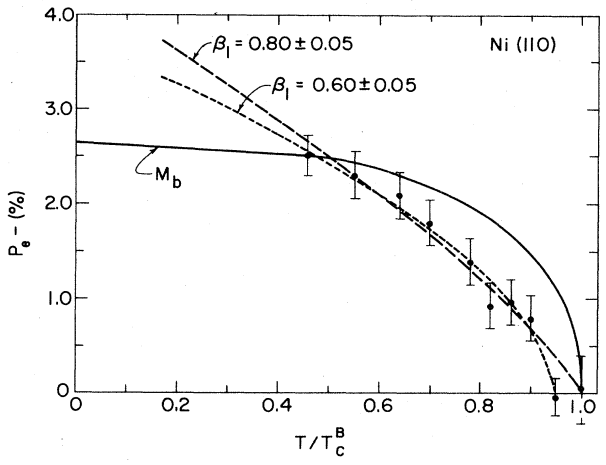

FIG. 88. Temperature dependence of the spin polarization P_e of the electron captured at a Ni(110) surface to form Ps. The solid curve is based on the bulk magnetization properties of Ni (normalized to the lowest-temperature data), and the dashed and dotted curves are models for surface magnetization with the critical temperature $T_c=T_c^B$ and T_c unconstrained, respectively (from Gidley, Köymen, and Capehart, 1982).

As discussed in the previous section, temperature-dependent measurements of both positron and electron work functions or of Ps formation potentials are representative of bulk changes in the solid, since

$$\Delta E_3=\Delta\varepsilon_{Ps}=\Delta(\varphi_+ +\varphi_-)=-\Delta(\mu_+ +\mu_-)\equiv\Delta\varphi_0\ , \tag{41}$$

where μ_+ and μ_- are the bulk solid positron and electron chemical potentials, respectively, and $\Delta\varphi_0$ is the magnitude of the change in the sum of the chemical potentials. Rosenberg *et al.* (1987) have compiled measurements of $\Delta\varepsilon_{Ps}$ for a variety of materials, and their results are shown in Fig. 89. The strong temperature dependences observed are consistent with previous observations for Cu (Schultz and Lynn, 1982) and recent studies of Al

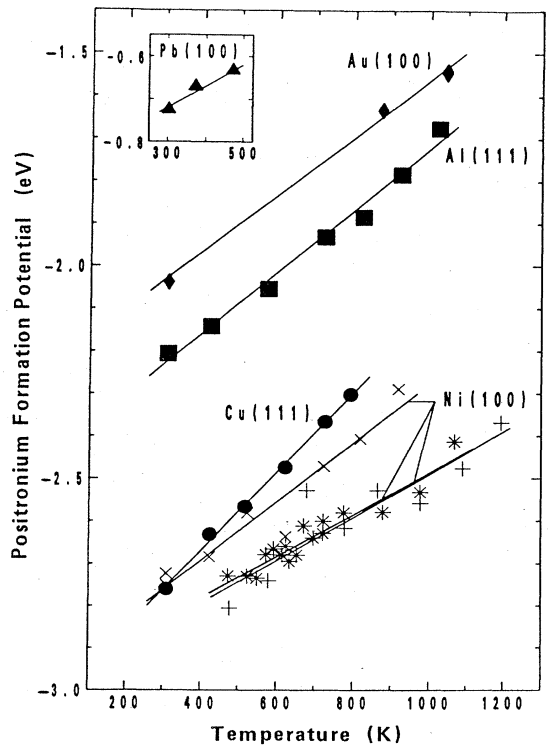

FIG. 89. Temperature dependence of Ps formation potentials ε_{Ps} for various surfaces. This is related to the change in the bulk chemical potentials of the solids in Eq. (41). From Rosenberg *et al.*, 1987.

(Gullikson and Mills, 1987a), which are shown in Fig. 90. For experiments performed at constant pressure, one can write the temperature dependence of a work function as (see, for example, Hölzl and Schulte, 1979)

$$\frac{d\varphi}{dT}=\alpha V\left[\frac{\partial\varphi}{\partial V}\right]_T+\left[\frac{\partial\varphi}{\partial T}\right]_V, \tag{42}$$

where the thermal coefficient of expansion $\alpha=(1/V)(\partial V/\partial T)_p$. Gullikson and Mills pointed out that the sum $\varphi_0=\varphi_+ +\varphi_-$ substituted in Eq. (42) above would exhibit a dependence on temperature that is

$$\frac{d\varphi_0}{dT}=-\alpha\varepsilon_d+\left[\frac{\partial\varphi_0}{\partial T}\right]_V. \tag{43}$$

This follows from the definition given by Bergersen *et al.* (1974) for the deformation potential [Eq. (32)], which can be written in the alternate form

$$\varepsilon_d=V\frac{\partial}{\partial V}(\mu_+ +\mu_-)=-V\left[\frac{\partial\varphi_0}{\partial V}\right]. \tag{44}$$

They suggest that if the right-hand term of Eq. (43), which is due to the electrostatic effects of lattice vibrations (Herring and Nichols, 1949), vanishes, one could extract ε_d from the slope of the data after correcting for thermal expansion. Applying this analysis to their results for Al [Fig. 90(b)], they obtain $\varepsilon_d=-11.7\pm0.5$ eV, which is somewhat larger than the theoretical estimates of Bergersen *et al.* (−8.6 eV) and of Farjam and Shore (1987; −9.83 eV). The data of Schultz and Lynn (1982) when analyzed as above yield $\varepsilon_d\sim-11.9$ eV for Cu, which compares favorably with the theoretical estimate of Farjam and Shore (−10.42 eV). It is possible that the above discrepancy between theory and experiment is due to the incomplete cancellation of the lattice vibrational term, $(\partial\varphi_0/\partial T)_V$, in Eq. (43). This is reasonable, since temperature-induced changes of the potentials for positrons and electrons in a solid lattice do not necessarily lead to equal and opposite shifts in μ_+ and μ_-. If it could be made reliably, an experimental determination of the deformation-potential constant would be useful in estimating the numerical value of the positron diffusion coefficient, as well as determining electron and hole mobilities in semiconducting materials.

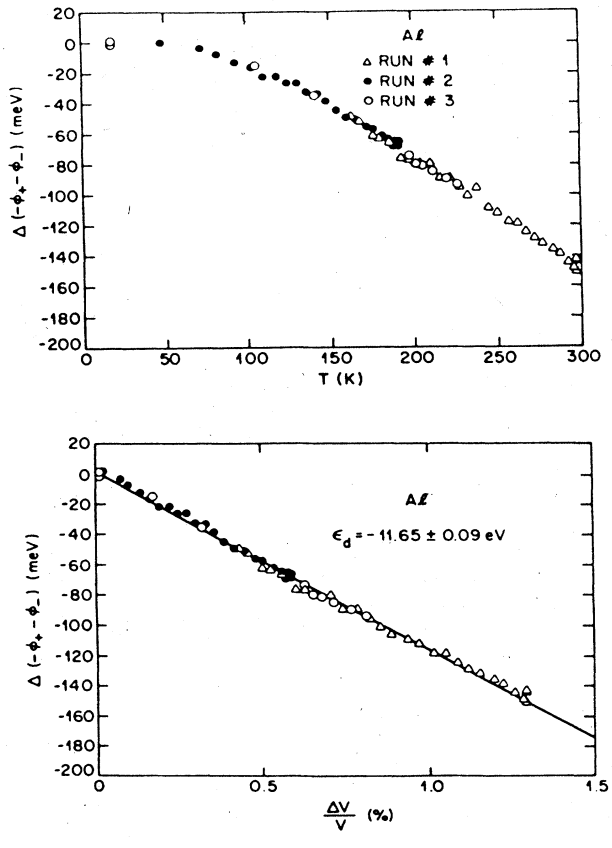

FIG. 90. Temperature and volume-change dependence of the Ps formation potential for Al. The slope can be related to the bulk deformation potential of Al by Eq. (43). From Gullikson and Mills, 1987a).

A related study (Howell *et al.*, 1988) indicates that the temperature dependence of the Ps work function φ_{Ps} is similar for an insulator (LiF) to that observed for $d\varphi_0/dT$ [Eq. (43)] for positrons in metals. They find that $d\varepsilon_{Ps}/dT=-0.95\pm0.1$ meV/K for LiF. This result is sensible in view of the fact that φ_{Ps} depends on the sum of the e^- and e^+ chemical potentials in the solid, just as the emission potential ε_{Ps} does.

3. The surface state and thermal positronium

The earliest theories of the positron surface state were developed in response to the relatively long lifetimes (≈400 to 500 psec) that were being measured in the early 1970's for positrons localized at radiation-induced vacancy clusters or voids. The existence of a surface-localized state for positrons was predicted theoretically by Hodges and Stott (1973a), who suggested *matching* the image potential with the internal correlation energy of the positron, producing the same kind of single-particle potential that Cole and Cohen (1969) described for localized electron bands on He surfaces. This type of picture, which is shown schematically in Fig. 91, is still the most common physical description used. Following an improved (although still static) description of the potential (Nieminen and Manninen, 1974), the model was superseded by a variational calculation of the positron coupled to the screening cloud of the many-electron system by Nieminen and Hodges (1978). Their assumption of a nondispersive distribution of surface plasmons was corrected by Barberan and Echenique (1979), and finally the most complete variational calculations extending the same basic hydrodynamic approach were presented in a series of papers by Barton (1981, 1982) and Barton and Babiker (1981). For most of the early theoretical work on the positron surface state there was no direct experimental support. However, by the time Barton's work was published, the first observations of thermally activated Ps

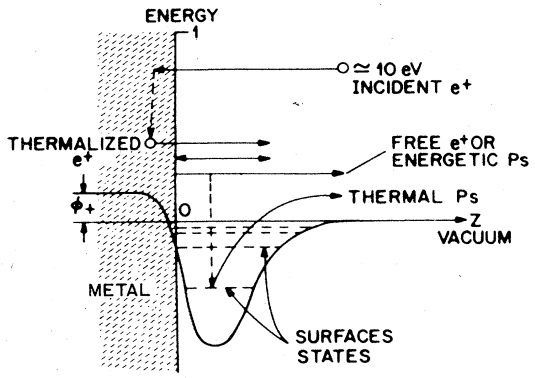

FIG. 91. Schematic representation of the surface state and possible desorption as "thermal" Ps (from Chu, Mills, and Murray, 1981).

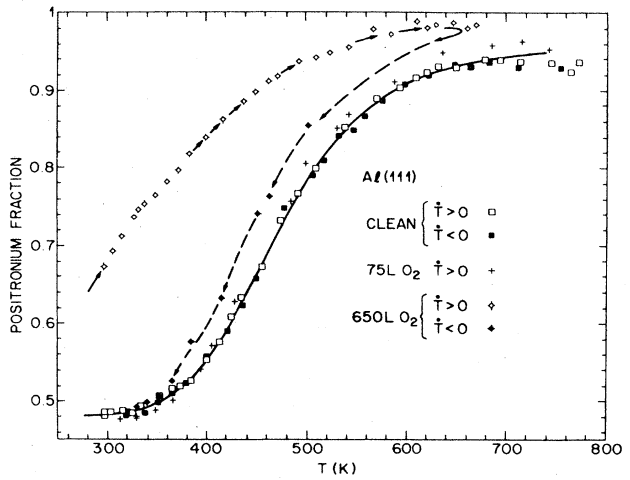

FIG. 92. Ps fraction vs temperature for clean and oxygen-exposed Al(111) surfaces, showing the thermally activated component. The solid line is a fit to the data of Eq. (45). From Mills and Pfeiffer, 1985.

were available. His conclusion was that many-body aspects alone are not sufficient, and that single-particle properties are also required to describe the positron in the idealized surface state.

Positrons that localize in the surface state are typically bound with energies E_b on the order of a few eV. The first observations of the temperature dependence of Ps emitted from solid surfaces (Lynn, 1980; Mills, 1979b; Rosenberg, Weiss, and Canter, 1979b) showed that the process could be described in terms of the activation energy for desorption, E_a, in a curve of the form

$$f=\mathcal{F}_0+\mathcal{F}_s=\mathcal{F}_0+\frac{\Gamma\exp(-E_a/k_BT)}{\lambda_s+\Gamma\exp(-E_a/k_BT)}f_s\ , \quad (45)$$

where the prefactor Γ is discussed below and $\mathcal{F}_0$ and $\mathcal{F}_s$ are the fractions of incident positrons emitted as Ps directly (i.e., ε_{Ps} energetic) and from the surface state, respectively. Those positrons that are trapped in the surface state (fraction $=f_s$) have an annihilation rate of λ_s. An example of thermally activated Ps emitted from an Al(111) surface is shown in Fig. 92. Guided by the exponential activation evident in the experimental data, Chu, Mills, and Murray (1981) and Manninen and Nieminen (1981) considered the process thermodynamically in a model for which the positron is confined to the surface, the electrons are in both bulk and surface states, and the Ps forms an ideal gas in the vacuum. The model requires that the chemical potentials be in equilibrium, as given previously in Eq. (5): $\mu_+ + \mu_- = \mu_{Ps}$. This formalism is equivalent to the Richardson-Dushman equation governing thermionic emission. Their solution for the preexponential factor Γ in Eq. (45), which comes from a detailed mass balance (i.e., the flux into the solid must equal the Ps thermally activated), is given by

$$\Gamma=\frac{4k_BT}{\hbar}(1-\langle\beta_{Ps}\rangle)\ , \quad (46)$$

where $\langle\beta_{Ps}\rangle$ is the velocity-averaged Ps reflection coefficient. A velocity dependence of β_{Ps} could lead to a modification of the Maxwellian distribution of Ps velocities, but most measurements (described below) are consistent with velocity-independent reflection.

Chu *et al.* suggest that Γ can be described as an "attempt rate" for escape from the surface trap, which is of the order of the ratio of positron thermal velocity to image well width, or $\approx 10^{15}$ sec^{-1}. In detailed calculations, they obtain an anomalously large value of Γ for Cu(100) + *S*, which they suggest may be compensated by a temperature-dependent activation energy. Such a dependence on temperature is not unreasonable, since it is well known that contaminated surfaces often have strongly temperature-dependent work functions (Hölzl and Schulte, 1979). This is most likely associated with temperature-dependent changes in the surface dipole. The activation energy E_a in Eq. (45) is given in terms of the positron binding energy to the surface state E_b, the electron work function φ_-, and the Ps binding energy

$$E_a=E_b+\varphi_- -\tfrac{1}{2}R_\infty\ . \quad (47)$$

The energy distribution of Ps activated from the surface was demonstrated to be thermal by Mills and Pfeiffer (1979), whose data are shown in Fig. 93. To measure this Ps velocity distribution they used a pulsed positron beam coupled with an apparatus similar to that shown in Fig. 31. The data shown in Fig. 93(a) are difference spectra for Ps emitted at 1060 and 300 K, measured for various slit positions in front of the target. The lower curve represents the Boltzmann velocity distribution

$$C(v_z)=A(v_z)\exp(-mv_z^2/k_BT)\ , \quad (48)$$

where the preexponential $A(v_z)$ is the absorption coefficient of Ps incident on the surface. The velocities determined by fitting these data were in excellent agreement with the measured sample temperatures. Since $A(v_z)$ is not a constant, Mills and Pfeiffer concluded that

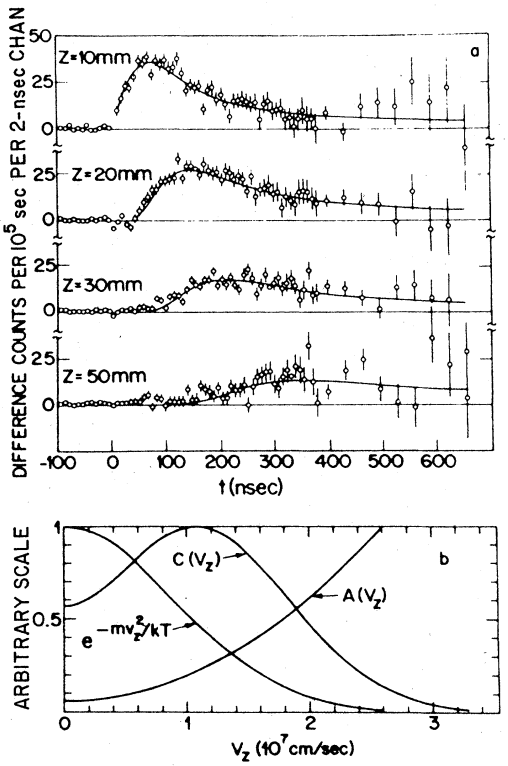

FIG. 93. Velocity distribution for thermal Ps activated from Cu(111). The time-of-flight measurements in the upper portion of the figure are fit by the velocity distribution $C(v_z) = A(v_z)\exp\{-mv_z^2/k_BT\}$ shown in the lower portion (from Mills and Pfeiffer, 1979).

the angular distribution of Ps velocities would be different from the usual cosine law. In their more recent study (1985), they again found good agreement with a thermally activated process for an Al(111) sample. Their conclusion that the Ps reflection coefficient β_{Ps} is independent of velocity is in disagreement with the model proposed by Pendry (1981), in which β_{Ps} is proportional to velocity v_z.

Precise measurements of thermally activated Ps in a larger variety of well-characterized situations will be of value to the understanding of the activation process. The clear sensitivity of E_a to impurities demonstrated in Fig. 92 shows that a quantitative description of thermal activation may in turn lead to increasing studies of unknown surface and image potentials.

In addition to Ps momentum distributions already discussed, 2D ACAR measurements have been used to characterize the positron/Ps localized at the image-induced surface state. In order to perform these experiments in relatively short times (necessary for surface cleanliness), one requires a high flux of moderated positrons. Two systems of this type have been reported; one uses a LINAC beam (Howell, Fluss, *et al.*, 1985) and the other uses a reactor-based beam (Lynn, Mills, *et al.*, 1985). Because of the two-dimensional nature of the trap, it was expected that there would be a large anisotropy in the surface-state momentum distributions. However, this has not been observed for those metal surfaces studied so far (Al, Cu, and Ni). The momentum broadening predicted perpendicular to the surface relative to the parallel component is due to the localization of the positron at the surface, and it is as much as a factor of 2 in some calculations. Figure 94 shows a contour plot for a recent calculation (Brown, Walker, and West, 1987) that uses a mixed-density approximation (MDA) and modified potential to minimize the anisotropy. The agreement with the experimental results of Chen *et al.* (1987), also shown in Fig. 94, is still clearly less than adequate. Lou *et al.* (1988) have shown that the perpendicular component of electron momentum at the surface is reduced by the model potential they used. Their calculated 2D ACAR distribution is nearly isotropic, consistent with the experimental results.

One of the most intriguing clues to the nature of the surface state was presented by Gidley, Köymen, and Capehart (1988; also Köymen *et al.*, 1984). They determined that a reduction of about 3 eV in the magnitude of the electron work function for Ni, caused by chemisorption of alkali metals, made almost no change in the amount of Ps thermally desorbed from the surface state. Their conclusions about this, as based on the Born-Haber energy balance represented by Eq. (47) above, is that the alkali-metal overlayer causes an effective broadening of the image potential well, thereby increasing E_b enough to counter the shift in φ_-. Calculations for Na and Cs overlayers on Ni(100) and Ni(110) indicate that the positron is actually localized at the interface (Nieminen and Jensen, 1988). This theoretical work supports the above observations by predicting that the alkali overlayer leads to very little change of the Ps desorption energy as well as a decrease in the surface-state lifetime.

An alternate suggestion presented by Platzman and Tzoar (1986) is that the positron at a metal surface is actually bound as weakly physisorbed Ps, rather than, as in the conventional picture, a positron wave function in a potential well (which might equivalently be termed *chemisorbed* e^+). This would explain the lack of sensitivity of

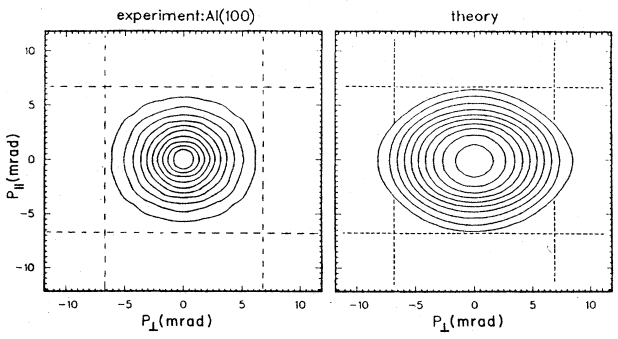

FIG. 94. Contour plots for positrons annihilating from surface-localized states. The experimental results (left) are those of Chen *et al.* (1987), and the theoretical prediction (right) is from Brown *et al.* (1987).

E_a to alkali-metal coverage, since the interaction between the neutral Ps and the metal surface would be a van der Waals interaction, and this polarization potential would not be tied to changes in φ_-. Manson and Ritchie (1984) first treated the Ps-surface interaction quantum mechanically, associating the interaction energy with virtual excitation of the Ps atom and surface plasmons. They found that the potential varies as $1/z^3$ for large separation and as $1/z$ nearer the surface. This change in the functional form was associated with quantum effects, and is affected by the speed of the atom relative to the surface. More recently Paranjape and Mahanty (1985) extended this work beyond the dipolar approximation to include the multipole excitations of the Ps atom. Figure 95 shows the $1/z^3$ potential of this model in comparison with the normal image potential. The reactivity of Ps near a metal surface (that may be expected by analogy with atomic hydrogen) would suggest that the van der Waals description of the interaction is valid only at very large distances from the surface.

The possibility of Ps localization at the surface was also adopted by Cuthbert (1985) in an independent theory. His model extends the variational approach (referred to at the beginning of this section) by including short-range effects through a single, distinguishable electron. The Ps-like contribution to the wave function that this introduces reduces the energy, thereby improving the solution, and the binding is due to the van der Waals attraction on the center-of-mass composite wave function (Fig. 96). It is important to note that this cannot be thought of as a true Ps atom near the surface because, as the author points out, the wave function is highly distorted. Although this model is not used to predict a surface 2D ACAR spectrum, the exceptionally small overlap of the *correlated* positron and electron means that the momentum distribution would be expected to represent all the electrons at the surface. This has recently been observed for positrons/Ps localized at graphite surfaces (Sferlazzo *et al.*, 1987).

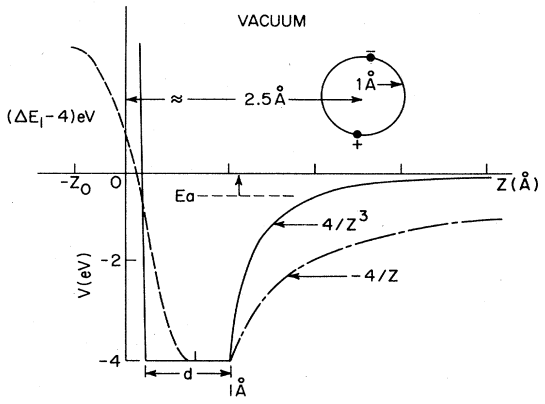

FIG. 95. The effective potential for Ps "physisorbed" at a surface. The solid curve represents the van der Waals attraction of the Ps to the surface, while the dashed curve shows the bare positron single-particle potential.

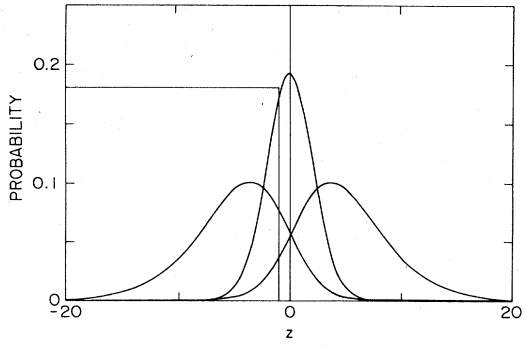

FIG. 96. Electron (left), positron (right), and center-of-mass (middle) probability distributions as a function of perpendicular distance from the surface (angstroms). The "Ps-like" center-of-mass wave function reduces the total energy of the positron localized at the surface (from Cuthbert, 1985).

Whether the positron is in a highly screened or a bound Ps-like state at the surface, its lifetime is known to be much longer than in the bulk solid. Until recently, theoretical calculations were usually performed by the use of a local-density approximation (LDA), neglecting dynamic correlations. In addition, the maximum positron lifetime in the low-density limit of a locally homogeneous electron gas was previously expected to be the spin-averaged Ps lifetime

$$\langle \lambda_{\mathrm{Ps}} \rangle \equiv \tau_{\mathrm{Ps}}^{-1} = \tfrac{3}{4}\lambda_{o\text{-Ps}} + \tfrac{1}{4}\lambda_{p\text{-Ps}} , \tag{49}$$

which yields $\tau_{\mathrm{Ps}} \approx 500$ psec. The most recent calculations of this type were done by Nieminen and Puska (1983; also, Puska and Nieminen, 1983), who found a positron surface-state lifetime of $\tau_s \approx 400$ psec for Al, which is more or less independent of the crystal orientation. Their model, which is the first to include microscopic differences of the surface through the use of a *corrugated* image plane, also predicts that the positron would localize in surface vacancies, at least for Al(110) surfaces. Their result is shown in Fig. 97, and the increase in lifetime they expect for the surface vacancy is only marginal (to ≈ 410 psec).

So far the only direct measurement of τ_s was that made for Al(110) using the apparatus shown in Fig. 28 (Lynn, Frieze, and Schultz, 1984). The lifetime they reported was 580 ± 10 psec, which is apparently inconsistent with the LDA calculations. To determine this lifetime from the data, the simple two-state trapping model had to be modified to include the effect of spatial variations of the positron density on the solution of the diffusion equation (Frieze, Lynn, and Welch, 1985). Nieminen, Puska, and Manninen (1984) showed that the discrepancy can be removed if the *bare* positron lifetime ($\tau = \infty$) is used rather than the spin-averaged lifetime shown above. However, the remaining uncertainty about dynamical screening effects coupled with the paucity of experimental results leaves the discussion still largely unsettled. In the end, it may turn out that surface defects

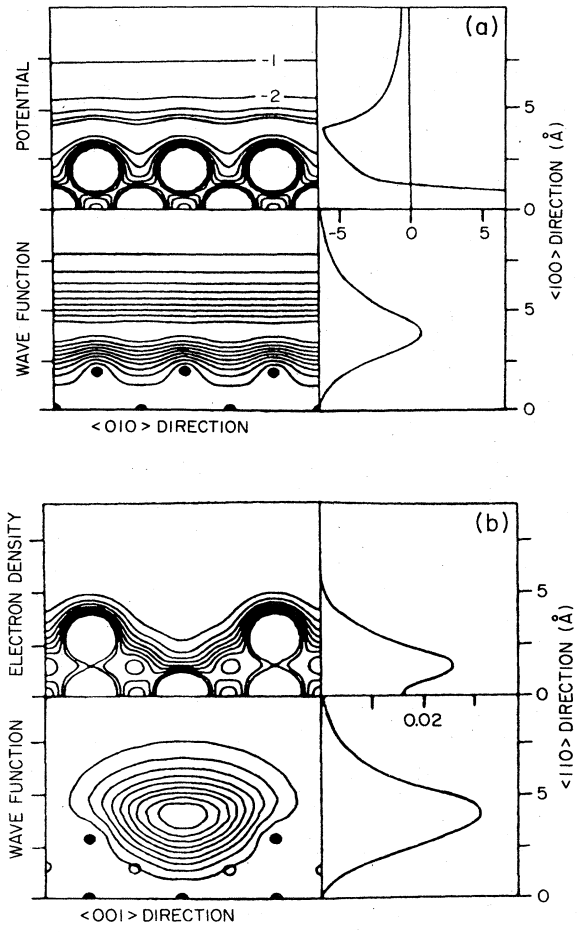

FIG. 97. Contour plots of positron potential (a) and wave function (b) at an Al(110) surface using the corrugated mirror model. The right-hand sides illustrate the (weak) tendency of the positron to localize at a surface vacancy for this surface (from Nieminen and Puska, 1983).

or impurities (like that pictured in Fig. 97) are in fact dominating all of the experimental studies of the surface state (Lynn, 1979b). Positron sensitivity to a variety of surface conditions has now been demonstrated (see Sec. II.E), and as we learn more about these interactions it becomes increasingly obvious that they must be included in any complete description of energy-loss, surface-state localization and subsequent desorption as thermal Ps.

It has been demonstrated that one can calculate core electron-positron annihilation rates with high accuracy (Lynn, MacDonald, *et al.*, 1977). Weiss *et al.* (1988) have recently observed Auger electron emission caused by positrons annihilating while localized in the surface state of Ni(110) and polycrystalline Cu. This may turn out to be a highly sensitive probe of the exact nature of the positron state at a surface, and specifically of whether the wave function is localized at surface defects or impurities. It also has the potential of being the only surface probe that creates Auger electrons from the outer surface layer only.

4. Ps emission from insulators and molecular crystals

In many insulators and molecular crystals Ps can form in the bulk solid, diffusing in a delocalized Bloch state (for a general review of Ps in solids, see Dupasquier, 1981). Some of the materials in which Ps will form will actually emit the Ps into the vacuum if it is formed sufficiently close to the surface. This process is characterized by a potential difference, which we define to be the Ps work function ϕ_{Ps}, because of the obvious analogy with the electron or positron work function (Sec. C.1). It is important to note that this is quite different from any of the above discussions of Ps, since it is not formed specifically at the surface.

The first positron beam study of "*excitonic*" Ps formed *near* a surface was that done in crystalline and amorphous ice (Eldrup *et al.*, 1983, 1984, 1985). This work was discussed briefly in Sec. II.B.4 in the context of positron energy loss in insulators, and an example of the excitonic Ps emitted from ice as a function of incident positron energy was shown in Fig. 63. The value of ϕ_{Ps} obtained in this study was -2 ± 1 eV. Other measurements of excitonic Ps emission have been made recently for ionic solids (Mills and Crane, 1984), and in quartz (SiO_2) and MgO single crystals (Sferlazzo, Berko, and Canter, 1987). Sferlazzo *et al.* found $\varphi_{Ps}=-3.27\pm0.04$ eV for quartz, but they found no evidence for the excitonic component in MgO. Their data, presented in terms of the Ps time of flight, are shown in Fig. 98. The inset in the upper right-hand corner shows the essentially monoenergetic component of the SiO_2 data, which they attribute to work-function emission of excitonic Ps.

In a similar experiment Sferlazzo, Berko, and Canter (1985) suggested that physisorbed Ps was stable on the surface of quartz. This conclusion was reached by fitting

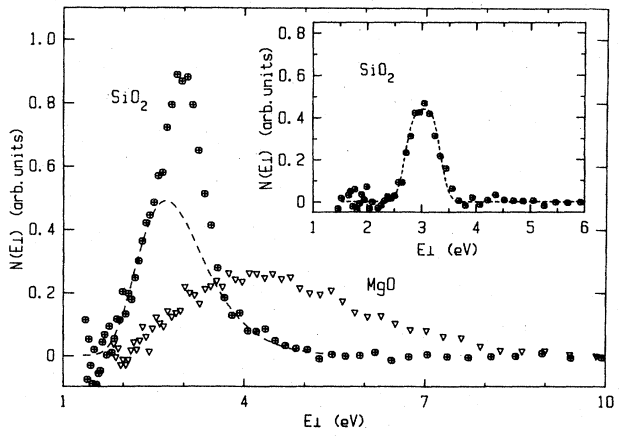

FIG. 98. Positronium formation in solid quartz and MgO. The continuous, broad energy distribution results from inelastic losses of the Ps to the solid. The authors state that the data for quartz (inset, upper right) also include a contribution due to excitonic Ps formation, like that shown for ice in Fig. 64 (from Sferlazzo *et al.*, 1987).

Eq. (45) to their data for Ps fraction versus temperature and deducing an activation energy of ≈ 0.15 eV, with a prefactor more than 30 times that found for metals. The thermal activation in this work is not nearly as well defined as that for most metal surfaces (e.g., Fig. 92), and future studies, such as the surface 2D ACAR described previously or the laser desorption experiments in progress at Livermore, may be required to confirm these conclusions. It may in fact turn out that a mechanism similar to the phonon-assisted Ps emission described earlier for graphite is responsible for the observations for quartz, since the data have in both cases the same unusual dependence on temperature.

E. Defects

One of the most widely adopted research areas for positrons has been the identification and study of various types and concentrations of defects in crystalline solids (West, 1973). It is therefore no surprise that, soon after the first UHV positron beams were operating, studies of defect properties *at* and *near* crystal surfaces were initiated (Lynn, 1979a). One of the most striking advantages of the positron beam technique follows from the narrow energy width and controllable energy it makes possible allowing nondestructive measurements on a greater variety of defect-related problems than any other method, positron or otherwise.

For studies of equilibrium defects in bulk solids (Sec. II.E.1), one particular advantage of the diffusion-length type of study relative to conventional *bulk* positron techniques (Sec. I.B) is the fact that the measurement of a diffusion length will continue to decrease with increasing defect density long after a bulk Doppler-broadening or lifetime parameter indicates saturation trapping. The procedure is (in principle) limited only by the need to inject positrons at energies high enough to prevent significant nonthermal positron reemission and/or nonthermal Ps formation. The variety of surface-specific interactions that can be observed, together with the low incident positron energies available, make the study of near-surface defects possible (Sec. II.E.2). Such studies have so far been restricted to indirect methods (e.g., LEED) or more spatially limited direct measurements (e.g., scanning tunneling microscopy). The variable energy of positron beams allows (at least in principle) somewhat selective studies of interfaces and multilayer structures (Secs. II.E.3 and II.E.4). This is because the mean depth at which the positrons thermalize is proportional to energy [Eq. (12)].

The present state of nonuniform defect studies with positron beams is far from its full potential, as is true of many of the areas already described for this relatively new probe of solids. However, it is clear from the work reviewed in the following sections that defect studies will in the future be one of the more actively pursued research areas for variable-energy positron beam facilities.

1. Bulk defects

The concept of bulk studies of solids with most of the positron beams that currently exist is slightly distorted, since the penetration depth [Eq. (12)] is limited to a maximum of a few microns. In particular, the way defects are often characterized is to use the "half-energy" for positron back-diffusion to an interface (solid/vacuum, solid/liquid, solid/solid), which is the parameter E_0 described in Sec. II.C [Eq. (28)]. This means that the portion of the bulk solid being sampled is within a few multiples of the mean diffusion length (of order 10^3 Å) of the interface. Nevertheless, for systems with supposedly "equilibrium" distributions of defects (such as thermally activated vacancies), the present evidence is that the shallow penetration depths are sampling uniform defect densities.

The first measurements of thermally activated vacancy trapping using a positron beam were for silver (Lynn, 1979a) and copper (Lynn and Welch, 1980). These were followed by studies in a variety of other materials, including aluminum (Lynn, 1981; Lynn and Schultz, 1985; Huomo *et al.*, 1987) and niobium (Nielsen, Lynn, Hurst, Vehanen, and Schultz, 1985). The ability to study difficult materials (e.g., chemically reactive, high-melting-point, or thin foil) without the same restriction of source-specimen geometry inherent to conventional positron annihilation techniques is a principle benefit of the positron beam. The vacancy formation energy E_{1v}^f is found by measuring E_0 as a function of sample temperature and modeling the effective lifetime of the diffusing positron [τ_{eff} in Eq. (28)] by

$$\lambda_{\text{eff}} \equiv \tau_{\text{eff}}^{-1} = \lambda_b + \frac{\lambda_v \kappa_{bv}}{\lambda_v + \kappa_{vb}} , \tag{50}$$

where λ_b and λ_v are the annihilation rates in the bulk solid and a vacancy, respectively, and κ_{bv} is the trapping rate into vacancies. The probability for detrapping, κ_{vb}, is generally assumed to be zero for monovacancies. The trapping rate, determined from the above, is then related to E_{1v}^f by the expression

$$\begin{aligned} \kappa_{bv} &= \nu_0 \exp(S_{1v}^f / k_B) \exp(-E_{1v}^f / k_B T) \\ &= \kappa_0 \exp(-E_{1v}^f / k_B T) , \end{aligned} \tag{51}$$

where ν_0 is the so-called "*specific*" trapping rate, and S_{1v}^f is the entropy of formation for a monovacancy. An example is shown in Fig. 99. In this study it was found that reasonable values of the formation energy ($E_{1v}^f \approx 0.6$–0.7) could only be obtained by using an energy dependence for the mean depth of the stopping profile (Sec. II.B.1) of $\bar{z} = AE$ that was known *not* to be correct for Al. This discovery has in part led to the present realization that diffusion and nonthermal trapping-related phenomena of positrons near surfaces must be studied in much greater detail before accurate parameters (such as E_{1v}^f) can be extracted reliably.

Although the problems mentioned above limit the pre-

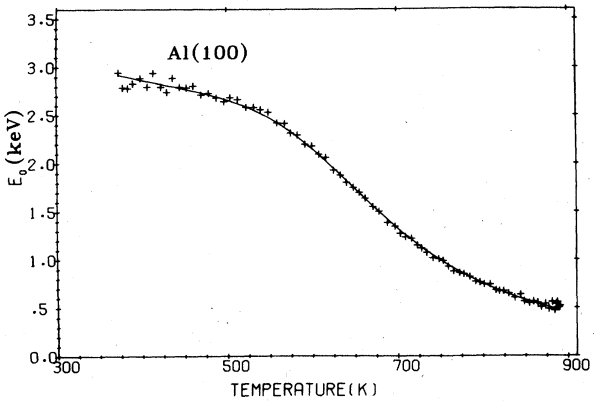

FIG. 99. Temperature dependence of the diffusion-related parameter E_0 for aluminum. The increased slope above ~500 K is due to trapping in thermally generated vacancies (from Lynn and Schultz, 1985a, 1985b).

cision of measurements of E_{1v}^f to about 10%, such measurements have still resulted in useful information for some difficult problems. One example was the determination (Nielsen, Lynn, Hurst, Vehanen, and Schultz, 1985) that the effect of vacancy trapping in Nb is much smaller than was previously thought (Maier *et al.*, 1979). These data, shown in Fig. 100, are inconsistent with the previous value of $E_{1v}^f = 2.6$ eV, although they are now in agreement with the most recent Doppler-broadening bulk study of Nb (Smedskjaer *et al.*, 1985). Another application of the technique to a difficult materials problem was the study of thin foils of amorphous alloys (Vehanen, Lynn, *et al.*, 1984). In this study the extreme sensitivity of positrons to open-volume defects was reconfirmed by the discovery that positron trapping continues in these alloys at temperatures well above the crystallization temperatures (T_c). Prior to this study most evidence supported the view that annealing above T_c would result in bulk recovery of the alloys, and that positrons would therefore annihilate from a more delocalized state than was observed.

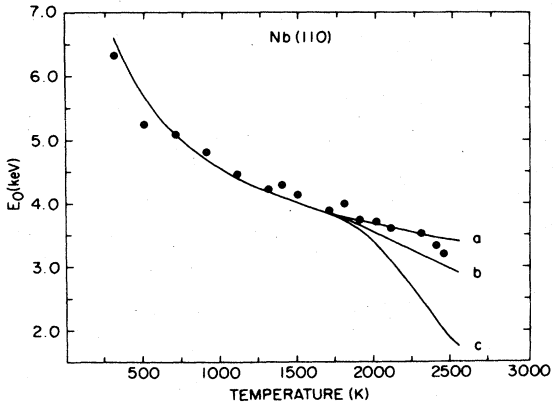

FIG. 100. Temperature dependence of E_0 for niobium. The solid curves are generated assuming $D_+ \alpha T^{-1}$ and (a) no vacancy trapping, (b) $E_{1v}^f = 3.3$ eV, (c) $E_{1v}^f = 3.0$ eV, (d) $E_{1v}^f = 2.6$ eV (from Nielsen, Lynn, Hurst, Vehanen, and Schultz, 1985).

Nielsen, Lynn, and Chen (1986) have recently shown that positrons below 1 eV in aluminum have a relatively high probability of trapping in vacancies prior to complete thermalization. Their results were shown previously in Fig. 57. Before these results, prethermalized trapping was not expected to be significant (Hodges, 1970). McMullen and Stott (1986) subsequently recalculated the trapping rate as a function of energy by modeling the vacancy as a simple spherical well (radius $= 2.99a_0$; depth $= V_0$) and using the exact positron scattering states in place of the normally used orthogonalized plane-wave approximation. Their results are shown in Fig. 101, where it can be seen that in all cases they predict finite trapping rates for positrons in the eV energy range (~0.1 Ry). Lynn, McKay, and Nielsen (1987) have extended the McMullen and Stott model by including the vacancy concentration in their estimates of trapping rates. They showed that most of the nonthermal trapping occurs at energies between $\frac{3}{2}k_BT$ and $10k_BT$ (because of the longer thermalization times at low energy), and they obtained good agreement with the data of Nielsen, Lynn, and Chen when they used the shallow well depths ($V_0 \approx -0.6$ to -0.7 Ry) calculated previously by Manninen *et al.*

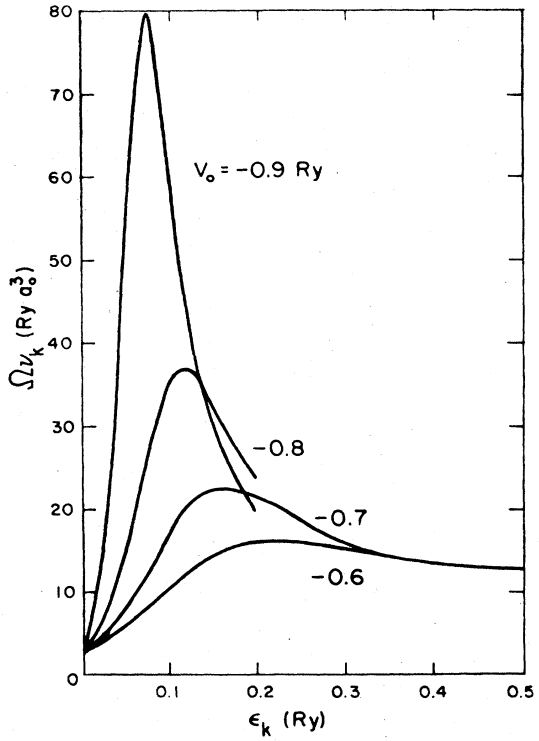

FIG. 101. Cross section for positron trapping at vacancies as a function of positron energy during slowing down. The curves show that for increasing depths of the potential well (V_0) there is an increased probability of prethermalized (≥ 0.01 Ry) trapping of the positron. The symbol V_0 is the authors' and is not related to our use for zero-point potential (from McMullen and Stott, 1986).

(1975) and Nieminen, Boronski, and Lantto (1985). More extensive calculations of this type have been carried out by Puska and Manninen (1987) and by Shirai and Takamura (1987).

2. Surface defects

As discussed in Sec. II.D, the image-induced potential well at a surface (Fig. 8) means that the surface is itself a two-dimensional defect as far as a positron is concerned. It has, however, been observed that structural imperfections on the surface (i.e., steps, islands, surface vacancies) that are either intrinsic or caused by some thermal or adsorbate-mediated reconstruction are often detectable with low-energy positrons. The first observation of this type was for Al_xO_y on Al (Lynn, 1980), where a low value of the reemitted Ps fraction f was observed to increase following heating of the sample. This result, shown in Fig. 102, was attributed to the crystallization of the amorphous oxide overlayer, although a more recent interpretation (Mayer and Lynn, 1986) suggests that the recovery of f is associated with oxygen leaving the surface, rather than crystallizing. In any event, the efficient trapping of positrons before heating in the surface oxide or at the metal/oxide interface is clearly evident in Fig. 102.

This sensitivity to surface defects has been confirmed in several subsequent studies as well. As discussed in Sec. II.D.3 (see Fig. 97), it is possible that the unexpected long surface lifetime measured for Al(110) (Lynn, Frieze, and Schultz, 1984) is attributable to an exceptional sensitivity to defects or impurities. In other words, it may be almost impossible to measure a delocalized positron surface state for any metal surface, since the highly mobile positron in such a state would always seek out a lower-energy site.

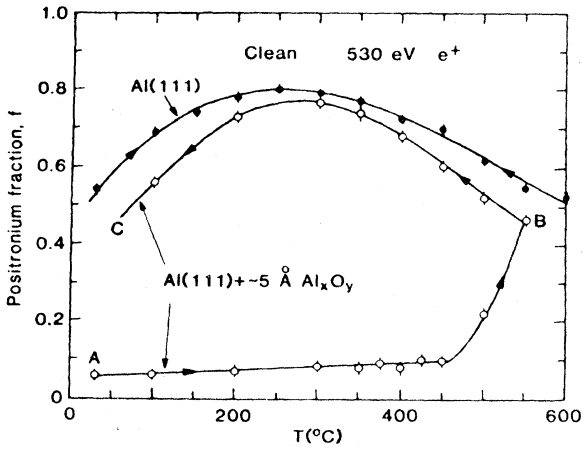

FIG. 102. Positronium fraction as a function of sample temperature for aluminum. The oxygen exposure causes positrons to trap at the surface, inhibiting the usual near-room-temperature activation of thermal Ps. High-temperature treatment of the oxygen-exposed surface has been reinterpreted as the oxygen diffusing into the bulk Al, leaving a clean surface (from Lynn and Lutz, 1980a; and Mayer and Lynn, 1986).

Possible evidence that this is the case is the fact that introducing even a small amount of surface damage by low-dose ion bombardment causes observable differences in the commonly measured surface "signal," which is the branching ratio to Ps (f_0) in Eq. (24). This was demonstrated in the work of Nielsen, van Veen, and Lynn (1985) for Mo(100).

Trapping of positrons at surface imperfections was recently studied by Köymen, Gidley, and Capehart (1987), who produced a variable number of surface steps by epitaxially depositing Ni on a clean Ni(110) substrate. They calibrated their measurements by using LEED to determine the step density, which they were able to do up to the coherence limit (~180 Å) of the electron gun. The results they present, which are reproduced in Fig. 103, show that the positronium fraction formed at the surface is sensitive well beyond the LEED limit. The authors suggest that the steps are the predominant trapping sites of the positrons on the surface, but point out that their measurements do not preclude other possibilities.

The reconstructed Si(111)-7×7 surface, first observed in 1959, is the most studied in all of surface science. Recent advances in diffraction techniques and transmission and tunneling microscopy are now leading to consistent structural models for this surface (Takayanagi *et al.*, 1985, and references therein). It is now fairly widely accepted that the surface unit cell contains stacking faults which terminate in open surface voids about one or two atomic layers deep, and spaced a few tens of angstroms apart. It was suspected that these voids might trap positrons efficiently, therefore reducing the amount of Ps which ultimately will form at the surface. An attempt to

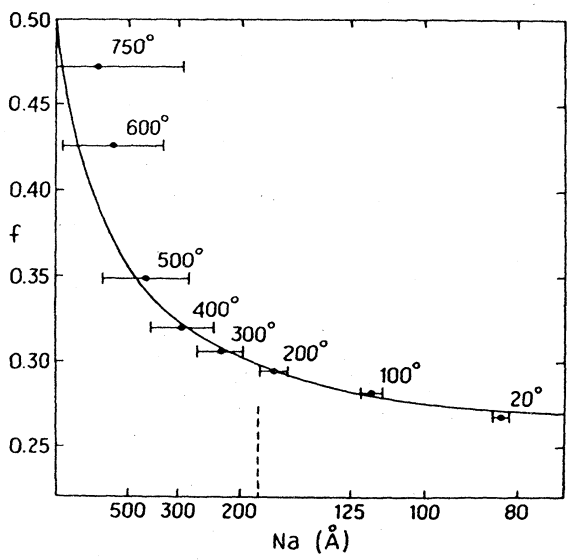

FIG. 103. Positronium fraction as a function of surface ledge size for Ni(110). The ledges, which are known to be monatomic height, are formed by evaporating Ni on the Ni(110) substrate. The dashed line is the coherence limit of the LEED system used to measure the small ledge dimensions (from Köymen *et al.*,

look for evidence of this revealed no change in f_0 upon formation of the 7×7 reconstructed surface, and a slight increase (from ~0.5 to ~0.6) after subsequent exposure to hydrogen (Nielsen, Lynn, Vehanen, and Schultz, 1985).

More recently surface 2D ACAR from Brookhaven National Laboratory (Sec. I.E.2; Lynn, Mills, West, Berko, Canter, and Roellig, 1985) was used to measure the two-dimensional electron momentum distributions for positrons annihilating at reconstructed Si surfaces (Chen, 1987). The data (shown in Fig. 104) are much closer to what would be expected for positrons annihilating with electrons from the bulk band structure after exposure to hydrogen. These results suggest that the positrons are annihilating at the surface with electrons whose momentum is similar to those from the bulk solid. Chen (1987) also found that the hydrogen-covered Si surface resulted in a decreased Ps fraction f_0, in apparent contradiction with the previous study described above.

3. Interface and multilayer effects

Figure 105 shows a highly simplified schematic of positron interface trapping. The first observation that positrons were trapped at interfacial defects was for copper overlayers on a W(110) crystal (Schultz, Lynn, Frieze, and Vehanen, 1983). The Cu, which forms an epitaxial overlayer of Cu(111), takes up the strain of the lattice mismatch in the first two atomic layers. From the results shown in Fig. 106, it can be seen that the yield of 2-keV incident positrons reemitted from the Cu(111) overlayer is only ~30% of the anticipated yield. This reduced yield continued until the Cu/W(110) system was annealed to above 1225 K, which is very close to the temperature required to thermally activate the first atomic layer of Cu on W(110) (Bauer *et al.*, 1974) and is well above the temperature required to anneal out any point defects in the bulk Cu itself.

The observed recovery of the interfacial defects at the Cu/W(110) interface was supplemented with measurements of the yield versus energy in the as-deposited state.

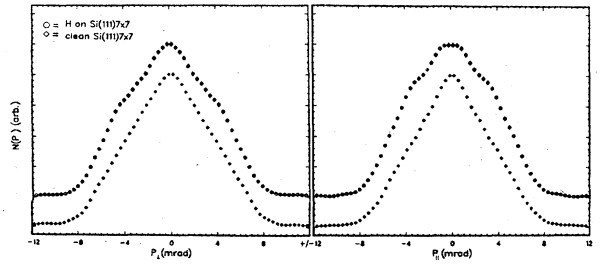

FIG. 104. Electron momentum distributions measured by surface 2D ACAR at a clean and hydrogen-exposed Si(111) 7×7 reconstructed surface. The lower curve is more representative of the bulk electronic band structure than the results for the clean surface (from Chen, 1987).

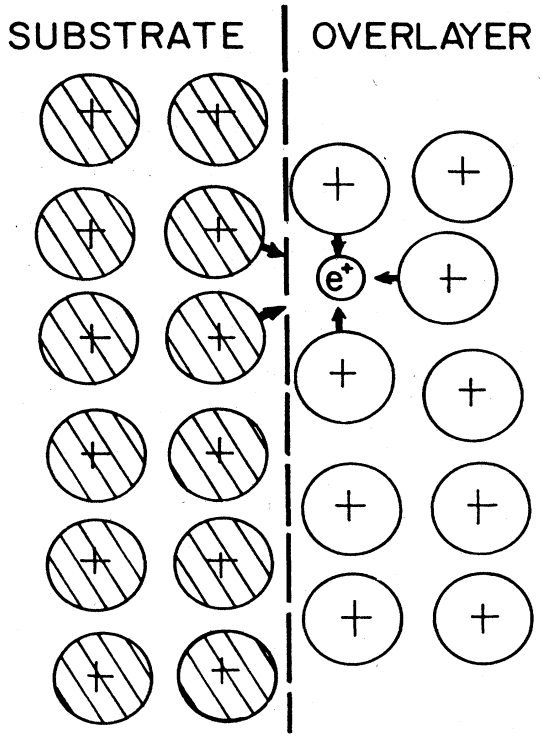

FIG. 105. Schematic representation of positron trapping at an open-volume defect at an interface.

These results showed approximately a 50% decrease in the reemitted yield for incident positron energies above ~1 keV, which is consistent [Eq. (28)] with the interfacial trapping. Monte Carlo simulations of the stopping profile were carried out for the Cu/W(110) system (Lynn and McKeown, 1988), using the partial-wave scattering cross sections discussed in the second paper by Valkealahti and Nieminen (1984). Examples of the simu-

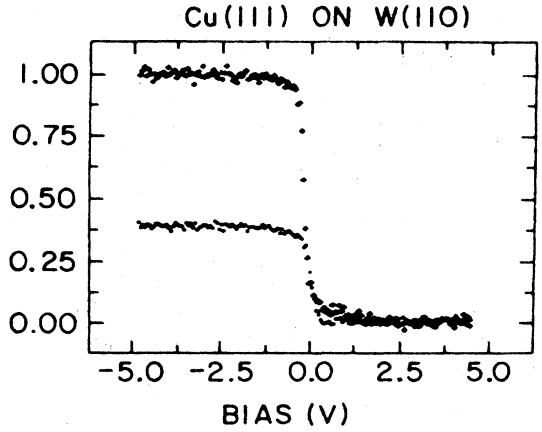

FIG. 106. Reemitted positron energy distribution for epitaxial Cu(111) evaporated on a W(110) substrate. The data are normalized to the defect-free yield of 30% reemission (upper curve), which was observed only after the as-evaporated system (lower curve) was briefly annealed to temperatures above 1225 K (from Schultz, Lynn, Frieze, and Vehanen, 1983).

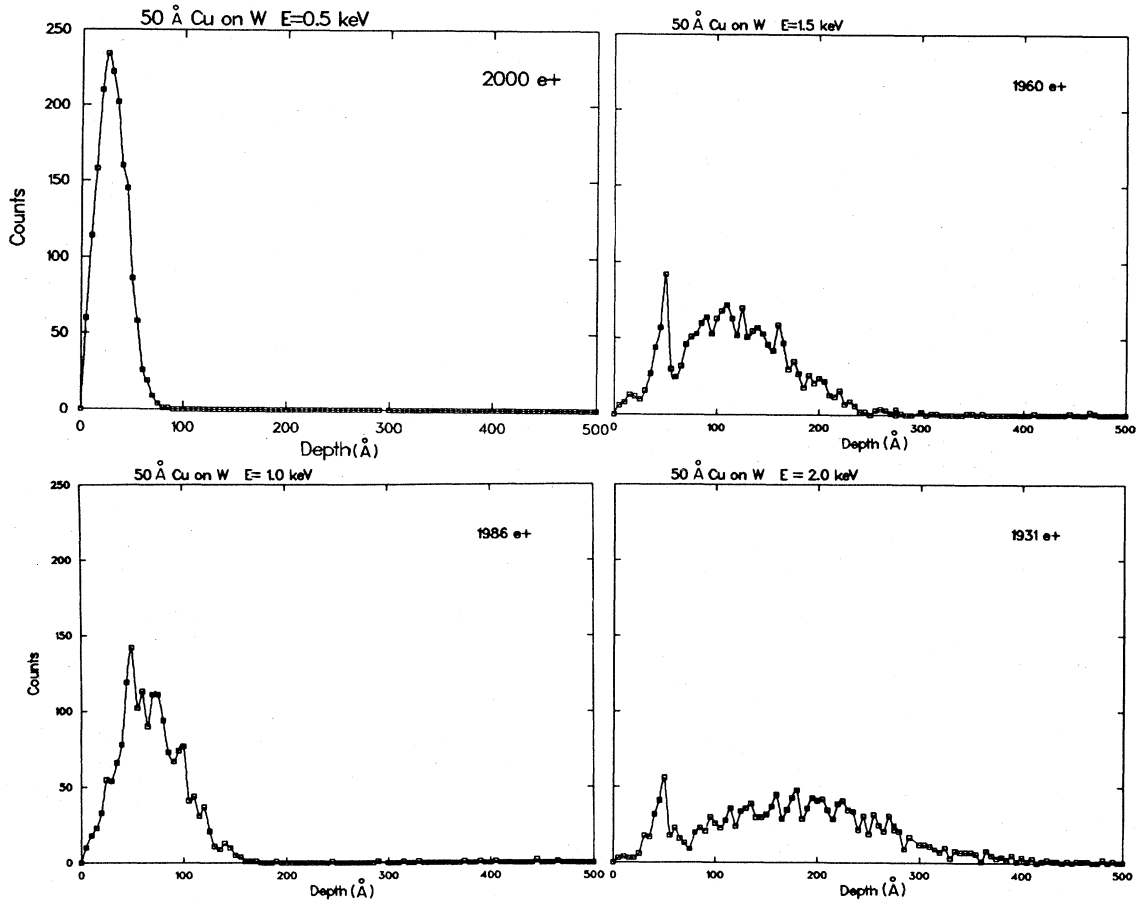

FIG. 107. Monte Carlo simulations of positron stopping profiles for 50 Å Cu on tungsten (from Lynn and McKeown, 1988).

lated profiles are shown in Fig. 107, illustrating the unusual effects of the large density mismatch of the episystem on positron stopping. These profiles show the starting positions of the positrons as thermally diffusing particles, and the simulation of yield involves the iterative solution for diffusion and trapping discussed in Sec. II.E.4, which has to include an interfacial dipole term.

In multilayer systems where the positron does not diffuse, such as oxides, glasses, or other amorphous materials, the interpretation of the results is considerably easier. Vehanen, Saarinen, Hautojärvi, and Huomo (1987) have studied multiple layers of ZnS and Al_2O_3 on a glass substrate by measuring the S parameter as a function of incident positron energy (Fig. 108). This particular heterostructure has application as an electroluminescent display. A high field is placed across the ZnS layer (usually with Mn or rare-earth trace impurities), which is sandwiched between insulating Al_2O_3 layers, and information about interfacial and breakdown properties is useful for the development of these devices. Using a Gaussian-derivative profile [Eq. (25)], Vehanen, Saarinen

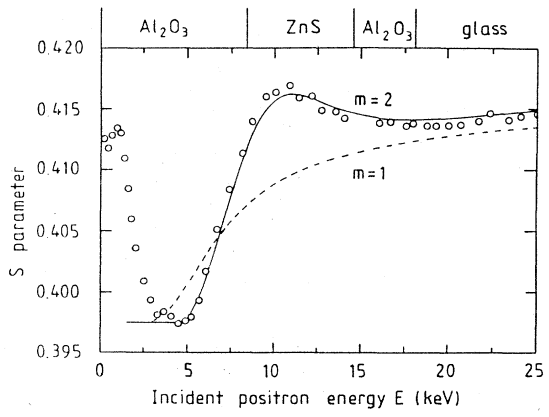

FIG. 108. Doppler-broadening parameter "S" as a function of incident positron energy in a multilayerd heterostructure. The solid curve is a fit to the data using the Gaussian-derivative stopping profile [Eq. (25)] and a linear combination of the known parameters for the various materials in the structure (from Vehanen *et al.*, 1987).

et al. were able to model their data with considerable success, as shown by the solid line ($m=2$) in the figure. The application of the modeling technique to this set of data was simplified considerably by the fact that there was no positron diffusion in the amorphous layers, so that a good test of the implantation profile was possible. The shape reflects the broadening introduced by the finite width of the profile, and a linear superposition of contributions from annihilations at the surface ($S=0.415$), in the Al_2O_3 ($S=0.398$), in the ZnS ($S=0.430$), and in the glass substrate ($S=0.416$). This result is an important demonstration of the applicability of the Gaussian-derivative profile for systems in which the layers do not introduce significant density changes.

An example of a "trapping" overlayer on a crystalline substrate, in which the positron diffuses, is that of SiO_2 on Si. Iwase, Uedono, and Tanigawa (1985) first reported qualitative measurements in this system, showing an increase in the overall fraction of positrons trapped following γ irradiation. More recently Nielsen, Lynn, Chen, and Welch (1987) have made measurements in SiO_2 on Si(110) which fit with a superposition of parameters, including the diffusion in the substrate. Their results, shown in Fig. 109, yield the same value for L_+ as unmodified Si(110) for the portion at energies ≥ 7.5 keV, and the interface is seen very clearly to be near 7 keV. Using Eq. (28) for the mean penetration length, this corresponds to 3200 Å, which is in adequate agreement with the known thickness of 3500 Å.

In another study of this type, Nielsen, Lynn, Leung, *et al.* (1987) found a different behavior when a 520-Å oxide was grown on a Si(100) substrate. To reduce the effects of the electric field, the authors measured the sample at 500 °C, obtaining the data shown in Fig. 110. At depths greater than the interface, the bulk diffusion length for the data shown was consistent with the field-free value. The increase of the line-shape parameter observed at the SiO_2/Si interface indicates positron trapping in open-volume defects. Nielsen *et al.* (private communication) have associated this increase with 3γ annihilations, suggesting that *o*-Ps is being formed in what may be large open-volume spaces (voids) near the interface.

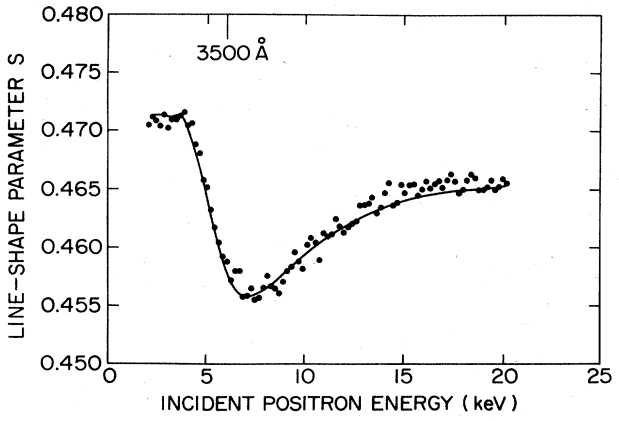

FIG. 109. Doppler-broadening parameter "*S*" as a function of incident positron energy in SiO_2 on Si(110). The curvature for energy greater than ~7 keV corresponds to positron diffusion in the crystalline Si (e.g., Fig. 66). The influence of the interface is observable in the limiting value of the line-shape parameter, which the curve approaches (from Nielsen, Lynn, Chen, and Welch, 1987).

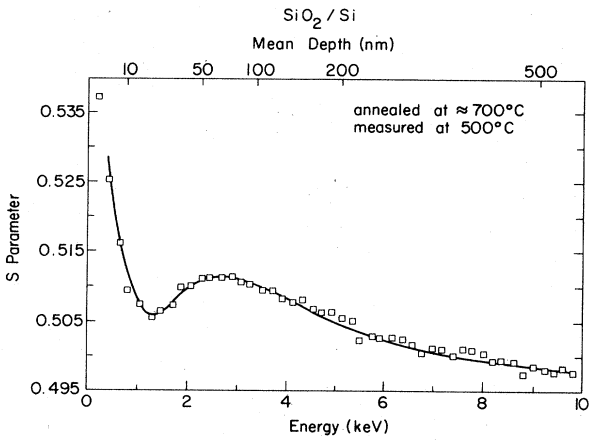

FIG. 110. Positron line-shape parameter *S* measured vs incident energy for Si(100) with a 52-nm overlayer of thermally grown SiO_2. The sample had been heat treated at ~700 °C, and the measurement was done at 500 °C (from Nielsen, Lynn, Leung, Welch, and Rubloff, 1987).

4. Depth profiling of defects

The discussion above and the data presented in Figs. 106–110 are special cases of the more general topic of depth profiling of defects with variable-energy positrons. This technique is generally complicated by positron diffusion, which must be considered together with the detailed shape of the implantation profile to properly *deconvolute* the unknown defect distribution. Since the first reported observations of subsurface defect profiles with positrons (Triftshäuser and Kögel, 1982a, 1982b, 1982c), several advances have brought us to the point where more reliable profiles can be extracted from the data, so long as they are smoothly varying. At the time of writing, the emphasis of the work in this area is on more sophisticated analysis of the measurable data (e.g., *S* parameter, or Ps fraction *f*), and it will likely soon be possible to resolve more complicated distributions with this technique routinely.

In the first study, Triftshäuser and Kögel (1982a, 1982b, 1982c; also Kögel and Triftshäuser, 1983) studied the line-shape parameter for polycrystalline Ni and Cu samples irradiated with energetic He ions. Their results, shown in Fig. 111 for Ni, are presented as the parameter I_c vs incident positron energy. This parameter (sometimes referred to as "*W*") is analogous to the *S* parameter discussed in Sec. I.E.1, except that it is the relative fraction of counts in the wings of the Doppler-broadened annihilation line-shape spectrum. The depth dependence of

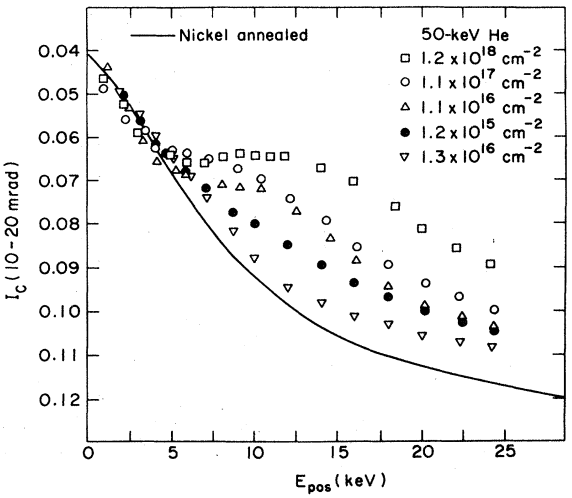

FIG. 111. A Doppler-broadening line-shape parameter as a function of incident positron energy for He^+-irradiated polycrystalline Ni specimens. The solid curve is the result of a fit to the data for annealed Ni (from Triftshäuser and Kögel, 1982a, 1982b, 1982c).

the He-induced damage is clearly visible in these results, as well as the increase of the trapping with dose, but so far they have not modeled the damage profile by anything more than the mean depth of the damage. Measurements similar to these were presented recently by Iwase, Uedono, Tanigawa, and Sakairi (1985).

The problem of modeling the damage caused by the energetic He ions was addressed by Lynn, Chen, Nielsen, Pareja, and Myers (1986; Lynn, 1986). For a distribution $n(z)$ of positrons in a solid with a bulk annihilation rate of λ_b, and a trapping rate

$$\kappa_t = \nu C(z) \tag{52}$$

for a one-dimensional distribution of defects $C(z)$, the steady-state diffusion equation is

$$D_+ \frac{\partial^2 n(z)}{\partial z^2} - (\lambda_b + \kappa_t) n(z) - \frac{\partial}{\partial z}[v_d n(z)] \tag{53}$$

where $P(z)$ is the normalized implantation or stopping profile of the positrons, and v_d [see Eq. (13)] is the field-dependent drift velocity ($v_d = \mu E$; μ = mobility; E = electric field). By integrating Eq. (53) it is seen that positrons annihilating from three distinguishable states have fractions (F_s represents surface; F_d, defect trapped; F_b, bulk) that are given for incident positron energy E by

$$F_s(E) = -J(E)\Big|_{z=0} = D_+ \frac{\partial n(z)}{\partial z}\Big|_{z=0} . \tag{54}$$

$$F_d(E) = \int_0^\infty \kappa_t n(z) dz , \tag{55}$$

and

$$F_b(E) = \int_0^\infty \lambda_b n(z) dz , \tag{56}$$

where $F_s + F_d + F_b = 1$. These formulas are, of course, completely general. In the work of Lynn, Chen, *et al.* (1986) for He-implanted Ni, it was demonstrated that the diffusion equation (53) could be solved exactly for a *reasonably* accurate profile, namely, the Gaussian derivative [Eq. (25)], and a simplified model of the defects as a "box" extending from depth z_1 to z_2. Their results for the difference in the S parameter for three different He implant energies relative to that for unirradiated Ni are shown in Fig. 112. The solid lines in the figure are the results of their model calculations, which correspond to defects extending over the ranges 40–220 nm, 125–400 nm, and 100–600 nm for the 30-, and 90-, and 180-keV curves, respectively. The fit is seen to be quite good in all cases, and the defect ranges are shown to agree with those calculated by Monte Carlo techniques. Uedono *et al.* (1988) have shown in a similar study that positrons are sensitive to defects in (70-keV) helium-implanted nickel at levels down to $\sim 1 \times 10^{13}$ He/cm^2.

A similar type of data analysis was employed by Keinonen *et al.* (1987), who studied the radiation-induced damage and its recovery with thermal annealing in n-type Si(100) crystals implanted with 1×10^{16} 35-keV H^+ ions/cm^2. The positron results, which provided information about the concentration and depth of the defects, were combined with Rutherford backscattering and channeling studies using 2.0-MeV $^4He^+$ ions, which provided profiles of the displaced Si. Through this combination of techniques, they were able to show that the vacancy and displaced-atom distributions in Si which remain after isochronal annealing are not related to the initial deposited energy distribution, contrary to previous expectations.

The first depth-dependent positron *lifetime* study has recently been reported by Schödlbauer *et al.* (1987); results are shown in Fig. 113. These data were obtained using the apparatus shown in Fig. 19 with a polycrystalline nickel sample that was uniformly implanted with helium

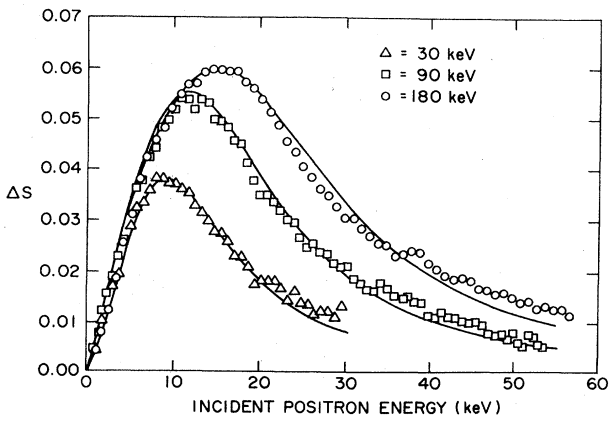

FIG. 112. Difference data obtained by subtracting a curve fit to the S parameter vs energy for annealed Ni from that for the He^+ irradiated Ni crystals. The solid curves are the result of fitting the simple model described in the text (from Lynn, Chen, Nielsen, Pareja, and Myers, 1986).

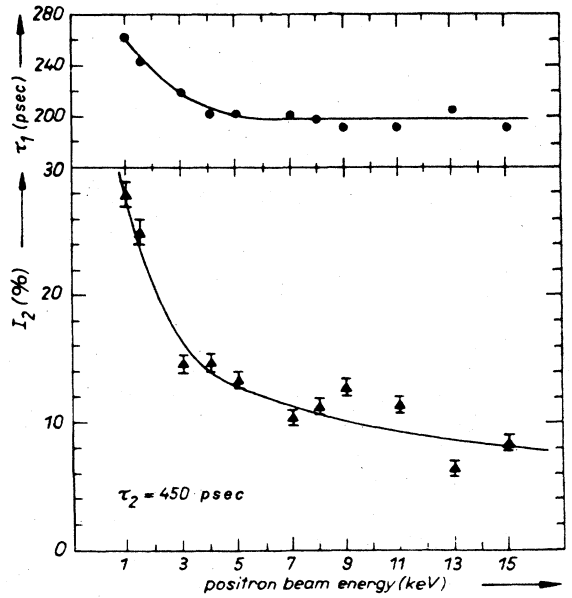

FIG. 113. Positron lifetime τ_1 and intensity I_2 in He-implanted nickel (5000 ppm He) as a function of positron beam energy (from Schödlbauer, Kögel, Sperr, and Triftshäuser, 1987).

(5000 ppm). The data show positron trapping (as evidenced by a short diffusion length), but quantitative results have so far not been obtained with this technique.

One of the reasons the simple model of the 1986 study done at Brookhaven National Laboratory works fairly well is that it is assumed (reasonable for this type of experiment) that the surface is a perfectly absorbing boundary. If, for example, Ps is emitted, it is clear by inspection of Figs. 2 and 29 that it would affect the measured annihilation line shape (Schultz, Lynn, and Jorch, 1984). It is in general true that depth profiling is simplified considerably by ensuring that the surface is absorbing. However, Schut *et al.* (1988) have demonstrated that a careful accounting of the positrons that end up in all available channels (including e^+ and Ps reemission) may be valuable for separating the surface and bulk contributions to the total trapping probability.

To analyze more complicated distributions of defects, it is no longer possible (in general) to solve the diffusion equation analytically. Vehanen, Mäkinen, Hautojärvi, and Huttunen (1985) have defined a parameter which by construction of Eqs. (54) through (56) above can be seen to be the ratio of the fraction returning to the surface in the defected sample, $F_s^{\rm def}$, to the fraction which would return to the surface in the absence of defects, $F_s^{\rm non}$. Their result is

$$K(E)=1-\frac{F_s^{\rm def}}{F_s^{\rm non}}=1-\frac{J_{\rm def}(E)}{J_{\rm non}(E)} . \tag{57}$$

The asymptotic limit of $K(E)$ is

$$K_\infty=1-\left[\cosh\left[\frac{2\langle z\rangle \nu \mathcal{C}_t}{D_+}\right]^{1/2}\right] , \tag{58}$$

where $\mathcal{C}_t$ is the *total* defect concentration, ν is the specific trapping rate, and $\langle z\rangle$ is the mean depth of defects (Mäkinen *et al.*, 1986). This analysis requires a measurable flux of positrons to return to the surface, although in such cases it is so far the most direct way of determining the total concentration and mean depth of $C(z)$. In general, the technique has been applied to cases in which the defect distribution is itself very narrow and near the surface, such as the characterization of defects caused by Ar^+ sputtering damage of Al(110) (Vehanen, Mäkinen, *et al.*, 1985) that is shown in Fig. 114. The Ar^+ energies (and established defect concentrations) ranged from 0.4 keV ($\sim 0.2\times 10^{15}/\text{cm}^2$) to 3 keV ($\sim 1.0\times 10^{15}/\text{cm}^2$). Other studies by these authors using this technique include variations of ion dose and/or angle of incidence (Mäkinen *et al.*, 1986) and an annealing study of the ion-induced defects in Mo(111) that is shown in Fig. 115 (Bentzon *et al.*, 1987).

Two independent techniques for actually modeling different profiles of defects against experimentally obtained data have been developed, although both result in essentially the same information and neither is yet at a stage where it may be reliably applied to totally unknown systems. The first was adapted from a model developed for ion desorption studies by van Gorkum and Kornelsen (1979). van Veen (1984, unpublished) applied their technique to e^+ beam measurements, and elements of this work have been partially described by Nielsen, van Veen, and Lynn (1985). The important components of the model are clearly outlined in part I of the paper by van

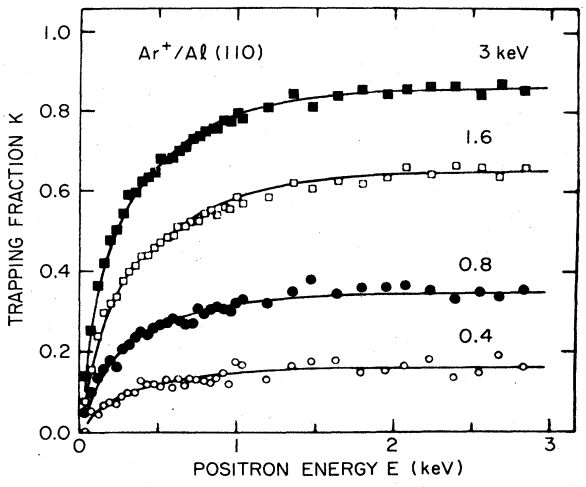

FIG. 114. Positronium parameters $K(E)$ [Eq. (57)] vs energy for Ar^+-ion-sputtered Al(110). The various incident energies are shown; the Ar^+ fluence was in all cases $\sim 10^{17}$ cm^{-2} at an incident angle of $\theta=75°$. From the asymptotic limit of $K(E)$ [Eq. (58)] the total concentration and mean depth of the defects can be deduced (from Vehanen, Mäkinen, Hautojärvi, and Huttunen, 1985).

Gorkum and Kornelsen (1979). A second method employing a Green's-function solution was developed by the Finnish group (Mäkinen *et al*, 1986; Bentzon *et al.*, 1987). Neglecting subtle complications of either technique, they both rely on an iterative approach to solving the diffusion equation (53).

After iteratively solving for the fractions of positrons which annihilate from surface (F_s), defect localized (F_d), and bulk (F_b) states, one compares the solution determined above with the experimental data. This is a direct comparison in the case of Ps fraction data, Eq. (24), or, in the case of line-shape parameter measurements, a linear combination given by

$$S=F_sS_s+F_dS_d+F_bS_b\ , \tag{59}$$

where S_s,S_d, and S_b are the line-shape parameters for positrons annihilating from the surface, defects, or in the undefected bulk solid, respectively

As yet, techniques that actually *deconvolute* an unknown distribution of defects are only in developmental stages. The techniques referred to above require that the implantation profile $P(z)$ and an assumed defect profile $C(z)$ be given and that the specific trapping rate be a known function for each type of defect. These parameters are adjustable, but the results become more time consuming as more parameters are varied.

Vehanen *et al.* (1985) have found a defect profile, $C(z)$, for Ar^+ sputtering damage in Al(110) using a similar technique to that described above. They parametrize $C(z)$ with a Gaussian distribution atop an exponential tail. Their results, shown in Fig. 116, are compared with molecular-dynamics calculations of the damage caused by 100 incident Ar^+ ions. The two curves in Fig. 116 were volume normalized for comparison.

Another more recent example from that same group is shown in Fig. 117 (Punkka *et al.*, 1987). In this example, a Si single crystal was irradiated with 100-keV As^+ ions (5×10^{16} cm^{-2}), which created defects leading to a change in the line-shape parameter ΔS, relative to that observed in the undefected sample. The profile of damage assumed was two "boxes," also shown in the figure. In this study it was demonstrated that laser annealing (1.9 J/cm^2; $\lambda=0.69$ μm) of the irradiated sample significantly reduced the defect concentration, as shown by the data and assumed defect profile also shown in Fig. 117. Other results from this study were presented by Hautojärvi *et al.* (1987).

There is considerable interest in epitaxially grown semiconductor/semiconductor interfaces, as well as hybrid structures made with metals, oxides, and/or semiconductors. An example described in the preceding section (Fig. 109) illustrated the sensitivity of the variable-

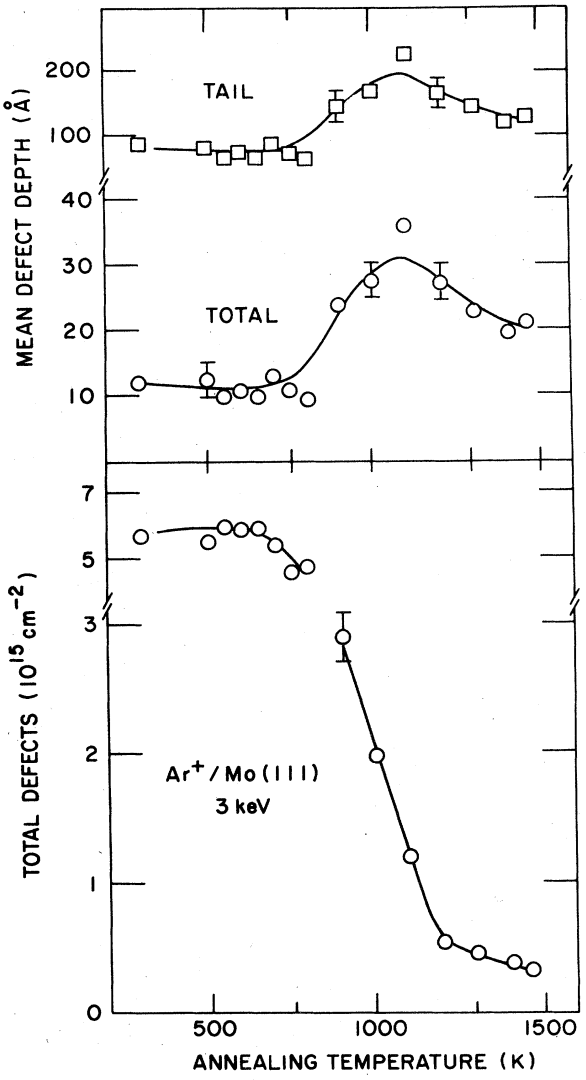

FIG. 115. Total defect concentration and mean depth vs annealing temperature for Mo(111) following sputtering with 3-keV incident Ar^+ ions. The migration of vacancylike defects between 900 and 1200 K leads to both a reduced total number and a deeper mean depth for the defects (from Bentzon *et al.*, 1987).

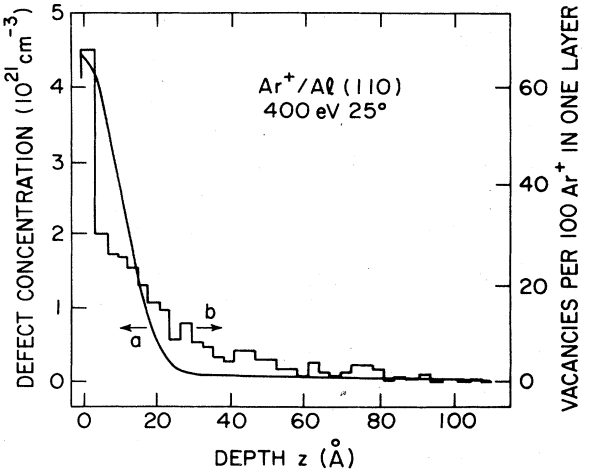

FIG. 116. Defect profiles determined (a) experimentally and (b) by molecular dynamics simulation for Al(110) sputtered with 400-eV Ar^+ ($\sim10^{17}$ cm^{-2}) (from Vehanen, Mäkinen, Hautojärvi, and Huttunen, 1985).

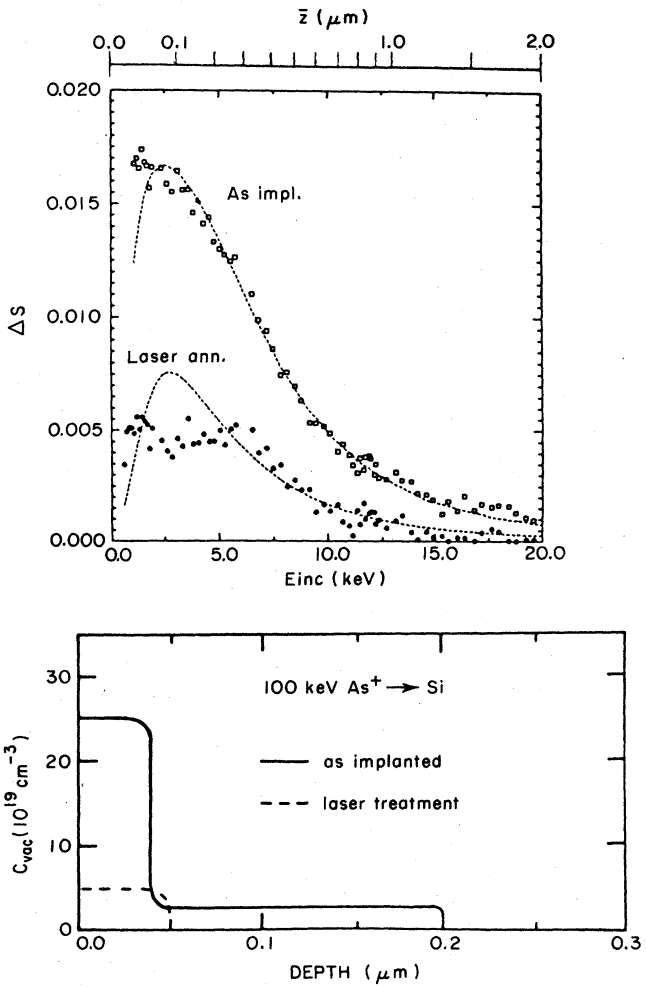

FIG. 117. Change in the S parameter relative to that for annealed Si for As^+-implanted Si. Data are shown for samples before and after laser annealing (from Punkka *et al.*, 1987).

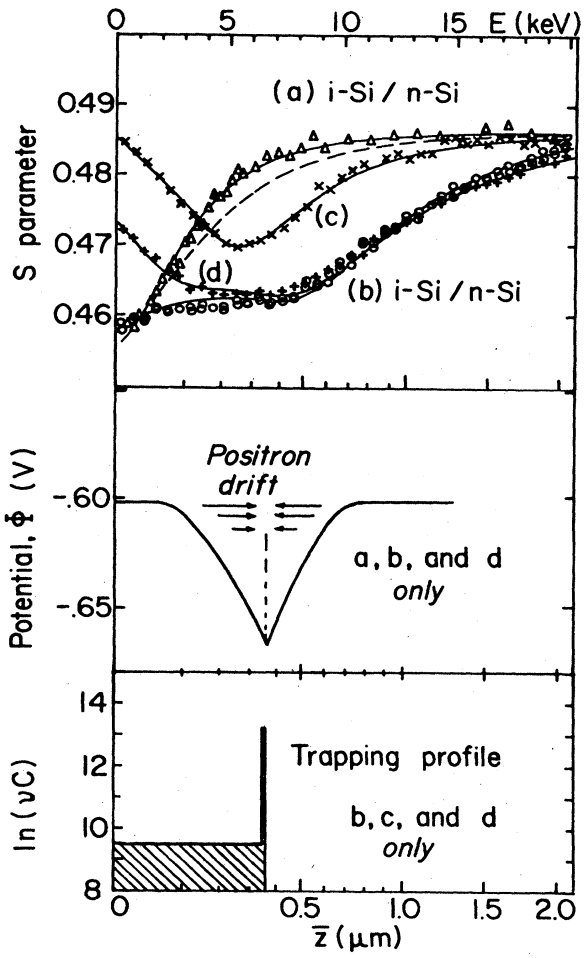

FIG. 118. S-parameter data for MBE-grown intrinsic Si epilayers on n-type Si(100). Data are (a) without defect trapping, and (b)–(d) for a sample containing oxide-type defects. All data are for samples at 20 °C, except (c), which is at 300 °C. The solid curves are obtained by iteratively solving the diffusion equation (53), including both defect trapping [profile $\nu C(z)$] and positron drift. The dashed curve is for bulk material (cf. Fig. 72). From Schultz, Tandberg, *et al.*, 1988.

energy positron technique to the SiO_2/Si(110) interface. New studies presently underway are investigating some of the structural and electronic properties of heterostructures that are *nominally* epitaxial, grown using standard MBE (molecular-beam epitaxy) techniques (e.g., Bean, 1986). Materials presently being investigated with variable-energy positrons include GaAs and Si_xGe_y alloys, which have (among others) applications as potential optical sources or detectors that can be matched to existing fiber optics. Other experiments have been performed for Si/Si superlattices, revealing new information about both electric field effects introduced by electrically active impurities in the epilayers and structural properties associated with the MBE fabrication of the material. Figure 118(a) shows data for a ~3000-Å epilayer grown on an N-type Si(100) substrate. The results are only slightly different from those for "bulk" material (dashed curve, taken from Fig. 72), due to a layer of boron trapped at the interface, which results in a bipolar field of $\sim 2\times 10^3$ V/cm directed *towards* the interface. The data in Figs. 118(b)–118(d) are for a ~3500-Å epilayer on Si(100) that contains oxidelike defects near the interface. The various data sets shown are Fig. 118(b) at 20 °C (as grown), Fig. 118(c) at 300 °C, and Fig. 118(d) after returning to 20 °C. The solid curves through the data are the result of the iterative modeling of the diffusion equation discussed above [see Sec. II.C.4 and Eq. (53)]. Included in the modeling are the effects of positron drift velocity and trapping in defects, observed to be concentrated at the interface and spread (dilutely) throughout the overlayer. The figure also shows the bipolar potential calculated for this sample, and the defect distribution used in the model (Schultz, Tandberg, *et al.*, 1988).

One of the important considerations for positron trapping in semiconductors is the charge state of the defect. For example, the data in Fig. 118 show clear signs of trapping in defects at the interface, which implies that

they are either neutral or negatively charged. On the other hand, studies of thick silicon epilayers (4–6 μm) on Si substrates containing varying numbers of dislocations (from $\sim 5\times 10^3$ to $\geq 10^8$ cm^{-2}) show no signs of positron trapping, indicating that these defects are positively charged. It is clear that more detailed studies of the charge states for various defects will be pursued in the future, and in particular studies will investigate whether or not the electric fields associated with charged defects are leading to prethermalized trapping of positrons. Puska *et al.* (1986) have discussed some theoretical aspects of positron states in defects in semiconductors, and Dlubek and Krause (1987) and Dannefaer (1987) have reviewed some of the bulk solid studies of semiconductors that have been conducted with positrons.

A promising area for investigation with variable-energy positrons is that of modification-induced damage in MBE-grown epilayers. An example that follows logically from the Si/Si study described above is shown in Fig. 119, where silicon epilayers of varying depths are doped using relatively low-energy (0.5–1.0 keV) arsenic ions. Electrical mobility studies show that carrier concentrations of 10^{19} cm^{-3} or more, when implanted during overlayer growth at $\sim$750 °C, can lead to mobilities that are only $\sim$75% of the theoretical values. By contrast, when the growth temperature is $\sim$500 °C the mobility reduction is evident at concentrations of a few times 10^{18} cm^{-3}. As the data in Fig. 119 show, not only is the positron sensitive to the structural damage that is presumably leading to this decreased mobility, but evidence of this damage is clear, even before electrical mobility shows an effect (+ data in the figure).

Although still preliminary, studies of this type are providing the groundwork for using positrons to determine nondestructively depth profiles of defects in the near-surface region of a solid. It is already possible to solve the problem without assuming a functional form for the defect profile, but without significant advancements in the numerical procedure the technique is limited by the experimental precision of the data. These concerns, and the correlation of defect and implantation profiles, will eventually establish the limits to which a profile of unknown defects can be uniquely determined experimentally.

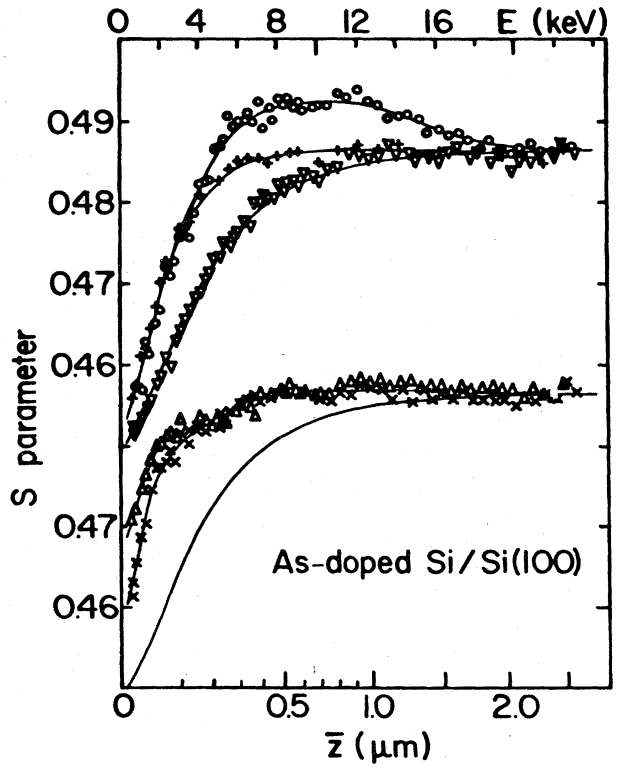

FIG. 119. *S*-parameter vs positron energy for As-doped MBE-grown Si on Si(100). The data are as follows: (a) ∇ symbols, 0.75–1.6-μm overlayers, various doping levels from 1.8×10^{18} to 6.6×10^{18} cm^{-3}, 0.5- and 1.0-keV As$^+$ ion energy, growth temperature $Tg = 750$ °C; (b) + symbols, 1.0-μm overlayer, 7×10^{18} cm^{-3} carriers, 0.5-keV As$^+$, $Tg = 500$ °C; (c) ○ symbols, 1.0-μm overlayer, 3×10^{18} cm^{-3} carriers, 1.0-keV As$^+$, $Tg = 500$ °C; (d) × symbols, 0.3-μm overlayer, 4.5×10^{19} cm^{-3} carriers, 1.0-keV As$^+$, $Tg = 750$ °C; (e) △ symbols, 0.6-μm overlayer, $>1\times 10^{20}$ cm^{-3} carriers, 1.0-keV As$^+$, $Tg = 750$ °C (from Jackman, Schultz, Tandberg, and Denhoff, 1988).

III. SUMMARY AND CONCLUSIONS

We have attempted to provide the reader with an understandable overview of studies of condensed matter with variable-energy beams of positrons. The positron interaction was described from its first encounter with a solid surface, through many of the possible processes until its eventual decay. Some of the applications of the probe are described, as well as many of the fundamental interactions of positrons with solids that are currently of interest to researchers in the field. This pursuit of the basic understanding is essential to the evolution of positron (or indeed even Ps) beams as quantitative probes of material properties.

Perhaps the fastest-emerging area of research with positron beam facilities is that of defect profiling in bilayer and multilayer systems. We expect this to be one of the most useful applications of the technique to materials science. Already, in the last 2 years, new information on metal-metal, semiconductor-semiconductor, and oxide-semiconductor systems has been revealed, some of which is described in this review. This area is not without difficulties, but as the profiling and data analysis capabilities improve we will see it evolve as a more quantitative defect and interface probe. Among the areas that could benefit from studies of this type are adhesion, wear, corrosion, and (as demonstrated) the various techniques used for growing epitaxial multilayer systems.

There has been a great deal written about new experiments that can be performed with positrons. One of the areas currently developing is that of the remoderated e^+ microbeam, which has application to imaging studies of near-surface or interfacial defects. A beam of this type

would complement electron probes (such as TEM or STM) and provide depth-dependent information about numbers and types of various defects. There are presently no fundamental problems in developing a working microbeam with $\sim 10^6$ e^+/sec, which would be useful not only for imaging but for all of the techniques discussed in this review.

In spite of a promising future in both pure and applied areas of materials research, it is clear that more experimental and theoretical work is needed to understand fully e^+ diffusion and interactions with real surfaces and adsorbates. The full description of emission processes will require more accurate estimates for energy-loss rates, which take account of large variations in electron density, including electric field and correlation effects. Future studies on liquids and liquid/solid interfaces will likely contribute to the understanding of the energy-loss and localization phenomena (e.g., Britton and Rice-Evans, 1988). The area of Ps chemistry at surfaces is another that has so far received very little attention. The use of polarized and unpolarized positrons to study molecules on surfaces that have metastable triplet states (e.g., induced by uv light) would be of interest to the study of excited molecular spin-state interactions with Ps atoms. Studies of this nature will not only provide new surface chemistry, but also contribute to the ongoing field of e^+ and Ps chemical interactions in bulk solids.

There are a variety of other research areas involving variable-energy positrons which have only just been initiated, but which will certainly receive more attention in the coming years. Foremost among these is the application of two-dimensional angular correlation techniques to surface and near-surface studies of solids. Some of the preliminary 2D ACAR experiments discussed in this review have already contributed to our understanding of Ps emission, the surface band gap, and positron interactions at a surface. These may yet be enhanced by angle-resolved Ps measurements, or by the use of spin-polarized incident positron beams. The applications of the probe will also be greatly expanded as the time resolution of various "tagging" or pulsing techniques is reduced to a few hundred picoseconds or less on a routine basis. Positron lifetime studies have been extremely useful for bulk solid-state research, and it is certain that similar capabilities will allow new and interesting problems to be addressed in solid surface research.

One undeveloped area is the use of variable-energy Ps beams for studying surfaces. The benefit of this probe is that it is neutral and therefore does not strongly interact with the surface potential. Whether or not Ps will provide unique information about solid surfaces that is not otherwise obtainable with more conventional atomic beams depends to some extent on what is learned in the early stages of the development of these beams, as well as on the (as yet uncertain) ability to make reasonably intense beams ($> 10^5$ Ps/sec) that are energy tunable. It is expected that because it is the "simplest" hydrogenic system available, with a mass three orders of magnitude less than hydrogen, there will indeed be a demonstrable advantage in using Ps scattering for a variety of problems. These questions can only really be answered by the pioneering studies currently underway.

ACKNOWLEDGMENTS

We are indebted to M. Charlton, L. R. Logan, I. K. MacKenzie, T. McMullen, R. M. Nieminen, and A. Vehanen for their detailed comments on the entire manuscript. We should also like to acknowledge D. M. Chen, M. Eldrup, E. M. Gullikson, W. N. Lennard, A. P. Mills, Jr., B. Nielsen, C. L. Snead, E. Tandberg, and D. O. Welch for their suggestions, comments, or discussions. This review could not have been written without the benefit of the various collaborative interactions we have enjoyed; we thank all those individuals with whom we have worked. The work was supported by the Natural Sciences and Engineering Research Council of Canada (P.J.S.) and by the U.S. Department of Energy Division of Materials Sciences, Contract No. DE-AC02-76CH00016 (K.G.L.).

REFERENCES

*In this list of references, ICPA denotes the International Conferences on Positron Annihilation held in 1965, 1979, 1982, and 1985. The proceedings of these conferences are identified by year (ICPA65, ICPA79, etc.), and full information on them is given in the I's under ICPA. Similarly, SLO84, SLO85, and SLO86 refer to Proceedings of International Workshops on Slow Positron Beams. Full information on these proceedings is given in the S's under SLO. POS81 denotes the Proceedings of the International School of Physics Enrico Fermi, Course LXXXIII, on Positron Solid-State Physics, and POS84 the NATO Advanced Research Workshop on Positron Scattering in Gases. Full information on these proceedings is given under POS.

Adesida, I., R. Shimizu, and T. E. Everhard, 1980, J. Appl. Phys. **51**, 5962.

Adkins, G., 1983, Ann. Phys. (NY) **146**, 78.

Andersen, J. U., W. M. Augustyniak, and E. Uggerhoj, 1971, Phys. Rev. B **3**, 705.

Anderson, Carl D., 1932a, Science **76**, 238.

Anderson, Carl D., 1932b, Phys. Rev. **41**, 405.

Anderson, Carl D., 1933, Phys. Rev. **43**, 491.

Ashcroft, Neil W., and N. David Mermin, 1976, *Solid State Physics* (Holt, Rinehart, and Winston, Philadelphia).

Baker, J. A., M. Touat, and P. G. Coleman, 1988, unpublished.

Barberan, N., and P. M. Echenique, 1979, Phys. Rev. B **19**, 5431.

Bardeen, J., 1956, Can. J. Phys. **34**, 1171.

Bardeen, J., and W. S. Shockley, 1950, Phys. Rev. **80**, 72.

Barton, G., 1981, J. Phys. C **14**, 3975.

Barton, G., 1982, J. Phys. C **15**, 4727.

Barton, G., and M. Babiker, 1981, J. Phys. C **14**, 4951.

Bauer, E., H. Poppa, G. Todd, and F. Bonczek, 1974, J. Appl. Phys. **45**, 5164.

Bauer, W., K. Maier, J. Major, H.-E. Schaefer, A. Seeger, H.-D.

Carstanjen, W. Decker, J. Diehl, and H. Stoll, 1987, Appl. Phys. A **43**, 261.
Bean, J., 1986, Physics Today **39** (10), 36.
Beling, C. D., R. I. Simpson, M. Charlton, F. M. Jacobsen, T. C. Griffith, P. Moriarty, and S. Fung, 1987, Appl. Phys. A **42**, 111.
Beling, C. D., R. I. Simpson, M. G. Stewart, Y. Y. Wang, S. Fung, J. C. H. Wai, and T. N. Sun, 1987, Phys. Status Solidi **102**, 537.
Bell, R. E., and R. L. Graham, 1953, Phys. Rev. **90**, 644.
Bell, R. E., and M. H. Jorgensen, 1960, Can. J. Phys. **38**, 652.
Bellotti, E., M. Corti, E. Fiorini, C. Liguori, A. Pullia, A. Sarracino, P. Sverzellati, and L. Zanotti, 1983, Phys. Lett. B **124**, 435.
Bentzon, M. D., H. Huomo, A. Vehanen, P. Hautojärvi, and J. Lahtinen, 1987, J. Phys. F **17**, 1477.
Bergersen, B., E. Pajanne, P. Kubica, M. J. Stott, and C. H. Hodges, 1974, Solid State Commun. **15**, 1377.
Bergersen, B., and M. J. Stott, 1969, Solid State Commun. **7**, 1203.
Berglund, C. N., and W. E. Spicer, 1964, Phys. Rev. A **136**, 1044.
Berko, S., 1981, in POS81, p. 64.
Berko, S., K. F. Canter, K. G. Lynn, A. P. Mills, Jr., L. O. Roellig, and M. Weber, 1985, in ICPA85, p. 961.
Berko, S., and Hugh N. Pendleton, 1980, Annu. Rev. Nucl. Part. Sci. **30**, 543.
Bisc, A., and L. Braicovich, 1964, Nucl. Phys. **58**, 171.
Blackett, P. M. S., and G. P. S. Occhialini, 1933, Proc. R. Soc. London, Ser. A **139**, 699.
Boev, O. V., and K. P. Arefiev, 1985, in ICPA85, p. 783.
Boev, O. V., M. J. Puska, and R. M. Nieminen, 1987, Phys. Rev. B **36**, 7786.
Brandes, G. R., K. F. Canter, T. N. Horsky, and P. H. Lippel, 1987, Bull. Am. Phys. Soc. **32**, 439.
Brandes, G. R., K. F. Canter, T. N. Horsky, and P. H. Lippel, 1988, Rev. Sci. Instrum. **59**, 228.
Brandt, W., 1965, in ICPA65, p. 155.
Brandt, W., 1976, in *Radiation Effects on Solid Surfaces, Advances in Chemistry Series,* edited by M. Kaminsky (American Chemical Society, Washington, D.C.), Vol. 158, p. 219.
Brandt, W., and N. R. Arista, 1979, Phys. Rev. A **19**, 2317.
Brandt, W., and A. Dupasquier, 1983, Eds., *Positron Solid-State Physics* ("POS81"), Proceedings of the International School of Physics Enrico Fermi, 1981, Course LXXXIII (North-Holland, Amsterdam).
Brandt, W., and R. Paulin, 1968, Phys. Rev. Lett. **21**, 193.
Brandt, W., and R. Paulin, 1972, Phys. Rev. B **5**, 2430.
Brandt, W., and R. Paulin, 1977, Phys. Rev. B **15**, 2511.
Britton, D. T., and P. C. Rice-Evans, 1988, Phys. Lett. **126**, 444.
Brown, A. P., A. B. Walker, and R. N. West, 1987, J. Phys. F **17**, 2491.
Brown, B. L., 1986, in *Positron Studies of Solids, Surfaces, and Atoms,* edited by A. P. Mills, Jr., W. S. Crane, and K. F. Canter (World Scientific, Singapore),
Brusa, R. S., R. Grisenti, S. Oss, A. Zecca, and A. Dupasquier, 1985, Rev. Sci. Instrum. **56**, 1531.
Canter, K. F., 1986, in *Positron Studies of Solids, Surfaces, and Atoms,* edited by A. P. Mills, Jr., W. S. Crane, and K. F. Canter (World Scientific, Singapore), p. 102.
Canter, K. F., P. G. Coleman, T. C. Griffith, and G. R. Heyland, 1972, J. Phys. B **5**, L167.
Canter, K.F., and K. G. Lynn, 1984, J. Vac. Sci. Technol. A **2**, 916.
Canter, K. F., and A. P. Mills, Jr., 1982, Can. J. Phys. **60**, 551.
Canter, K. F., A. P. Mills, Jr., and S. Berko, 1974, Phys. Rev. Lett. **33**, 7.
Canter, K. F., A. P. Mills, Jr., and S. Berko, 1975, Phys. Rev. Lett. **34**, 177.
Carbotte, J. P., and H. L. Arora, 1967, Can. J. Phys. **45**, 387.
Case, K. M., and P. F. Zweifel, 1967, *Linear Transport Theory,* (Addison-Wesley, Reading, MA), Chap. 8.
Chang, Tianbao, Hsiaowei Tang, and Yaoqing Li, 1985, in ICPA85, p. 212.
Charlton, M., 1985, Rep. Prog. Phys. **48**, 737.
Chen, D. M., 1987, Ph.D. dissertation (City College, New York).
Chen, D. M., S. Berko, K. F. Canter, K. G. Lynn, A. P. Mills, Jr., L. O. Roellig, P. Sferlazzo, M. Weinert, and R. N. West, 1987, Phys. Rev. Lett. **58**, 921.
Chen, D. M., K. G. Lynn, R. Pareja, and Bent Nielsen, 1985, Phys. Rev. B **31**, 4123.
Chen, D. M., P. J. Schultz, and K. G. Lynn, 1984, unpublished.
Cherry, W., 1958, Ph.D. dissertation (Princeton University).
Chu, S., and A. P. Mills, Jr., 1982a, Phys. Rev. Lett. **48**, 1333.
Chu, S., and A. P. Mills, Jr., 1982b, Appl. Phys. B **28**, 279.
Chu, S., A. P. Mills, Jr., and J. L. Hall, 1984, Phys. Rev. Lett. **52**, 1689.
Chu, S., A. P. Mills, Jr., and C. A. Murray, 1981, Phys. Rev. B **23**, 2060.
Cohen, E. R., and B. N. Taylor, 1973, J. Phys. Chem. Ref. Data **2**, 663.
Cole, Milton W., and Morrel H. Cohen, 1969, Phys. Rev. Lett. **23**, 1238.
Connors, D. C., and R. N. West, 1969, Phys. Lett. A **30**, 24.
Conwell, E. M., 1967, Ed., *High Field Transport in Semiconductors,* Suppl. 9 of *Solid State Physics: Advances in Research and Applications* (Academic, New York).
Cook, D. R., T. N. Horsky, and P. G. Coleman, 1984, Appl. Phys. A **34**, 237.
Corbel, C., 1987, Scanning Microsc. **1**, 545.
Cosslett, V. E., and R. N. Thomas, 1964, Br. J. Appl. Phys. **15**, 1283.
Cosslett, V. E., and R. N. Thomas, 1965, Br. J. Appl. Phys. **16**, 779.
Costello, D. G., D. E. Groce, D. F. Herring, and J. W. McGowan, 1972, Phys. Rev. B **4**, 1433.
Crane, W. S., and A. P. Mills, Jr., 1985, Rev. Sci. Instrum. **56**, 1723.
Cuthbert, A., 1985, J. Phys. C **18**, 4561.
Dale, J. M., L. D. Hulett, and S. Pendyala, 1980, Surf. Interface Anal. **2**, 199.
Dale, J. M., L. D. Hulett, and S. Pendyala, 1981, Appl. Surf. Sci. **8**, 472.
Dale, J. M., L. D. Hulett, and S. Pendyala, 1983, Appl. Spectrosc. Rev. **19**, 105.
Dannefaer, S., 1987, Phys. Status Solidi (a) **102**, 481.
DeBenedetti, S., C. E. Cowan, and W. R. Konneker, 1949, Phys. Rev. **76**, 440.
Deutsch, M., 1951, Phys. Rev. **83**, 866 (1951).
Dirac, P. A. M., 1930, Proc. Cambridge Philos. Soc. **26**, 361.
Dlubek, G., and R. Krause, 1987, Phys. Status Solidi (a) **102**, 443.
Dorikens, M., L. Dorikens-Vanpraet, D. Segers, and I. Lemahieu, 1987, Appl. Phys. A **43**, 257.
Dupasquier, A., 1981, in POS81, p. 510.
Dupasquier, A., 1984, Lett. Nuovo Cimento **41**, 443.
Dupasquier, A., and L. Quartapelle, 1987, Appl. Phys. A **44**,

239.
Dupasquier, A., and A. Zecca, 1985, Riv. Nuovo Cimento **8**, 3.
Eldrup, M., 1981, in POS81, p. 644.
Eldrup, M., A. Vehanen, Peter J. Schultz, and K. G. Lynn, 1983, Phys. Rev. Lett. **51**, 2007.
Eldrup, M., A. Vehanen, Peter J. Schultz, and K. G. Lynn, 1984, Phys. Rev. Lett. **53**, 954.
Eldrup, M., A. Vehanen, Peter J. Schultz, and K. G. Lynn, 1985, Phys. Rev. B **32**, 7048.
Farjam, Mani, and Herbert B. Shore, 1987, Phys. Rev. B **36**, 5089.
Feldman, Leonard C., James W. Mayer, and S. Thomas Picraux, 1982, *Materials Analysis by Ion Channeling* (Academic, New York).
Fischer, D. A., 1984, Ph.D. dissertation (SUNY, Stony Brook). Available from University Microfilms International (No. 85-13537).
Fischer, D. A., K. G. Lynn, and W. E. Frieze, 1983, Phys. Rev. Lett. **50**, 1149.
Fischer, D. A., K. G. Lynn, and D. W. Gidley, 1986, Phys. Rev. B **33**, 4479.
Fluss, M. J., L. C. Smedskjaer, M. Chason, D. G. Legnini, and R. W. Siegel, 1978, Phys. Rev. B **17**, 3444.
Frieze, W. E., D. W. Gidley, and K. G. Lynn, 1985, Phys. Rev. B **31**, 5628.
Frieze, W. E., K. G. Lynn, and D. O. Welch, 1985, Phys. Rev. B **31**, 115.
Gemmell, D. S., 1974, Rev. Mod. Phys. **46**, 129.
Gidley, D. W., and W. E. Frieze, 1986, private communication.
Gidley, D. W., and W. E. Frieze, 1988, Phys. Rev. Lett. **60**, 1193.
Gidley, D. W., A. R. Köymen, and T. Weston Capehart, 1982, Phys. Rev. Lett. **49**, 1779.
Gidley, D. W., A. R. Köymen, and T. Weston Capehart, 1988, Phys. Rev. B **37**, 2465.
Gidley, D. W., R. Mayer, W. E. Frieze, and K. G. Lynn, 1987, Phys. Rev. Lett. **58**, 595.
Gidley, D. W., A. Rich, E. Sweetman, and D. West, 1982, Phys. Rev. Lett. **49**, 525.
Gidley, D. W., and P. W. Zitzewitz, 1978, Phys. Lett. A **69**, 97.
Gidley, D. W., P. W. Zitzewitz, K. A. Marko, and A. Rich, 1976, Phys. Rev. Lett. **37**, 729.
Graff, G., R. Ley, A. Osipowicz, and G. Werth, 1984, Appl. Phys. A **33**, 59.
Gramsch, E., J. Throwe, and K. G. Lynn, 1987, Appl. Phys. Lett. **51**, 1862.
Groce, D. E., D. G. Costello, J. W. McGowan, and D. F. Herring, 1968, Bull. Am. Phys. Soc. **13**, 1397.
Groce, D. E., D. G. Costello, J. W. McGowan, and D. F. Herring, 1969, in *Proceedings of the VIth International Conference on the Physics of Electronic and Atomic Collisions* (MIT, Cambridge, MA), p. 757.
Gryziński, M., 1965, Phys. Rev. **138**, 305 A (Part I), 322 A (Part II), and 336 A (Part III).
Gullikson, E. M., and A. P. Mills, Jr., 1986, Phys. Rev. Lett. **57**, 376.
Gullikson, E. M., and A. P. Mills, Jr., 1987a, Phys. Rev. B **35**, 8759.
Gullikson, E. M., and A. P. Mills, Jr., 1987b, Phys. Rev. B **36**, 8777.
Gullikson, E. M., A. P. Mills, Jr., W. S. Crane, and B. L. Brown, 1985, Phys. Rev. B **32**, 5484.
Gullikson, E. M., A. P. Mills, Jr., and E. G. McRae, 1988, Phys. Rev. B **37**, 588.
Gullikson, E. M., A. P. Mills, Jr., and C. A. Murray, 1988, Phys. Rev. B (to be published).
Gullikson, E. M., A. P. Mills, Jr., and Julia M. Phillips, 1988, Surf. Sci. **195**, L150.
Haghgooie, M., J. J. Mader, and S. Berko, 1978, Phys. Lett. A **69**, 293.
Hamann, D. R., 1966, Phys. Rev. **146**, 277.
Hansen, H. E., and U. Ingerslev-Jensen, 1988, "Penetration of fast electrons and positrons," Technical University of Denmark preprint.
Hansen, H. E., S. Linderoth, and K. Petersen, 1982, Appl. Phys. A **29**, 99.
Hansson, G. V., and S. A. Flodström, 1978, Phys. Rev. B **18**, 1562.
Hautojärvi, P., 1979, Ed., *Positrons in Solids,* Topics in Current Physics No. 12 (Springer, Berlin).
Hautojärvi, P., P. Huttunen, J. Mäkinen, E. Punkka, and A. Vehanen, 1987, in *Defects in Electronic Materials,* edited by M. Stavola, S. J. Pearton, and G. Davies (Materials Research Society Symposia Proceedings, Boston, MA).
Held, A., and S. Kahana, 1964, Can. J. Phys. **42**, 1908.
Heine, V., and C. H. Hodges, 1972, J. Phys. C **5**, 225.
Heitler, W., 1947, *The Quantum Theory of Radiation,* 2nd ed. (Oxford, London).
Herring, C., and M. H. Nichols, 1949, Rev. Mod. Phys. **21**, 185.
Hodges, C. H., 1970, Phys. Rev. Lett. **25**, 284.
Hodges, C. H., 1975, J. Phys. C **8**, 1849.
Hodges, C. H., and M. J. Stott, 1973a, Solid State Commun. **12**, 1153.
Hodges, C. H., and M. J. Stott, 1973b, Phys. Rev. B **7**, 73.
Hölzl, J., and F. K. Schulte, 1979, in *Solid Surface Physics,* Springer Tracts in Modern Physics No. 85 (Springer, Berlin), pp. 1–150.
Horsky, T. N., G. R. Branbes, K. F. Canter, C. B. Duke, A. P. Mills, Jr., and A. Paton, 1988 (unpublished).
Howell, R. H., R. A. Alvarez, and M. Stanek, 1982, Appl. Phys. Lett. **40**, 751.
Howell, R. H., M. J. Fluss, I. J. Rosenberg, and P. Meyer, 1985, Nucl. Instrum. Methods **B10-11**, 373.
Howell, R. H., P. Meyer, I. J. Rosenberg, and M. J. Fluss, 1985, Phys. Rev. Lett. **54**, 1698.
Howell, R. H., I. J. Rosenberg, and M. J. Fluss, 1986, Phys. Rev. B **34**, 3069.
Howell, R. H., I. J. Rosenberg, M. J. Fluss, R. E. Goldberg, and R. B. Laughlin, 1987, Phys. Rev. B **35**, 5303.
Howell, R. H., I. J. Rosenberg, and T. McMullen, 1988, unpublished.
Howell, R. H., I. J. Rosenberg, P. Meyer, and M. J. Fluss, 1987, Phys. Rev. B **35**, 4555.
Hulett, L. D., J. M. Dale, and S. Pendyala, 1980, Surf. Interface Anal. **2**, 204.
Humberston, J. W., and M. R. C. McDowell, 1984, Eds., *Positron Scattering in Gases* ("POS84"), Proceedings of the 2nd NATO Advanced Research Workshop, 1983 (Plenum, New York).
Huomo, H., A. Vehanen, M. D. Bentzon, and P. Hautojärvi, 1987, Phys. Rev. B **35**, 8252.
Huomo, H., A. Vehanen, and P. Hautojärvi, 1987, unpublished.
Hutchins, S. M., P. G. Coleman, A. Alam, and R. N. West, 1985, in ICPA85, p. 983.
Hutchins, S. M., P. G. Coleman, and R. N. West, 1986, in *Positron (Electron)-Gas Scattering,* edited by W. E. Kauppila *et al.* (World Scientific, Singapore), p. 342.
Hutchins, S. M., P. G. Coleman, R. J. Stone, and R. N. West,

1986, J. Phys. E **19**, 282.
Hyodo, T., 1985, in ICPA85, p. 643.
Hyodo, T., T. McMullen, and A. T. Stewart, 1986, Phys. Rev. B **33**, 3050.
ICPA65, *Positron Annihilation,* Proceedings of the 1st International Conference on Positron Annihilation, Detroit, 1965, edited by A. T. Stewart and L. O. Roellig (Academic, New York/London, 1967).
ICPA79, *Positron Annihilation,* Proceedings of the 5th International Conference on Positron Annihilation, Lake Yamanaka, Japan, 1979, edited by R. R. Hasiguti and K. Fujiwara (Japan Institute Met., Tokyo, 1982).
ICPA82, *Positron Annihilation,* Proceedings of the 6th International Conference on Positron Annihilation, Arlington, Texas, 1982, edited by P. G. Coleman, S. C. Sharma, and L. M. Diana (North-Holland, Amsterdam, 1982).
ICPA85, *Positron Annihilation,* Proceedings of the 7th International Conference on Positron Annihilation, New Delhi, 1985, edited by P. C. Jain, R. M. Singru, and K. P. Gopinathan (World Scientific, Singapore, 1985).
ICRU, 1984, "Stopping powers for electrons and positrons" (International Commission on Radiation Units and Measures, Bethesda, Maryland), Report No. 37.
Ishii, Akira, 1987, Phys. Rev. B **36**, 1853.
Ishii, Akira, and Shigeru Shindo, 1987a, Phys. Rev. B **35**, 6521.
Ishii, Akira, and Shigeru Shindo, 1987b, Surf. Sci. **189/190**, 988.
Isii, Akira, 1982, Phys. Lett. A **88**, 417.
Isii, Akira, 1984a, Surf. Sci. **147**, 277.
Isii, Akira, 1984b, Surf. Sci. **147**, 295.
Isii, Akira, 1985, Surf. Sci. **163**, 498.
Ito, Y., T. Axuma, O. Sueoka, S. Mori, Y. Katsumura, H. Kobayashi, and Y. Tabata, 1985, in ICPA85, p. 993.
Ito, Shin, Sakae Shimizu, Tatsumi Kawaratani, and Ken-ichi Kubota, 1980, Phys. Rev. A **22**, 407.
Iwase, Y., A. Uedono, and S. Tanigawa, 1985, in ICPA85, p. 977.
Iwase, Y., A. Uedono, S. Tanigawa, and H. Sakairi, 1985, in ICPA85, p. 868.
Jackman, T. E., P. J. Schultz, E. Tandberg, and M. Denhoff, 1988, unpublished.
Jean, Y. C., K. G. Lynn, and M. Carroll, 1980, Phys. Rev. B **21**, 4935.
Jennings, P. J., and D. Neilson, 1988, unpublished.
Jensen, Kjeld O., and R. M. Nieminen, 1987, Phys. Rev. B **35**, 2087.
Jona, F., D. W. Jepsen, P. M. Marcus, I. J. Rosenberg, A. H. Weiss, and K. F. Canter, 1980, Solid State Commun. **36**, 957.
Jorch, H. H., K. G. Lynn, and I. K. MacKenzie, 1981, Phys. Rev. Lett. **47**, 362.
Jorch, H. H., K. G. Lynn, and T. McMullen, 1984, Phys. Rev. B **30**, 93.
Kahana, S., 1960, Phys. Rev. **117**, 123.
Kakimoto, M., T. Hyodo, and K. Fujiwara, 1985, in ICPA85, p. 776.
Kato, M., and A. Ishii, 1987, Surf. Sci. **189/190**, 996.
Katz, L., and A. S. Penfold, 1952, Rev. Mod. Phys. **24**, 28.
Keinonen, J., M. Hautala, E. Rauhala, M. Erola, J. Lahtinen, H. Huomo, A. Vehanen, and P. Hautojärvi, 1987, Phys. Rev. B **36**, 1344.
Kim, Longhuan, R. H. Pratt, S. M. Seltzer, and M. J. Berger, 1986, Phys. Rev. A **33**, 3002.
Klemperer, O., 1934, Proc. Cambridge Philos. Soc. **30** , 347 (1934).
Kögel, G., Qin-Min Fan, P. Sperr, W. Triftshäuser, and B. Viswanathan, 1985, J. Nucl. Mater. **127**, 125.
Kögel, G., D. Schodlbauer, W. Triftshauser, and J. Winter, 1988, Phys. Rev. Lett. **60**, 1550.
Kögel, G., and W. Triftshäuser, 1983, Radiat. Eff. **78**, 221.
Köymen, A. R., D. W. Gidley, and T. W. Capehart, 1984, in SLO84.
Köymen, A. R., D. W. Gidley, and T. W. Capehart, 1987, Phys. Rev. B **35**, 1034.
Knudsen, M., 1915, Ann. Phys. (Leipzig) **48**, 1113.
Kreuzer, H. J., D. N. Lowy, and Z. Gortel, 1980, Solid State Commun. **35**, 781.
Kubica, P., and A. T. Stewart, 1975, Phys. Rev. Lett. **34**, 852.
Kuzminikh, V. A., I. A. Tsekhanouski, and S. A. Vorobev, 1974, Nucl. Instrum. Methods **118**, 269.
Lahtinen, J., A. Vehanen, H. Huomo, J. Mäkinen, P. Huttunen, K. Rytsölä, M. Bentzon, and P. Hautojärvi, 1986, Nucl. Instrum. Methods B **17**, 73.
Lambrecht, R. M., 1975 (Brookhaven National Laboratory), Report No. BNL50510.
Lang, N. D., 1983, Phys. Rev. B **27**, 2019.
Lang, N. D., and W. Kohn, 1973, Phys. Rev. B **7**, 73.
Laricchia, G., M. Charlton, S. A. Davies, C. D. Beling, and T. C. Griffith, 1987, J. Phys. B **20**, L99.
Lennard, W. N., G. R. Massoumi, and Peter J. Schultz, 1988, unpublished.
Lennard, W. N., Peter J. Schultz, and G. R. Massoumi, 1988, Nucl. Instrum. Methods B **33**, 128.
Leventhal, M., and C. J. MacCallum, 1985, in ICPA85, p. 1003.
Levine, R. Y., and L. Sander, 1982, Solid State Commun. **42**, 5.
Ley, R., K. D. Niebling, A. Osipowicz, A. Picard, and G. Werth, 1985, in ICPA85, p. 996.
Lindhard, J., 1965, K. Dan. Vidensk. Selsk. Mat.-Fys. Medd. **34**.
Logan, L. R., Peter J. Schultz, J. A. Davies, and T. E. Jackman, 1988, Nucl. Instrum. Methods B **33**, 58.
Lou, Yongming, Binglin, Gu, Jialin Zhu, Chang Lee, and Jiajiong Xiong, 1988, unpublished.
Lowy, D. N., and A. D. Jackson, 1975, Phys. Rev. B **12**, 1689.
Luhr-Tanck, W., Th. Kurschat, and Th. Hohenkamp, 1985, Phys. Rev. B **31**, 6994.
Lynn, K. G., 1979a, Phys. Rev. Lett. **43**, 391.
Lynn, K. G., 1979b, J. Phys. C **12**, L435.
Lynn, K. G., 1980, Phys. Rev. Lett. **44**, 1330.
Lynn, K. G., 1981, in POS81, p. 609.
Lynn, K. G., 1986, in *Positron Studies of Solids, Surfaces, and Atoms,* edited by A. P. Mills, Jr., W. S. Crane, and K. F. Canter (World Scientific, Singapore).
Lynn, K. G., D. M. Chen, Bent Nielsen, R. Pareja, and S. Myers, 1986, Phys. Rev. B **34**, 1449.
Lynn, K. G., and J. E. Dickman, 1978, Bull. Am. Phys. Soc. **23**, 427.
Lynn, K. G., and D. A. Fischer, 1986, unpublished.
Lynn, K. G., W. E. Frieze, and Peter J. Schultz, 1984, Phys. Rev. Lett. **52**, 1137.
Lynn, K. G., and H. Lutz, 1978, unpublished.
Lynn, K. G., and H. Lutz, 1980a, Phys. Rev. B **22**, 4143.
Lynn, K. G., and H. Lutz, 1980b, Rev. Sci. Instrum. **51**, 977.
Lynn, K. G., J. R. MacDonald, R. A. Boie, L. C. Feldman, J. D. Gabbe, M. F. Robbins, E. Bonderup, and J. Golovchenko, 1977, Phys. Rev. Lett. **38**, 241.
Lynn, K. G., T. McKay, and M. McKeown, 1987, unpublished.
Lynn, K. G., T. McKay, and Bent Nielsen, 1987, Phys. Rev. B **36**, 7107.
Lynn, K. G., and B. T. A. McKee, 1979, Appl. Phys. **19**, 247.

Lynn, K. G., and M. McKeown, 1988, unpublished.
Lynn, K. G., A. P. Mills, Jr., R. N. West, S. Berko, K. F. Canter, and L. O. Roellig, 1985, Phys. Rev. Lett. **54**, 1702.
Lynn, K. G., and B. Nielsen, 1987, Phys. Rev. Lett. **58**, 81.
Lynn, K. G., B. Nielsen, and J. H. Quateman, 1985, Appl. Phys. Lett. **47**, 239.
Lynn, K. G., and Peter J. Schultz, 1985a, Appl. Phys. A **37**, 31.
Lynn, K. G., and Peter J. Schultz, 1985b, Appl. Phys. A **38**, 293(E).
Lynn, K. G., P. J. Schultz, and I. K. MacKenzie, 1981, Solid State Commun. **38**, 473.
Lynn, K. G., and Alan Wachs, 1982, Appl. Phys. A **29**, 93.
Lynn, K. G., and D. O. Welch, 1980, Phys. Rev. B **22**, 99.
MacKenzie, I. K., T. L. Khoo, A. B. McDonald, and B. T. A. McKee, 1967, Phys. Rev. Lett. **19**, 946.
Madanski, L., and F. Rasetti, 1950, Phys. Rev. **79**, 397.
Maier, K., M. Peo, B. Saile, H. E. Schaefer, and A. Seeger, 1979, Philos. Mag. A **40**, 701.
Makhov, A. F., 1960a, Fiz. Tverd. Tela (Leningrad) **2**, 2161 [Sov. Phys. Solid State **2**, 1934 (1960)].
Makhov, A. F., 1960b, Fiz. Tverd. Tela (Leningrad) **2**, 2172 [Sov. Phys. Solid State **2**, 1942 (1960)].
Makhov. A. F., 1960c, Fiz. Tverd. Tela (Leningrad) **2**, 2176 [Sov. Phys. Solid State **2**, 1945 (1960)].
Mäkinen, J., 1987, M. Sc. thesis (Helsinki University of Technology).
Mäkinen, J., A. Vehanen, P. Hautojärvi, H. Huomo, J. Lahtinen, R. M. Nieminen, and S. Valkealahti, 1986, Surf. Sci. **175**, 385.
Manninen, M., and R. M. Nieminen, 1981, Appl. Phys. A **26**, 93.
Manninen, M., R. M. Nieminen, P. Hautojärvi, and J. Arponen, 1975, Phys. Rev. B **12**, 4012.
Manson, J. R., and R. H. Ritchie, 1984, Phys. Rev. B **29**, 1084.
Manuel, A. A., 1981, in POS81, p. 581.
Marder, S., V. Hughes, C. S. Wu, and W. Bennet, 1956, Phys. Rev. **103**, 1258.
Massoumi, G. R., Peter J. Schultz, W. N. Lennard, and J. Ociepa, 1988, Nucl. Instrum. Methods B **30**, 592.
Mayer, R., and K. G. Lynn, 1986, Phys. Rev. B **33**, 3507.
Mayer, R., Chun-Si Zhang, K. G. Lynn, W. E. Frieze, F. Jona, D. W. Jepsen, and P. M. Marcus, 1987, Phys. Rev. B **35**, 3102.
Mayer, R., Chun-Si Zhang, K. G. Lynn, J. Throwe, P. M. Marcus, D. W. Gidley, F. Jona, 1987, Phys. Rev. B **36**, 5659.
McGowan, J. William, 1972, unpublished.
McKay, T., and K. G. Lynn, 1986, unpublished.
McKee, B. T. A., G. J. C. Carpenter, J. F. Watters, and R. J. Schultz, 1980, Philos. Mag. A **41**, 65.
McKee, B. T. A., A. T. Stewart, L. Manis, and H. Sang, 1979, in ICPA79.
McMullen, T., 1977, J. Phys. F **7**, 2041.
McMullen, T., 1978, J. Phys. F **8**, 87.
McMullen, T., 1984, unpublished.
McMullen, T., 1985, in ICPA85, p. 657.
McMullen, T., and M. J. Stott, 1986, Phys. Rev. B **34**, 8985.
Melezhik, V. S., and F. R. Vukajlovic, 1987, Phys. Rev. Lett. **59**, 641.
Mikeska, H. J., 1967, Phys. Lett. A **24**, 402.
Mills, A. P., Jr., 1978, Phys. Rev. Lett. **41**, 1828.
Mills, A. P., Jr., 1979a, Appl. Phys. Lett. **35**, 427.
Mills, A. P., Jr., 1979b, Solid State Commun. **31**, 623.
Mills, A. P., Jr., 1980a, Appl. Phys. **22**, 273.
Mills, A. P., Jr., 1980b, Appl. Phys. **23**, 189.
Mills, A. P., Jr., 1980c, Appl. Phys. Lett. **37**, 667.
Mills, A. P., Jr., 1981a, in POS81, p. 432.
Mills, A. P., Jr., 1981b, Phys. Rev. Lett. **46**, 717.
Mills, A. P., Jr., 1982, Science **218**, 335.
Mills, A. P., Jr., 1983, Phys. Rev. Lett. **50**, 671.
Mills, A. P., Jr., and S. Chu, 1983, At. Phys. **8**, 83
Mills, A. P., Jr., and W. S. Crane, 1984, Phys. Rev. Lett. **53**, 2165.
Mills, A. P., Jr., and W. S. Crane, 1985a, Phys. Rev. A **31**, 593.
Mills, A. P., Jr., and W. S. Crane, 1985b, Phys. Rev. B **31**, 3988.
Mills, A. P., Jr., and W. S. Crane, and K. F. Canter, 1986, Eds., *Positron Studies of Solids, Surfaces, and Atoms* (World Scientific, Singapore).
Mills, A. P., Jr., and E. M. Gullikson, 1986, Appl. Phys. Lett. **49**, 1121.
Mills, A. P., Jr., and C. A. Murray, 1980, Appl. Phys. **21**, 323.
Mills, A. P., Jr., and Loren Pfeiffer, 1976, Phys. Rev. Lett. **36**, 1389.
Mills, A. P., Jr., and Loren Pfeiffer, 1977, Phys. Lett. **63A**, 118.
Mills, A. P., Jr., and Loren Pfeiffer, 1979, Phys. Rev. Lett. **43**, 1961.
Mills, A. P., Jr., and Loren Pfeiffer, 1985, Phys. Rev. B **32**, 53.
Mills, A. P., Jr., Loren Pfeiffer, and P. M. Platzman, 1983, Phys. Rev. Lett. **51**, 1085.
Mills, A. P., Jr., and P. M. Platzman, 1980, Solid State Commun. **35**, 321.
Mills, A. P., Jr., P. M. Platzman, and B. L. Brown, 1978, Phys. Rev. Lett. **41**, 1076.
Mills, A. P., Jr., and R. Wilson, 1982, Phys. Rev. A **26**, 490.
Mogensen, O. E., 1974, J. Chem. Phys. **60**, 998.
Mogensen, O. E., 1975, Appl. Phys. **6**, 315.
Mogensen, O. E., 1986, Phys. Lett. A **118**, 357.
Mohorovicic, 1934, Astron. Nachr. **253**, 94.
Murray, Cherry A., and Allen P. Mills, Jr., 1980, Solid State Commun. **34**, 789.
Murray, Cherry A., Allen P. Mills, Jr., and J. E. Rowe, 1980, Surf. Sci. **100**, 647.
Neilson, D., R. M. Nieminen, and J. Szymanski, 1986a, Phys. Rev. B **33**, 1567.
Neilson, D., R. M. Nieminen, and J. Szymanski, 1986b, "Angular distribution of positrons emitted from metal surfaces," University of New South Wales, preprint.
Nielsen, Bent, K. G. Lynn, and Yen-C. Chen, 1986, Phys. Rev. Lett. **57**, 1789.
Nielsen, Bent, K. G. Lynn, Yen-C. Chen, and D. O. Welch, 1987, Appl. Phys. Lett. **51**, 1022.
Nielsen, B., K. G. Lynn, J. Hurst, A. Vehanen, and P. J. Schultz, 1985, in ICPA85, p. 464.
Nielsen, Bent, K. G. Lynn, T. C. Leung, D. O. Welch, and G. Rubloff, 1987, in *Defects in Electronic Materials,* edited by M. Stavola, S. J. Pearton, and G. Davies (Materials Research Society Symposia Proceedings, Boston, MA).
Nielsen, Bent, K. G. Lynn, A. Vehanen, and Peter J. Schultz, 1985, Phys. Rev. B **32**, 2296.
Nielsen, B., A. van Veen, and K. G. Lynn, 1985, in ICPA85, p. 836.
Nieminen, R. M., 1983, Phys. Scr. **T4**, 29.
Nieminen, R. M., E. Boronski, and L. J. Lantto, 1985, Phys. Rev. B **32**, 1377.
Nieminen, R. M., and C. H. Hodges, 1976a, J. Phys. F **6**, 573.
Nieminen, R. M., and C. H. Hodges, 1976b, Solid State Commun. **18**, 1115.
Nieminen, R. M., and C. H. Hodges, 1978, Phys. Rev. B **18**, 2568.
Nieminen, R. M., and Kjeld O. Jensen, 1988, unpublished.

Nieminen, R. M., and M. Manninen, 1974, Solid State Commun. **15**, 403.
Nieminen, R. M., and J. Oliva, 1980, Phys. Rev. B **22**, 2226.
Nieminen, R. M., and M. J. Puska, 1983, Phys. Rev. Lett. **50**, 281.
Nieminen, R. M., M. J. Puska, and M. Manninen, 1984, Phys. Rev. Lett. **53**, 1298.
Oliva, J., 1979, Ph.D. dissertation (University of California at San Diego).
Oliva, J., 1980a, Phys. Rev. B **21**, 4909.
Oliva, J., 1980b, Phys. Rev. B **21**, 4918.
Ore, A., and J. L. Powell, 1949, Phys. Rev. **75**, 1696.
Paranjape, U. V., and J. Mahanty, 1985, Phys. Rev. **32**, 3502.
Paulin, R., 1979, in ICPA79, p. 601.
Pedersen, M. J., J. U. Andersen, and W. M. Augustyniak, 1972, Radiat. Eff. **12**, 47.
Pendry, J. B., 1980, J. Phys. C **13**, 1159.
Pendry, J. B., 1981, in POS81, p. 408.
Pendyala, S., 1973, Ph.D. dissertation (University of Western Ontario).
Pendyala, S., and J. W. McGowan, 1980, J. Electron Spectrosc. Relat. Phenom. **19**, 161.
Pendyala, S., P. W. Zitzewitz, J. W. McGowan, and P. H. R. Orth, 1973, Phys. Lett. A **43**, 298.
Perkins, A., and J. P. Carbotte, 1970, Phys. Rev. B **1**, 101.
Platzman, P. M., and N. Tzoar, 1986, Phys. Rev. B **33**, 5900.
POS81, 1981, *Positron Solid-State Physics,* Proceedings of the International School of Physics Enrico Fermi, Course LXXXIII, edited by W. Brandt and A. Dupasquier (North-Holland, Amsterdam, 1983).
POS84, 1984, *Positron Scattering in Gases,* Proceedings of the 2nd NATO Advanced Research Workshop, 1983, edited by J. W. Humberston and M. R. C. McDowell (Plenum, New York).
Punkka, E., A. Vehanen, J. Mäkinen, and P. Hautojärvi, 1987, unpublished.
Puska, M. J., O. Jepsen, O. Gunnarsson, and R. M. Nieminen, 1986, Phys. Rev. B **34**, 2695.
Puska, M. J., and M. Manninen, 1987, J. Phys. F **17**, 2235.
Puska, M. J., and R. M. Nieminen, 1983, J. Phys. F **13**, 333.
Read, M. N., 1983, Solid State Commun. **47**, 1.
Read, M. N., and D. N. Lowy, 1981, Surf. Sci. **107**, L313.
Rice-Evans, P. C., D. T. Britton, and B. P. Cowan, 1987, Appl. Phys. A **44**, 283.
Rich, A., 1981, Rev. Mod. Phys. **53**, 127.
Rich, A., 1986, in *Positron Stuides of Solids, Surfaces, and Atoms,* edited by A. P. Mills, Jr., W. S. Crane, and K. F. Canter (World Scientific, Singapore), p. 177.
Rich, A., J. Van House, D. W. Gidley, R. S. Conti, and P. W. Zitzewitz, 1987, Appl. Phys. A **43**, 275.
Rohrlich, F., and B. C. Carlson, 1954, Phys. Rev. **93**, 38.
Rosenberg, I. J., R. H. Howell, and M. J. Fluss, 1987, Phys. Rev. B **35**, 2083.
Rosenberg, I. J., A. H. Weiss, and K. F. Canter, 1980a, Phys. Rev. Lett. **44**, 1139.
Rosenberg, I. J., A. H. Weiss, and K. F. Canter, 1980b, J. Vac. Sci. Technol. **17**, 253.
Schödlbauer, D., G. Kögel, P. Sperr, and W. Triftshäuser, 1987, Phys. Status Solidi A **102**, 549.
Schödlbauer, D., P. Sperr, G. Kögel, and W. Triftshäuser, 1985, in ICPA85, p. 957.
Schoepf, D. C., S. Berko, K. F. Canter, and A. H. Weiss, 1982, in ICPA82, p. 165.
Schrader, David M., 1985, in SLO85, p. 166.
Schultz, P. J., 1988, Nucl. Instrum. Methods B **30**, 94.
Schultz, P. J., and John L. Campbell, 1985, Phys. Lett. A **112**, 316.
Schultz, P. J., E. M. Gullikson, and A. P. Mills, Jr., 1986, Phys. Rev. B **34**, 442.
Schultz, P. J., T. E. Jackman, H. H. Jorch, and K. G. Lynn, 1983, unpublished.
Schultz, P. J., R. Logan, T. E. Jackman, and J. A. Davies, 1988, Phys. Rev. B (in press).
Schultz, P. J., and K. G. Lynn, 1982, Phys. Rev. B **26**, 2390.
Schultz, P. J., K. G. Lynn, and W. E. Frieze, 1984, in SLO84.
Schultz. P. J., K. G. Lynn, W. E. Frieze, and A. Vehanen, 1983, Phys. Rev. B **27**, 6626.
Schultz, P. J., K. G. Lynn, and Harald H. Jorch, 1984, in SLO84.
Schultz, P. J., K. G. Lynn, and Bent Nielsen, 1985, Phys. Rev. B **32**, 1369.
Schultz, P. J., K. G. Lynn, R. N. West, C. L. Snead, Jr., I. K. MacKenzie, and R. W. Hendricks, 1982, Phys. Rev. B **25**, 3637.
Schultz, P. J., and I. K. MacKenzie, 1982, in ICPA82, p. 640.
Schultz, P. J., E. Tandberg, K. G. Lynn, Bent Nielsen, T. E. Jackman, M. W. Denhoff, and G. C. Aers, 1988, Phys. Rev. Lett. (in press).
Schut, H., A. Van Veen, B. Nielsen, and K. G. Lynn, 1988, unpublished.
Seeger, Alfred, Janos Major, and Frank Jaggy, 1985, in ICPA85, p. 137.
Seltzer, S. M., and M. J. Berger, 1974, Nucl. Instrum. Methods **119**, 157.
Sferlazzo, P., S. Berko, and K. F. Canter, 1985, Phys. Rev. B **32**, 6067.
Sferlazzo, P., S. Berko, and K. F. Canter, 1987, Phys. Rev. B **35**, 5315.
Sferlazzo, P., S. Berko, K. G. Lynn, A. P. Mills, Jr., L. O. Roellig, A. J. Viescas, and R. N. West, 1988, Phys. Rev. Lett. **60**, 538.
Shindo, Shigeru, and Akira Ishii, 1987a, Phys. Rev. B **35**, 8360.
Shindo, Shigeru, and Akira Ishii, 1987b, Phys. Rev. B **36**, 709.
Shirai, Y., and J. Takamura, 1987, Mater. Sci. Forum. **15**, 1.
Singh, M., S. Y. Tang, and O. L. Chow, 1988, unpublished.
Skalsey, M., and J. Van House, 1988, Nucl. Instrum. Methods B (in press).
SLO84, 1984, *Slow Positrons in Surface Science,* Proceedings of the International Workshop, Pajulahti, Finland, edited by A. Vehanen (Helsinki University of Technology Report No. 135).
SLO85, 1985, *Proceedings of the MURR Slow Positron Beam Workshop,* University of Missouri, Columbia, Missouri, edited by Daniel C. Reichel and William B. Yelon (unpublished).
SLO86, 1986, *Proceedings of the International Workshop on Slow Positron Beams for Solids and Surfaces,* Norwich, England, edited by P. G. Coleman and A. B. Walker (unpublished).
Smedskjaer, L. C., C. D. Loper, M. K. Chason, S. B. Gerber, and R. W. Siegel, 1985, in ICPA85, p. 546.
Stein, T. S., and W. E. Kauppila, 1982, Adv. At. Mol. Phys. **18**, 53.
Stein, T. S., W. E. Kauppila, and L. O. Roellig, 1974, Rev. Sci. Instrum. **45**, 951.
Sueoka, Osamu, Yasuo Ito, Toshiyuki Azuma, Shigeki Mori, Yosuke Katsumura, Hitoshi Kobayashi, and Yoneho Tabata, 1985, Jpn. J. Appl. Phys. **24**, 222; also in ICPA85, p. 993.
Sze, S. M., 1981, *Physics of Semiconductor Devices,* 2nd ed. (Wiley-Interscience, New York).
Takayanagi, K., Y. Tanishiro, M. Takahashi, and S. Takahashi,

1985, J. Vac. Sci. Technol. A **3**, 1502.
Thiel, P. A., R. J. Behm, P. R. Norton, and G. Ertl, 1983, J. Chem. Phys. **78**, 7448.
Tong, B. Y., 1972, Phys. Rev. B **5**, 1436.
Triftshäuser, W., and G. Kögel, 1982a, Phys. Rev. Lett. **48**, 1741.
Triftshäuser, W., and G. Kögel, 1982b, in ICPA82, p. 142.
Triftshäuser, W., and G. Kögel, 1982c, J. Nucl. Mater. **111&112**, 687.
Uedono, A., S. Tanigawa, and H. Sakairi, unpublished.
Uggerhoj, E., 1966, Phys. Lett. **22**, 382.
Uggerhoj, E., and J. U. Andersen, 1968, Can. J. Phys. **46**, 543.
Valkealahti, S., and R. M. Nieminen, 1983, Appl. Phys. A **32**, 95.
Valkealahti, S., and R. M. Nieminen, 1984, Appl. Phys. A **35**, 51.
Valkealahti, S., and R. M. Nieminen, 1987, Nucl. Instrum. Methods B **18**, 365.
van Gorkum, A. A., and E. V. Kornelsen, 1979, Radiat. Eff. **42**, 93 (Part I); **42**, 113 (Part II).
Van House, James, and Arthur Rich, 1988, Phys. Rev. Lett. **60**, 169.
Van House, J., A. Rich, and P. W. Zitzewitz, 1984, Phys. Rev. Lett. **53**, 953.
Van House, J., and P. W. Zitzewitz, 1984, Phys. Rev. A **29**, 96.
van Veen, A., 1984, unpublished.
Vehanen, A., 1987, Appl. Phys. A **43**, 269.
Vehanen, A., 1988, private communication.
Vehanen, A., P. Huttunen, J. Mäkinen, and P. Hautojärvi, 1987, J. Vac. Sci. Technol. A **5**, 1142.
Vehanen, A., J. Lahtinen, H. Huomo, J. Mäkinen, K. Rytsölä, and P. Hautojärvi, 1985, in ICPA85, p. 989.
Vehanen, A., K. G. Lynn, Peter J. Schultz, E. Cartier, H.-H. Güntherodt, and D. M. Parkin, 1984, Phys. Rev. B **29**, 2371.
Vehanen, A., K. G. Lynn, Peter J. Schultz, and M. Eldrup, 1983, Appl. Phys. A **32**, 163.
Vehanen, A., and J. Mäkinen, 1985, Appl. Phys. A **36**, 1.
Vehanen, A., J. Mäkinen, P. Hautojärvi, H. Huomo, J. Lahtinen, R. M. Nieminen, and S. Valkealahti, 1985, Phys. Rev. B **32**, 7561.
Vehanen, A., J. Mäkinen, P. Hautojärvi, and P. Huttunen, 1985, in ICPA85, p. 954.
Vehanen, A., and K. Rytsölä, 1981, in POS81, p. 659.
Vehanen, A., K. Saarinen, P. Hautojärvi, and H. Huomo, 1987, Phys. Rev. B **35**, 4606.
Waite, T. R., 1957, Phys. Rev. **107**, 463.
Walker, A. B., and R. M. Nieminen, 1986, J. Phys. F **16**, L295.
Warburton, W. K. and M. A. Shulman, 1977, Phys. Lett. A **60**, 448.
Weber, M., 1988, private communication.
Weiss, Alex H., Mohammed Jibaly, Chun Lei, David Mehl, R. Mayer, and K. G. Lynn, 1988, "Auger electron emission resulting from the annihilation of core electrons with low energy positrons," University of Texas at Arlington preprint.
Weiss, Alex H., and Karl F. Canter, 1982, in ICPA82, p. 162.
Weiss, Alex H., I. J. Rosenberg, K. F. Canter, C. B. Duke, and A. Paton, 1983, Phys. Rev. B **27**, 867.
West, R. N., 1973, Adv. Phys. **22**, 263.
West, R. N., 1985, in ICPA85, p. 11.
Wilson, R. J., 1982, in ICPA82, p. 153.
Wilson, R. J., 1983, Phys. Rev. B **27**, 6974.
Wilson, R. J., and A. P. Mills, Jr., 1983a, Phys. Rev. B **27**, 3949.
Wilson, R. J., and A. P. Mills, Jr., 1983b, Surf. Sci. **128**, 70.
Woll, E. J., and J. P. Carbotte, 1967, Phys. Rev. **164**, 985.
Yu, M. L., and N. D. Lang, 1983, Phys. Rev. Lett. **50**, 127.
Zhang, C., N. Tzoar, and P. M. Platzman, 1988, Phys. Rev. B **37**, 7326 (1988).
Zitzewitz, P. W., J. Van House, A Rich, and D. W. Gidley, 1979, Phys. Rev. Lett. **43**, 1281.

FIG. 1. One of Anderson's (1933) original photographs illustrating the historic discovery of the positron. In the cloud chamber, there is a lead plate 6 mm thick and a magnetic field oriented in the page. The change of energy (63 MeV below the plate to 23 MeV above) with the known thickness of lead and magnitude of the field proves that the particle is positive and of the same mass as the electron.

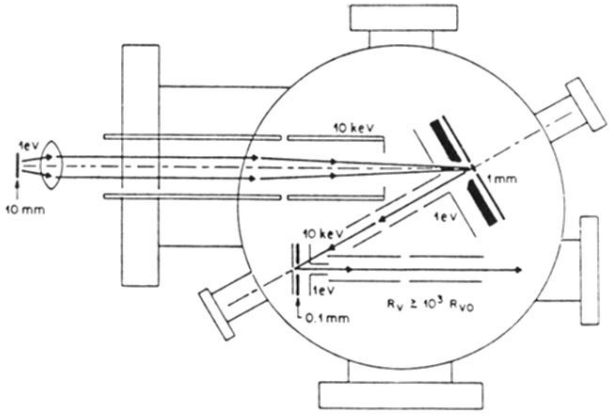

(a)

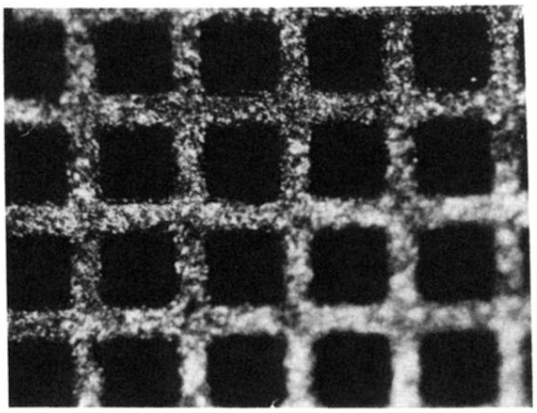

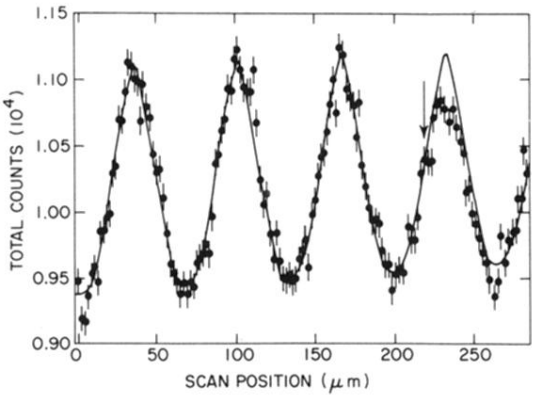

(b)

FIG. 21. A doubly remoderated electrostatic positron beam. The increase of the brightness of the beam is a factor of 10^3. This apparatus produces a focused spot size of $\sim$15-μm diam. The resolution of the beam is indicated in (b), where the one-dimensional image of a fine-mesh grid is obtained by rastering the beam across it (after Brandes *et al.*, 1988).